THE UNIVERSITY OF MICHIGAN

INDUSTRY PROGRAM OF THE COLLEGE OF ENGINEERING

CRYOGENIC HEAT TRANSFER

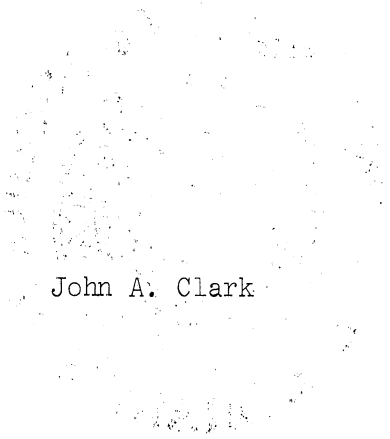

John A. Clark

August, 1968

IP-823

CRYOGENIC HEAT TRANSFER*

by

John A. Clark
Chairman
Department of Mechanical Engineering
University of Michigan
Ann Arbor

* Prepared for Advances in Heat Transfer, Vol. V, edited by T. F. Irvine, Jr. and J. P. Hartnett, Academic Press, Inc. Reproduced by permission.

TABLE OF CONTENTS

TABLE OF CONTENTS (CONTINUED)

I. INTRODUCTION

The first half of this century has seen intensive progress in the physics of low temperatures. This has been followed by the natural development of engineering applications in design and research. One consequence of this has been the introduction of a new word -cryogenic- into the lexicon of technology. This word means the production of cold or a process involving very low temperatures. It is a combination of two Greek words kryos and -gen, kryos meaning icy-cold and -gen indicating an act of production. Hence, kryos plus gen becomes cryogen which, accordingly means a refrigerant. The suffix -ic is appended giving it the adjectival form cryogenic, although the word also may be used as a noun as it frequently is. An -s is sometimes also added forming the word cryogenics, which implies a broad connotation for low temperature phenomena. Thus, today cryogenics is used to describe the science and technology of low temperature phenomena that is, below -150°C (-238F), where marked changes occur in the physical properties of materials.

The growth of cryogenic technology in recent years has been exceptionally rapid and has led one observer to predict that "cryogenics will be to the second half of the 20th century what high temperature processing was to the first".(1)

By 1965 the cryogenics industry had developed into a $650-million a year business with expectation that by 1970 it would surpass $1-billion in yearly sales.(2) Although much of the early impetus to this growth as well as its principal market has been the missile and space programs of the United States Government much development is occuring in private industry. Natural gas, mostly methane, can be liquified

and easily shipped in insulated containers by barge or ship for ultimate use great distances from its source. Liquified natural gas (LNG), for example, from North African and American fields is shipped to England[3,4] and for peak load service a 290,000 bbl LNG storage facility has been built in the Hackensack Meadows, New Jersey, by the Transcontinental Gas Pipeline Corporation.[4] The use of very low temperature in medicine has permitted quick freezing processes important to brain surgery and the preservation of living cells for biological use and research.[2,5,6,14] In a similar application many foods are frozen for storage and transportation and a technique known as "freeze-drying" has introduced a new concept in food preservation.

At low temperatures many materials exhibit extremely low resistance to the flow of electricity. This is called "superconductivity" and at present 24 elements and numerous alloys have been found to possess this property. Cryoelectronics is a developing science devoted to the exploitation of "zero" resistance electrical components for magnetic devices, computer memories and circuits and other electrical apparatus. (References 2, 7, 8, 9). The cooling of surfaces by cryogens, usually liquid nitrogen, is used to produce very low pressures in high vacuum systems. Called cryopumping it is extensively employed in space simulation systems.[2,10,11] Liquid oxygen (LOX) is used by the steel industry in blast furnace operations to increase production and improve plant efficiency. It is produced in LOX plants adjacent to the mills some having a capacity in excess of 500 tons per day.[18]

Liquid hydrogen (LH_2) and liquid oxygen are used in large quantities by the NASA, the AEC and the U.S. Air Force in doubtless the most widely publicized use of cryogens. Owing to its high specific impulse

of approximately 1000 lb_f/lb_m-sec, liquid hydrogen is chosen as the coolant/propellant for a solid core nuclear rocket.[12,13] The ROVER program at Los Alamos is set up to operate at a flow rate of liquid hydrogen of 100 lb_m/sec at 1200 psi for 500 sec. Cryogenic rockets and weapon systems employ both liquid hydrogen and kerosene as fuels and LOX as the oxidizer. Although the specific impulse of these combinations is not as high as pure LH_2 in the nuclear rocket their choice provides the distinct advantages of easy handling, storability and transportation without deterioration. The early rocket of Prof. Goddard in 1926 used LOX as did the German V-2. Liquid hydrogen is now used in bubble chambers[15] and for industrial hydrogenation processing. The production of liquid hydrogen is growing in the U. S. with one plant producing about 65 tons per day with an expected U. S. consumption by 1966 to be 4000 tons per month.[16] The Linde Co. has designed and operated a 28,000 gal railroad tank car for the transcontinental shipment of LH_2 safely and with negligible loss.[17] Liquid hydrogen also is commonly transported conveniently and safely interstate in large tank trucks.

Some of the typical cryogenic fluids in common industrial use are listed in the following table as given by Zenner.[18] A few cryogenic gases, such as CO and Neon, are omitted since they are presently of minor industrial importance as cryogenic gases. Scott[19] lists approximately 35 fluids as cryogens. The transport properties of several cryogens as related to liquid water of 100F and 1- atmosphere pressure are listed in Table II. The properties of water also are given for comparison.

TABLE I

THERMODYNAMIC PROPERTIES OF COMMON CRYOGENS

(p = 1 atm)

Cryogenic Substance	Boiling Point °F	Liquid Density Lb_m/Ft^3	Heat of Vaporization		Ft^3 of Gas at STP per Ft^3 of Liquid
			BTU/Lb_m	BTU/Ft^3 Liquid	
Oxygen	-297	71.3	91.6	6531	862
Nitrogen	-320	50.4	85.6	4319	696
Argon	-303	87.5	70.0	6126	846
Methane	-259	26.5	219.0	5808	637
Flourine	-307	94.3	74.0	6975	959
Hydrogen	-423	4.4	193.0	849	844
Helium	-452	7.8	8.8	69	754

TABLE II

TRANSPORT PROPERTIES OF CRYOGENIC LIQUIDS AT 1 ATMOSPHERE
(Relative to liquid water at 100F, except Prandtl number)

Cryogenic Liquid	T °R	$\frac{k}{k_w}$	$\frac{\rho}{\rho_w}$	$\frac{c_p}{c_{p_w}}$	$\frac{\mu}{\mu_w}$	$\frac{\nu}{\nu_w}$	$\frac{a}{a_w}$	$\frac{\sigma}{\sigma_w}$	Pr	$\left(\frac{B}{B_w}\right)^*$
N_2	139	0.221	0.815	0.488	0.220	0.263	0.556	$150(10^{-3})$	2.20	0.425
O_2	162	0.239	1.150	0.406	0.287	0.240	0.510	$225(10^{-3})$	2.21	0.430
H_2	36.7	0.186	0.071	2.30	0.021	0.285	1.145	$32.7(10^{-3})$	1.17	0.667
He-I	7.6	0.040	0.126	1.15	0.0047	0.036	0.277	$1.58(10^{-3})$	0.613	0.0118
He-II	3.6	$2(10^5)$	0.148	1.15	0.00117	0.0076	$1.17(10^6)$	----------	$3.05(10^{-8})$	------

PROPERTIES OF LIQUID WATER AT 1 ATMOSPHERE AND 100F

	T °R	k_w BTU/HR-R-FT	ρ_w $Lm_m/Ft3$	cp_w BTU/Lb_m-R	μ_w Lb_m/HR-FT	ν_w Ft^2/HR	a_w Ft^2/HR	σ_w Dynes/cm	Pr (1)	B* cm
H_2O	560	0.364	62	1.0	1.65	$27.6(10^{-3})$	$5.88(10^{-3})$	58.8	4.52	0.250

*B is related to the "most unstable wave length", λ_d by $\lambda_d = 2\pi\sqrt{3}\,B$, where $B = \left[\frac{g_o\sigma}{g(\rho_\ell - \rho_V)}\right]^{1/2}$, (20)

The use of cryogenic substances has introduced several unique problems in heat transfer. The handling and transport of these fluids at very low temperatures in the presence of an atmospheric ambient has necessitated the development of specialized insulating methods and design techniques. Because of these large temperature differences new insulation systems consisting of multiple layer aluminum foil separated by a low conducting glass fiber matrix in a vacuum have been developed. These insulations, sometimes called super insulation or multiple layer vacuum insulation, are very effective in reducing the rate of heat leakage into cryogenic systems. One type, which has as many as 150 layers of aluminum foil per inch, has a mean thermal conductivity at 0.05 microns of mercury of 1/700 of that of air.[24] Thermal conduction effects in the supporting structure of cryogenic containers require special attention in their design for minimum heat loss. Another consequence of the large temperature differences in the high probability for the existence of boiling and two-phase flow in storage containers and transfer lines. This has required considerable research on these topics for cryogenic fluids. The condensation of water vapor, carbon dioxide and other gases on cryogenic cooled surfaces is another problem of importance in cryogenic systems. At low temperatures the physical properties of many substances are significantly temperature dependent. This has introduced the need to consider the question of variable properties in the analysis and calculation of heat transfer processes at cryogenic temperatures. Important cases in point are thermal conduction at low temperatures and convective phenomena in the region of the critical point, a circumstance fairly commonly encountered with cryogens. An example of this is the variation of the specific heat of hydrogen with both temperature and pressure, as shown in Figure 1.

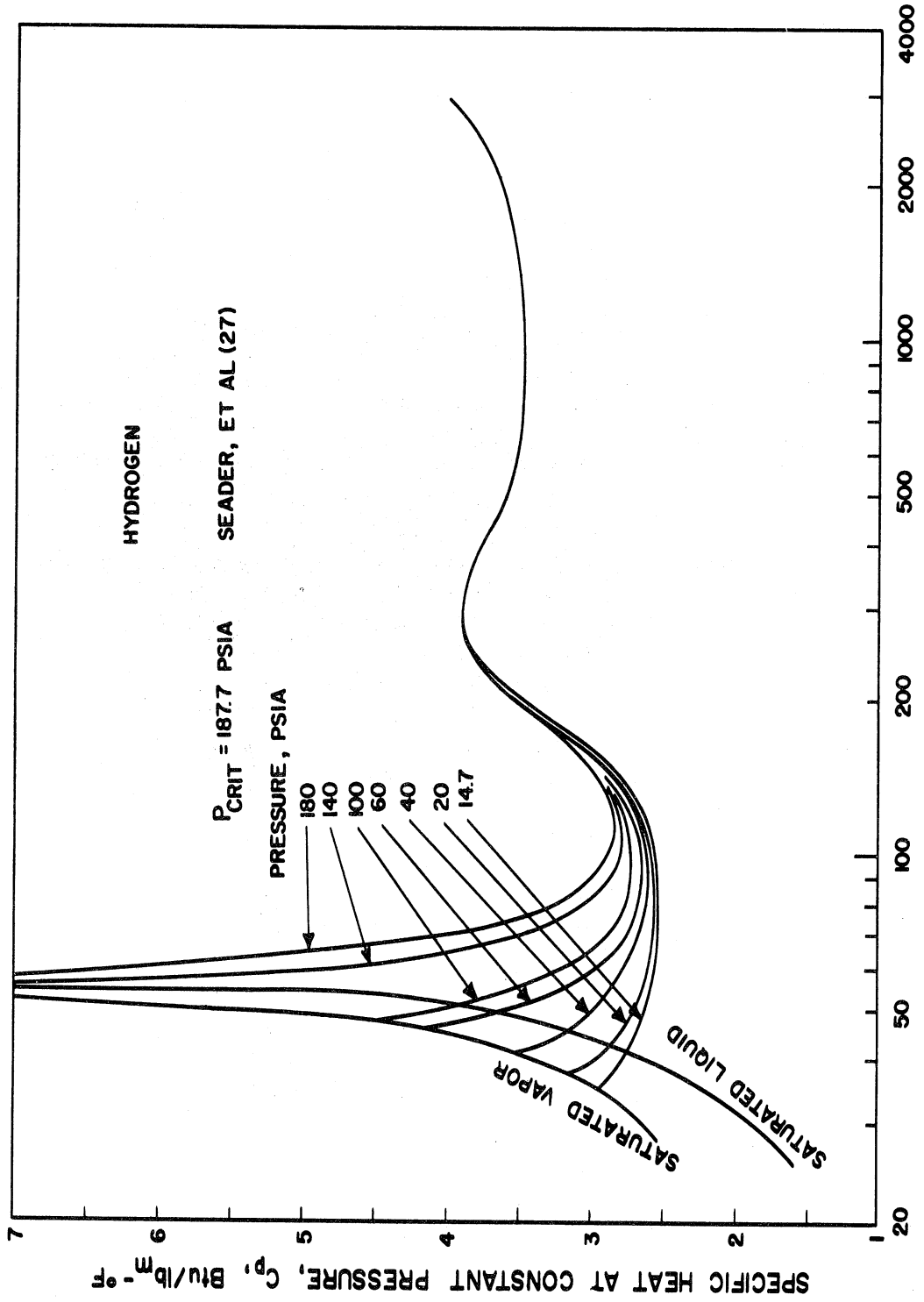

Figure 1. Specific Heat at Constant Pressure of Para-Hydrogen.

A significant characteristic of most cryogens is that they behave as "classical" fluids. That is, their physical behavior follows the well established principles of mechanics and thermodynamics and they obey the laws of similarity. This means that the principles of similitude may be applied and that the scaling laws are valid. Thus, the fundamental concepts of fluid behavior based on the classical laws of physics may be expected and the formulation of the governing elevations for analysis may be carried out in the same manner as is so familiar in the case of non-cryogenic fluids. Accordingly, convective heat transfer correlations can be formulated in terms of such well-known dimensionless quantities as Nusselt number, Reynolds number, Prandtl number, Grashof number and length-to equivalent diameter ratio, among others.

An important exception to the "classical" behavior which has become known at very low temperatures is the behavior of liquid helium (He-II) at temperatures below 2.19K and certain other "electron gases" in solids.[22] Under these circumstances the substances exhibit what is known as "superfluid" behavior, which among other characteristics includes an enormous increase in the heat conducting ability. This is a relatively unexplored field at present from the standpoint of transport phenomena although a few of the available results, principally regarding helium, will be cited later. At the present time the engineering applications of superfluids is limited but they promise to increase. Examples of "superfluid" properties of helium, silver and copper are shown in Figures 2 and 3 for the thermal conductivity and specific heat. The shape of the specific heat curve in Figure 3 resembles the Greek letter lambda which has given rise to the identification of this transition from normal to superfluid characteristic in helium as the "λ-point".

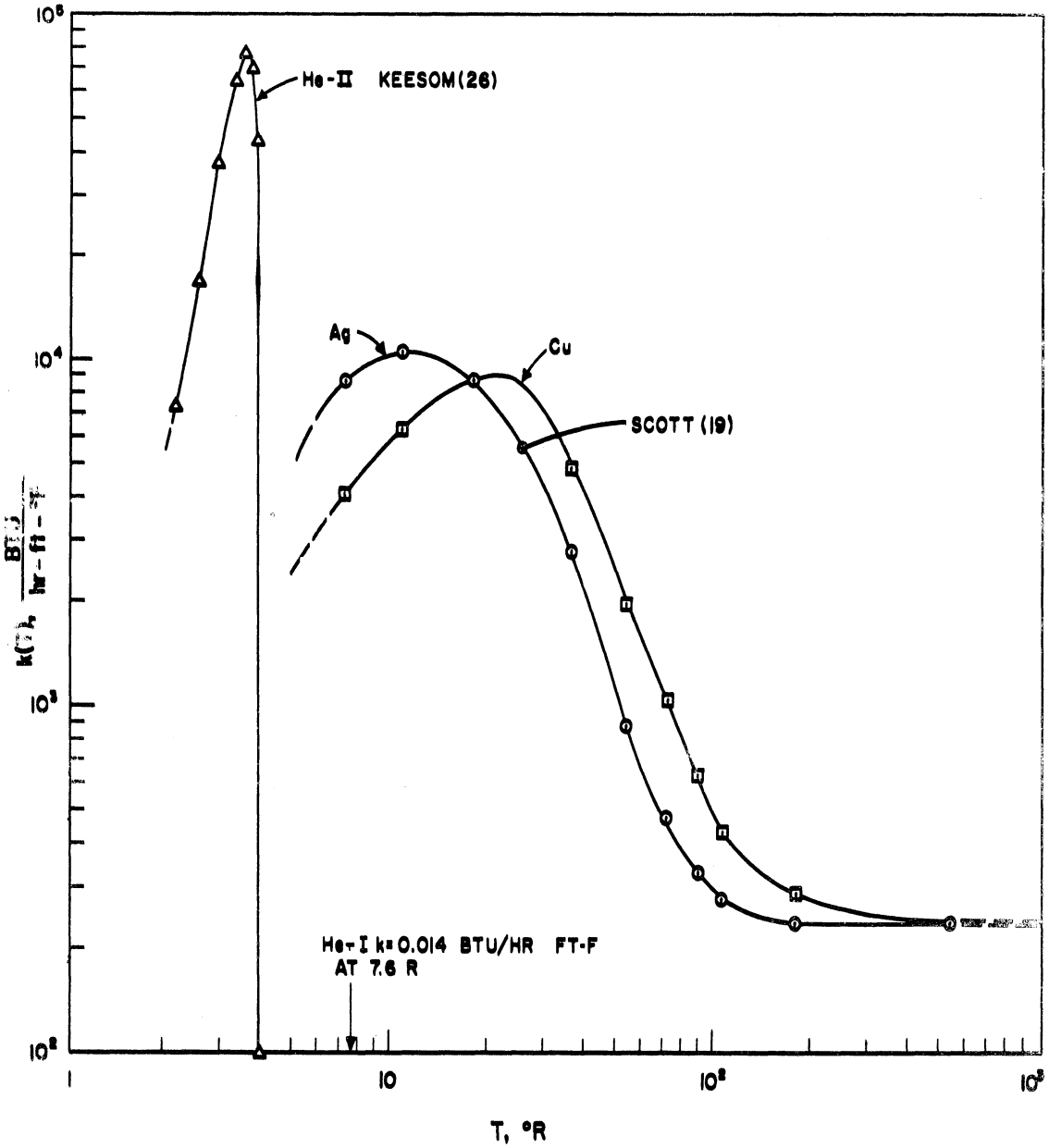

Figure 2. Superconductivity at Cryogenic (Below -150°C) Temperatures.

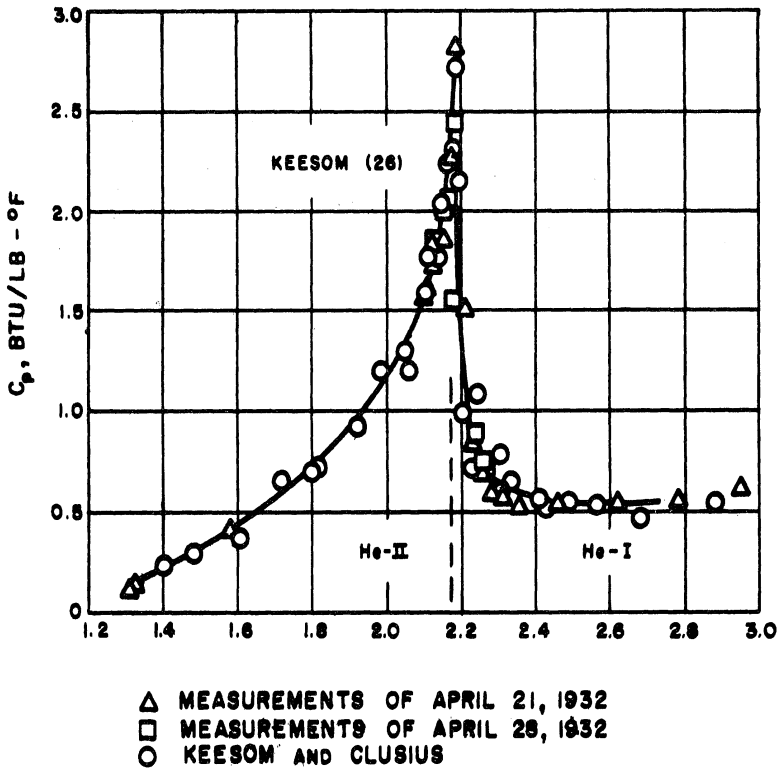

Figure 3. Specific Heat for Helium I and II.

Several of the important and useful sources of reference for information on the subject of cryogenics, including discussions on heat transfer, will now be given. Each year the proceedings of the Cryogenic Engineering Conference held in the United States is published under the title Advances in Cryogenic Engineering, (Plenum Press). This publication is now (1967) in its twelfth volume and contains reviewed papers on all aspects of cryogenic engineering. The journal Cryogenics, published in England by Heywood and Co., Ltd., London since 1960, devotes its pages to papers on low temperature engineering and research. Probably the original book to broadly treat this subject is Cryogenic Engineering by R. B. Scott (1959), Reference (19). This has been followed by Technology and Uses of Liquid Hydrogen, edited by R. B. Scott, W. H., W. H. Denton and C. M. Nicholls (1964), Reference (16). Two additional volumes on low temperature technology are Applied Cryogenic Engineering, edited by R. W. Vance and W. M. Duke (1962), Reference (13) and Cryogenic Technology edited by R. W. Vance (1964), Reference (14). The specialized topic of superfluid behavior is discussed in Superfluid Physics by C. T. Lane (1962) Reference (22), as previously mentioned. The subject of materials behavior is presented by the ASTM in Behavior of Materials at Cryogenic Temperatures (1966), Reference (23), Symposium on Evaluation of Metallic Materials in Design For Low-Temperature Service, (1962), Reference (24) and Report on Physical Properties of Metals and Alloys From Cryogenic to Elevated Temperatures (1961), Reference (25). A valuable source for information on physical properties at cryogenic temperatures is the Cryogenic Data Center, Institute for Materials Research, Cryogenics Divisions (formerly the Cryogenics Engineering Laboratory) of the National Bureau of Standards in Boulder, Colorado. This Institute also publishes reports and papers on cryogenic

science and technology as well as frequent bulletins listing their available publications. The publications of the various commissions in the Proceedings of the International Congress of Regrigeration contains frequent papers on cryogenics.

Other U. S. sources having occasional papers and reports on cryogenic heat transfer and related subjects are the Transactions of the American Society of Mechanical Engineers (ASME), especially its Journal of Heat Transfer (series C) and Journal of Basic Engineering (series D), the Journal of the American Institute of Chemical Engineers (AIChE) and the Journal of the American Institute of Aeronautics and Astronautics (AIAA). Reports and technical notes treating cryogenic processes also are issued periodically by the National Aeronautics and Space Administration (NASA).

This chapter will summarize some of the available information relating specifically to heat transfer phenomena at low temperatures. The technical presentation will include conduction, insulation and interfacial processes, forced and natural convection processes, pressurized-discharge processes, stratification phenomena in vessels, multi-phase processes including two-phase flow and frost formation, among others, radiation and transport phenomena in the superfluid helium II. Although most of the material to be presented may be applied to non-cryogenic behavior, the emphasis will be on applications valid for the cryogens. Where possible or available cryogenic data will be cited and the uniqueness of low temperature application high-lighted. Surveys of heat transfer results appropriate to low temperature may be found in References (13, 14, 16, and 19). The author has published an extensive discussion of the general subject in Reference (14). The present contribution will differ from that presentation in the sense of a specific emphasis on cryogenic heat transfer and the inclusion of the more recently available material.

II. CONDUCTION HEAT TRANSFER

Probably the principal new problems associated with conduction heat transfer at cryogenic temperatures are those of variable thermal properties and low temperature insulation, as indicated in the Introduction. In addition, the principles of conduction heat transfer and diffusion phenomena have been recently applied to some important applications in cryogenics, namely, interfacial processes in single and multicomponent systems. These will be discussed later in this section.

A. Conduction in Solids*

The differential equation governing the steady and unsteady conduction of heat in isotropic substances having variable thermal properties and including the influence of internal heat generation is

$$\frac{\partial T}{\partial t} = \frac{1}{\rho C_p}\left[\frac{\partial}{\partial x}\left(k\,\frac{\partial T}{\partial x}\right) + \frac{\partial}{\partial y}\left(k\,\frac{\partial T}{\partial y}\right) + \frac{\partial}{\partial z}\left(k\,\frac{\partial T}{\partial z}\right)\right] + \frac{P_S''(x,y,z,t)}{\rho C_p} \qquad (1)$$

This equation is written in cartesian coordinates for convenience only. The properties k, ρ, C_p are usually temperature dependent for a given substance. Typical low temperature variations in k and C_v (for solids C_v and C_p are essentially the same) are shown in Figures 4 and 5. Equation (1) is non-linear owing to the temperature dependency in k, ρ and c_p and accordingly is very difficult to solve. A simple transformation (28), however, can be used to aid in the solution. A new vari-

---

* The emphasis in this section will be on the influence of temperature dependent physical properties. Heat conduction analysis and calculation for uniform properties is well documented in References (29, 30, 31 and 32).

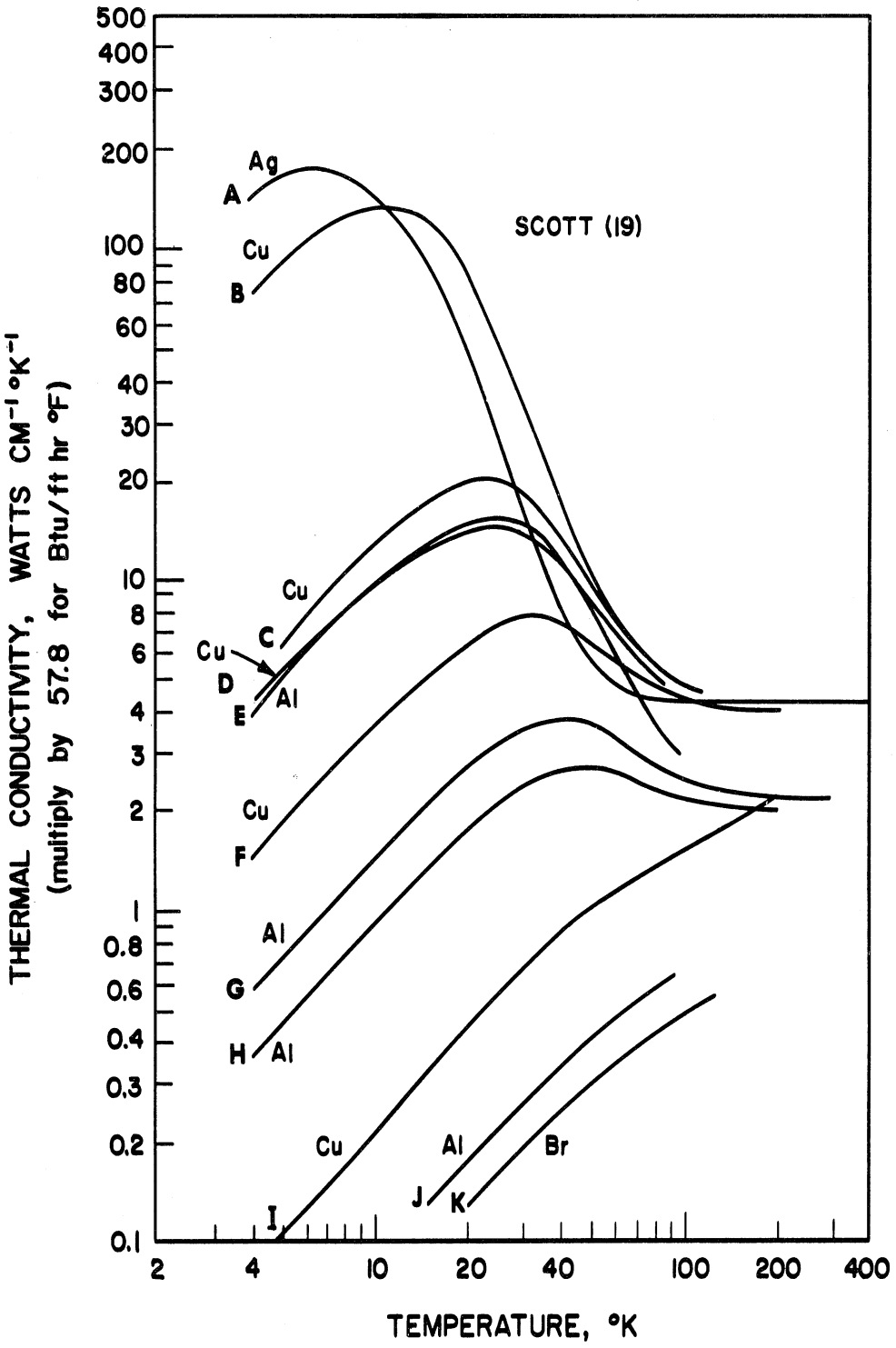

Figure 4. Low Temperature Thermal Conductivity of Metals. A, silver 99.999% pure; B, high purity copper; C, coalesced copper; D, copper, electrolytic tough pitch; E, aluminum single crystal; F, free-machining tellurium copper; G, aluminum, 1100F; H, aluminum, 6063-T5; I, copper, phosphorus deoxidized; J, aluminum, 2024-T4; K, free-machining leaded brass.

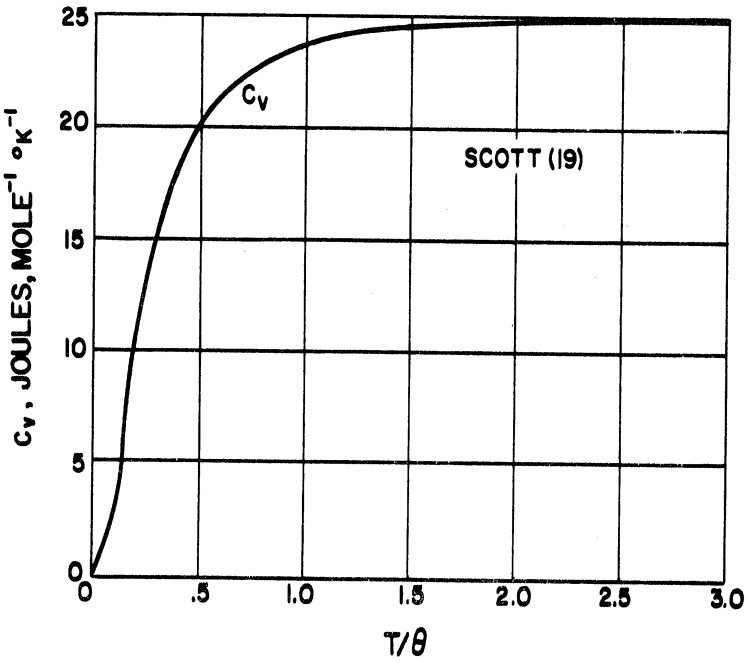

To convert these units to (BTU per lb-mole-deg R) divide the numberical values given in the figure by 4.184. Thus, the asymptotic value of 25 becomes its classical value of 3R, cal/gr-mole, which has exactly the same numerical as units in BTU/lb-mole-°R.

Substance	θ(°K)	Substance	θ(°K)
Li	430	Hg	95
Na	160	Ga	125
K	100	In	100
Be	980	Tl	96
Mg	320	Ti	350
Ca	230	Zr	280
Sr	170	Hf	213
Al	390	Ta	245
Diamond	1850	Cr	440
Graphite	1500	Mo	375
Si	625	W	315
Ge	290	Mn	350
Sn (white)	165	α-Fe	430
Sn (gray)	240	γ-Fe	320
Pb	86	Co	385
Sb	140	Ni	375
Bi	110	Ru	400
Ne	63	Rh	370
A	85	Pd	275
Cu	310	Pt	225
Ag	220	LiF	650
Au	180	NaCl	275
Zn	240	MgO	800
Hf	213		

Figure 5. Temperature Dependence of Specific Heat, C_v .

able E is defined as

$$E = \int_{T_R}^{T} k(T)dT \ , \tag{2}$$

where T_R is an arbitrary reference temperature. Hence, we may formulate the space and time derivatives of T in Equation (1) as

$$\frac{\partial T}{\partial t} = \frac{1}{k(T)} \left(\frac{\partial E}{\partial t} \right) \tag{3}$$

and

$$\frac{\partial}{\partial x} \left(k \frac{\partial T}{\partial x} \right) = \frac{\partial^2 E}{\partial x^2} \ , \text{ etc.} \tag{4}$$

With these transformations solutions to heat conduction problems are sought in terms of the function E. Since E is a unique function of T by Equation (2) the temperature distribution $T(x,y,z,t)$ is determined from the function $E(x,y,z,t)$. Thus, Equation (1) becomes

$$\frac{\partial E}{\partial t} = a(T) \left[\frac{\partial^2 E}{\partial x^2} + \frac{\partial^2 E}{\partial y^2} + \frac{\partial^2 E}{\partial z^2} \right] + a(T) \ p_s''(x,y,z,t), \tag{5}$$

where $a(T)$ is the variable thermal diffusivity, defined as $k(T)/\rho(T)C_p(T)$, and is a function of temperature. Equation (5) is still non-linear since both $a(T)$ and E are functions of temperature. However, it has been put into a more useful form than Equation (1). In case $a(T)$ is a severe function of temperature it will be necessary to employ numerical methods to the integration of Equation (5), something which will be discussed later. For numerical formulations Equation (5) is a more convenient and useful representation than Equation (1).

There are certain practical circumstances in which $a(T)$ is much less variable with temperature than is $k(T)$. This is a consequence of similar temperature variations of $k(T)$ and $c_p(T)$ in some regions

such that their ratio remains essentially independent of temperature. For these conditions $a(T)$ may be approximated by a constant value, designated as a^*. Equation (5), for no internal heat generation, then becomes,

$$\frac{\partial E}{\partial t} = a^* \left[\frac{\partial^2 E}{\partial x^2} + \frac{\partial^2 E}{\partial y^2} + \frac{\partial^2 E}{\partial z^2} \right] \tag{6}$$

This result will be recognized as the classical linear diffusion equation for which a vast number of analytical solutions have been generated for various boundary conditions (29, 30). For a one-dimensional case equation (6) is written

$$\frac{\partial E}{\partial t} = a^* \left(\frac{\partial^2 E}{\partial x^2} \right) \tag{7}$$

Further, for a convective heat transfer at $x = 0$ and $x = 2L$, Figure 6, with an ambient fluid at T_∞, the typical convective boundary condition is (28),

$$\frac{\partial E(0,t)}{\partial x} = \frac{h}{k_\infty} [E(0,t) - E_\infty] \tag{8}$$

where, $k_\infty(T_\infty - T_R) = E_\infty$. The initial condition would be written $E(x,0) = E_i$. Hence, we may write Equation (7) and its boundary condition Equation (8) in the following form,

$$\frac{\partial E^*(x^*, F_o)}{\partial F_o} = \frac{\partial^2 E^*(x^*, F_o)}{\partial x^{*2}} \tag{9}$$

and

$$\frac{\partial E^*(0, F_o)}{\partial x^*} = B_i [E^*(0, F_o)] \tag{10}$$

where

$$E^* = \frac{E(x,t)-E_\infty}{E_i-E_\infty} \quad , \quad B_i = \frac{hL}{k_\infty}$$
$$F_o = \frac{a^* t}{L^2} \quad , \quad x^* = \frac{x}{L} \quad . \tag{11}$$

in which L is a characteristic length.

A comparison of Equations (9) and (10) for variable properties with the corresponding differential equation and boundary conditions for uniform properties shows them to be identical. Hence, for the same geometrical shape and initial condition their solutions also will be identical. This means that the various heat conduction charts formulated on the basis of uniform properties, such as the extensive tabulation of Schneider,[31] can be employed for the solution of a variable property problem in terms of the function E. Multidimensional problems also may be solved by the product method for those geometric shapes for which analytical solutions are available.

The analytical solution to Equations (9) and (10) for a slab is given in Figure 6 in chart form as $(1-E^*)$ for variable properties of k, ρ, and c_p for the case of constant thermal diffusivity a^*.

Analytical solutions for steady-state heat conduction problems having variable properties may be obtained from solutions to Equation (5) with $(\partial E/\partial t)$ set equal to zero. Thus, the governing equation is,

$$\frac{\partial^2 E}{\partial x^2} + \frac{\partial^2 E}{\partial y^2} + \frac{\partial^2 E}{\partial z^2} + p_S''(x,y,z) = 0 \quad . \tag{12}$$

For a convective heat transfer to a wetting fluid at T_∞ the boundary condition would be of the type given in Equation (8). In the absence

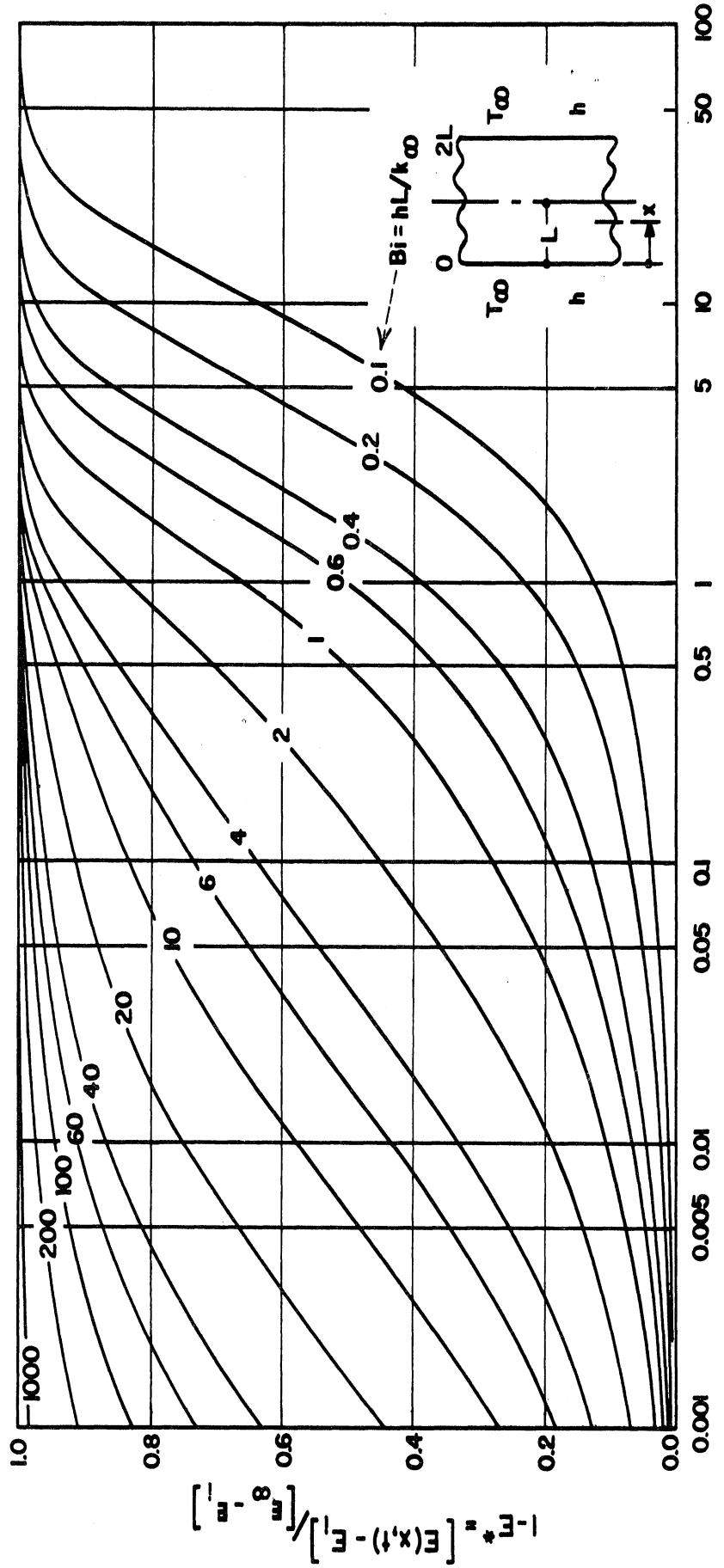

Figure 6. Temperature Response of a Slab, $0 \leq x \leq \delta$ after sudden exposure to a uniform-temperature convective ambient T_∞ at $x = 0$. From Schneider.(31)

of internal heat generation, we have then

$$\frac{\partial^2 E}{\partial x^2} + \frac{\partial^2 E}{\partial y^2} + \frac{\partial^2 E}{\partial z^2} = 0 \,. \qquad (13)$$

This is the classical La Place equation well-known in field theory and in the study of diffusion phenomena. As may be noted the variable property problem in this case involves only variations in $k(T)$ and not in the thermal diffusivity $a(T)$.

Analytical solutions to Equations (12) or (13) are rather broadly available in the standard literature[28,29,32] for a wide variety of problems. Such solutions also may be found by analogical techniques such as the analog field plotter. For these reasons they will not be reproduced here. The main difference in the present formulations from those currently available rests in the treatment of the function E , Equation (2), to determine the temperature distribution rather in the temperature itself. This is the principal distinction of the variable property problem.

For those cases of unsteady heat conduction in which the property variation is very great and the constant thermal diffusivity approximation of Equation (6) cannot be made satisfactorily it will be necessary to solve Equation (5) by numerical methods using a digital computer. In this discussion we shall study the case without internal heat generation, $p''_s(x,y,z,t) = 0$ as this function even with spatial and time variations is a simple additive term in the numerical formulation which does not complicate the calculation in any special way. The most convenient from for a numerical calculation is to arrange the equations in an explicit formulation. This enables a marching-type solution

and avoids the time-consuming iterative computer procedures of the implicit-type formulations. The development to be given here will be for the two-dimensional region shown in Figure 7 which has a convective heat transfer at the wetted boundary. For the interior point $\underline{0}$, using a square grid, the value of the function E_0 at the (n+1) time interval may be computed in terms of the functions at the adjacent lattice points at the (nth) time interval[28] as,

$$E_0^{n+1} = \frac{E_1^n + E_2^n + E_3^n + E_4^n + (M_0 - 4)E_0^n}{M_0} \tag{14}$$

where

$$M_0 = \frac{(\Delta x)^2}{a(T_0)\Delta t} \tag{15}$$

For variable properties $a(T_0)$ will vary with time and space and it will be necessary to up-date the calculation of M_0 at the start of each new sequence of calculations. This may require adjustment in the time interval Δt. The numerical value of M_0 is related to the stability of the calculation and will be discussed below.

For the surface point $\underline{S}$ the value of the function E_S at the (n+1) time interval is given[28] as

$$E^{n+1} = \frac{2E_8^n + E_6^n + E_7^n + 2N_S E_\infty^n + [M_S - (2N_S+4)]E_S^n}{M_S} \tag{16}$$

where

$$M_S = \frac{(\Delta x)^2}{a(T_S)\Delta t} \tag{17}$$

$$N_S = \frac{h\Delta x}{k^*} \tag{18}$$

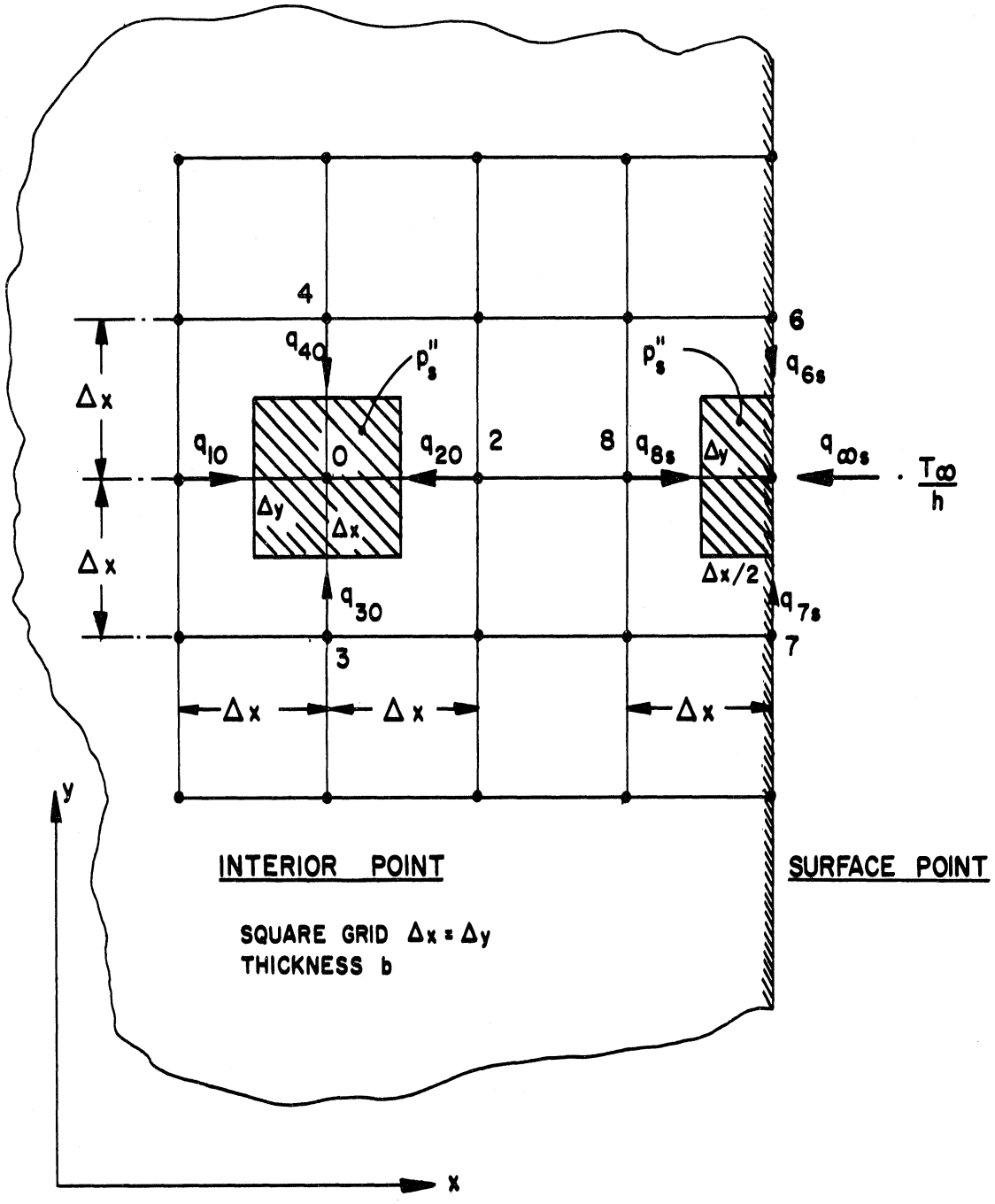

Figure 7. Finite-Difference Network for Typical a Interior and Surface Point Using a Square Grid $\Delta x = \Delta y$.

$$k^* = \frac{1}{T_\infty - T_s^n} \int_{T_s^n}^{T_\infty} k(T)dT \qquad (19)$$

and,

$$E_\infty^n = \int_{T_R}^{T_\infty} k(T)dT \ . \qquad (20)$$

The stability of the numerical calculation requires that,

$$M_s \geq 2N_s + 4, \qquad (21)$$

$$M_o \geq M_s \ , \qquad (22)$$

for constant grid size. Because $a(T_s)$ and to a lesser extent k^* will vary during the calculation owing to changes in T_s , the value of M_s must be up-dated at each step to check the compliance with the stability criterion, Equation (21). Should changes in M_s become necessary it is probably best done by altering the size of the time interval, Δt , rather than the grid size, Δx .

Equations (14) and (16) will be recognized as "marching" type explicit formulations. Because of the restrictions on the time interval, Δt , this kind of formulation can require considerable computer time to complete a calculation. Its advantage, however, rests with its "explicit" form. Another type of "explicit" formulation suitable for this kind of a problem and which is unconditionally stable without restriction on the size of Δt is given in Reference (33). Owing to space limitations it will not be outlined here. The calculation is complete when the computed values of E are related to their corresponding values of T , using Equation (2).

Steady heat conduction problems also usually require the use of numerical methods when the geometry of a region or the boundary conditions are not simple. The general formulation of the equations for the steady

case corresponding to the system in Figure 7 are given as follows[28] for the interior and surface points,

$$E_1 + E_2 + E_3 + E_4 - 4E_o = R_o \ , \qquad (23)$$

and,

$$2E_8 + E_6 + E_7 + 2N_s E_\infty - [N_s+2]E_s = R_s. \qquad (24)$$

The solution of Equations (23) and (24) is usually accomplished by the "relaxation" method[29] or by iterative procedures on a digital computer. The desired value of R_o and R_s, the residuals, is zero but as a practical matter they are reduced to as small a value (positive or negative) as required by the demands of accuracy of the problem. The quantities N_s, E_∞ and E_s are defined above.

B. Low Temperature Insulation

Since the end of World War II many new applications have been found for low temperature fluids. Probably the most significant of these in terms of quantity of liquid consumed is the use of liquid oxygen and hydrogen in rockets and other such applications in missiles and space exploration. A widening industrial use of these low temperature fluids can be identified, however, such as the use of oxygen in steel manufacture and nitrogen in food preservation. Associated with cryogenic application has been the important problem of insulation of the low temperature fluids from the ambient, both terrestrial and in space. This is actually an old problem as Sir James Dewar devoted considerable effort to the development of low temperature insulations at the turn of the century. The vacuum bottle, or thermos, can be credited to him Many of our modern techniques such as the use

of vacuum and low emissivity multiple-layer surfaces were recognized as important by Dewar.

In this section we shall mention some of the principal features of insulations for cryogenic application. Kropschot[34,35,36] has published a thorough summary of this subject. The topic is discussed by Scott et al[16], Scott[19] and found in the periodical Cryogenics and in the annual report of the Cryogenic Engineering Conference.[37] Owing to the effectiveness and the high performance requirements of these new insulants they are sometimes referred to as "super-insulations".

The types of low temperature insulation may be divided into four categories (i) high vacuum; (ii) multiple-layer; (iii) powder; and (iv) rigid foam. Insulation systems may include combinations of these categories.

High vacuum (less than 1 μ of Hg) insulation is similar to that used in a thermos bottle. The transfer to heat is predominantly by radiation although there may be a significant contribution due to gaseous conduction if the vacuum is not sufficiently high. Insulation is achieved by maintaining as low a pressure as possible in the vacuum space which is enclosed by low emissivity surfaces, usually consisting of highly polished metallic coatings.

Multiple-layer insulation is made of alternate layers of low conductivity fibers and thin, low emissivity metallic foil (usually aluminum) in high vacuum. As many as 150 layers of foil per inch is used giving as apparent thermal conductivity as low as 0.025×10^{-3} BTU/hr-ft-°F which is one of the lowest of any bulk cryogenic insulation developed to date. Figure 8 is a photograph of a typical multiple layer insulation without its vacuum jacket. The low vacuum reduces gas conduction

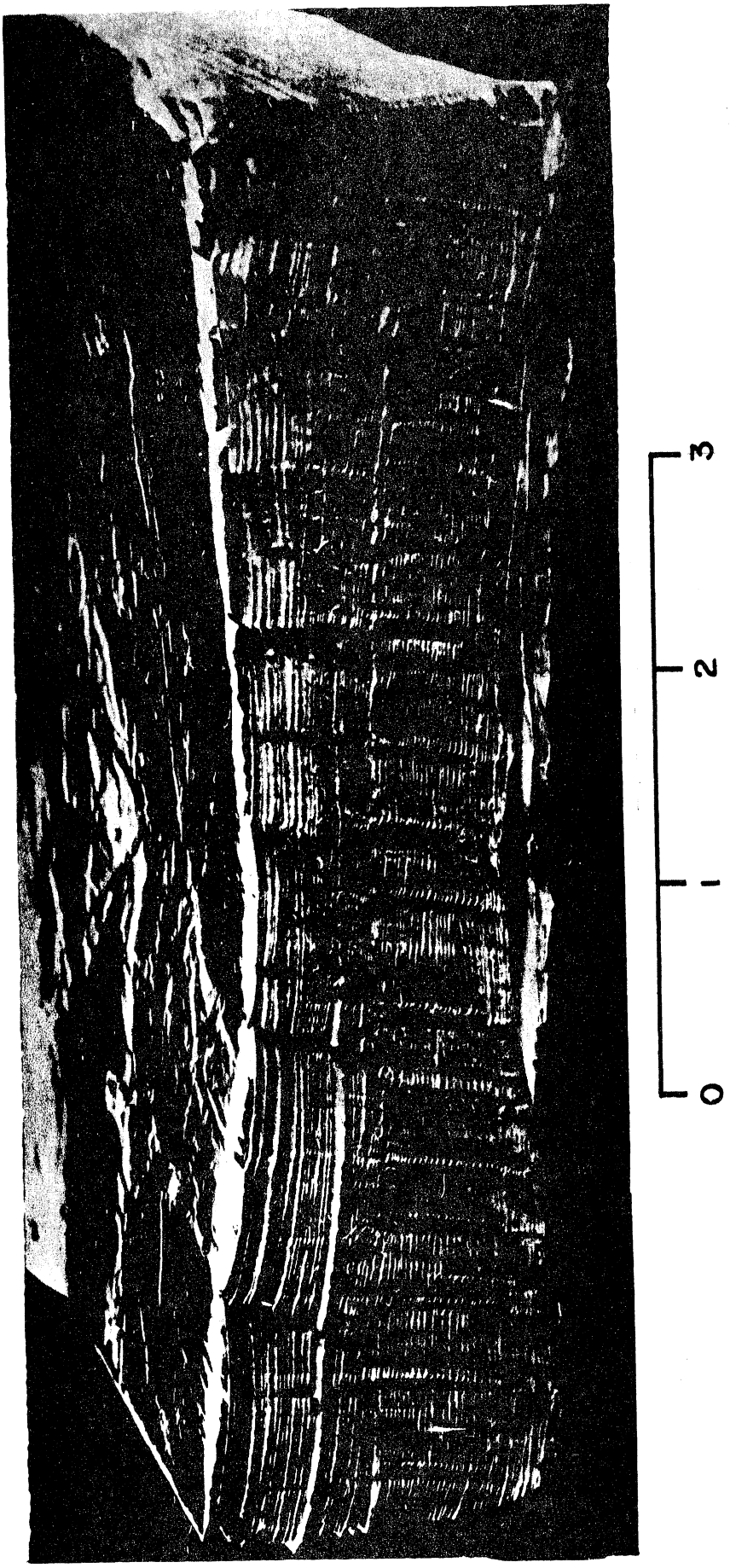

FIGURE 8. MULTI-LAYER VACUUM INSULATION FOR CYROGENIC APPLICATION (COURTESY LINDE COMPANY).

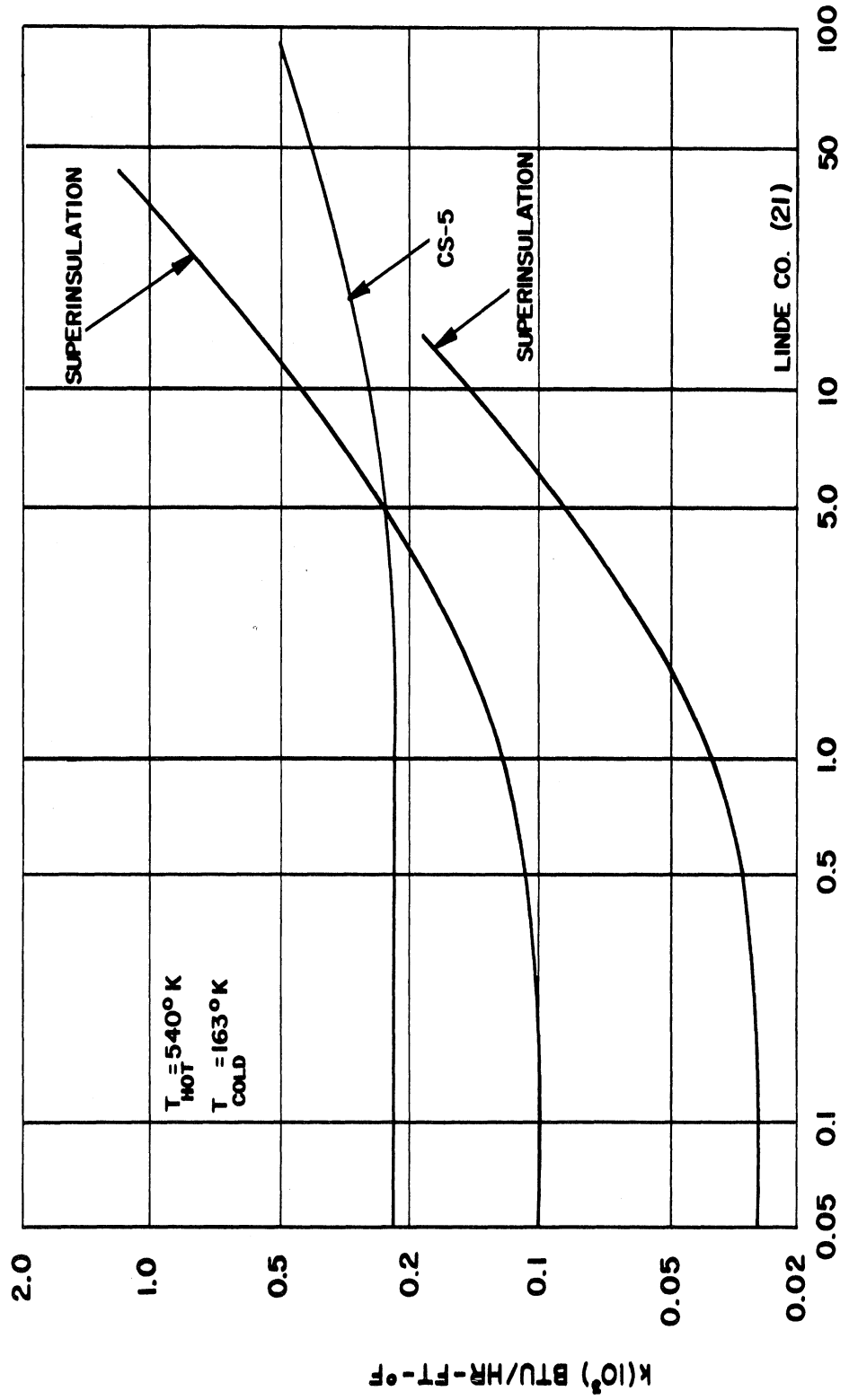

Figure 9. Performance of Multiple-layer Insulations as Functions of Vacuum.

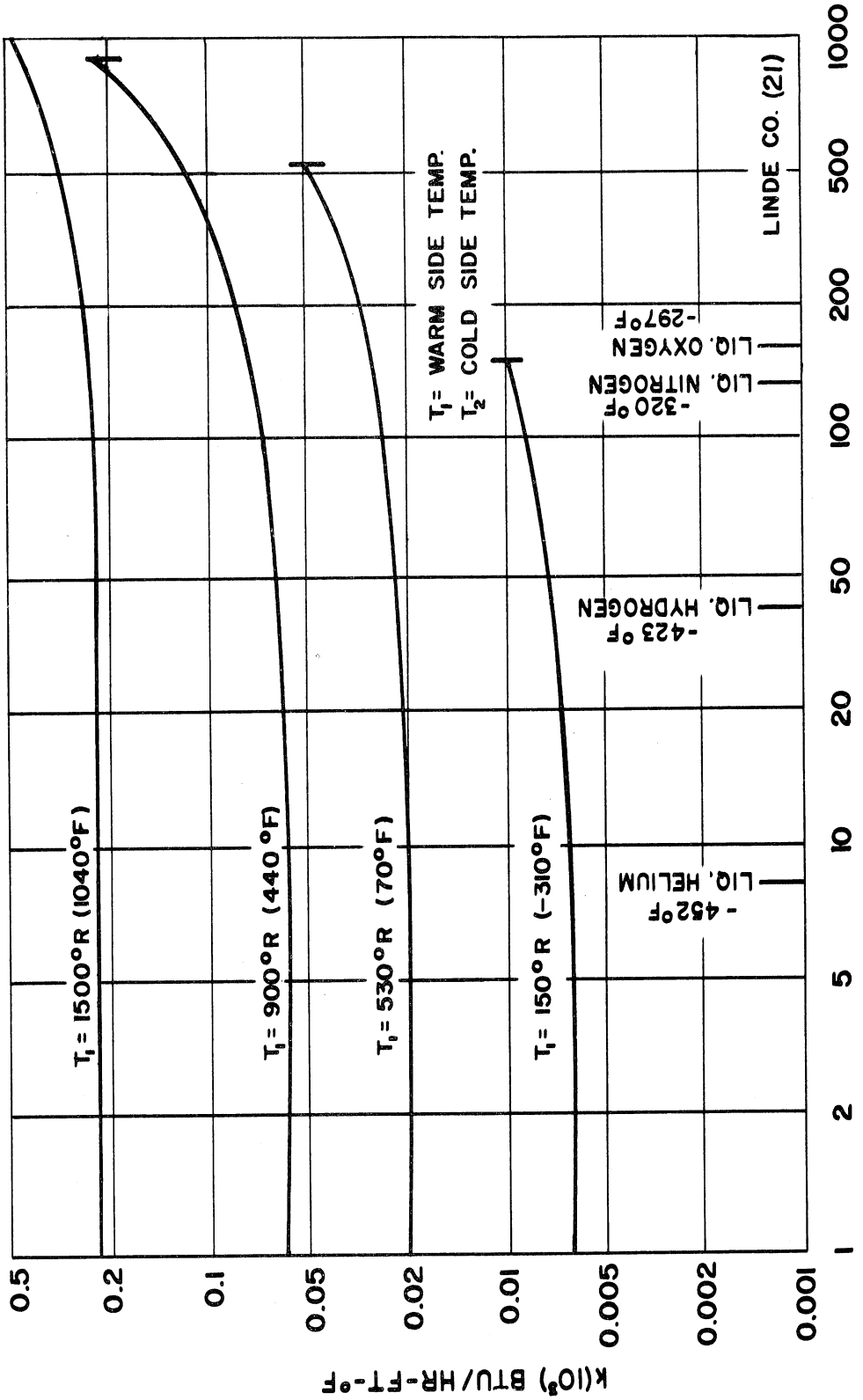

Figure 10. The Apparent Thermal Conductivity of a Multiple-layer Insulation at Various Boundary Temperatures.

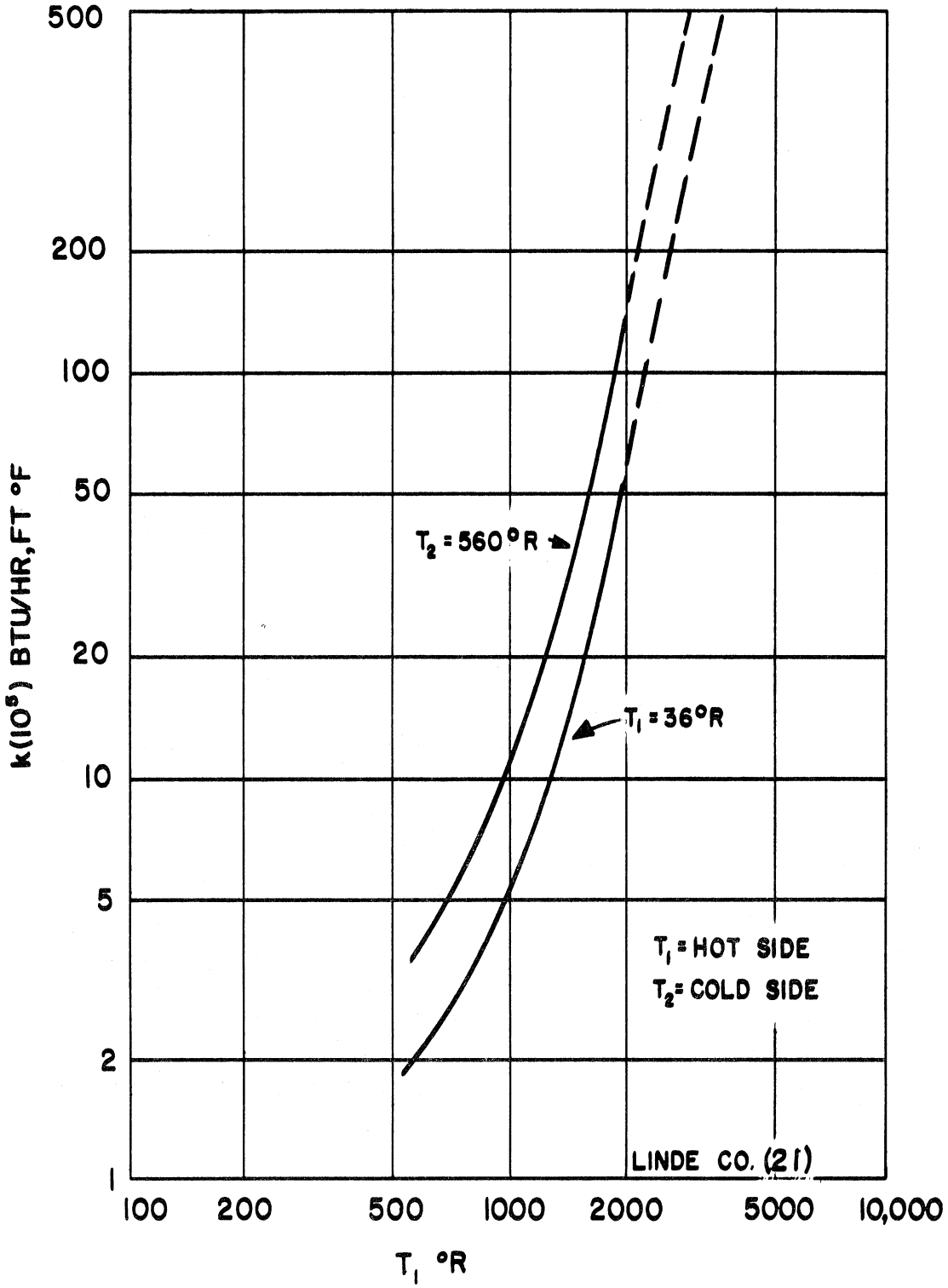

Figure 11. The Apparent Thermal Conductivity of a Multiple-layer Insulation at High Temperature.

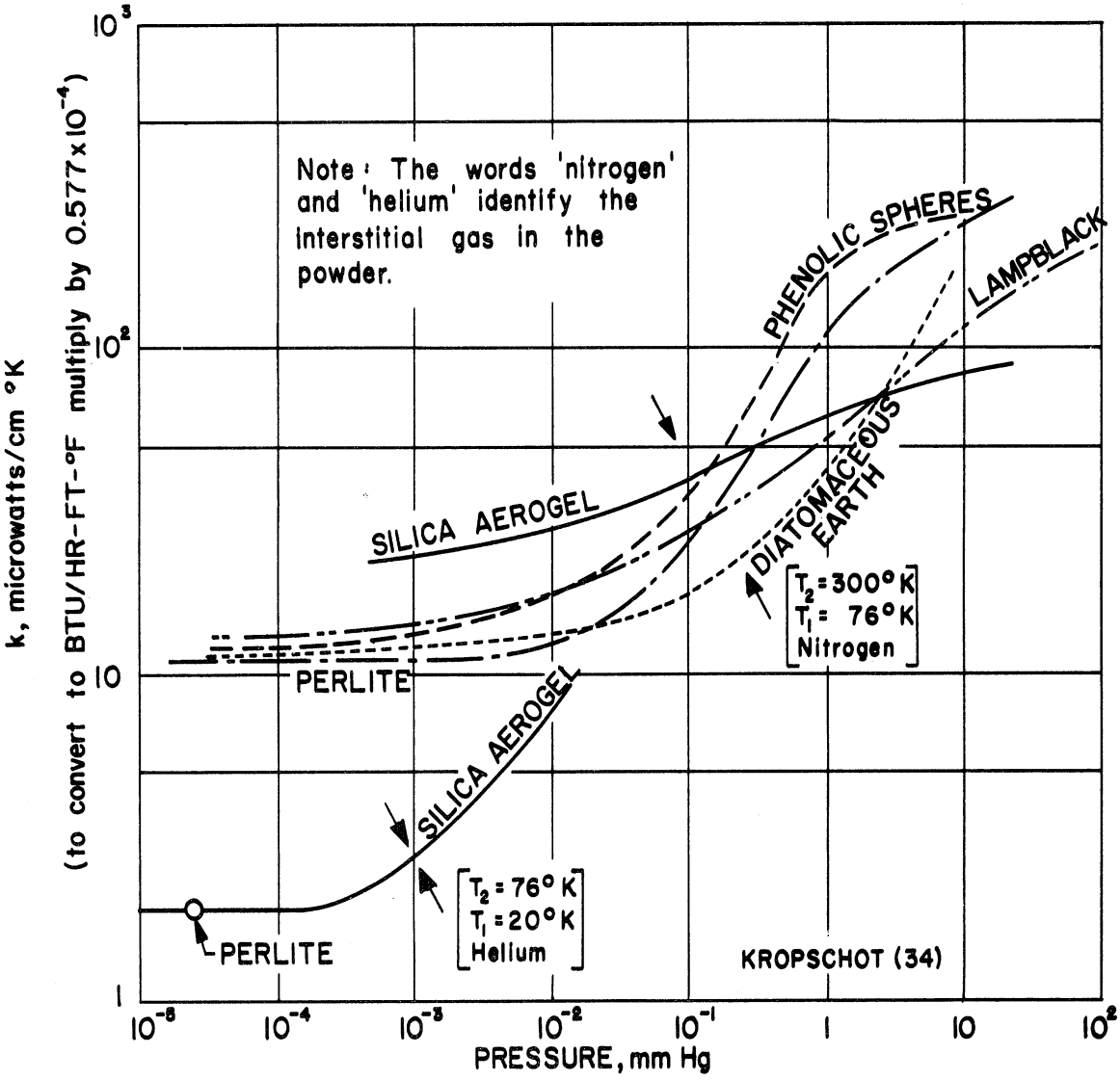

Figure 12. Thermal Conductivities of Evacuated Powders.

to a negligible amount and the multiple-layers of polished foil decreases the radiation contribution. The influence of pressure on the apparent thermal conductivity of a superinsulation reported by the Linde Co.[21] is shown in Figure 9. Values of the apparent thermal conductivity of the insulation for various boundary temperatures is given in Figure 10. The low values of this property are to be noted. The thermal conductivity of multiple-layer insulation is called "apparent" thermal conductivity because the mechanism of transfer is not purely diffusion. At low pressures where gaseous conduction is negligible heat is transferred primarily by radiation. For this reason the apparent thermal conductivity is a function of the boundary temperatures as shown in Figure 10. Multiple-layer insulation also can be used at high temperatures and some data on the performance of this material in this range of temperatures is given in Figure 11.

Multiple-layer vacuum insulations also are discussed by Riede and Wang[39] and Paivanas, et al[40].

The thermal conductivity of several powders commonly employed in vacuum insulation systems is shown in Figure 12 as a function of the pressure of the interstital gas. Below approximately 10^{-3} mm Hg the effect of gas pressure is negligible indicating that the principal mechanism of the transfer is radiation. Additional discussion of perlite as an insulant is given by Kropschot and Burgess.[41]

Rigid foams which have found application in low temperature insulation are those which have a relatively closed cellular structure. Such a structure has the advantage of being inprevious to water vapor, an important characteristic in systems to be used in contact with the

atmosphere. Foams commonly used include polystyrene, epoxy, polyurethane, rubber and glass. Heat conduction through a foam is determined by convection and radiation within the cells and by conduction in the solid structure. Evacuation of a foam is effective in reducing its thermal conductivity although it still will be considerably higher than either multiple-layer or evacuated powder insulations. Data on the thermal conductivity of some selected foams presented by Kropschot[34] is given in Table III. The thermal properties of foams are also discussed by Haskins and Hertz[42] and Miller, et al.[43] Evacuation of most foams reduces the apparent thermal conductivity, indicating a partially open cellular structure. Data on this effect for polystyrene and epoxy forms, among others, are given by Kropschot,[34] as indicated in Table III. The opposite effect, diffusion of ambient gases into the cells of a foam, can cause an increase in its apparent thermal conductivity. This is especially significant in the case of the diffusion of hydrogen or helium.

C. Interfacial Phenomena

Interfacial transfer of heat and mass is intimately associated with both pressurization and stratification phenomena in cryogenic vessels containing coexistent liquid and vapor phases. It is, of course, the conditions at the liquid-vapor interface which couple the simultaneous transport processes in the liquid and gas phases. In a generalized sense knowledge of these interfacial phenomena is very incomplete. Yet, in terms of an idealized model, which is a reasonable representation of many practical circumstances, exact solutions for these transfer processes are known. The basis for most of these is the classical treatise of Carslaw and Jaeger.[30] In this section the subject of interfacial phenomena will parallel that given in Reference 44.

TABLE III

THERMAL CONDUCTIVITY OF SOME SELECTED FOAMS*

Foam	Density Lbm/ft3	Boundary Temperatures	Pressure	Thermal Conductivity BTU/hr-ft-F
Polystyrene	2.4	540-140°R	1 Atm	0.0191
	2.9	540-140°R	1 Atm	0.0150
	2.9	140-36°R	10^{-5}mm Hg	0.0047
Epoxy	5.0	540-140°R	1 Atm	0.0191
	5.0	540-140°R	10^{-2}mm Hg	0.0097
	5.0	540-140°R	$4x10^{-3}$mm Hg	0.0075
Polyurethane	5-8.8	540-140°R	1 Atm	0.0191
		540-140°R	10^{-3}mm Hg	0.0069
Rubber	5	540-140°R	1 Atm	0.0208
Silica	10	540-140°R	1 Atm	0.0318
Glass	8.8	540-140°R	1 Atm	0.0202

*Data Taken from Kropschot(34)

Experience to-date points to three important generalizations (a) the interfacial temperature is essentially that of equilibrium (saturation) conditions corresponding to system pressure,* (b) during pressurized-discharge of a liquid from a vessel both condensation and evaporation of the cryogenic propellants at the interface are possible but usually are not significant factors, and (c) during self-pressurization of liquid containers interfacial evaporation occurs and the system pressure is governed by the vapor-pressure characteristics of the phases at the interfacial temperature.

Schrage[45] presents the basic equations based on the statistical behavior of molecules from the kinetic theory applicable to condensation and vaporization phenomena. Balekjian and Katz[46] give experimental data on the depression of the liquid-vapor interface temperature below saturation temperature during the condensation of superheated vapors of Freon and water. Analytical and experimental investigations of liquid surface configurations for adiabatic processes in containers including the effects of low gravity, surface tension and draining are presented by Saad and Oliver[47] and Satterlee and Reynolds.[48] Knuth[49,54] in a series of two theoretical papers solved the laminar transport equations governing interfacial growth for a single component system. The same problem was studied independently by Thomas and Morse[53] who presented both an exact solution and an approximate solution yielding an explicit expression for the interfacial mass transfer. The phase change of single component liquids and vapors in contact with various sub-strates is reported in Reference (50) and by Yang.[51] Yang, et al.[52,55] have

*This has been the subject of direct measurement in many investigations in single component phases and is thought to be a reasonable assumption in multi-component systems although no known experimental confirmations of this have come to the author's attention. Departures from this are discussed later in this section.

applied the source theory to the solution of interfacial heat and mass transfer in multi-component phases producing approximate but simple formulations for the rates of phase growth and transient temperature and concentration distributions in liquid and vapor. An extension of the analytical work on single component systems to binary systems is given by Yang, et al.[56] where exact solutions to the simultaneous transient, heat and mass transfer between phases for a suddenly pressurized system are presented. Because this work is representative of the current analytical studies on interfacial phenomena it will be used as source material for much of the following discussion.

Mass transfer by condensation or evaporation at a vapor-liquid interface depends on the relative rates of heat transfer from each phase at the interface. Should heat transfer from the vapor dominate that to the liquid, evaporation will occur at the interface; if the opposite is true, the vapor will condense; if the respective heat transfer rates are the same, neither evaporation nor condensation occurs and the interface remains stationary. These circumstances will exist generally. For physical systems having convective action in both phases adjacent to the interface there is little known at present for predicting the interfacial transport of heat and mass. Clark, et al[54] treat the subject for cryogenic containers. The influence of liquid and vapor velocities in both laminar and turbulent motion on this process, the magnitude of molecular and eddy diffusion coefficients controlling simultaneous heat and mass transfer over an extended range of conditions and a model of the general mechanics for this process are largely unknown.

However, significant progress has been made by adopting a simple, but reasonable model for study. One such model is shown in Figure 13 in

which a two-phase binary system initially in thermodynamic equilibrium ($t < 0$) is suddenly subjected to temperature, pressure and concentration transients ($t = 0$) in the vapor phase. The resulting transient, transport process ($t > 0$) is governed by the following equations, assuming the origin of the X-coordinate to be at the initial location of the interface, thus causing the liquid to have a zero velocity,

Vapor:

$$\frac{\partial T''}{\partial t} + u''(t) \frac{\partial T''}{\partial X} = \alpha'' \frac{\partial^2 T''}{\partial X^2} \tag{25}$$

$$\frac{\partial C''}{\partial t} + u''(t) \frac{\partial C''}{\partial X} = D'' \frac{\partial^2 C''}{\partial X^2} \tag{26}$$

Liquid:

$$\frac{\partial T'}{\partial t} = \alpha' \frac{\partial^2 T'}{\partial X^2} \tag{27}$$

$$\frac{\partial C'}{\partial t} = D' \frac{\partial^2 C'}{\partial X^2} \tag{28}$$

with boundary and initial conditions as shown in Figure 13 and outlined in Reference (56). Conditions at the interface are taken to be those of thermodynamic equilibrium for $t > 0$. For uniform initial conditions the displacement of the interface $X(t)$ from $X = 0$ is characterized by

$$X(t) = 2\lambda\sqrt{\alpha' t}\,, \tag{29}$$

where λ is the interfacial growth parameter and is positive for condensation and negative for evaporation. The interfacial and vapor velocities and interfacial mass flux are then,(56)

$$\frac{dX(t)}{dt} = \lambda\sqrt{\frac{\alpha'}{t}} \tag{30}$$

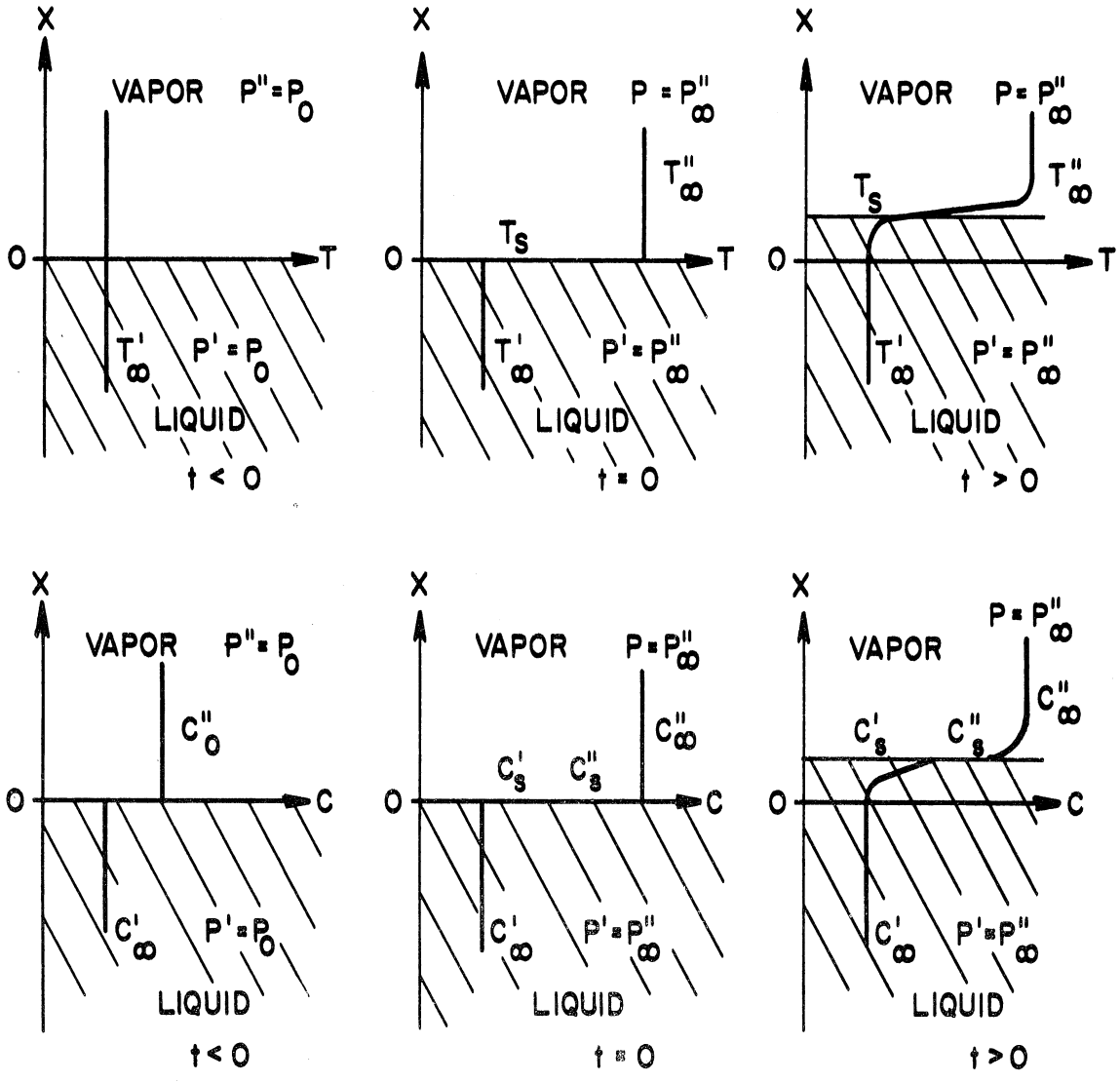

Figure 13. Schematic Illustration of Temperature and Concentration Distributions in the Liquid and Vapor Regions at Several Different Times.

$$u''(t) = -\frac{\rho'-\rho''}{\rho''}\,\lambda\sqrt{\frac{\alpha'}{t}} \tag{31}$$

$$\frac{w}{A} = \rho'\,\frac{dX(t)}{dt} = \rho'\,\lambda\sqrt{\frac{\alpha'}{t}} \tag{32}$$

The general solutions for $T'(t)$ and $T''(t)$ are Reference (56)

$$\frac{T'(x,t) - T_\infty'}{T_\infty'' - T_\infty'} = A'(\lambda)\left[1 + \operatorname{erf}\frac{X}{2\sqrt{\alpha' t}}\right] \tag{33}$$

$$\frac{T_\infty'' - T''(x,t)}{T_\infty'' - T_\infty'} = A''(\lambda)\,\operatorname{erfc}\left[\frac{x}{2\sqrt{\alpha' t}} + \frac{\lambda(\rho'-\rho'')}{\rho''}\sqrt{\frac{\alpha'}{\alpha''}}\right] \tag{34}$$

where

$$A'(\lambda) = \frac{\delta_T\,\lambda\,\operatorname{erfc}(\gamma_T\lambda) + \sigma_T\,e^{-\lambda^2\gamma_T^2}}{e^{-\lambda^2}\operatorname{erfc}(\gamma_T\lambda) + \sigma_T e^{-\lambda^2\gamma_T^2}\,(1 + \operatorname{erf}\lambda)} \tag{35}$$

$$A''(\lambda) = \frac{e^{-\lambda^2} - \delta_T\,\lambda(1 + \operatorname{erf}\lambda)}{e^{-\lambda^2}\operatorname{erfc}(\gamma_T\lambda) + \sigma_T\,e^{-\lambda^2\gamma_T^2}(1 + \operatorname{erf}\lambda)} \tag{36}$$

and

$$\delta_T = \frac{h_{fg}\sqrt{\pi}}{c_p'\,(T_\infty'' - T_\infty')} \tag{37}$$

$$\gamma_T = \frac{\rho'}{\rho''}\sqrt{\frac{\alpha'}{\alpha''}} \tag{38}$$

$$\sigma_T = \sqrt{\frac{(k\rho c_p)''}{(k\rho c_p)'}} \tag{39}$$

The interfacial temperature T_S at $X(t) = 2\pi\sqrt{\alpha' t}$ is given by

$$\frac{T_S - T_\infty'}{T_\infty'' - T_\infty'} = A'(\lambda)\,(1 + \operatorname{erf}\lambda) \tag{40}$$

For a single component system λ is determined from Equation (40) by specifying the interfacial temperature T_S, usually taken to be that of thermodynamic equilibrium. In a binary system it is necessary to

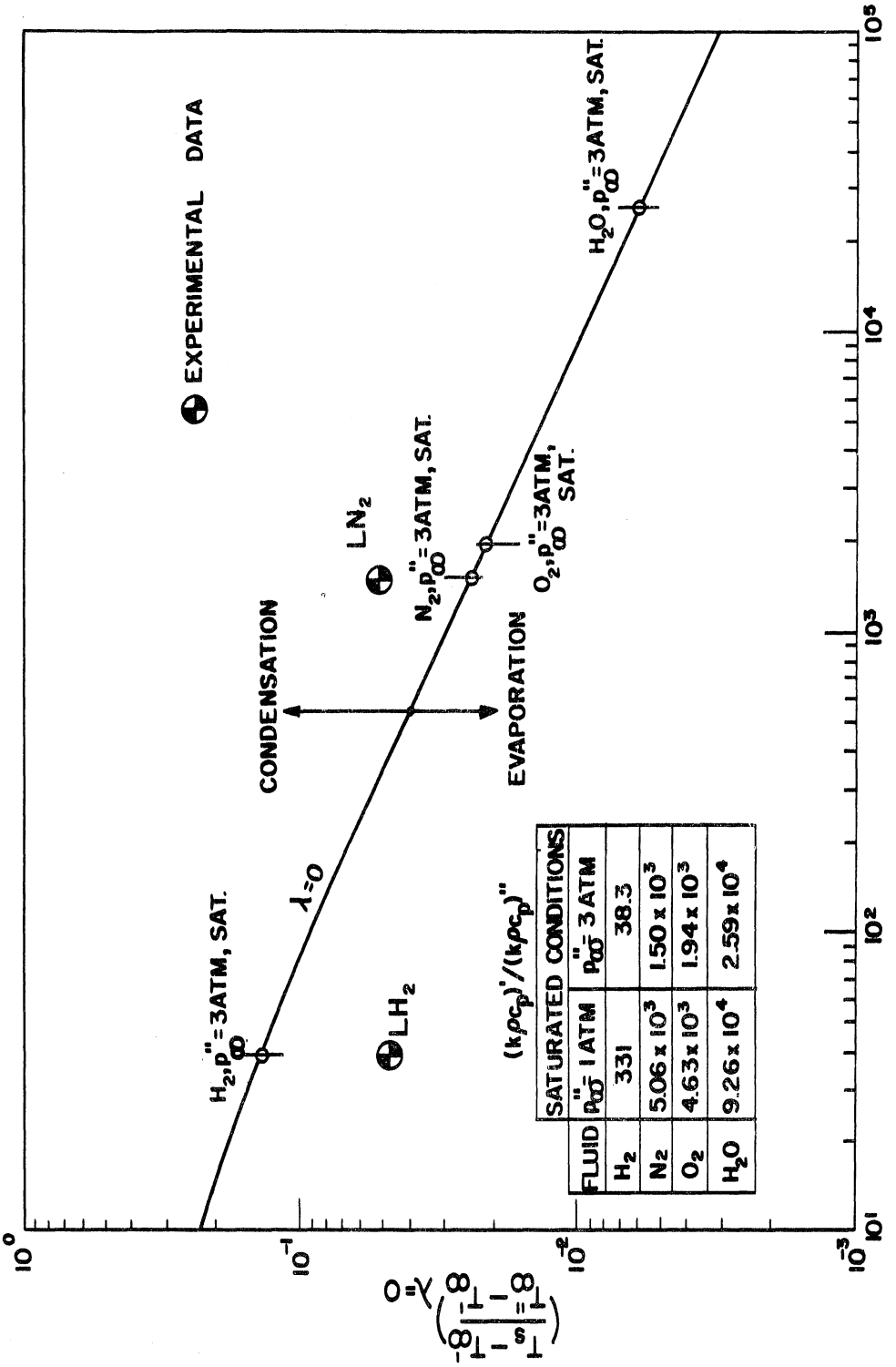

Figure 14. Interfacial Temperature for No Condensation Nor Evaporation, $\lambda = 0$.

determine λ by a coupling of T_s as expressed in Equation (40) with a similar expression for interfacial concentration C_s' and C_s'' and the thermodynamic equilibrium data for the binary mixture. These results will not be given here but may be found in Reference (56).

The vapor and liquid heat flux at the interface are expressed as

$$\frac{(q/A)'}{k'(T_\infty'' - T_\infty')} = \frac{A'(\lambda)}{\sqrt{\pi\alpha' t}} e^{-\lambda^2} \tag{41}$$

and

$$\frac{(q/A)''}{k''(T_\infty'' - T_\infty')} = \frac{A''(\lambda)}{\sqrt{\pi\alpha'' t}} e^{-\lambda^2\gamma_T^2} \tag{42}$$

A particularly useful case is that of $\lambda = 0$, which separates the conditions corresponding to evaporation and condensation. A simple formulation may be used as a criterion for judging in a particular instance which process may be expected to occur. The interfacial temperature for $\lambda = 0$ is found from Equation (40) as

$$\left(\frac{T_s - T_\infty'}{T_\infty'' - T_\infty'}\right)_{\lambda=0} = A'(0) = \frac{\sigma_T}{1 + \sigma_T} = \frac{1}{1 + \sqrt{\dfrac{(k\rho c_p)'}{(k\rho c_p)''}}} \tag{43}$$

It may be shown that if $(T_s - T_\infty')/(T_\infty'' - T_\infty')$ is greater than $A'(0)$, then $\lambda > 0$ and condensation occurs, whereas if this temperature ratio is less than $A'(0)$, then $\lambda < 0$ and evaporation occurs. The usefulness of this criterion is that it provides a simple expression in terms of known system parameters and the thermal property ratio $(k\rho c_p)'/(k\rho c_p)''$. This expression is shown in Figure 14 along with

representative values of the thermal property ratio for O_2 , N_2 , H_2 and H_2O at 1 and 3 atmospheres, saturated conditions. From this result it may be observed that interfacial evaporation may reasonably be expected in the pressurization of sub-cooled liquid hydrogen, whereas much larger temperature differences, $T_\infty''-T_\infty'$, are required to cause evaporation at liquid nitrogen, oxygen or water interfaces. In these latter systems condensation may more often prevail. Experimental data for both liquid hydrogen systems,(58) where vaporization was reported, and liquid nitrogen systems,(59) where condensation was reported, are included in Figure 14. The relative positions of these data points on the figure confirm the prediction of Equation (43). This is further borne out by the growth rate parameter-gas temperature calculations shown in Figures 15 and 16 for the pressurization of sub-cooled liquid hydrogen and nitrogen. Oxygen would behave similar to that of nitrogen in Figure 16. Experimental observations in both liquid hydrogen, liquid oxygen and liquid nitrogen systems have indicated these same effects, References (60) and (61). Aydelott (251) reports evaporation from a liquid hydrogen interface in contact with its superheated vapor. The growth rate parameters for binary systems oxygen-nitrogen and helium-nitrogen systems are reported in References (55) and (56).

An important question relating to interfacial phenomena concerns the departure of the interfacial temperature from that corresponding to thermodynamic equilibrium. The difference between the equilibrium temperature T^* and the interfacial temperature T_S may be shown to be closely approximated by the following expression(56)

$$\frac{T^* - T_S}{\lambda/\sigma_1} = \frac{v_{fg}\, T_S^{3/2}}{J\, h_{fg}} \sqrt{\frac{2\pi R}{g_o}\, \frac{(k\rho/c_p)'}{t}} = \frac{C_F}{\sqrt{t}} \qquad (44)$$

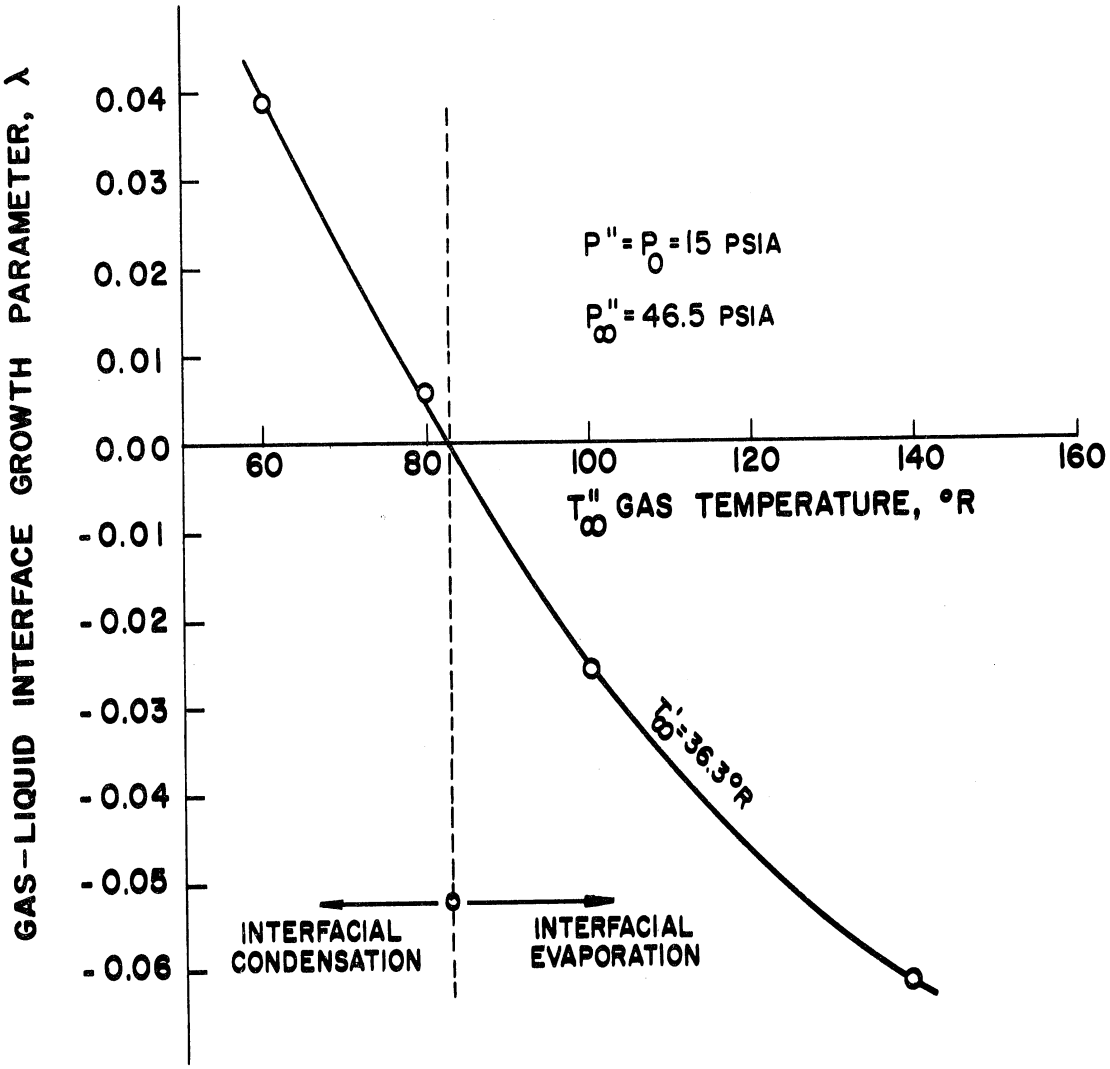

Figure 15. Gaseous Hydrogen-Liquid Hydrogen Interfacial Transfer for Non-Uniform Temperature and Interface Equilibrium.

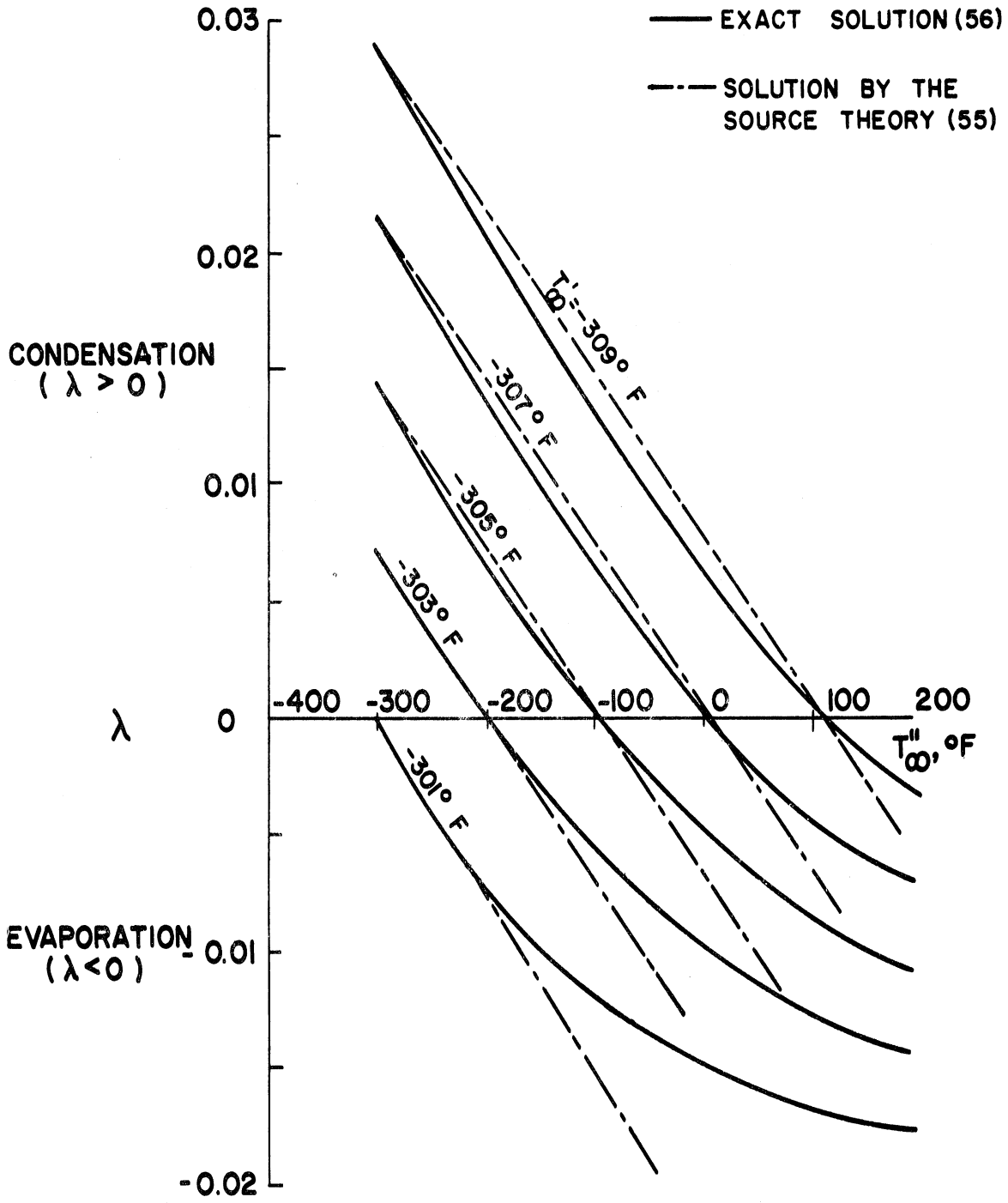

Figure 16. Growth Rate Parameter of Liquid-Vapor Nitrogen System Pressurized from 1 atm. To 3 atm.

Here σ_1 is called the Knudsen condensation coefficient, an experimentally determined parameter discussed in References (45) and (46). For estimating purposes T_s on the right hand side of Equation (44) may be taken as T^* with negligible error. At a pressure of 3 atm and for t in seconds, C_F has the approximate value of 5.31×10^{-4} for hydrogen and 87.0×10^{-4} for oxygen. Hence, it may be seen that hydrogen interfaces respond considerably faster than oxygen interfaces for equivalent values of λ/σ_1. For t equal to 1 second $(T^*-T_s)(\lambda/\sigma_1)$ is 0.000531°R for H_2 and 0.0087°R for O_2. Values of λ are of the order 10^{-1} to 10^{-2}. Thus, unless σ_1 is extremely small departures from thermodynamic equilibrium at the interface will be negligible except at vanishingly small times. Even thenthis departure will reduce rapidly at larger times. Olsen(62) has reported several degrees (F) superheat of a liquid hydrogen interface during pressurization. However, the superheat was observed to decay with time in a manner suggested by Equation (44).

The transient condensation of a cryogenic vapor on an insulating substrate is reported in Reference (50). One of the problems associated with pressurization of cryogenic vessels is the high rate of initial condensation of the pressurant on the internal surfaces, including the liquid-vapor interface, and the consequent loss in pressure. The presence of an insulating material on these surfaces allows for an increased response time of surface temperature and a fairly rapid re-evaporation of a condensed liquid layer. An important consideration then concerns the identification of those thermal properties which may be used to select insulants for this purpose. It turns out(50) that a single property group, namely, $k \zeta cp$, may be used to discriminate as to the suitability of insulants on whose surface a condensed layer of liquid will have

minimum residence time. Some typical values of $k \rho cp$ are listed in Table IV. The low value of this property for styrofoam indicates the rapid surface temperature response which may be expected for this material.

TABLE IV

VALUES OF $k \rho cp$

Substance	$(k\rho cp)10^3$, $(BTU/HR\text{-}F\text{-}Ft^2)^2 HR$
Aluminum (70°F)	3,000,000.
Water (Liquid, 70°F)	24,920.
Nitrogen (Liquid, -320°F)	2,310.
Cork (100°F)	56.
Fiberglas (70°F)	29.
Styrofoam (40°F)	9.

III. FORCED-CONVECTION PROCESSES

In general, single phase forced convection heat transfer processes for cryogens may be described by the same scaling parameters as found useful for other substances. The exceptions to this rule include all transport phenomena in the region of the critical point. Here variations in the values of c_p, μ, k, ρ and β with temperature and pressure are so great that correlation equations developed for "constant" property conditions are invalid. It is currently felt that heat transfer processes in the region of the critical point will be successfully described when the general problem of convective heat transfer in a system of severely variable properties in adequately solved. Some work has been accomplished along this line[64,65] for liquid hydrogen and will be discussed later. Another hypothesis tendered to explain near-critical point behavior is to ascribe it to a pseudo-boiling phenomena.[66] The frictional pressure drop for duct flow can be fairly reliably predicted using standard friction factor-Reynolds number correlations, except in the region of the critical point. The total pressure drop in many cases, however, is made up mostly of momentum changes resulting from density variations on heating or cooling. These can be computed using property data.[66]

The most useful results to date for design purposes are the generalized empirical and semi-empirical correlations. These include correlations formulated from studies conducted on both cryogenic and non-cryogenic substances. (Reference 14, Chapter 5). Richards, Steward and Jacobs[67] have summarized some results for cryogenic substances. Data from this reference are given in Reference 14. Compact heat exchangers have been sized for cryogenic application[68,69,80] using the

extensive tabulation of heat transfer and friction data of Kays and London.[70] For single phase flow the standard heat transfer and pressure-drop correlations have been employed for design.[69,71,81] Other heat exchanger design procedures for cryogenic application are reported by Bartlit and Williamson,[72] Hargis and Stokes[73] and Kroeger.[82] Some of the results of Hargis and Stokes, who worked on Saturn I and Saturn V pressurization heat exchangers, will be discussed later.

Single-phase convective heat transfer is characterized by the type of flow, laminar, transition of turbulent and the manner in which the flow is obtained, forced convection or natural convection. Heat transfer correlations depend on these characterizations as well as on the geometry of the flow, external, internal (duct flow) or separated. The principal scaling parameters are the Nusselt number $Nu = hDe/k$, the Reynolds number $Re = \rho V De/\mu$, the Grashof number $GR = De^3\rho^2 g\beta\Delta T_o/\mu^2$, the Prandtl number $Pr = c_p\mu/k$ and the length to diameter ratio L/De. Where variable property effects are important these parameters are either evaluated at a particular temperature, such as the film temperature $T_f = (T_w + T_b)/2$, or an additional parameter consisting of (T_w/T_b) or (ν_w/ν_b) may be included in the correlation.

A. Flows With Moderate Property Variation

Except for the superfluid condition most cryogens behave in a "classical" manner when their thermodynamic state is well removed from the critical state. For gases, this will always be true whenever an ideal gas equation of state describes the p, v, T relationship and the

transport properties (cp, μ , k) vary only slightly with temperature. Under these circumstances the heat transfer correlations may be written for a moderate property variation corresponding to low to moderate differences in temperature between the surface and that of the fluid bulk.

1. Laminar Flow

Laminar flow exists when disturbances decay when introduced into the flow. Generally, for flow inside of ducts this corresponds to a condition of a Reynolds number, based on diameter, less than approximately 2000. In this instance the Reynolds number is defined as

$$Re = \frac{\rho V D_e}{\mu} = \frac{D_e G}{\mu} \tag{45}$$

Here D_e is the equivalent diameter defined by

$$D_e = 4 \frac{\text{wetted flow area, } A_f}{\text{wetted perimeter, } p} = 4 \left(\frac{A_f}{p} \right) \tag{46}$$

which provides for consideration of ducts having non-circular cross section.

Heat transfer data for laminar flow inside ducts having uniform wall temperature is correlated by the following two equations for h based on the arithmetic mean temperature difference. The subscript b indicates that physical properties are evaluated at mixed mean fluid temperature.

(a) $$Re \cdot Pr / \frac{L}{D_e} \geq 10$$

$$\frac{h D_e}{k_b} = 1.86 \left[\frac{4}{\pi} \cdot \frac{A_f}{D_e^2} \cdot \frac{Re\ Pr}{L/D_e} \right]_b^{1/3} \left(\frac{\mu_b}{\mu_w} \right)^{0.14} \tag{47}$$

(b) $$\mathrm{Re}\ \mathrm{Pr}/\frac{L}{D_e} \leq 5$$

$$\frac{hD_e}{k_b} = \frac{1}{2}\left[\frac{\mathrm{Re}\cdot\mathrm{Pr}}{L/D_e}\right]_b \qquad (48)$$

These equations are shown on Figure 17 taken from McAdams[74] and compared with some experimental data for air in circular ducts. The agreement is good at low values of $\mathrm{Re}\cdot\mathrm{Pr}/\frac{L}{D_e}$ and satisfactory at higher values where the data fall slightly above the curve for Equation (47). This probably was caused by a superposed effect of free convection. The parabolic velocity profile correlation, Equation (47) is shown for circular tubes for which $A_f/D_e^2 = \pi/4$.

2. Turbulent Flow

Turbulent flow is found to exist when the flow Reynolds number is sufficiently large. For flow inside ducts a condition of fully turbulent flow occurs when the Reynolds number based on diameter, D_e , exceeds approximately 10,000. Between a Reynold number of 2000 and 10,000 the flow is in a transition state, being partly laminar and partly turbulent and characterized by some unsteadiness.

Heat transfer data for turbulent flow inside ducts is correlated ($\pm$ 25%) by the following equation for $1 \leq \mathrm{Pr} \leq 120$ and $10{,}000 \leq \mathrm{Re} \leq 500{,}000$,

$$\left(\frac{hD_e}{k}\right)_f = 0.023\left(\frac{D_eG}{\mu_f}\right)^{0.8}\mathrm{Pr}_f^{1/3}\left[1 + \left(\frac{D_e}{L}\right)^{0.7}\right] \qquad (49)$$

The subscript f in this expression indicates that the physical properties are to evaluated at the film temperature which is the arithmetic mean of the surface and mixed mean fluid temperature.

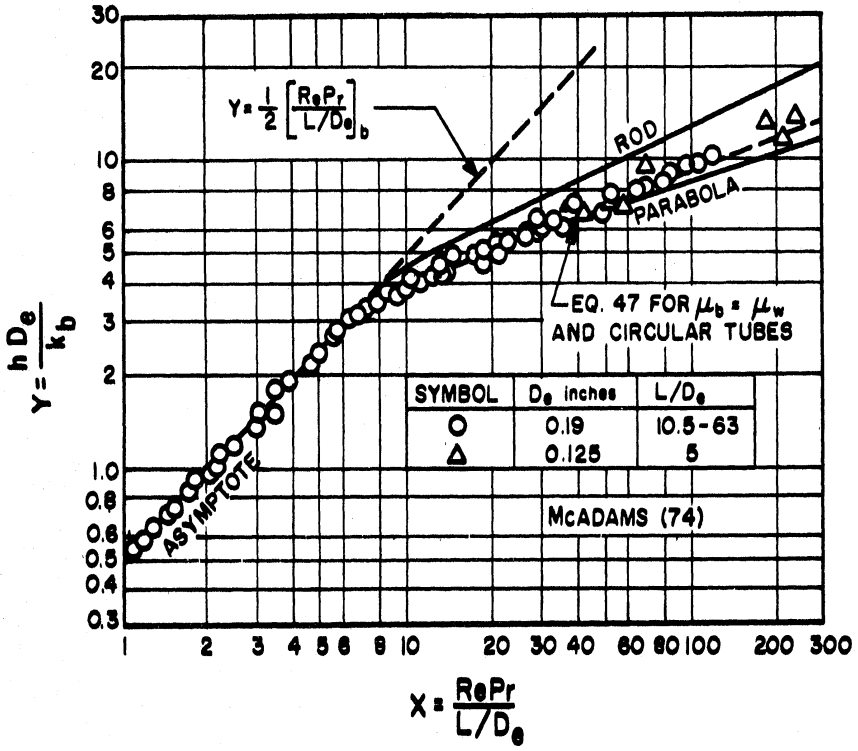

Figure 17. Correlation of Heat Transfer Data for Laminar Flow in Ducts.

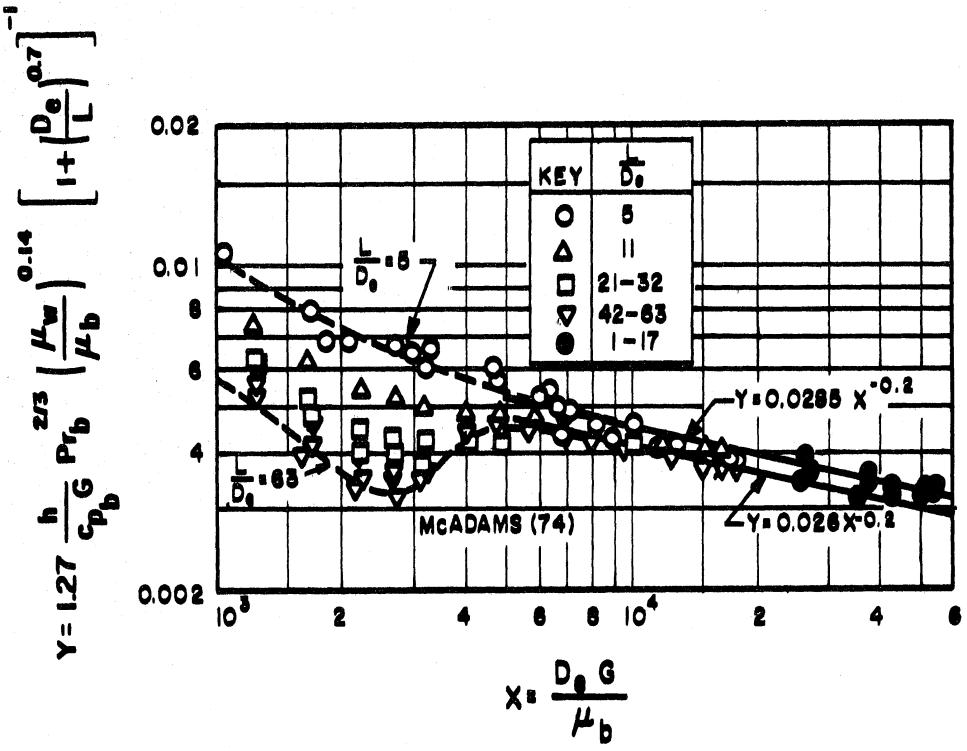

Figure 18. Correlation of Heat Transfer Data for Laminar, Transition and Turbulent Flow in Ducts.

Another correlation which may be used to compute heat transfer coefficients in turbulent flow (± 25%) and having the same restrictions as Equation(49), is written as follows:

$$\frac{h}{c_{p_b} G} Pr_b^{2/3} \left(\frac{\mu_w}{\mu_b}\right)^{0.14} = 0.0205 \left(\frac{D_e G}{\mu_b}\right)^{-0.2} \left[1 + \left(\frac{D_e}{L}\right)^{0.7}\right] \quad (50)$$

Except for the viscosity ratio correction factor, μ_w/μ_b, all physical properties are evaluated at the mixed mean bulk temperature, designated by the subscript b. A comparison of this expression with experimental data is shown in equivalent form in Figure 18. The influence of L/D_e as well as the general interrelationship of turbulent, transition and laminar heat transfer data also is shown.

Thompson and Geery(75) studied heat transfer to liquid hydrogen at super critical pressures (680-1344 psia and inlet temperatures 57 to 86°R) for turbulent flow in a 0.194 inch ID tube. Two regimes of flow were found characterized by the magnitude of the level of heat flux and wall-fluid temperature ratio. Except at low values of these quantities, the data were correlated (± 30%) by

$$Nu_b = 0.0217\ Re_b^{0.8}\ Pr_b^{0.4} \left(\frac{T_w}{T_b}\right)^{-0.34}, \quad (51)$$

as shown in Figure 19. Pressure drop was satisfactorily correlated by the conventional friction factor for Newtonian fluids.

In low pressure regions where hydrogen has almost ideal gas behavior, Hendrick's, et al(66) found that local heat transfer data could be correlated by

$$\frac{h_x D_e}{k_f} = 0.023 \left(\frac{\rho_f V\ D_e}{\mu_f}\right)^{0.8} \left(\frac{c_p \mu}{k}\right)_f^{0.4} \quad (52)$$

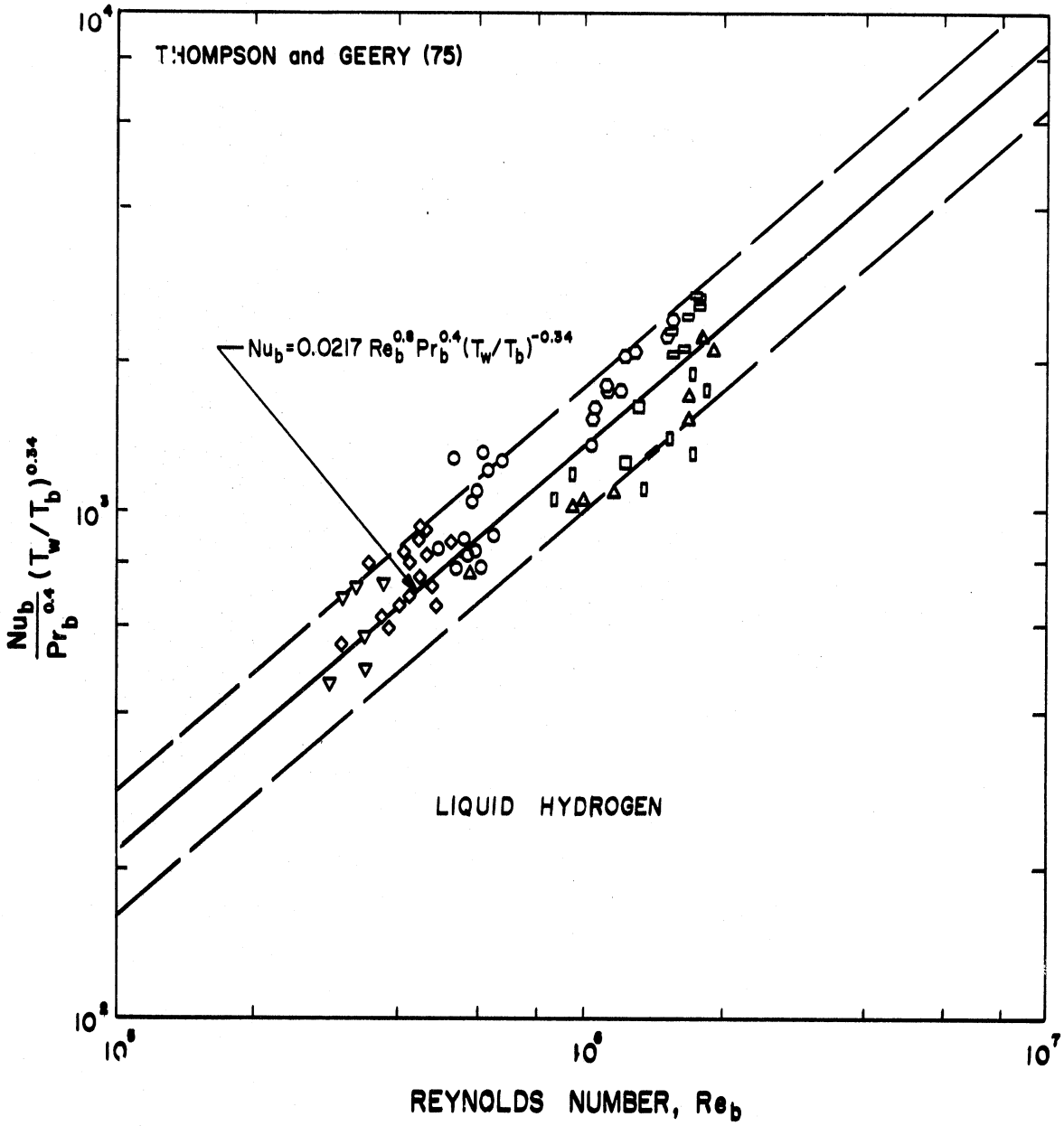

SYMBOL	PRESSURE (psia)	INLET TEMP (°R)
◇	1340	86
□	1270	74
○	1210	77
△	730	79
▽	730	82
▯	730	55
○	720	60
▭	680	57

PROPERTIES EVALUATED AT LOCAL BULK TEMPERATURES

L/D = 41.2

T_w/T_b = 3.85 TO 16.5

Q/A = 0.6 TO 8.0 BTU/IN^2 SEC

Figure 19. Correlation of Forced-Convection Heat Transfer.

At higher pressures (12-50 atm) and for fluid temperatures in excess of 90°R, these authors find their local heat transfer data to correlate approximately as Equation (52), as shown in Figure 20.

Hendricks, et al[66] summarize turbulent convective heat transfer correlations for hydrogen at pressures above and below the critical pressure (188 psia) in the range 1-100 atm, but not too close to the critical temperature (60°R). This summary is given in Table V and includes some results for helium as well.

A comparison of the various correlations in Table V is shown in Figure 21. Except for Equation (53) they all predict essentially the same magnitude of result over a large range of T_w/T_b . Equation (53) diverges severely for values of T_w/T_b greater than about 4. The range of actual experimental values of T_w/T_b is not great and since many modern power and propulsion systems require design at higher values of T_w/T_b additional data would be welcome. Hendricks, et al[66] recommend the use of Equation (57) at large ratios of T_w/T_b as this correlation is formulated in terms of local properties and consequently takes some account of property variation.

At low pressures the pressure drop may be computed by the standard turbulent flow Equation (66). For pressures above the critical pressure and temperatures in excess of 90°R the fluid friction appears to be similar to that observed with other gases in pipes of varying roughness. In Reference 77 the isothermal fluid friction was comparable to results in the literature. However it was noticed that the nonisothermal friction factors were less than the isothermal values at the same bulk Reynolds number.

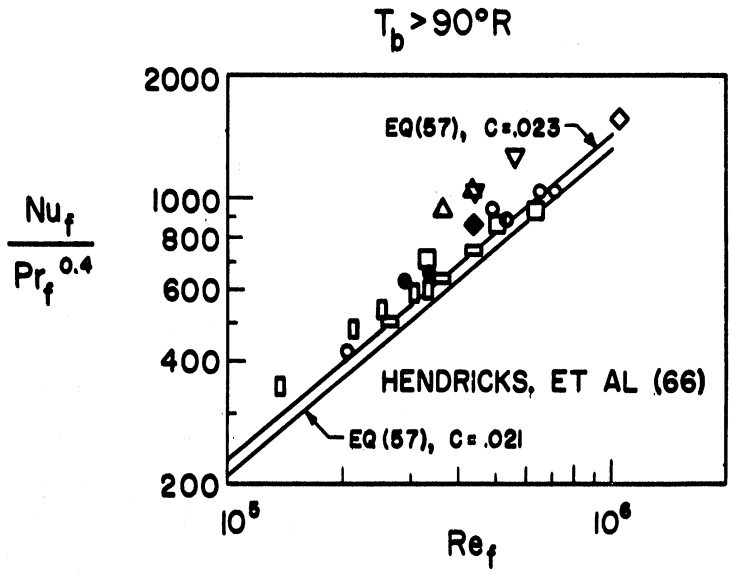

Figure 20. Correlation of Local Heat Transfer Data for Hydrogen p = 12 - 50 ATM .

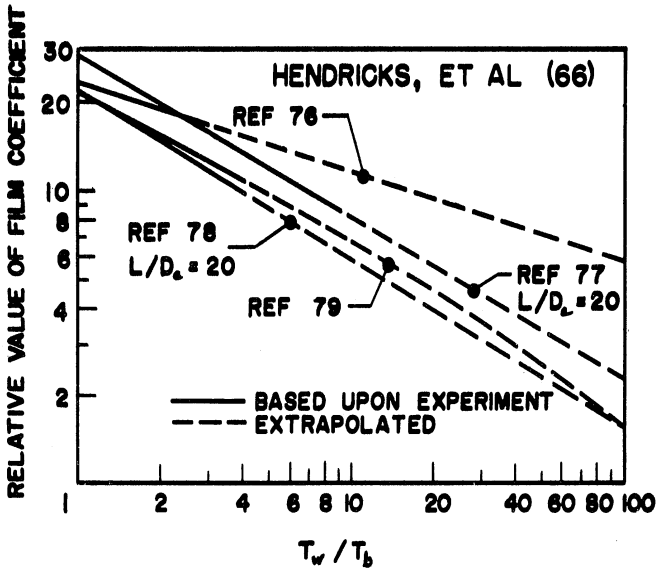

Figure 21. Comparison of Convective Film Correlations Over a Range of T_w/T_b .

TABLE V

SUMMARY OF HEAT TRANSFER CORRELATIONS FOR REGIONS REMOTE FROM THE CRITICAL POINT.[66]

Ref.	Fluids	Max $\frac{T_w}{T_b}$	Entrance bulk temp. range, °R	Correlation
76	Hydrogen	2.8	360 to 560	$Nu_b = 0.023 Re_b^{0.8} Pr_b^{0.4} \left(\frac{T_w}{T_b}\right)^{-0.3}$ (overall) (53)
77	Hydrogen	9	135 to 515	$Nu_b = 0.045 Re_b^{0.8} Pr_b^{0.4} \left(\frac{T_w}{T_b}\right)^{-0.55} \left(\frac{L}{D_e}\right)^{-0.15}$ (overall) (54)
	Helium	11		
78	Hydrogen	4	88 to 130	$Nu_b = 0.021 Re_b^{0.8} Pr_b^{1/3} \left(\frac{T_w}{T_b}\right)^{-0.575} \left(1 + \frac{6}{L/De}\right)$ (overall) (55)
79	Helium	4	1500 max	$Nu_f = 0.034 Re_f^{0.8} Pr_f^{0.4} \left(\frac{L}{De}\right)^{-0.1}$ (overall) (56)
	Unpublished hydrogen[66]			$Nu_f = C Re_f^{0.8} Pr_f^{0.4}$, $C = 0.021$ (overall) (57)

In Reference 79 the friction coefficient with helium at high wall temperatures was observed to be predictable by the Karman-Nikuradse relation for turbulent flow:

$$\frac{1}{\sqrt{f}} = 4 \log_{10}(Re \sqrt{f}) - 0.4 \qquad (58)$$

where f is the Fanning friction factor, defined as

$$f = \frac{\tau_w}{\rho V^2/2g_o} , \qquad (59)$$

and

$$\Delta p = 4f \left(\frac{L}{D_e}\right) \frac{\rho V^2}{2g_o} . \qquad (60)$$

McAdams[74] recommends a modified form of Equation (58) for flow in heated tubes having T_w/T_b up to 2.5. The result is a reduction in the friction factor for the higher values of T_w/T_b, as was observed in Reference (77). For compressible flows, a significant contribution of momentum change to the total pressure drop must be anticipated.

Hargis and Stokes[73] report on the design of heat exchangers for the Saturn I and Saturn V pressurization systems. These units consist of a helical tube coil through which the gaseous pressurant (H_2, O_2 or H_e) is pumped. The heat exchanger coil is heated by combustion gases from the rocket exhaust which flows over the outside of the coil. A comparison of test data and computer performance predictions for an oxygen heat exchanger is shown in Figure 22. The heat transfer correlation used for average tube side coefficient for oxygen which best fitted the data is

$$Nu_b = 0.023\ Re_b^{0.8}\ Pr_b^{0.4} \left(\frac{T_w}{T_b}\right)^{-0.34} \phi_1\phi_2 , \qquad (61)$$

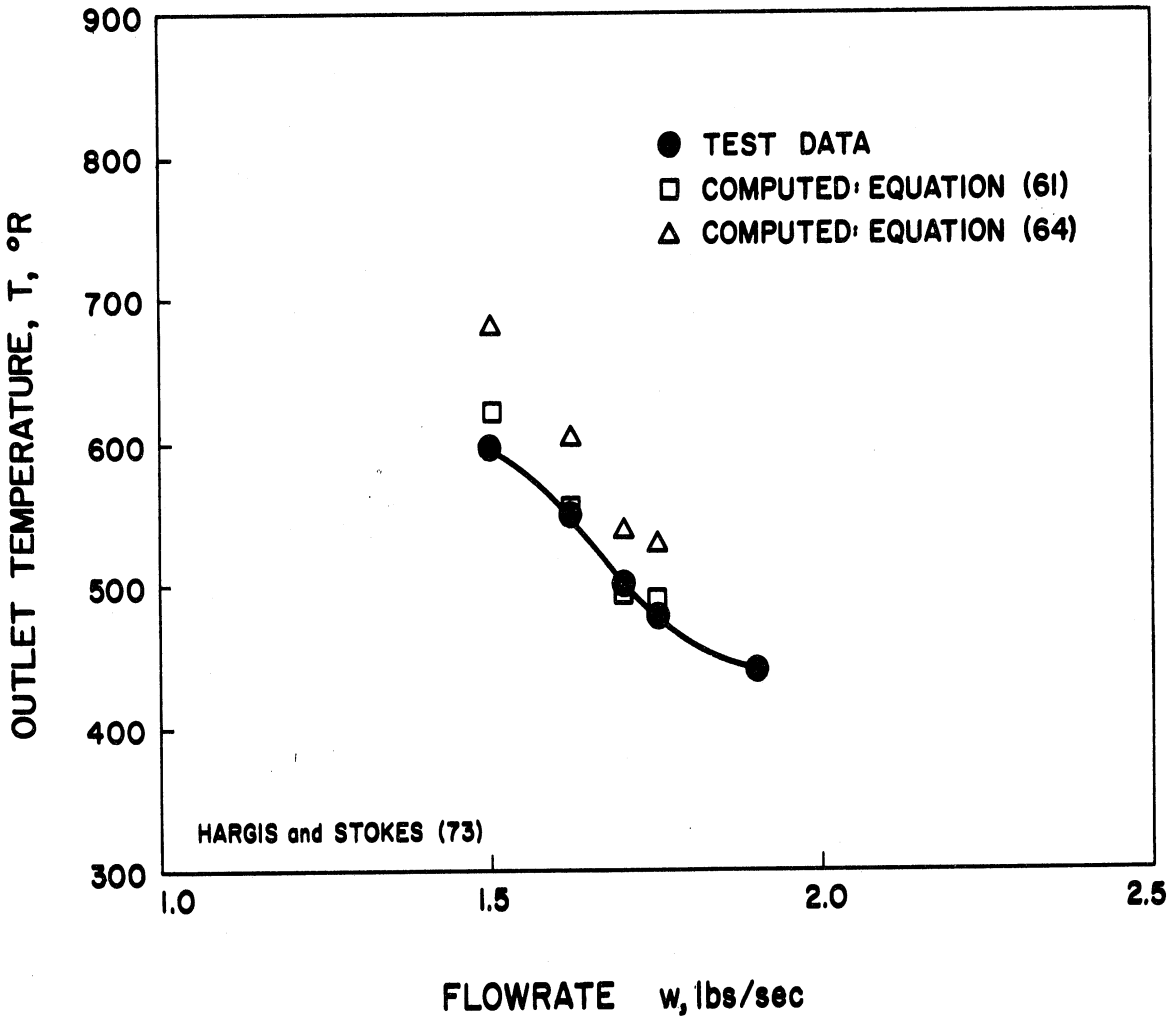

Figure 22. Comparison of Test Data and Computed Performance Predictions for a Typical Oxygen Heat Exchanger.

where ϕ_1 and ϕ_2 are correction factors, given below.

TABLE VI

(a) OXYGEN CORRECTION FACTOR ϕ_1 FOR EQUATION (61)

T_b °R	T_w °R		
	600	1000	1800
200	1.3	0.95	-----
278	0.58	0.42	0.32
300	0.68	0.556	0.434
350	0.836	0.764	0.655
400	1.0	1.0	1.0
Over 400	1.0	1.0	1.0

(b) Correction Factor ϕ_2 For Equation (61)

For $L/D_e \leq 50$:

$$\phi_2 = \frac{1.48}{(L/D_e)^{0.1}} \tag{62}$$

For $L/D_e \geq 50$:

$$\phi_2 = 1.0 \tag{63}$$

Equation (61) is shown in Figure 22 and agrees satisfactorily with the experimental data. As a demonstration of the need for property value correction Hargis and Stokes(73) include a comparison with a simplified correlation sometimes used in heat transfer correlations. This equation also shown in Figure 22 is

$$Nu_b = 0.023\ Re_b^{0.8}\ Pr_b^{0.4} . \tag{64}$$

This result compares much less favorably with the experimental data than does Equation (61).

As may be observed Equation (61) for oxygen at temperatures above 400°R and L/D_e in excess of 50 is essentially the same correlation found to predict the behavior of supercritical hydrogen, Equation (51) and Equation (53).

A discussion of the application of these various correlations to hydrogen cooled rocket nozzles is given by Benser and Graham.(83) The cooling of large masses by ducted supercritical helium is reported by Koln(84) and Koln, et al.(85) To maintain superconducting magnets at low temperature (40K) these investigators employed a forced circulation system of liquid helium at pressures above 100 atmospheres in small tubing integral with the object to be cooled. Performance data but not heat transfer data are reported.

3. Transition Flow

Between the Reynolds numbers of 2000 to 10,000, the flow in a duct is in a transition condition. This is a flow region in which the characteristics of both laminar and turbulent flow co-exist. There also is a tendency for instability in the flow pattern. Very little is known about this flow regime and no really satisfactory method or correlation exists for computing its heat transfer coefficients. A residual L/D_e influence is observed which is greatest at the lower range of Reynolds numbers and gradually diminishes at higher Reynolds numbers. To obtain heat transfer coefficients in the transition region it is recommended that the data of Figure 18 be smoothed and the coefficients computed from the ordinate corresponding to the expected Reynolds number and the L/D_e .

4. Flow Outside of Ducts

An important configuration encountered frequently is flow external and normal to the axis of a duct. Heat transfer data for the case of round ducts are correlated[86] by the expression

$$\left(\frac{hD_o}{k}\right) = C \cdot \left(\frac{\rho_\infty V D_o}{\mu_f}\right)^n, \qquad (65)$$

the subscript f denotes the physical properties are evaluated at the film temperature. Both C and n are functions of the Reynolds and Prandtl numbers in accordance with Table VII below.

TABLE VII

$\frac{\rho_\infty V D_o}{\mu_f}$	n	C Gases	C Liquids
1 - 4	0.330	0.891	$0.989\ Pr^{1/3}$
4 - 40	0.385	0.821	$0.911\ Pr^{1/3}$
40 - 4,000	0.466	0.615	$0.683\ Pr^{1/3}$
4,000 - 40,000	0.618	0.174	$0.193\ Pr^{1/3}$
40,000 - 250,000	0.805	0.0239	$0.0266 Pr^{1/3}$

Experimental results for air are shown in Figure 23 and compared with the correlation, Equation (65). Data also are available for non-circular ducts and spheres and may be found in McAdams[74] and Knudsen and Katz.[86]

The flow around a bluff object is of a variable nature. It starts as a laminar condition at the forward stagnation point, undergoes transition to a turbulent boundary layer and finally separates from the surface in the downstream regions producing a highly turbulent wake.

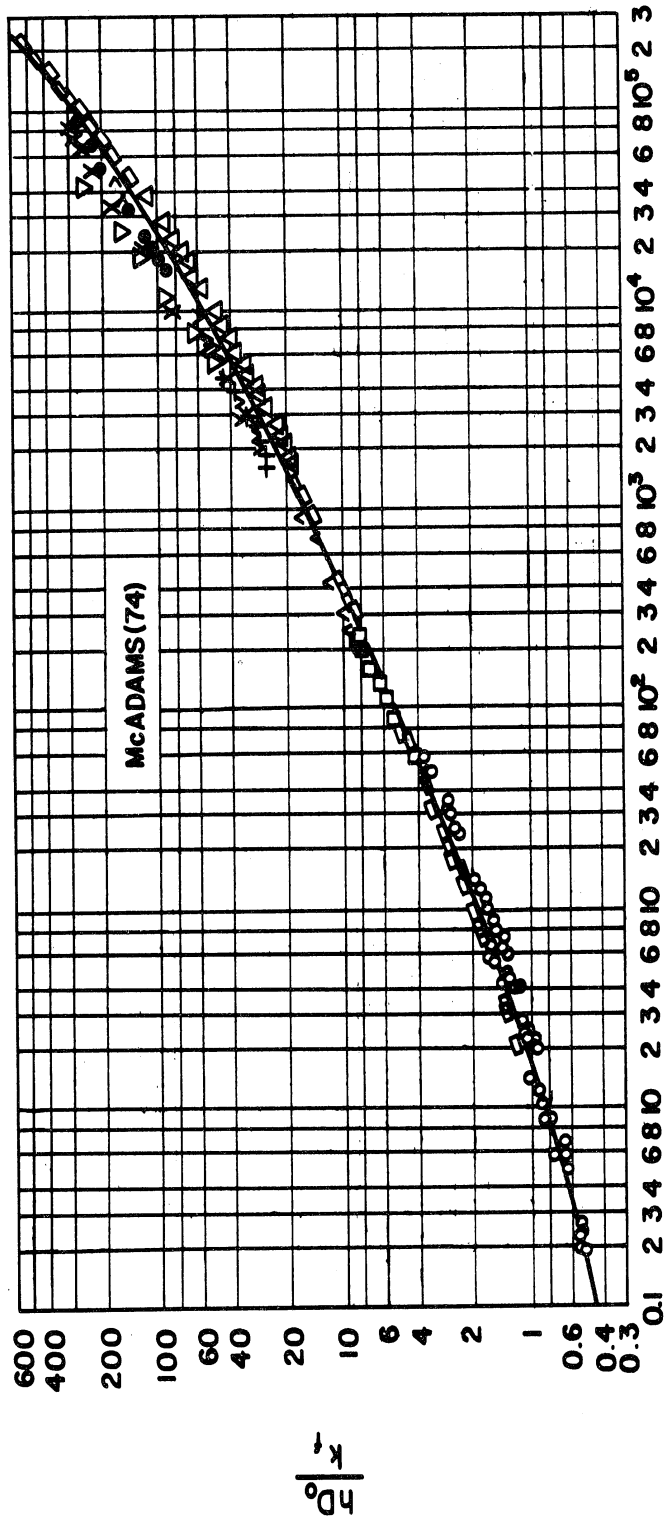

Figure 23. Heat Transfer Data for Air Flowing Normal to a Single Cylinder.

For this reason the flow is characterized by the Reynolds number only without reference to a laminar or turbulent description.

B. Flow With Large Property Variation

The conditions corresponding to the limits of application of constant or variable property correlations - the ideal gaseous or liquid states, on one hand, and the critical or superfluid states on the other - are fairly easily identified. Their intermediate or transition states, where fluid property variation with temperature and/or pressure becomes severe, are much less easily defined. No simple critierion exists. One is best guided by the magnitude of the variation in such properties as k , c_p and ν in the range of temperatures expected in a design. McAdams (Reference 74) reports the data of Desmon and Sams[87] which indicates the influence of large temperature variations on heat transfer to air in turbulent flow. These results are shown in Figures 24 and 25 where the data are correlated in accordance with a modified form of Equations (64) and (52), respectively. In this instance the Reynolds number is evaluated at the bulk temperature. The corresponding property variations for air suggests a limiting criterion for the application of "moderate" property variation correlations.

Hendricks, et al[66] present another guideline in the form of a dimensionless temperature ratio, originally suggested by E. R. G. Eckert. This ratio indicates the proximity of the fluid state to the critical state as measured by the temperature, T_m , at which the specific heat, c_p , reaches its maximum. The criterion is given in Figure 26. The ordinate in this figure is the ratio of the experimentally

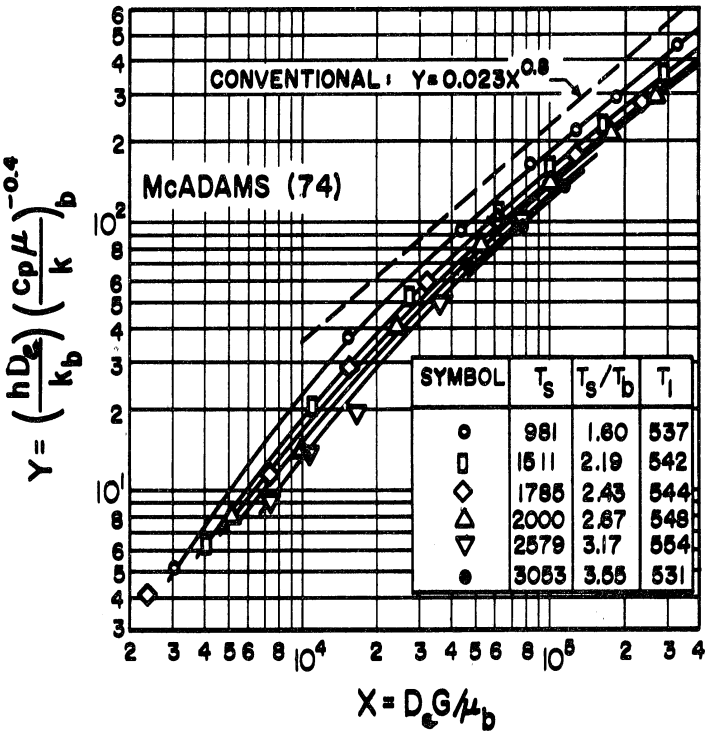

Figure 24. Heat-Transfer Data at Inlet-Air Temperature of 531 to 554°R. Physical properties of air evaluated at bulk temperature.

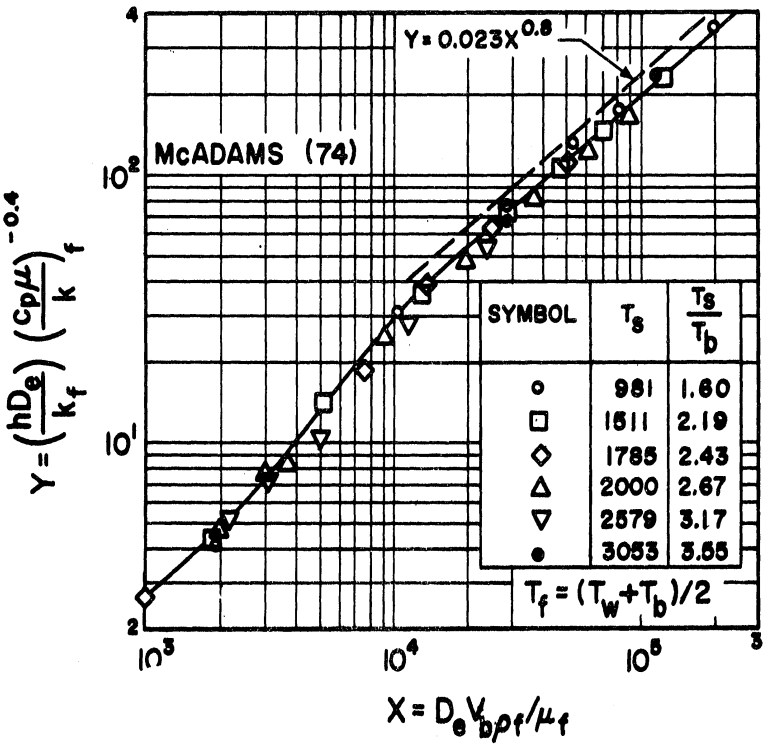

Figure 25. Correlation of Heat-Transfer Data at Inlet-air Temperature of 531 to 533°R Using Modified Film Reynolds Number.

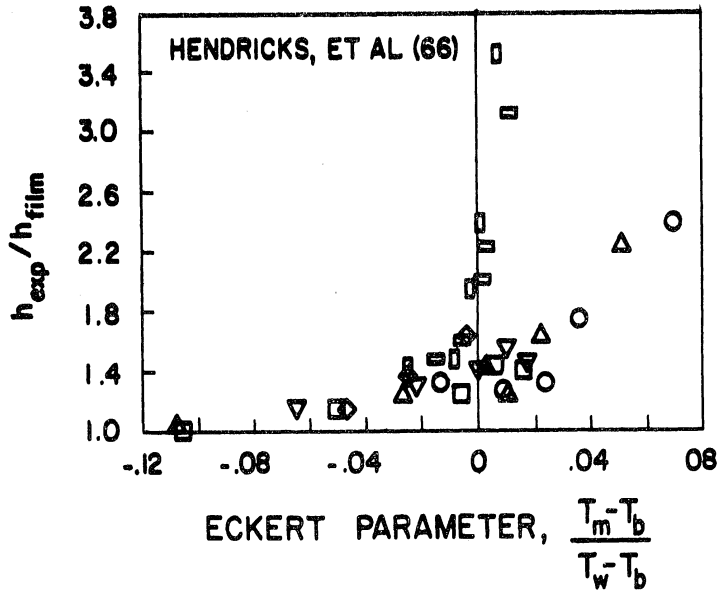

Figure 26. Comparison of Local Experimental and Computed h Near Critical Bulk Temperature, Computed h Based on Film Pipe Flow Correlation.

determined local heat transfer coefficient to that computed by Equation (57) (C = 0.023) for "moderate" property variation. As is shown, the ratio of the heat transfer coefficients increases sharpely as the fluid state approaches the critical state. The data shown are for liquid hydrogen and the bulk temperature where the largest coefficients were measured was approximately 90°R.

An analysis of the velocity and temperature distributions, the wall shear stress and the heat transfer rate for the fully developed turbulent flow of supercritical hydrogen is given by Hess and Kunz.[64] Their analysis accounts for the influence of variable physical properties on the universal velocity and temperature profiles. Based on the method of Wiederecht and Sonnemann,[88] these authors have solved the momentum and energy transport equations for variation in the eddy diffusivities of heat and momentum as well as the thermodynamic and transport properties. The influence of these property variations on the flow is shown in Figures 27, 28 and 29. The universal velocity profile for constant properties is given in Figure 27 for Reynolds numbers of 50,000 and 500,000. The constant property results are compared with both velocity and temperature profile calculations for supercritical hydrogen in Figures 28 and 29. The kinematic viscosity ratio, ν_w/ν_b , corresponding to the conditions of this calculation is 100, the inlet temperature and pressure is 67.2°R and 274 psia and the wall-bulk temperature ratio, T_w/T_b , is approximately 10. The influence of variable properties is most significant in the turbulent core.

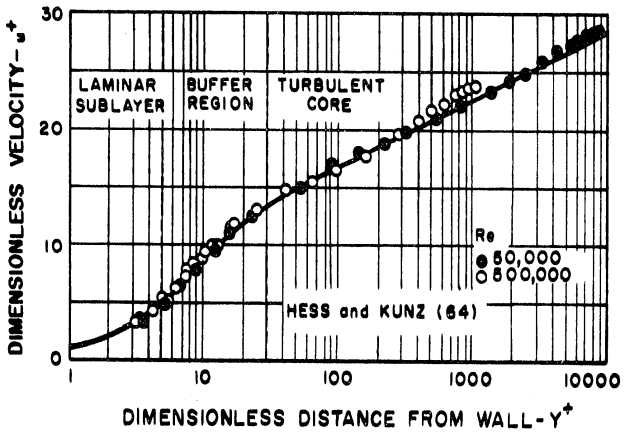

FIGURE 27. UNIVERSAL VELOCITY PROFILE.

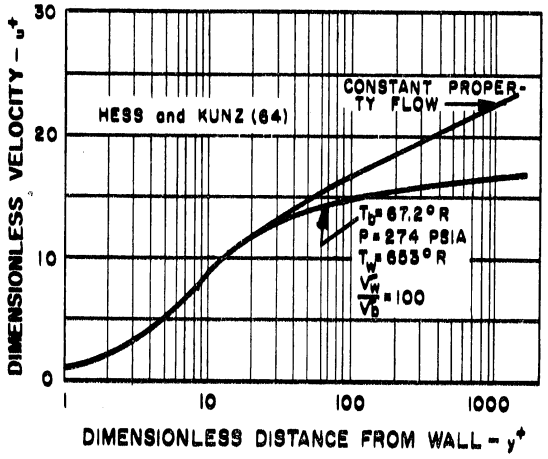

FIGURE 28. THE EFFECT OF FLUID PROPERTY VARIATIONS ON THE DIMENSIONLESS VELOCITY PROFILE.

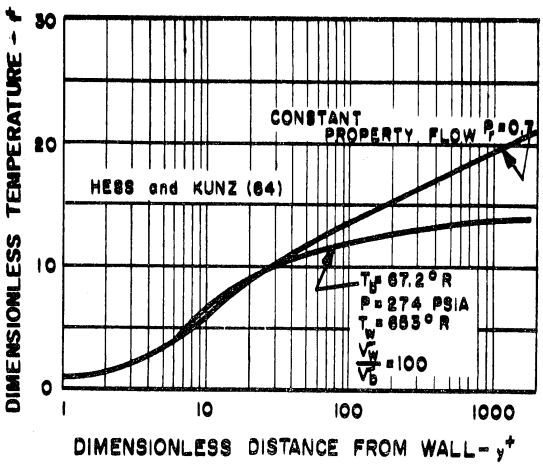

FIGURE 29. THE EFFECT OF FLUID PROPERTY VARIATIONS ON THE DIMENSIONLESS TEMPERATURE PROFILE.

It was found necessary to relate the viscous damping constant for the eddy diffusivity of momentum to the kinematic viscosity ratio, ν_w/ν_b , in order to describe the heat transfer to supercritical hydrogen. The specific form of the functional relationship to do this was determined by selectively fitting the results of the calculation to experimental data. As a consequence, however, reasonable agreement was found between the analytical calculations and the experimental heat transfer data of Hendricks, et al.(66) The results are shown in Figure 30 where the ratio of the experimental Nusselt number to the computed from the theory is plotted against the ratio ν_w/ν_b , the principal governing parameter for this system. As may be seen the comparison is within $\pm$ 20% , except for a few data in the range of ν_w/ν_b between 30 and 60.

As a further test of their analysis Hess and Kunz computed the local Nusselt numbers and the wall temperature distribution along the heated length of a tube and compared their results with the experimental hydrogen data of Hendricks, et al.(66) A typical result is shown in Figure 31. Except in the entrance region ($x/D < 30$) the comparison of computed and experimental results is favorable. The lack of agreement for x/D less than 30 is attributed to an extended influence of variable properties on the thermal entrance region. The unusual temperature distribution, which has a peak, had previously been found only in boiling experiments. The region downstream from the peak with the decreasing wall temperature appears to be predicted well by the analytical results based on the hypothesis of variable fluid properties.

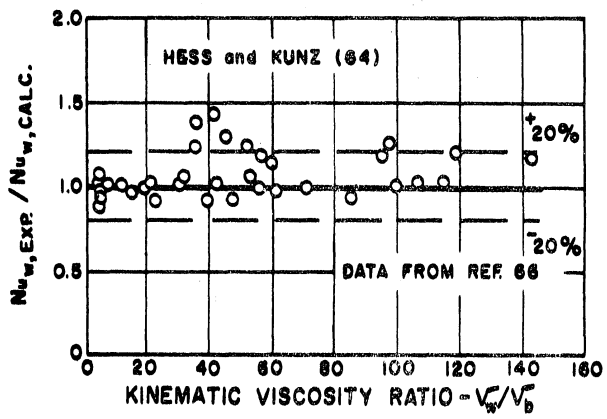

Figure 30. Comparison Between Experimental and Calculated Nusselt Numbers using the Proposed Analysis.

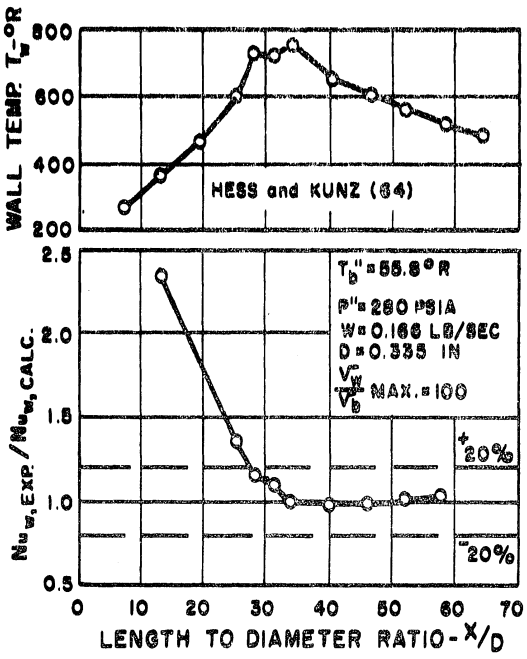

Figure 31. Experimental Data Exhibiting a Peak in the Tube Wall Temperature.

The analytic results obtained by Hess and Kunz, while providing some insight into the process, require extensive calculations using a digital computer in order to obtain useful numerical results. Hence, they are too complex for most practical design work. Because of this the following simpler formulation was obtained to fit the experimental data,

$$Nu_f = 0.0208\ Re_f^{0.8}\ Pr_f^{0.4} \left(1 + 0.01457\ \frac{\nu_w}{\nu_b} \right), \quad (66)$$

where all properties are evaluated at the film temperature, except that the bulk density is used to determine the velocity. Equation (66) is shown in relationship to the experimental data in Figure 32 as the ratio $Nu_{f\ exp}/Nu_{f\ calc}$. The value of $Nu_{f\ calc}$ is computed from Equation (52) and the solid line is the ratio of Equations (66) and (52). The work of Hess and Kunz points to the solution of the near critical region problem as one of a judicious consideration of property variation. They have found that the kinematic viscosity ratio, ν_w/ν_b, is one of the principal governing parameters for that proper description of heat transfer in a region of having large property variation.

Another explanation and correlation of near critical point heat transfer is the pseudofilm boiling hypothesis of Hendricks, et al.[66] This hypothesis is based on the similarity between the wall temperature distribution for heat transfer to supercritical hydrogen and that found in boiling experiments, as shown in Figure 31. It is thus postulated[66] that, "Instead of two-phases, there would be a continuum of densities between a light gas-like species and a heavy liquid-like species. Heavy, tightly packed clusters of molecules would migrate toward the wall and then would be broken up into smaller and lighter clusters and migrate

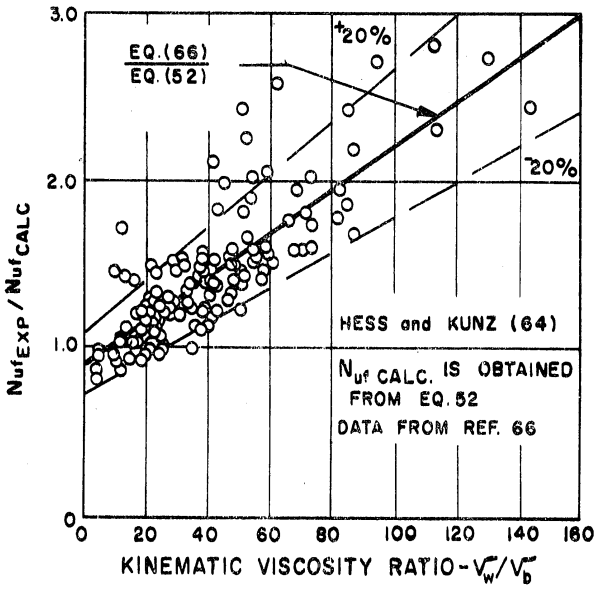

Figure 32. Comparison between Experimental and Calculated Nusselt Numbers Using Equation (52).

toward the core of the fluid". The heavy specie was taken to be a fluid at the melting point and the light specie to be that or an ideal gas. Using the concept of a "vapor" quality, X_2, to represent a mixture of these specie the mean bulk density is written

$$\frac{1}{\rho_b} = \frac{X_2}{\rho_{pg,b}} + \frac{1-X_2}{\rho_{melt}} . \qquad (67)$$

The analogy of supercritical hydrogen heat transfer with boiling is extended by introducing a modified form of the Martinelli two-phase parameter X'_{tt}, as

$$X'_{tt} = \left(\frac{1-X_2}{X_2}\right)^{0.9} \left(\frac{\mu_{melt}}{\mu_{pg,f}}\right)^{0.1} \left(\frac{\rho_{pg,f}}{\rho_{melt}}\right)^{0.5} . \qquad (68)$$

This parameter is then used to correlate heat transfer data to hydrogen in the near critical region. The correlation is in the form of plot of of $Nu_{f,exp}/Nu_{f,m}$ vs X'_{tt}, as shown in Figure 33. $Nu_{f,exp}$ is the experimental value of the Nusselt number and $Nu_{f,m}$ is computed from

$$Nu_{f,m} = 0.023\left(\frac{\rho'_{fm} V_{AV} D}{\mu_f}\right)^{0.8} \left(P_{R_f}\right)^{0.4} . \qquad (69)$$

The fluid density ρ'_{fm} is defined as

$$\frac{1}{\rho'_{fm}} = \frac{X_2}{\rho_{pg,f}} + \frac{1-X_2}{\rho_{melt}} , \qquad (70)$$

and the average velocity in Equation (69) is computed on the basis of ρ_b, Equation (67).

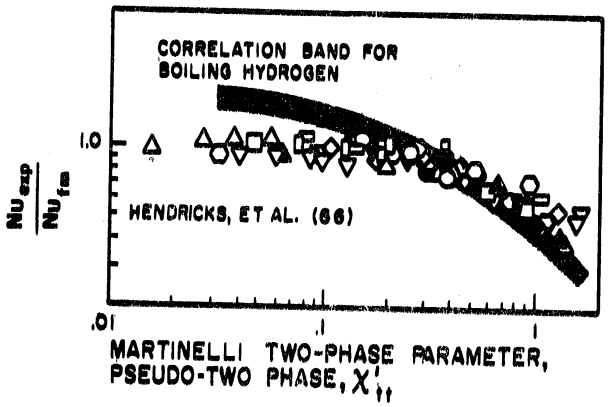

Figure 33. Correlation of Local Near Critical Heat Transfer Data Using Modified Martinelli Parameter.

As may be seen in Figure 33 the data tend to form a correlation. The range of correlation for boiling hydrogen, to be discussed later in section VII, is also shown. The same data correlated by the pseudo-film boiling hypothesis were correlated by Hess and Kunz in Figure 32. In addition, Hess and Kunz replotted the data of Hendricks, et al,[66] and obtained the following equation which fitted the data ± 20% ,

$$\frac{Nu_{f\ exp}}{Nu_{fm}} = -\ 0.21\ \log_e X'_{tt} + 0.549\ . \qquad (71)$$

this relationship is given in Figure 34.

Whether either the two correlating concepts is the "correct" one is unknown at the present. Each appears to represent the same data about equally well. In a sense both are "variable property" concepts. One gives recognition to the influence of property variation on the mechanics of the flow and the other employs an analogy with a boiling system which can be considered to have a variable mixture density. The correlation of Hess and Kunz[64] is probably a little easier to use and directs its attention more to the established principles of the mechanics of the flow.

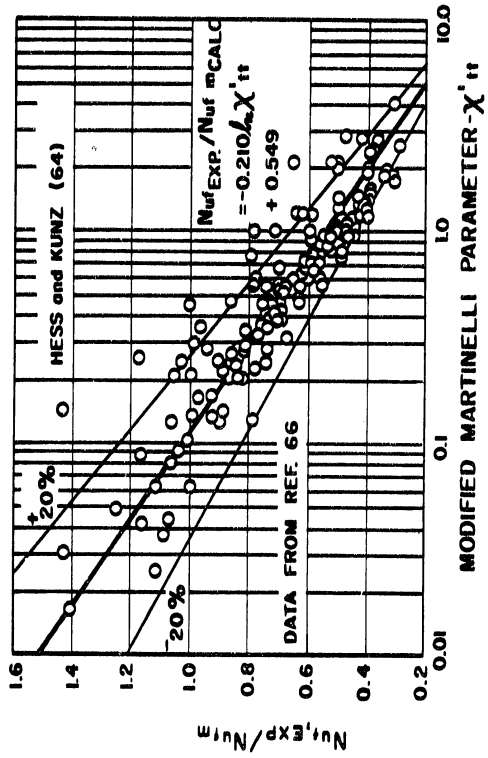

Figure 34. Pseudo Film Boiling Correlation of Reference (66).

IV. NATURAL CONVECTION PROCESSES

Natural convection describes a type of convective heat transfer process in which fluid motion is a direct consequence of bouyant and viscous forces in the fluid. The only requirements for flow is that the fluid have a temperature gradient and be in a force field such as a gravity or centrifugal field. The coupling of the fluid motion with the temperature distribution gives rise to complexities in the mathematical analysis of such processes. However, empirical correlations have been obtained which confirm those theoretical solutions that are available. It has been found that for both laminar and turbulent flow next to a heated (or cooled) surface of various geometry a correlation ($\pm$ 25%) of the following form is obtained:

$$\frac{hL}{k_f} = C \left[\frac{L^3 \rho_f^2 g \beta_f \Delta T_o}{\mu_f^2} \cdot \left(\frac{c_p \mu}{k} \right)_f \right]^n \qquad (72)$$

The term in the brackets is sometimes called the Rayleigh number and is the product of the Grashof and Prandtl numbers. The subscript f indicates that all physical properties are to be evaluated at the film temperature.

For vertical plates and cylinders the constant C and exponent n of Equation (72) are functions of the Grashof-Prandtl number product, $Gr \cdot Pr$, as shown in Table VIII below.

TABLE VIII

Gr·Pr	C	n	Type of Flow
10^4 - 10^9	0.59	1/4	laminar
10^9 - 10^{12}	0.13	1/3	turbulent

...s expression has been found to confirm experimental measurements on liquid and gaseous nitrogen.[89,90] Partial comparison of this correlation with experimental results of liqiid helium and liquid hydrogen indicate qualitative agreement, except for helium data at approximately half an atmosphere pressure. (Reference 67, p. 14).

Correlations of the form of Equation (72) are available for other geometry as well. Some of these are given by the following expressions:[74]

Horizontal cylinders, $10^3 \leq Gr \cdot Pr \leq 10^9$

$$\frac{hD_o}{k_f} = 0.53 \left[\frac{D_o^3 \rho_f^2 g \beta_f \Delta T_o}{\mu_f^2} \cdot \left(\frac{c_p \mu}{k} \right)_f \right]^{1/4} \qquad (73)$$

This equation with the constant slightly less than 0.53 correlates natural convection data from a 1-inch sphere for subcooled liquid nitrogen at 3 and 5 atmospheres.[91] These data are shown in Figure 35.

Heated horizontal square plates facing upward and cooled plates facing downward:

Laminar flow, $10^5 \leq Gr \cdot Pr \leq 2 \times 10^7$

$$\frac{hL}{k_f} = 0.54 \left[\frac{L^3 \rho_f^2 g \beta_f \Delta T_o}{\mu_f^2} \cdot \left(\frac{c_p \mu}{k} \right)_f \right]^{1/4} \qquad (74)$$

Turbulent flow, $2 \times 10^7 \leq Gr \cdot Pr \leq 3 \times 10^{10}$

$$\frac{hL}{k_f} = 0.14 \left[\frac{L^3 \rho_f^2 g \beta_f \Delta T_o}{\mu_f^2} \cdot \left(\frac{c_p \mu}{k} \right)_f \right]^{1/3} \qquad (75)$$

This expression has been confirmed experimentally for unbounded plates in force-fields resulting from system accelerations up to 21 times standard gravity.[92] Results from this investigation are given in Figure 36

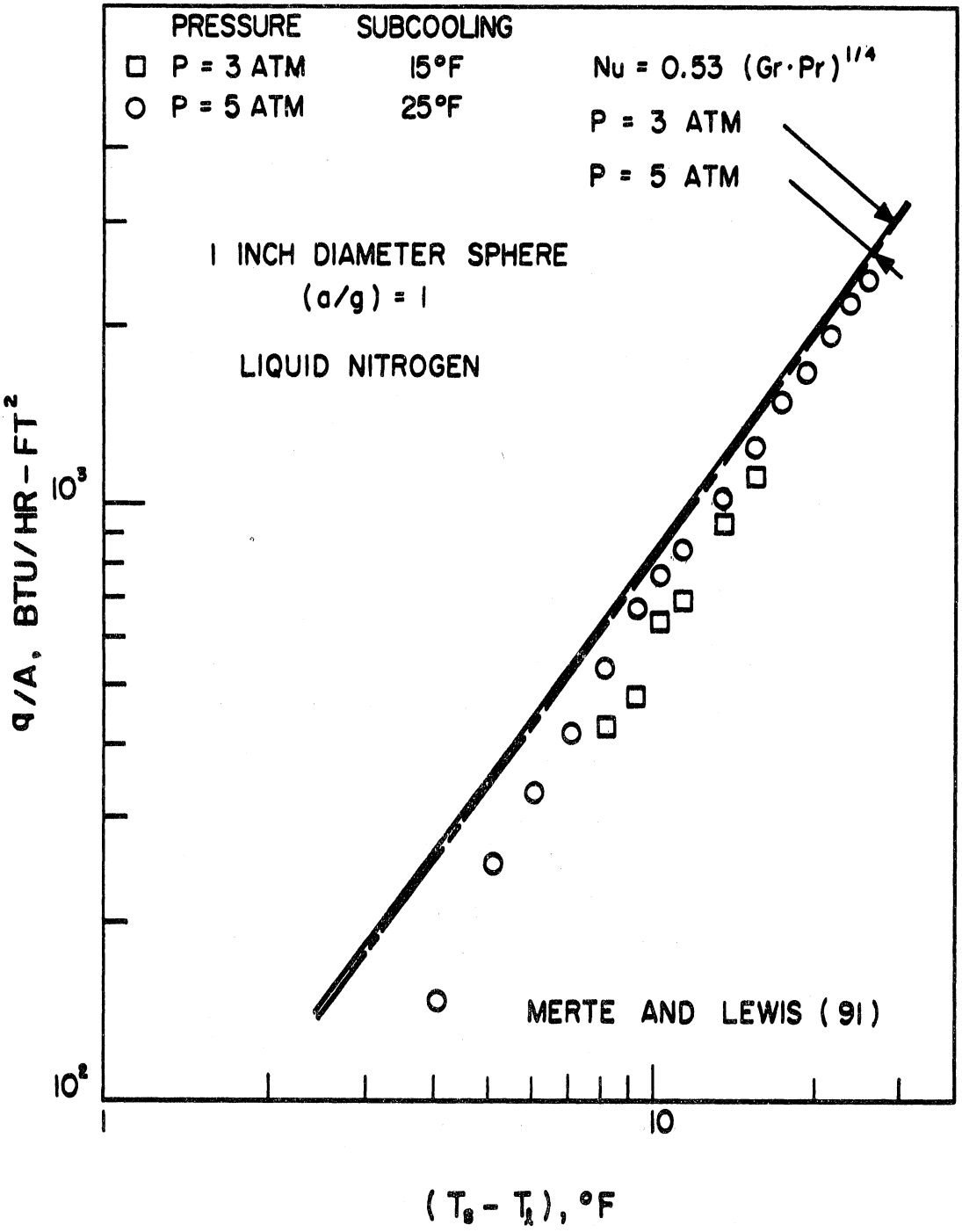

Figure 35. Heat Transfer in Natural Convection with Liquid Nitrogen.

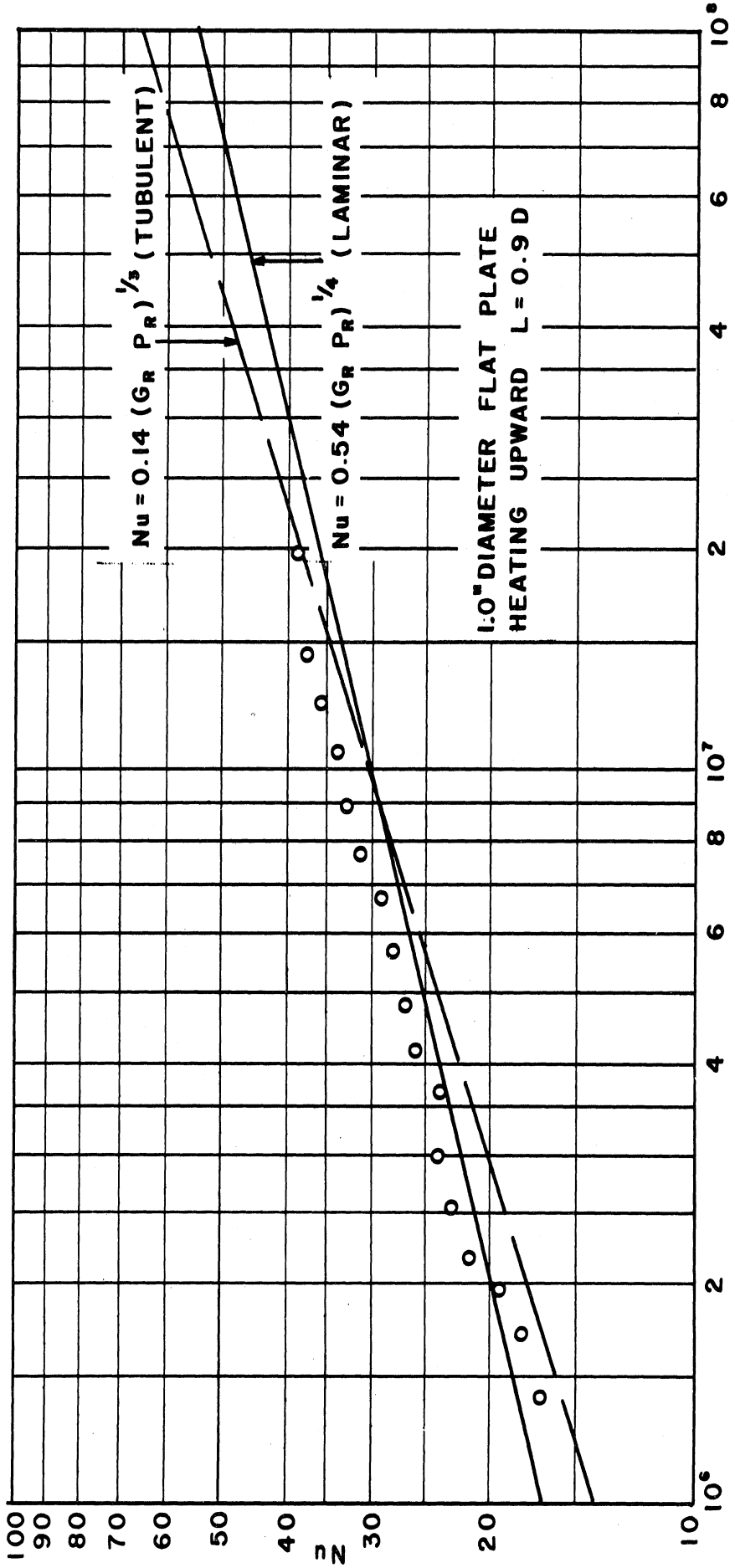

FIGURE 35a. NATURAL CONVECTION OF LIQUID HYDROGEN ON A HORIZONTAL FLAT PLATE.(260)

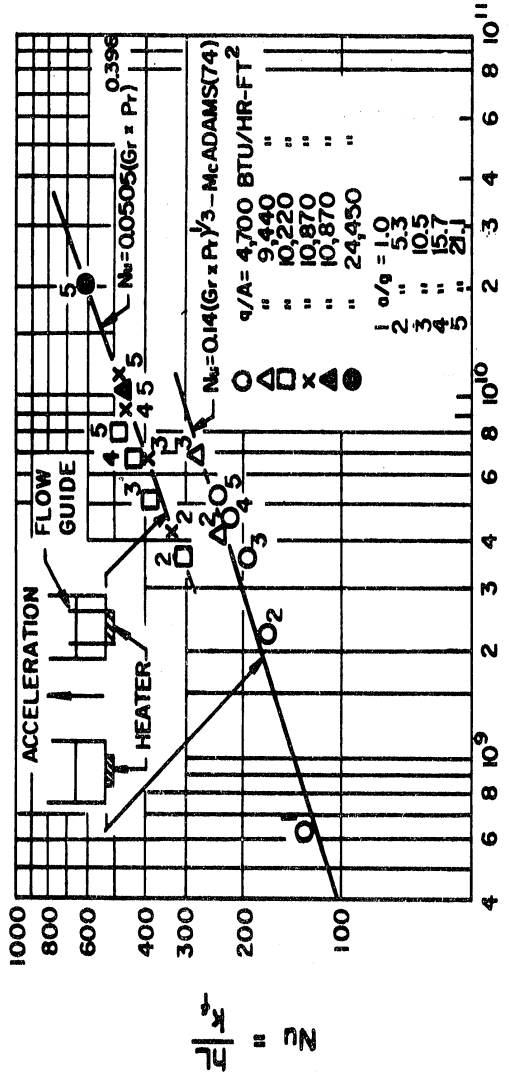

FIGURE 36. CORRELATION OF NATURAL CONVECTION DATA FOR SYSTEMS HAVING ACCELERATION NORMAL TO HEATED SURFACE.

for both a bounded and unbounded plate. The results for the bounded plate fall significantly above the correlation for the bounded plate, Equation (75), probably owing to increased eddy motion in the fluid. Similar results were found[93] for liquid nitrogen in the range a/g from 1 to 20, as shown in Figure 111. Natural convection data for liquid hydrogen on a horizontal flat plate is shown in Figure 35a. Agreement with Equations (74) and (75) is favorable.[260]

Heated square plates facing downward or cooled plate facing upward, $3 \times 10^5 \leq Gr \cdot Pr \leq 3 \times 10^{10}$

$$\frac{hL}{k_f} = 0.27 \left[\frac{L^3 \rho_f^2 g \beta_f \Delta T_o}{\mu_f^2} \cdot \left(\frac{c_p \mu}{k} \right)_f \right]^{1/4} \qquad (76)$$

The characteristic dimension L in these correlations is the edge of the plate. It will be noted that for the laminar condition, exponent of 1/4, the length dependency is weak, $L^{-1/4}$, and for the turbulent condition, exponent 1/3, it is completely absent. For non-square geometry an estimate of a mean L is recommended for use in the foregoing expressions.

During the orbital flight test of the Saturn I B, vehicle AS-203, the above correlations were found to be satisfactory for the prediction of heat transfer to liquid hydrogen and oxygen in a low gravity (a/g as low as 8×10^{-4}) environment.[94,95]

V. PRESSURIZED-DISCHARGE PROCESSES FOR CRYOGENS

During the past decade a great deal of research, engineering design effort and testing has been devoted to the problem of the pressurized-discharge of a cryogenic liquid from a container. Most of this effort has been directed at the optimization of the propellant tank design, determination of the pressurant requirements and the selection of the operating parameters for large rocket vehicles. Similar problems arise, however, in other applications such as the pressurized-transfer and storage of cryogens from vessels in ground installations. The discussion of the problems of pressurization included here will parallel that published by the author in Reference 44. Although the results are general they have been used almost exclusivly on cryogenic propellant systems for both ground and flight application.

Considerations of propellant or storage tank design and performance characteristics and the interaction of these with other sub-systems requires an examination of several related processes. Of primary importance among these are: (a) pressurization, including the calculation of the transient temperature, velocity and concentration profiles in the gas space and the flow rate and quantity of pressurant; (b) liquid stratification, including the calculation of transient temperature, velocity and concentration distribution in the liquid; and (c) interfacial phenomena, including the study and prediction of mass and heat transfer rates across gas-liquid and gas-solid interfaces. Part (b) will follow this section as Section VI and Part (c) was discussed earlier in Section II, paragraph c.

A typical flight propellant feed system to which these kinds of problems apply is shown schematically in Figure 37, taken from the paper of

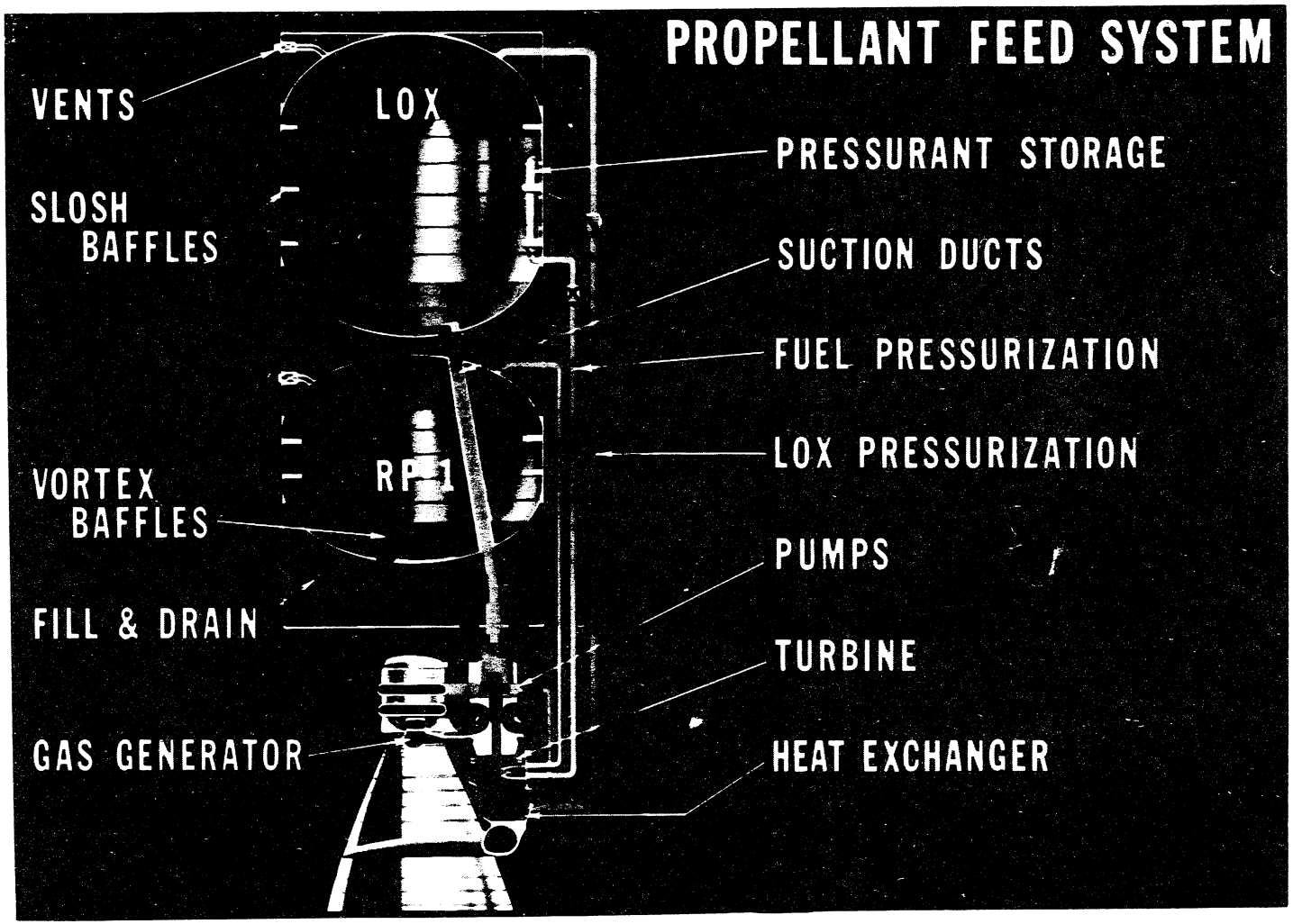

Figure 37. Typical Propellant Feed System for Flight Vehicle.

Platt, et al. (96). The liquid oxygen (LOX) tank is pressurized by a side stream of vaporized oxygen from the LOX pumps. The temperature, pressure and flow rate of gaseous oxygen (GOX) pressurant for the LOX tank is controlled by a heat exchanger and pressure regulating system. During the LOX tank discharge pressurized GOX at high temperature is introduced into the top of the tank through a diffuser, which is not shown. Heat is transferred between the LOX and the GOX as well as between these fluids and the tank walls. Mass transfer in the form of vaporization or condensation may occur between the fluids. (See Figure 14). As a result of these interactions temperature and concentration distributions are established in both the liquid and gas phases. These control the process dynamics as will as the total pressurant gas consumption and liquid heating. The level of pressure of the pressurant is governed by the vehicle structural and weight limitations and the suction head requirements for the turbo-pumps. The final residual mass of pressurant in the tanks at the end of engine firing is fixed by its pressure and mean temperature. It is desired, of course, to keep this mass of pressurant at a minimum. Temperature stratification in the liquid, if severe, can cause reduced engine burning time or loss of thrust owing to pump cavitation resulting from the passage of warmer liquid from the region of the LOX-GOX interface through the pumps.

Because of oscillations imparted to the vehicle during flight, baffles are mounted inside the tank to reduce the sloshing tendency of the propellants. The effect of sloshing and splashing is to break up the layer of heated liquid at the interface. This results in rapid condensation of the pressurant and consequent undesirable fluctuations in tank pressure and pressurant flow rate.

An indication of the importance of the pressurizing system to flight vehicle weight is shown in Figure 38, which is from a study by Nein and Thompson (60) The representation presented in this figure shows an approximate relationship between vehicle thrust and the mass/pressure ratio of the pressurant for several large rocket systems. For a Saturn V S1C Stage LOX tank pressure of about 22 psia at engine cut-off, for example, the mass of pressurant remaining in the LOX tank would be approximately 4500 pounds. Should the vehicle design be altered by reversing the relative positions of the LOX and fuel tanks a higher pressure would be required in the LOX to supply sufficient suction head for the turbo-pumps. An increase in tank pressure to 64 psia, for example, would result in a residual pressurant in the Saturn V S1C Stage of approximately 12,800 pounds. Figure 38 also shows the relationships between GOX, helium and LOX self-pressurization systems. Weight penalties are evident in the later two in comparison with a system using a heated GOX pressurant.

For purposes of classification the analytical approaches to the calculation of the pressurant properties in a pressurized-discharge process will be divided into two classes, namely, (a) distributed systems and (b) lumped systems. A distributed system is one in which the temperature, composition, velocity or pressure are determined as functions of both space and time within the gas space. Such an analysis is the most general and usually provides the greatest amount of information concerning the process. The calculations are produced from rate-type (non-equilibrium) equations of mass, energy and momentum. Although for many purposes such analysis as these are the most desirable, they also are the most complex and often involve parameters and terms about which little is generally known 'a priori. Analytical

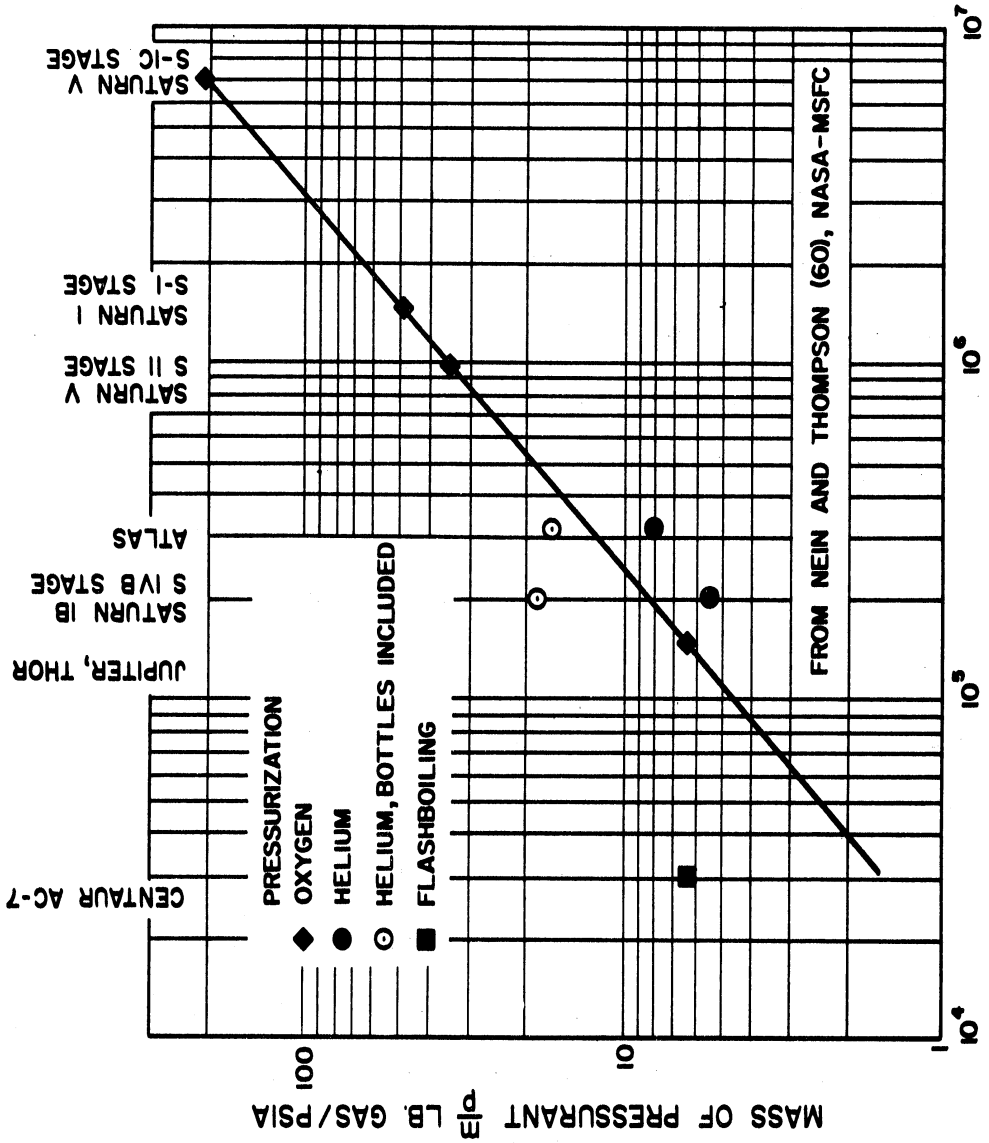

Figure 38. Relationship Between Vehicle Thrust and Final Oxygen Tank Pressurant Mass-Pressure Ratio.

solutions of this kind in one-dimensional space and in time, which have the advantages of exactness and the disadvantages of certain idealizations, include the work of Arpaci, et al. (97, 98) and Clark, et al. (99). Arpaci (100) has presented an analysis of the gas space processes including axial heat transport, interfacial heat transfet and wall heat transfer. Recently numerical methods using the finite-difference approximation programmed on a digital computer have been employed to compute the gas space processes. Notable a among these is the paper by Epstein, et al. (101) and a paper by Roudebush (102). Owing to the considerable flexibility of the finite-difference approximation this method represents a fruitful approach to the calculation of pressurization phenomena for propellant tank design.

A lumped-system is one in which only the mean properties of the gas space and tank wall are determined. Hence, such a property as the gas temperature is not found as a function of position within the gas space but rather the mean gas temperature is computed as a function of time only. Sometimes the calculation consists of determining over-all changes resulting from specified displacements of gas volume. These analyses are basically thermodynamic (equilibrium) in character and provide the minimum amount of useful information. Lumped-system studies have been reported by Burke, et al. (103), Moore, et al. (104), Bowersock and Reid (105), Bowersock, et al. (106), Humphrey (107), Gluck and Kline (61), Coxe and Tatom (108), Canty (109) and Momenthy (110). Most of these authors also report experimental data. Papers which are primary experimental in nature include the work of Van Wylen, et al. (111), Fenster, et al. (112), Oridn, et al. (113) and Nein and Head (114).

For our present purposes emphasis will be placed on analysis or a distributed system.

In a series of two papers Arpaci, et al. (97, 98) have presented an analytical solution of the transient processes within the gas space of a pressurized-discharge system which predicts the response of both the gas, $T(x,t)$, and the wall, $T_w(x,t)$, as functions of space and time. This work appears to be the only analytical solution of a distributed character available. As such it possesses all the advantages of an exact solution, namely, it is continuous in space and time, it is subject to parameterization, it can be used to judge the completeness of an approximate solution and it can be employed with confidence to determine the influence of a single variable. Exact analytical solutions also are beset with inherent disadvantages as well. Among these are the limitations on the solution resulting from certain idealizations necessary to make the problem mathematically tractable. The analytical results are fairly complicated to use and require several tabulated or plotted functions to carry out numerical calculations. However, the idealizations are chosen to fit a great many practical systems and the results can be employed to evaluate experimental data and used in certain design and pre-design calculations. This method has been used by the NASA - Marshall Space Flight Center for preliminary design on the Saturn V, S1C stage and other designs.

A unique feature of the results in Reference 98, which are an extension of those in Reference 97, is the allowance made in the computations of $T(x,t)$ and $T_w(x,t)$ for completely arbitrary and simultaneous time-dependent inputs of (1) inlet gas temperature, $T_g(t)$, (2) ambient temperature, $T_o(t)$, and/or (3) ambient heat flux $(q/A)_o(t)$. The analytical model and the nature of the arbitrary time-dependent inputs which may be handled by this solution are shown in Figure 39. The idealizations imposed on the analysis are constant physical properties, including gas density, constant discharge rate, constant cross sectional area of container, constant pressure and

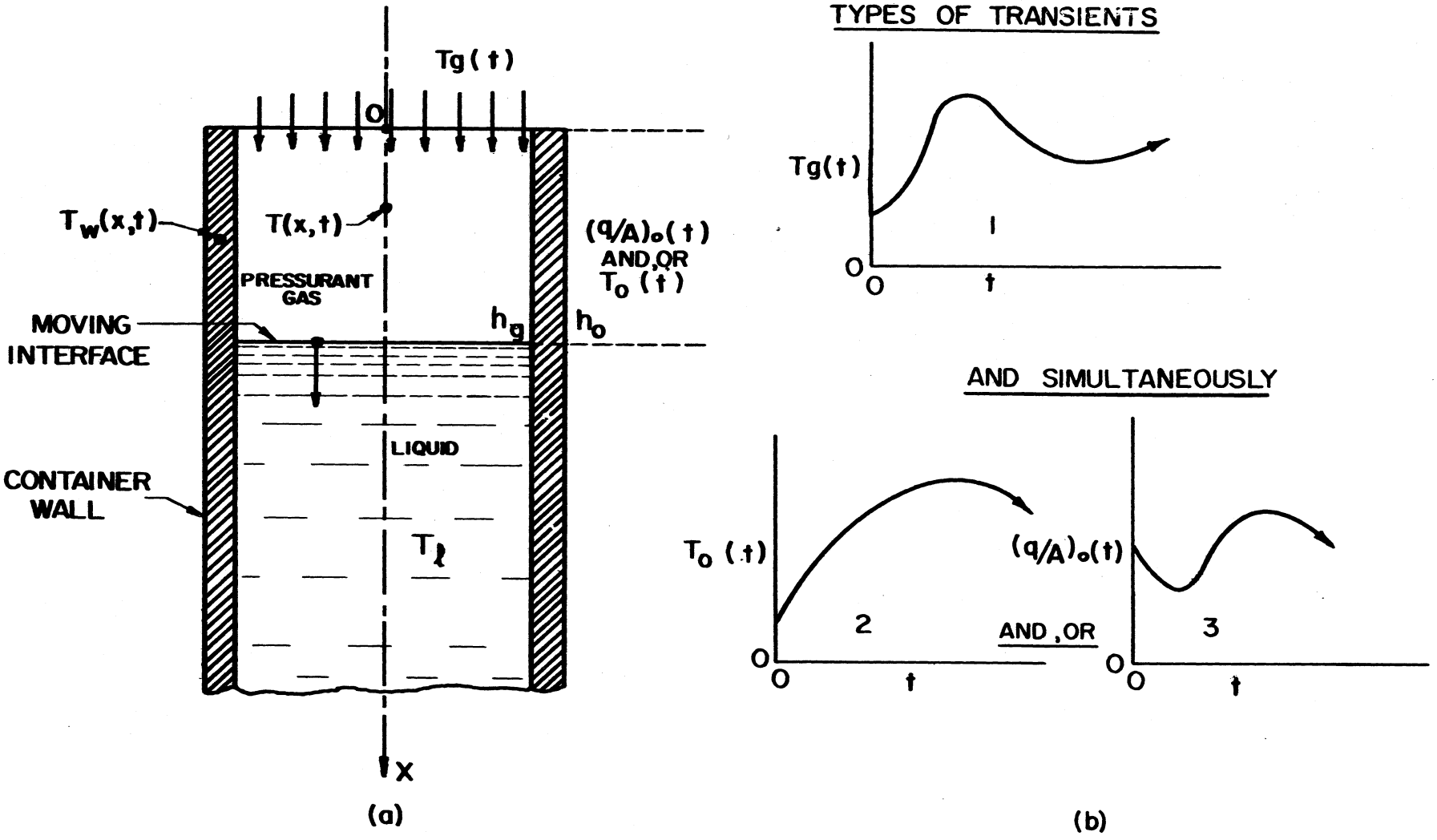

Figure 39. Analytical Model and Time-Dependent Inputs for the Analysis of Arpaci, Et. Al.(98)

constant heat transfer coefficients.* The imposition of constant gas density is less severe than may first appear since the effects of this can be adequately circumvented by an iterative process of calculation described in Reference 97. In terms of dimensionless space and time variables, s and δ, and the dimensionless parameter η, the response of the pressurant gas and wall temperatures to these simultaneous, arbitrary, time-dependent inputs of the type 1, 2 and 3, Figure 39, are written,

$$T(s,\delta,\eta) - T_\ell = T_1(s,\delta,\eta) + T_2(s,\delta,\eta) + T_3(s,\delta) \qquad (77)$$

and

$$T_w(s,\delta,\eta) - T_\ell = T_{w_1}(s,\delta,\eta) + T_{w_2}(s,\delta,\eta) + T_{w_3}(s,\delta) \qquad (78)$$

Expressions for $T_1 \ldots T_3$ and $T_{w_1} \ldots T_{w_3}$ are given (98) for arbitrary forms of the time-dependent inputs. Of particular interest is the linear time-dependent input disturbance of the form,

$$D(\delta) = D(0) + \frac{D(\delta_1)-D(0)}{\delta_1}\,\delta, \qquad (79)$$

as shown in Figure 40. The various forms of the disturbance $D(\delta)$ are summarized in Table IX. The temperatures $T_1 \ldots T_3$ and $T_{w_1} \ldots T_{w_3}$ of Equations (77) and (78) for the linear disturbances in inlet pressurant gas temperature (D_1), ambient temperature (D_2) and ambient heat flux (D_3) are given in terms of functions $F_1 \ldots F_3$, $f_1 \ldots f_3$, $G_1 \ldots G_3$ and $g_1 \ldots g_3$, which are functions of s, δ and η and defined and plotted in Reference 98.

*An axial variation in gas temperature only is considered in this analysis and in others. Radial variations have been shown to be small in test models of Saturn I and 1/3 scale model of Saturn V LOX tanks (60) and in smaller containers (97).

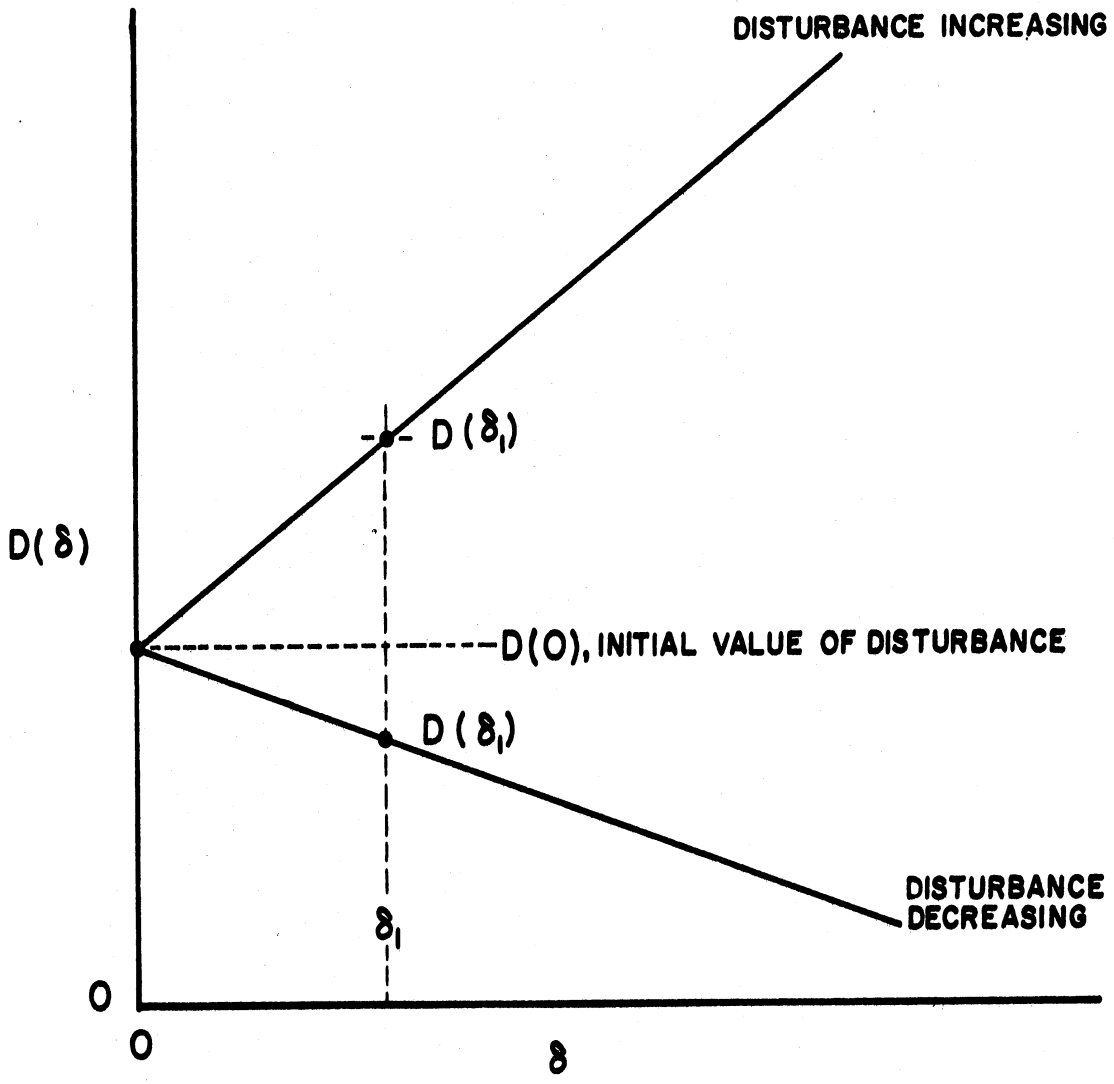

FIGURE 40. LINEAR TIME-DEPENDENT DISTURBANCE

TABLE IX

SUMMARY OF LINEAR DISTURBANCE FUNCTIONS

Case	Symbol	Type of Transient Disturbance	$D(0)$	$\frac{D(\delta_1)-D(0)}{\delta_1}$
1	D_1	Inlet Pressurant Gas Temp. $T_g(\delta)$	$T_g(0) - T_\ell$	$\frac{T_g(\delta_1)-T_g(0)}{\delta_1}$
2	D_2	Ambient Temp. $T_o(\delta)$	$T_o(0) - T_\ell$	$\frac{T_o(\delta_1)-T_o(0)}{\delta_1}$
3	D_3	Ambient Heat Flux $(q/A)_o(0)$	$\Phi(0) = \frac{(q/A)_o(0)p_o}{h_g\, p}$	$\frac{[(q/A)_o(\delta_1)-(q/A)_o(0)]}{\delta_1}$ $\frac{p_o}{h_g}$

The importance of the linear time-dependent disturbance may be seen in Figure 41 where an arbitrary disturbance in $T_g(\delta)$ is represented by a piece-wise fit of several linear combinations. In Reference 98 a method is outlined for computing the response of the pressurant gas and the wall temperatures for a typical disturbance as that shown in Figure 41. It is based on the superposition of solutions to linear systems.

The influence of h_g, the gas space heat transfer coefficient, was demonstrated in Reference 97 for an insulated container. The results are reproduced in Figure 42 showing the gas space mean temperature at the end of discharge as a function of h_g for the experimental system of Reference 97. This indicates that above a certain value of h_g the influences of this parameter is diminished.

A knowledge of h_g is necessary to carry out calculations of $T(x,t)$ and $T_w(x,t)$ using this method and most of the others. As may be seen from Figure 42 there is a range of h_g in which its influence is quite significant.

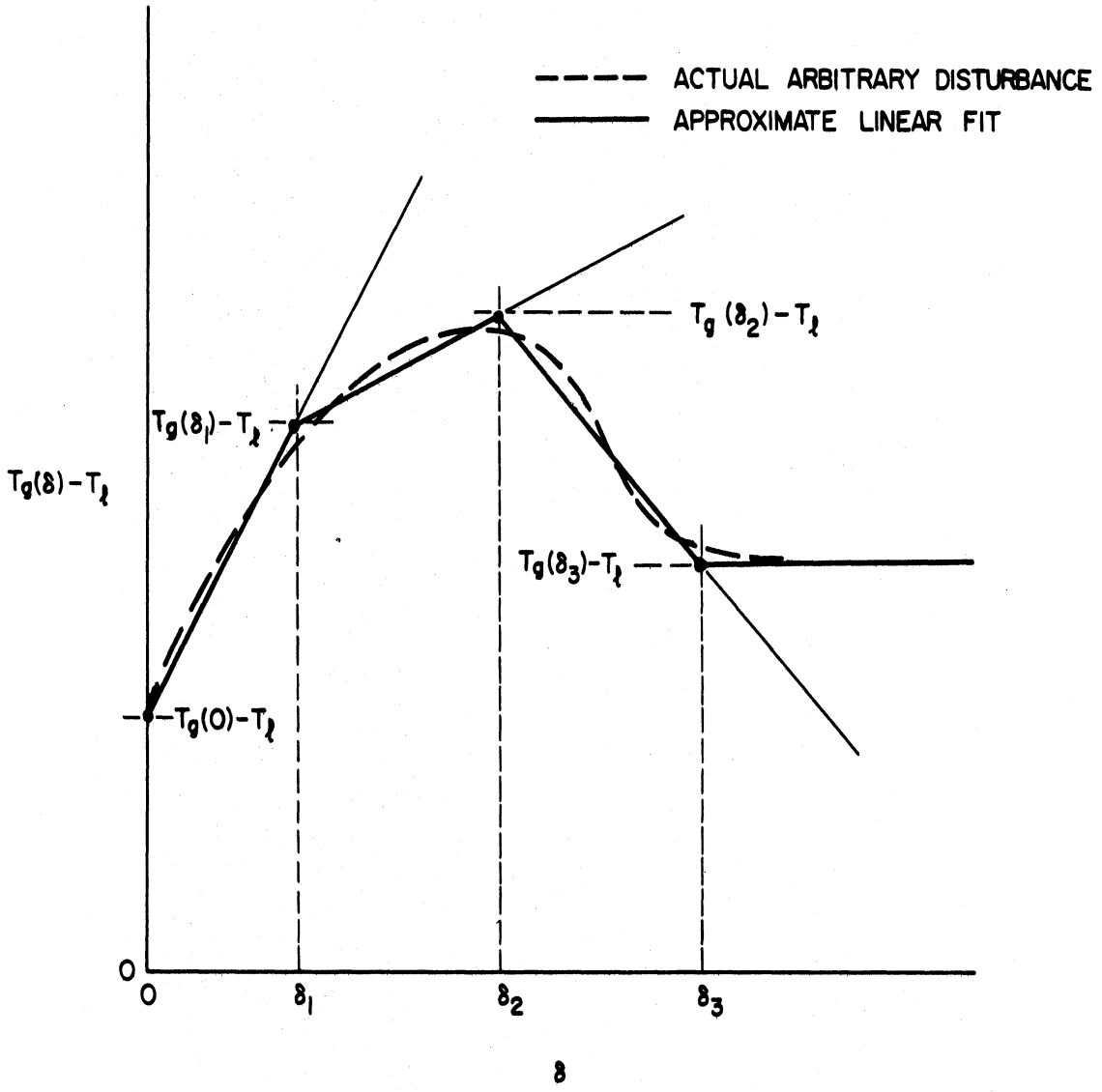

FIGURE 41. LINEAR PIECEWISE FIT TO AN ARBITRARY DISTURBANCE IN $T_g(\delta) - T_\ell$

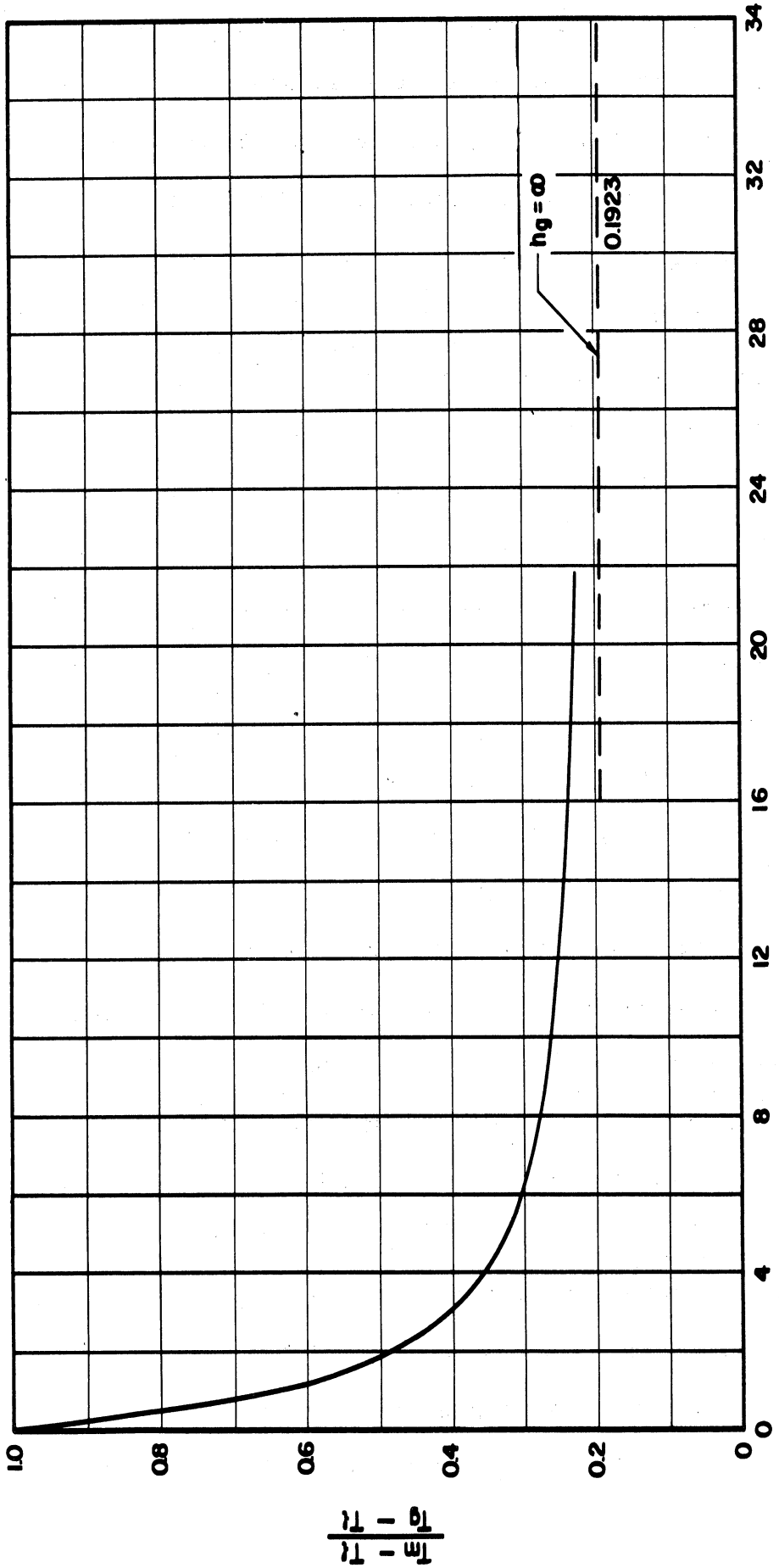

FIGURE 42. INFLUENCE OF h_g ON SPATIAL MEAN GAS TEMPERATURE FOR THE CONTAINER GEOMETRY OF FIGURE 43

Hence it is very important to have reliable estimates of the gas space heat transfer coefficient. Various approaches have been employed to obtain numerical values for h_g, none of them entirely satisfactory. In the experiments described in Reference 97 the theoretical curves for various values of h_g were superimposed on the experimental results in order to find an approximate fit for the suitable value of h_g which describes the experiments. For that system (liquid N_2 - gaseous N_2) the suitable value of h_g of 2 Btu/hr-ft^2-F adequately represented the data (see Figure 8, Reference 97). This is approximately the value one would obtain from natural convection heat transfer correlations and is reasonable in view of the low velocities expected in the gas space. In other systems, of course, different values of h_g must be expected depending on the type of pressurant, its flow rate and diffuser-tank design and arrangement.

The comparison of the theory (97) for a step-change in inlet gas temperature with the experimental results on a small insulated container (1 foot dia., 3 foot long) is given in Figure 43 for a LN_2 - GN_2 system and inlet gas temperatures from 200 to 1000 R. The same theory is compared with test data from Saturn I mock-up tanks 6.5 feet in dia. and 39 feet long in Figure 44 for various values of h_g (60). In this case h_g of 10 Btu/hr-ft^2-F represents the data very well. Experimental measurements in the same tank also indicated a heat transfer coefficient of about 10 Btu/hr-ft^2-F for the GOX pressurant.

In an attempt to avoid the limitations of the analytical solutions, Epstein, et al. (101) have presented a numerical method for calculation of the pressurization process. The computer program (101) has been modified by the NASA Marshall Space Flight Center to improve its correlation with test

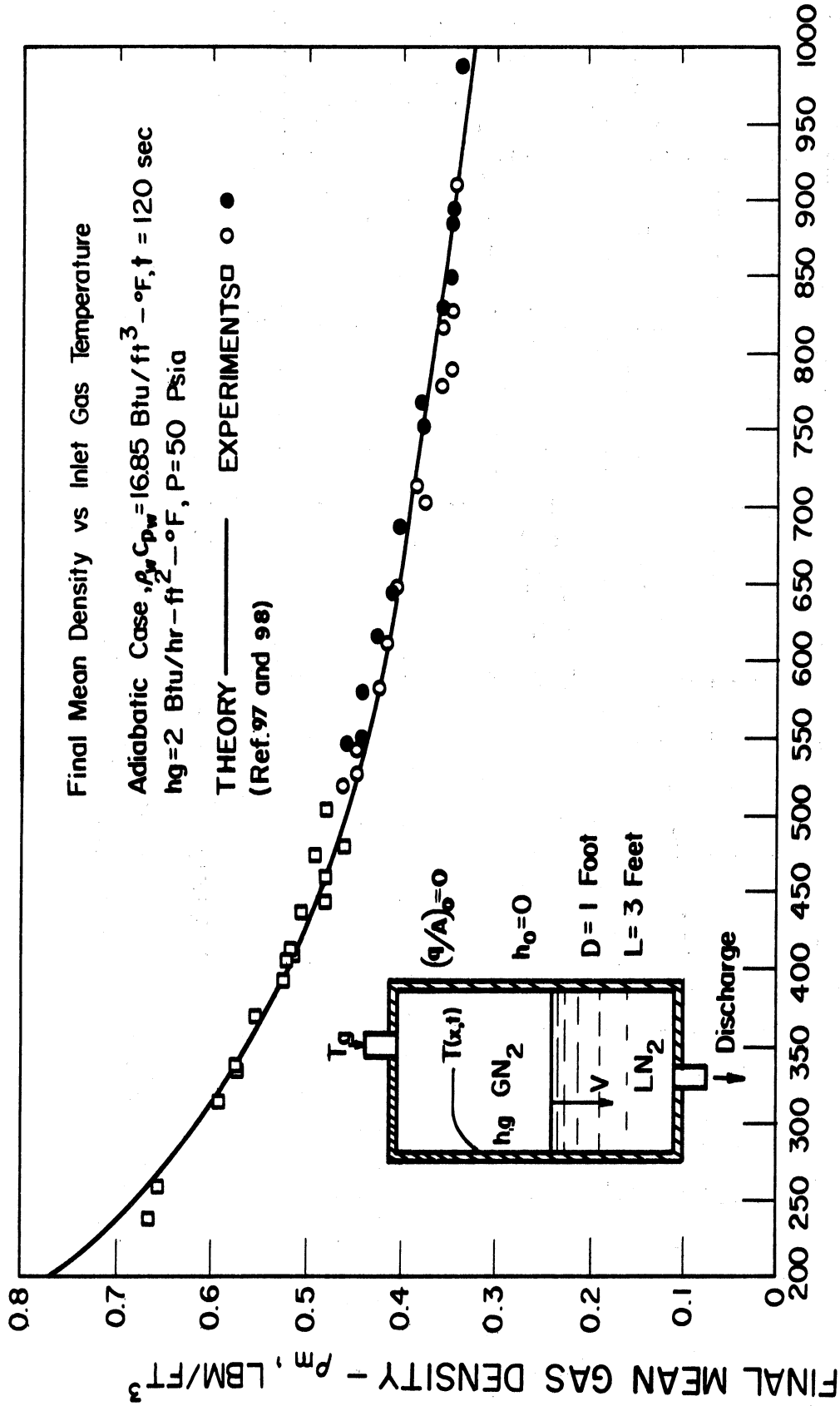

Figure 43 Comparison of Theory and Experiment for Pressurized-Discharge in Small Containers for Nitrogen as Pressurant.

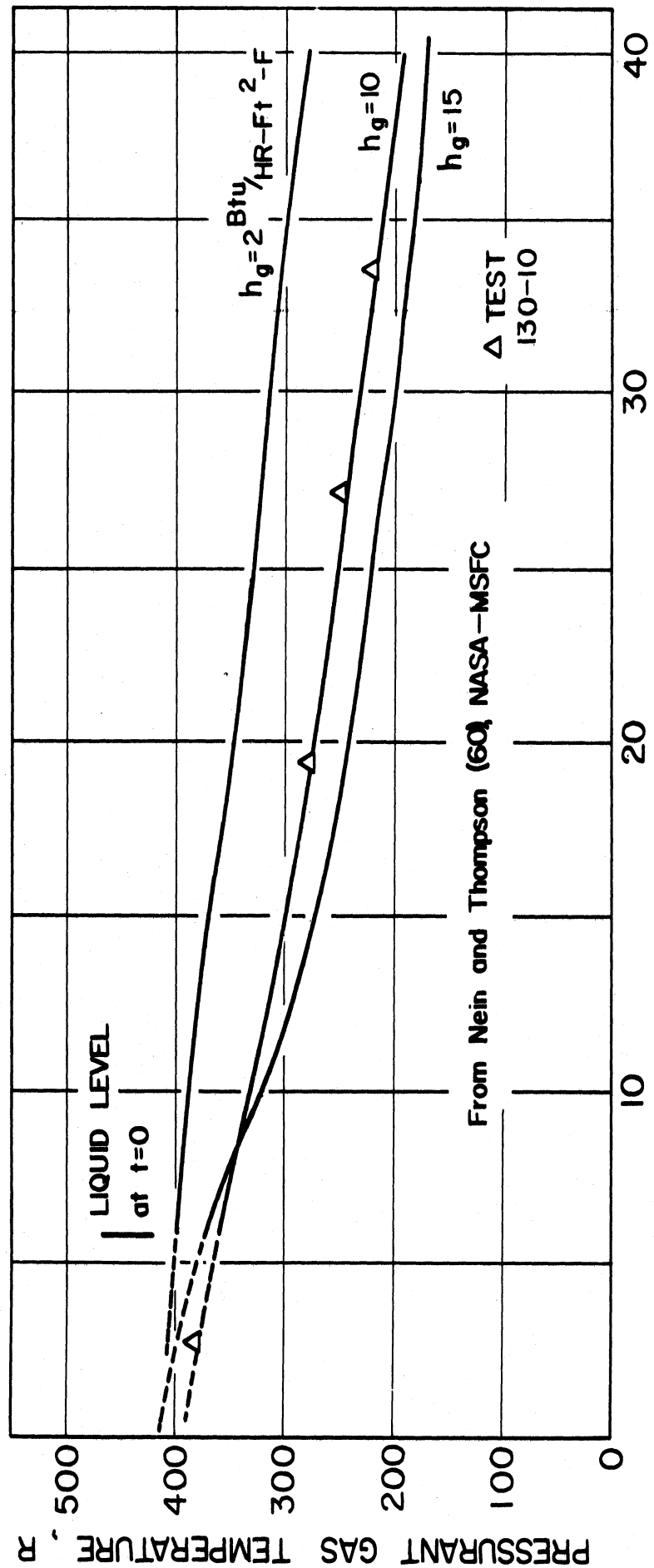

Figure 4 Comparison Between Experimental and Computed Pressurant Gas Temperature Gradient Facility 2, Oxygen as Pressurant, D = 6.5 Feet, L = 39 Feet

data on large tanks (60, 115). Comparison of these computer calculations with experimental data is given in Figure 45 which includes flight test data from Saturn SA-5. As can be seen a reasonable agreement is obtained for pressurant gas temperature distribution and pressurant flow rate. A distinct advantage of this computer program is that one output is the pressurant flow rate in terms of inputs such as measured propellant tank pressure and inlet temperature.

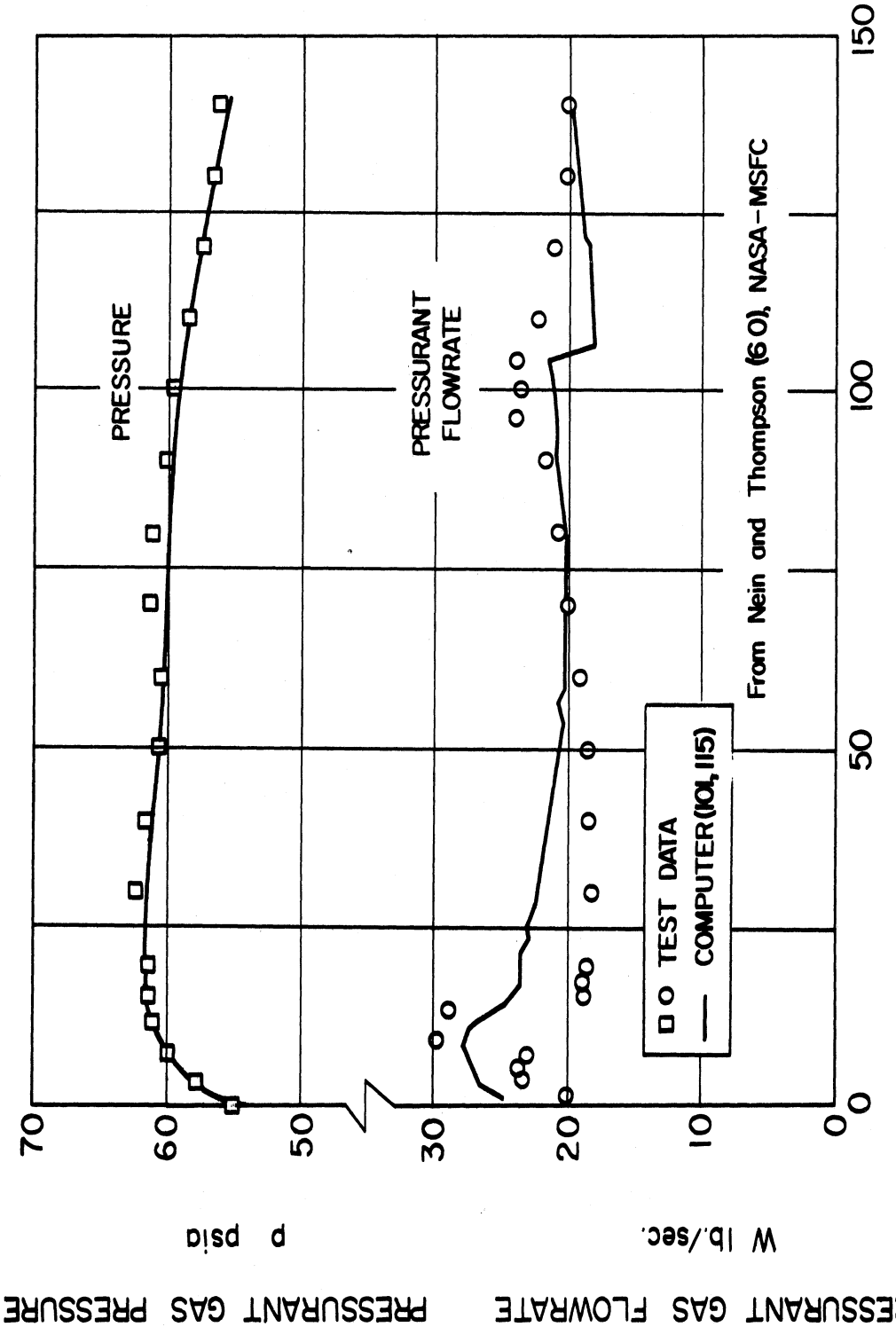

Figure 45 Comparison Between Experimental and Computed Pressurant Gas Flowrate Facility 1, SA - 5 Flight Test, Oxygen as Pressurant

VI. STRATIFICATION IN CRYOGENIC VESSELS

Thermal stratification of a cryogenic liquid in a vessel results from external heat exchange and consequent non-equilibrium phenomena within the liquid. In both flight vehicles and storage containers the most dominant influence is heat transfer through the (vertical) side walls of the vessels. Other effects may be important as well, such as nuclear energy absorption within the liquid, heating from the bottom of the vessel and both heat and mass exchange between the liquid surface and the pressurant. The phenomena of thermal stratification is important to propellant tank design and operation as it influences the selection of venting devices, insulation, pumps and tank structure, among others. The pressure in the tank is directly related to the interface temperature which is established by the convective transport processes with the tank. In the case of liquid hydrogen a 1°R increase in the liquid-vapor interface temperature represents approximately a 3 psi increase in tank pressure. As a result of stratification the pressure in cryogenic vessels has been found to be significantly greater than that corresponding to the vapor pressure at bulk (mixed) liquid temperature (58, 116, 133).

This discussion of stratification will follow that presented by the author in Reference (44) and will include certain new information which has recently become available.

Stratification is caused by the natural convective flow of heated liquid along the side-walls of a tank and into the upper regions near the liquid interface. Here it flows toward the center of the tank, dispersing and mixing, and causing a downward penetration of heated liquid, the depth of which increases with time. This depth is known as the thermal stratification layer. These processes of natural convective flow and mixing are extremely

complex and presently not well understood and only imperfectly described. Anderson and Kolar (117) have shown that the stratification pattern is very dependent on whether the liquid heating is from the side-wall, bottom or by internal absorption of energy. Schlieren photographs indicate that side-wall heating produces the greatest amount of thermal stratification. Schwind and Vliet (118) have taken schlieren and shadowgraph photographs of the natural-convective processes resulting from side-wall heating at various levels of heat flux. A boundary layer type phenomenon was observed with vortex motion in the regions where the flow changes direction. Experimental measurements of liquid hydrogen stratification are presented by Barnett, et al. (119) on a full size propellant tank from the Saturn S-IV stage.

As a result of these observations plus the application of physical intuition most analytical approaches to the prediction of stratification processes have started with the assumption of boundary layer flow along the wall. Essentially all analysis has been for side-wall heating only with uniform heat flux. Both laminar and turbulent layers have been studied. The model most commonly employed for these analyses is shown in Figure 46. Owing to a side-wall heat flux, $(q/A)_o$, a boundary-layer forms at $x = 0$, growing in thickness δ as it develops along the wall, intersecting with the bottom of the stratified layer, $A(t)$, and finally mixing with the stratified layer itself of volume $V(t)$. The unmixed bulk liquid is uniform at its initial temperature and the various analyses assume the heated stratified layer to be both mixed and unmixed at a higher temperature.

While the boundary layer type of flow may seem reasonable, it should be pointed out that analysis based on this assumption usually proceeds from the application of boundary layer theory to transient internal flows taken from steady-flow results on a vertical flat plate in an infinite, uniform

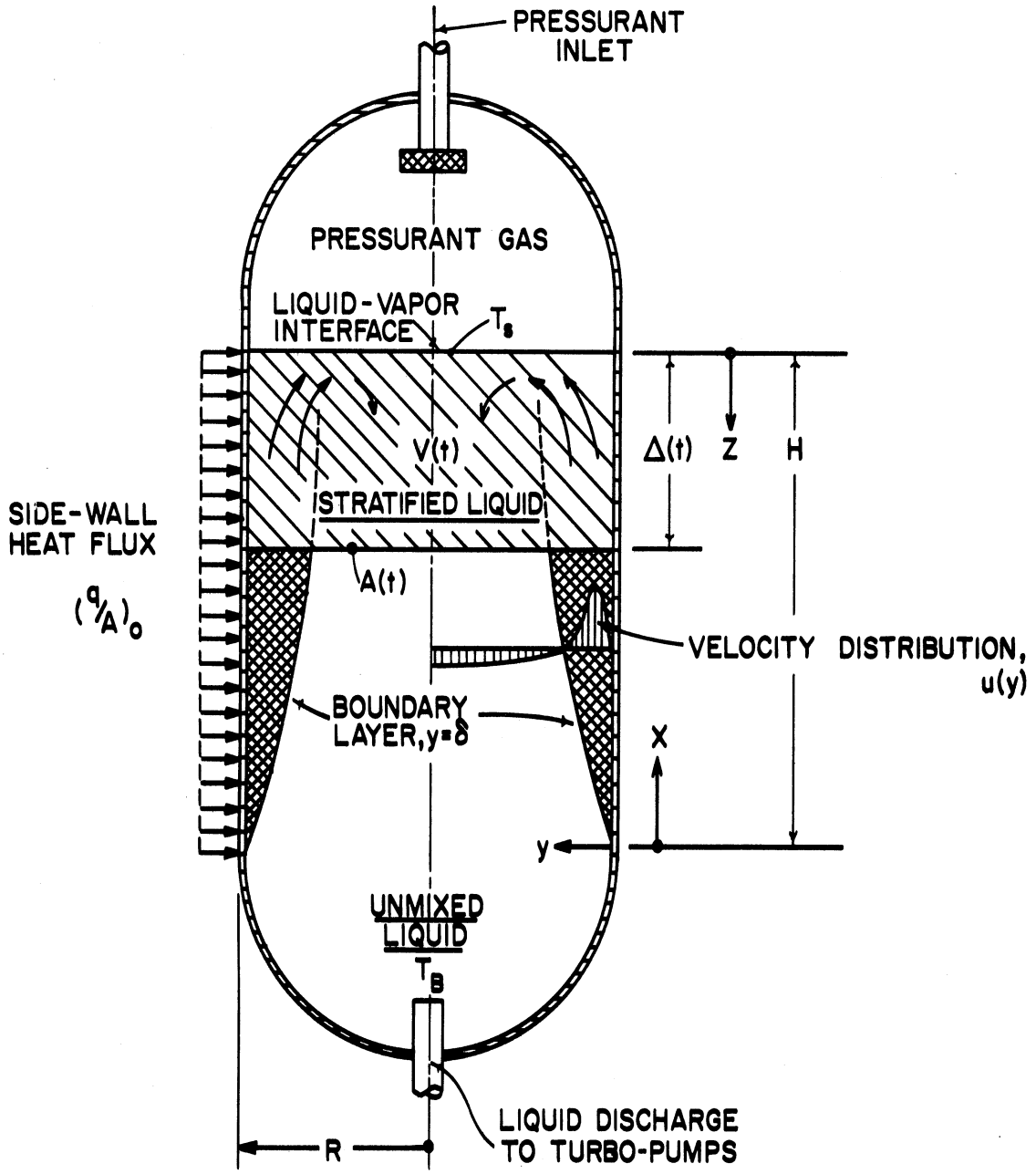

Figure 46. Typical Analytical Model for Liquid Stratification Analysis.

$$\frac{T_s - T_B}{(q/A)_o\,(H/k)} = \frac{2(H/R)}{I\ Pr\ \frac{\Delta(t)}{H}} \left(\frac{\upsilon t}{H^2} \right) \tag{80}$$

where,

$$I = \int \psi\, d\eta \tag{81}$$

$$\psi = \frac{T(z) - T_B}{T_s - T_B} \tag{82}$$

$$\eta = \frac{z}{\Delta(t)} \tag{83}$$

According to assumption (5), ψ should have "similarity" characteristics, i.e. constant values for a given η, in which case its integral I ought to be constant also. Experimental measurements of centerline temperatures during heating are shown in Figure 47 for a single run and in Figure 48 for several runs. The requirement for a constant value of I is met reasonably well over a broad range of modified Grashof numbers and it does not appear to be significantly influenced by Prandtl number. The break in the function at Gr^*_H of about 10^{11} may be a result of transition in the flow near the boundary.

For constant sidewall heat flux the principal scaling parameter governing the process is a modified Rayleigh number, Ra^*_X, the product of a modified Grashof number, Gr^*_X, and the Prandtl number, Pr. Hence,

$$Ra^*_X = Gr^*_X \cdot Pr = \frac{g\beta(q/A)o\ X^4}{k\upsilon^2} \left(\frac{c_p \mu}{k} \right) \tag{84}$$

Boundary layer transition from laminar to turbulent flow occurs at a modified Reyleigh number of approximately 10^{11} (120).

To carry out calculations using Equation (80) it is necessary to have information on $\Delta(t)/H$. This is provided by an analysis of the boundary layer flow, and the results depend on whether the boundary layer is laminar or turbulent. The following result is based on the need

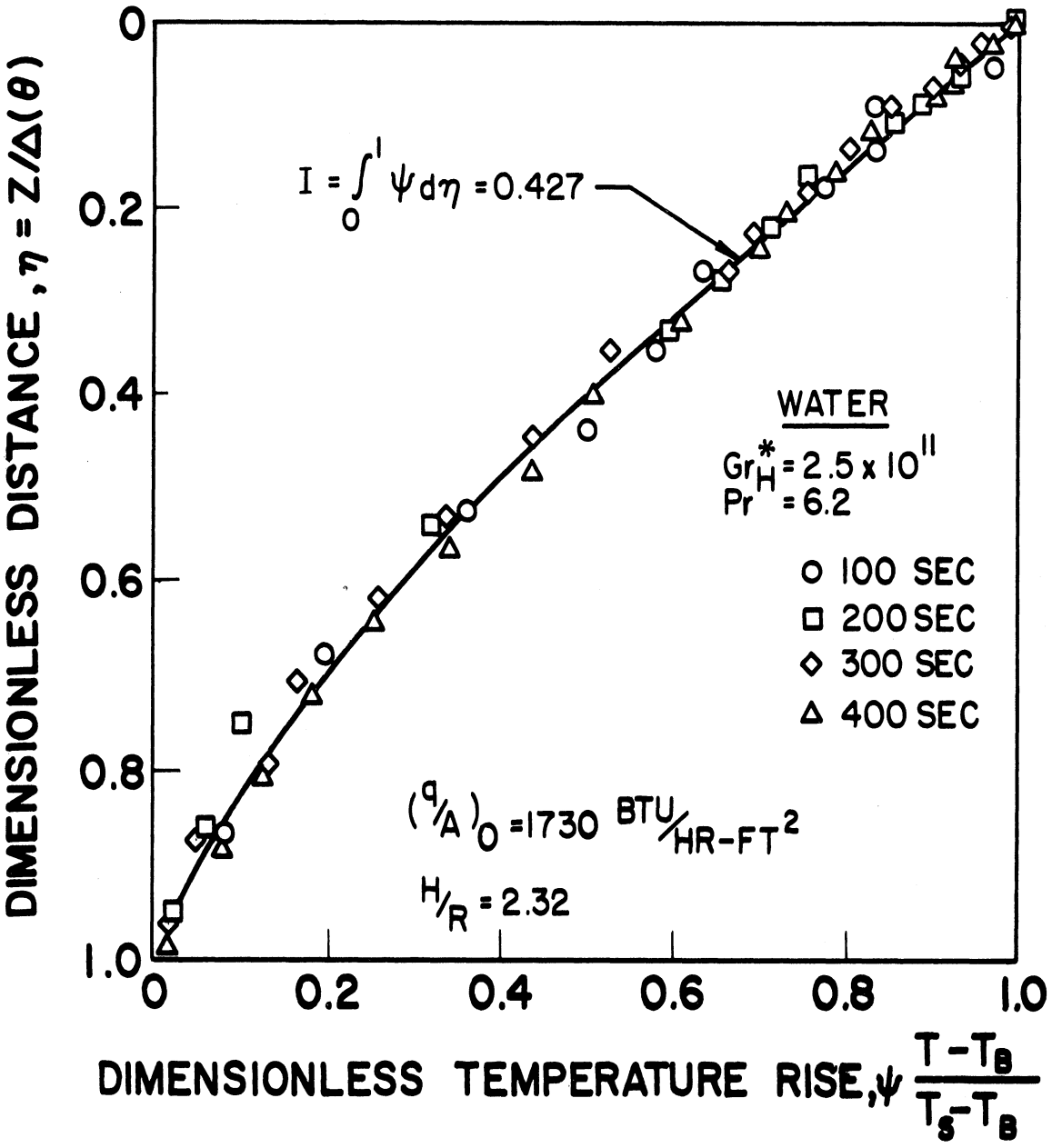

Figure 47 Dimensionless Stratification Temperature Profiles (120).

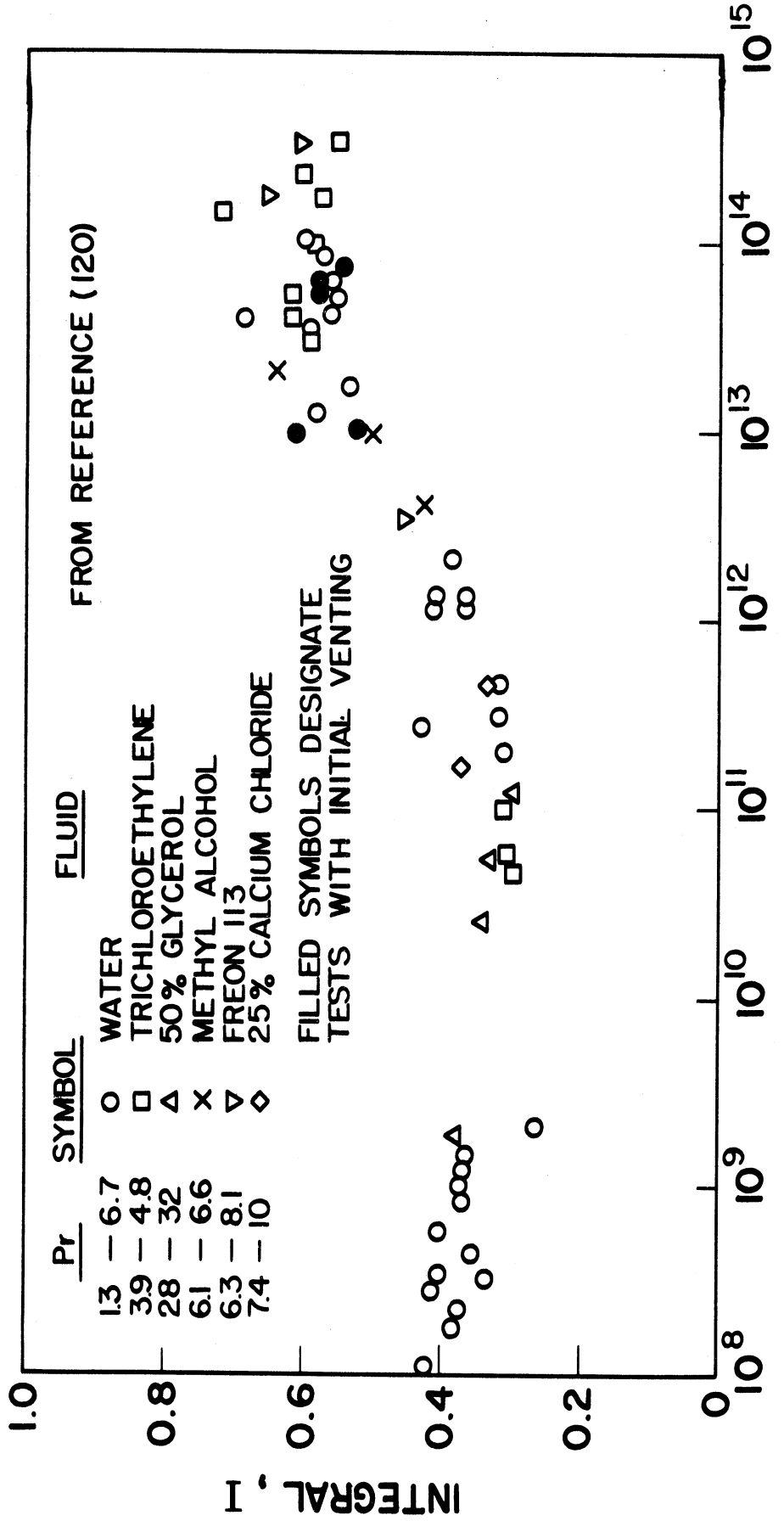

Figure 48 Energy Integral I as a Function of Modified Grashof Number for Prandtl Numbers Between 1.3 and 32 (with H/R = 2.3) (120)

to satisfy continuity requirements in the vessel. It is assumed that the rate of mass flow in the boundary layer at the plane $A(t)$ is identical with the rate of change of mass within the stratified layer of volume $V(t)$. Hence,

$$\left(2\pi R \int_0^{\delta} \rho u \, dy \right)_{x = H - \Delta(t)} = \frac{d[\rho V(t)]}{dt} = \pi R^2 \frac{d[\rho \Delta(t)]}{dt} . \qquad (85)$$

If the density is assumed to be constant, then this becomes,

$$\left(2\pi R \int_0^{\delta} u \, dy \right)_{x = H - \Delta(t)} = \pi R^2 \frac{d\Delta(t)}{dt} . \qquad (86)$$

Equation (86) is integrated using velocity distributions for both laminar and turbulent boundary layers. For the case of turbulent flow the result is (120),

$$\frac{\Delta(t)}{H} = 1 - \left(1 + 0.0924 \left(\frac{H}{R} \right) \frac{(\upsilon t / H^2)}{Pr^{2/3}} \left(\frac{Gr^*_H}{1 + 0.443 \, Pr^{2/3}} \right)^{2/7} \right)^{-7} \qquad (87)$$

This equation is compared with experimental data in Figure 49, where $\Delta(t)$ was determined from measurements of centerline temperature and time-zero corresponded with the instant the surface temperature started to increase. The general nature of the agreement with the shape and form of the data should be noted, although Equation (87) consistently predicts smaller stratification layers than those measured. It should be noted that in Equation (87) $\Delta(t)$ equals H only at infinite time, a circumstance which limits its application to small times following the start of transient. Equation (87) can be used in Equation (80) to compute surface temperature transients. It will be noted that the result in (87) is independent from that in (80), but the reverse is not

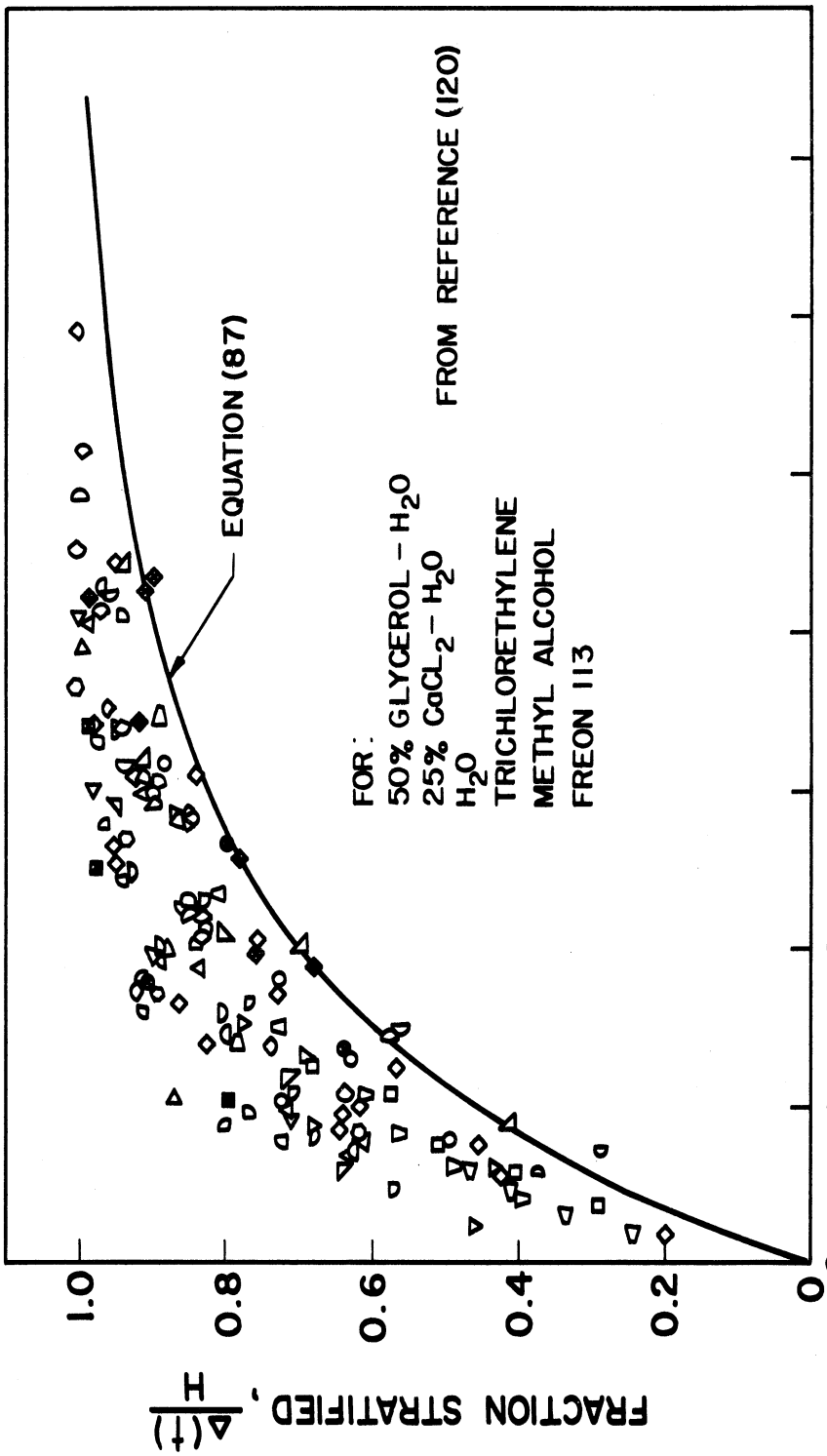

Figure 49 Comparison of Experimental Data for Stratified Layer Growth With Prediction by Equation (14) (with $Gr_H^* > 4 \times 10^{12}$ and H/R = 2.32)

true. The experimental results of surface temperature measurements are compared with Equation (80) in Reference (120) and a general agreement is found, as shown in Figure 50.

The transient laminar natural convection processes in both the liquid and vapor in a partically filled container, including the influence of heat sources have been studied by Barakat and Clark (130), Barakat (131) and Clark, et al. (57). These investigations have involved the finite-difference representation and solution on a digital computer of the two-dimensional transient, transport equations for rectangular and cylindrical geometry. Work on a spherical geometry is currently underway (133). Application of the results of these studies is to the internal flow, temperature stratification and pressure rise in cryogenic propellant containers when subjected to various gravity fields, external heat flux or wall temperature disturbance.

The isotherms and streamline pattern in a cylindrical container subjected to a sudden increase in wall heat flux of 2000 BTU/Hr - ft^2 is shown in Figure 51 at a time of 60 seconds following the disturbance (130). The bottom is insulated and the liquid vapor interface is maintained at 80F. It is evident from these results that, while a boundary-layer type of phenomenom is suggested, the bottom corner and the liquid interface intersection introduce effects causing a significant departure from boundary layer flow. Near the liquid interface two-dimensional effects are evident, also. Two vortices, one near the wall and the second at the centerline are evident. Numerical calculations indicated a shifting towards a steady-state position approximately at the midpoint in the liquid space. A comparison of the theoretical and experimental results for water at lg in a cylindrical container is shown in Figure 52. The spatial mean values of the heat transfer coefficient and

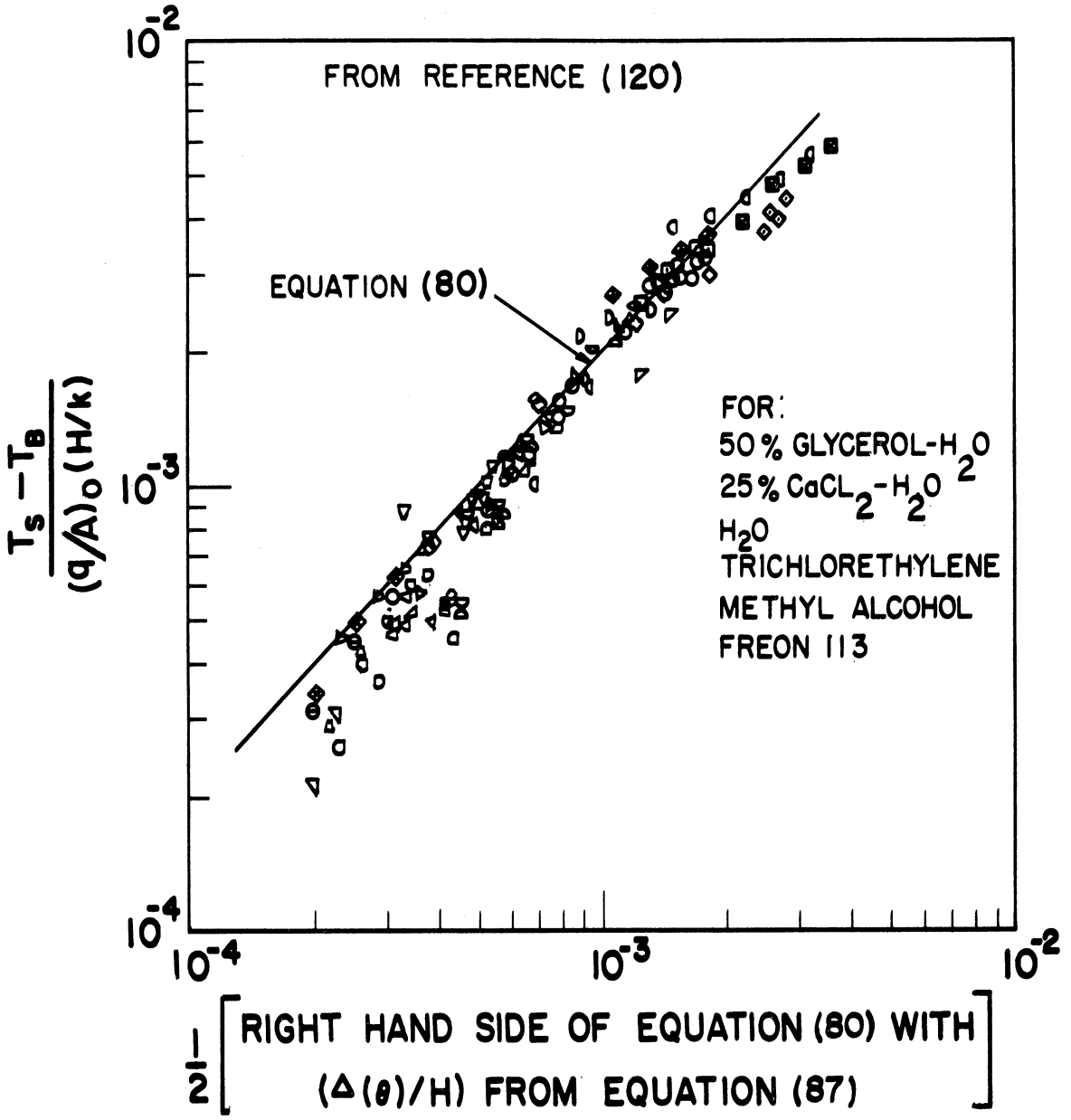

Figure 50 comparison of Experimental Data for Surface Temperature Rise with Prediction by Equations (80) and (87) (with $Gr_H^* Pr > 4 \times 10^{12}$ and H/R = 2.32)

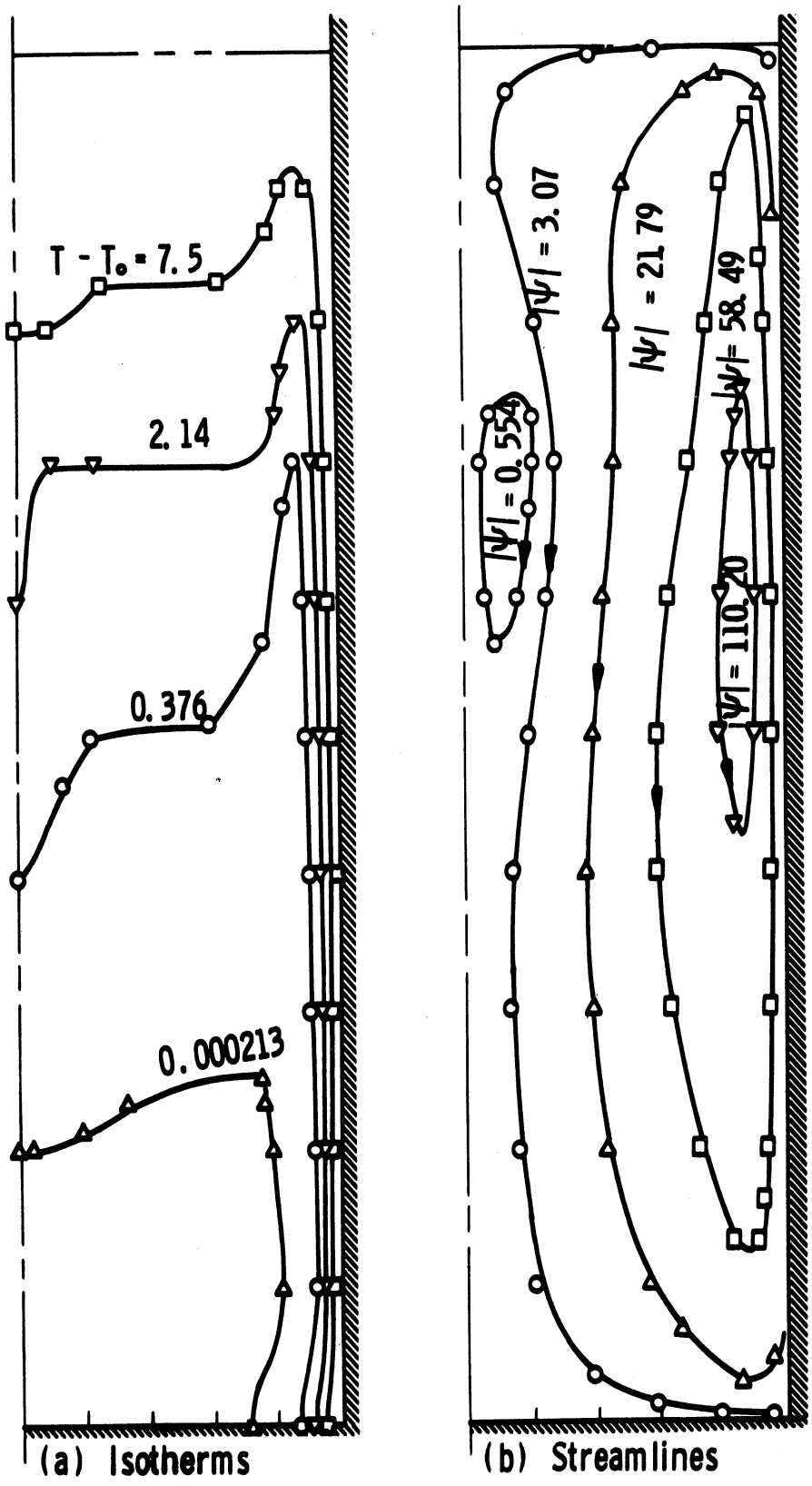

FIGURE 51. COMPUTED VALUES OF ISOTHERMS AND STREAMLINES IN A CYLINDRICAL CONTAINER[130] $(q/A)_o$ = 2000 BTU/HR FT^2, TIME = 60 SEC.

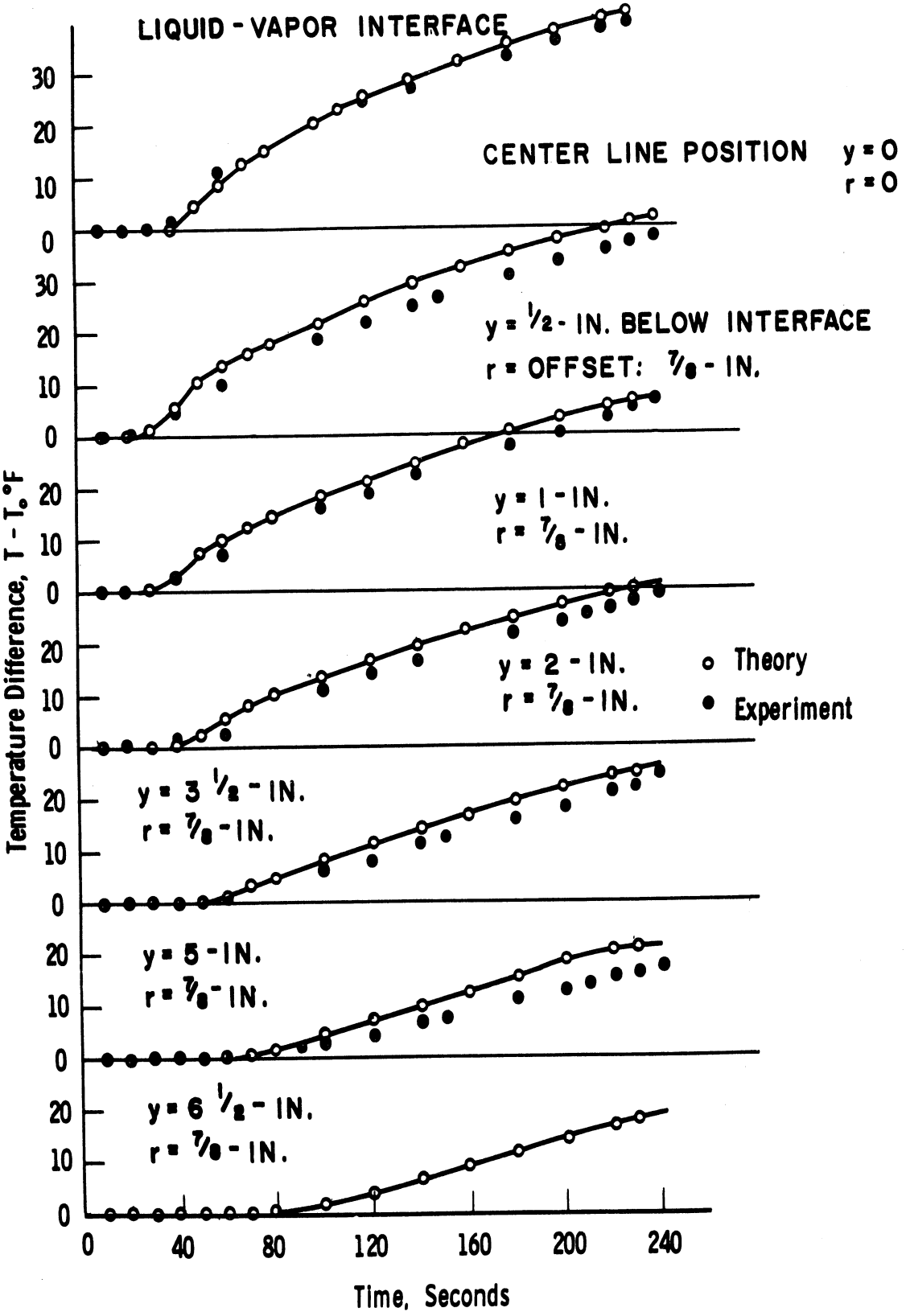

Fig. 52 Liquid temperature response in the cylindrical container,(130) run 4. $(q/A)_o$ = 2000 Btu/hr ft^2, T_o = 80°F. FW D: H_2O; a/g = 1.0

$\overline{Nu}/\overline{Ra}^{1/4}$ ratio were computed for the conditions in Figures 51 and 52. These results are shown in Figure 53 and correspond to a maximum $\overline{Ra}$ of approximately $6(10^9)$ based on height. Of interest is the rapid decrease in heat transfer coefficient and $\overline{Nu}$ following the start of the transient and their subsequent oscillation about a mean. The mean value about which $\overline{Nu}/\overline{Ra}^{1/4}$ oscillates is approximately 0.54, which is close to the value 0.59, recommended for steady laminar, natural-convection from vertical surfaces (74). A similar oscillation in the velocity and temperature distributions has been reported by Barakat (131).

One of the important consequences of thermal stratification in cryogenic propellant containers is the rate of pressure rise in the container resulting from the transfer of mass at the liquid-vapor interface. For a single component system the pressure in the vapor space corresponds very closely to the saturation pressure at the temperature of the interface. Thus, with stratification it is evident that container pressures can significantly exceed the pressure corresponding to saturation at the bulk liquid temperature. On the other hand, a sudden mixing of the fluid will result in rapid depressurization. These conditions have been studied by Huntley (133), among others. The computation of pressure-time histories in closed containers is given in Reference 57. This analysis is in the form of a numerical, finite-difference approximation to the transport equations in both liquid and gas phases with solution by a digital computer. A coupling of phase interaction at the interface is required in this analysis. Owing to the complexities of making detailed calculations at the interface, the limitations imposed by computer storage and uncertainties concerning the conditions at incipient boiling an approximation was introduced in the analysis. This consisted of establishing an arbitrary value of wall temperature rise, ΔT_w, max., above the saturation

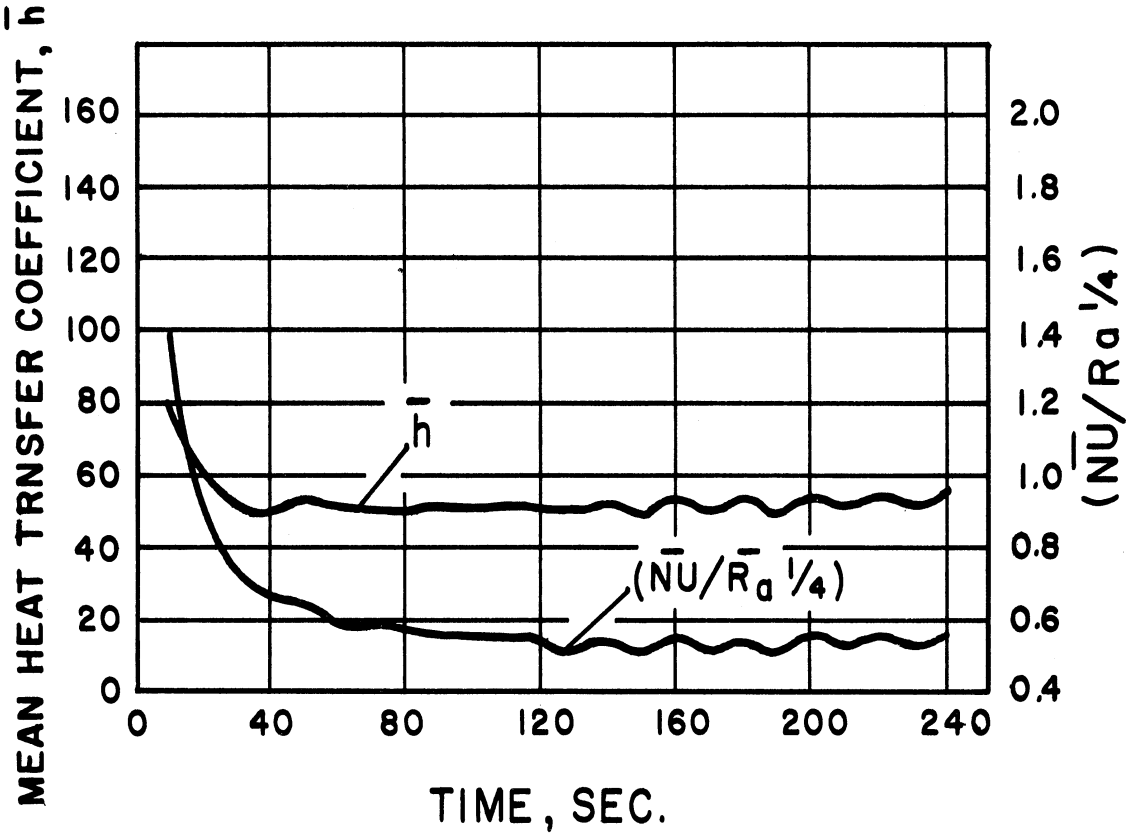

FIGURE 53. HEAT TRANSFER COEFFICIENT VS TIME.(130)

temperature, which the wall would not be permitted to exceed. The thermodynamic effect of this was introduced into the computer program by the evaporation of an appropriate amount of liquid directly into the vapor space, thus allowing for the superheat in the wall and the adjacent liquid. The influence of this arbitrary control is evident at heat flux as high as 180 BTU/He-Ft^2. However, at a heat flux more closely corresponding to that or an insulated propellant container subject to solar radiation is space, 1 BTU/Hr-Ft^2, the influence of ΔT_w, max is negligible. Under these conditions the actual wall temperature rise is less than 1°F.

Some typical temperature stratification patterns in both the liquid and vapor regions (57) are shown in Figure 54 for the self-pressurization of a closed cylindrical LOX container subjected to a uniform external heat flux of 180 BTU/Hr-Ft^2 and gravity level of 10^{-5}g. Except near the wall and liquid interface the liquid temperature rise is completely negligible but the relative stratification is quite large. The corresponding pressure rise and total mass of LOX evaporated is shown in Figure 55 for various values of ΔT_w, max. The influence of heat flux on the pressure rise and total mass evaporated for ΔT_w, max = 0°F is given in Figure 56. The pressure rise in the same LOX container for a heat flux of 1 BTU/Hr-Ft^2 is very much lower even for an exposure time exceeding 3 hours, as shown in Figure 57.

One of the principal problems of the finite-difference approximations used in (57, 130, 131) is that of numerical convergence and stability. This question is discussed in detail in (130) for the laminar transport equations and a simple stability criterion is given and its mathematical basis established. The numerical formulation is of an "explicit" form which reduces computer time to a practical minimum.

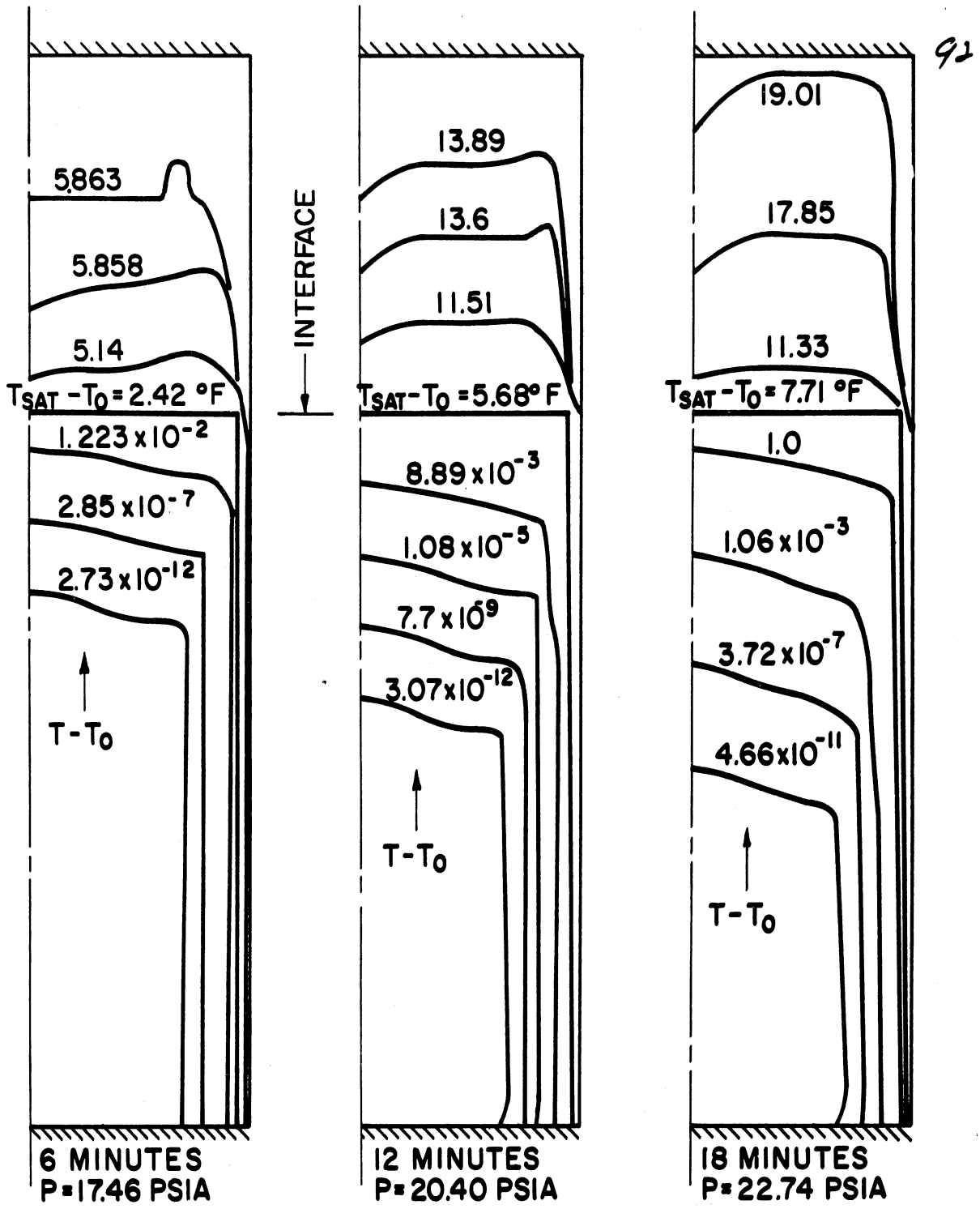

LIQUID OXYGEN IN CYLINDRICAL TANK

5 FT DIA. x 10 FT LONG	$q/A = 180$ BTU/HR-FT^2
21 x 31 GRID	$a/g = 10^{-5}$
33% INITIAL ULLAGE	$P_0 = 15$ PSIA

FIGURE 54. ISOTHERMS IN A CYLINDER LOX CONTAINER FOR $\Delta T_{w\ max} = 2°F$

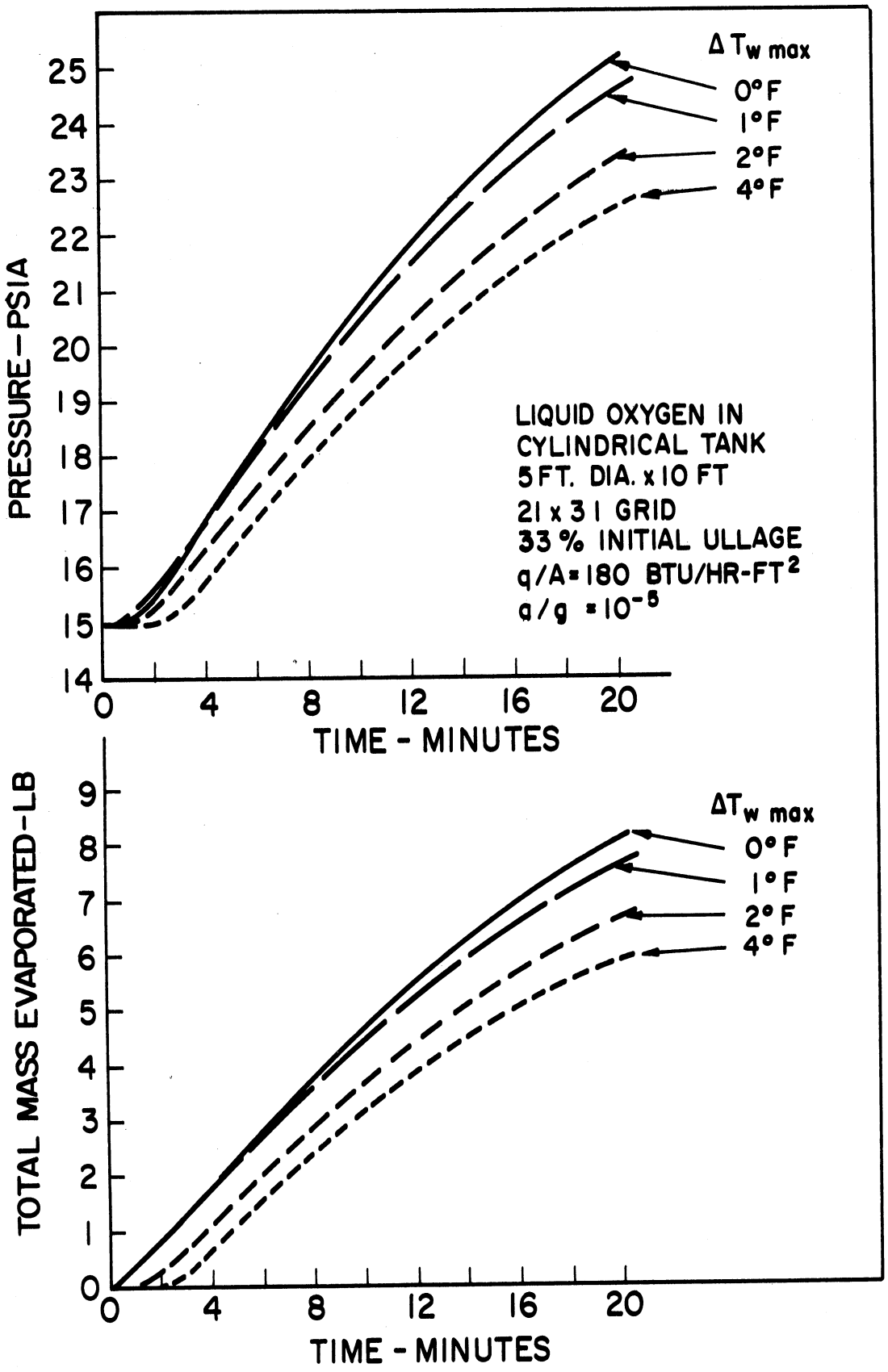

FIGURE 55. PRESSURE RISE AND TOTAL MASS EVAPORATED IN A CYLINDRICAL LOX CONTAINER

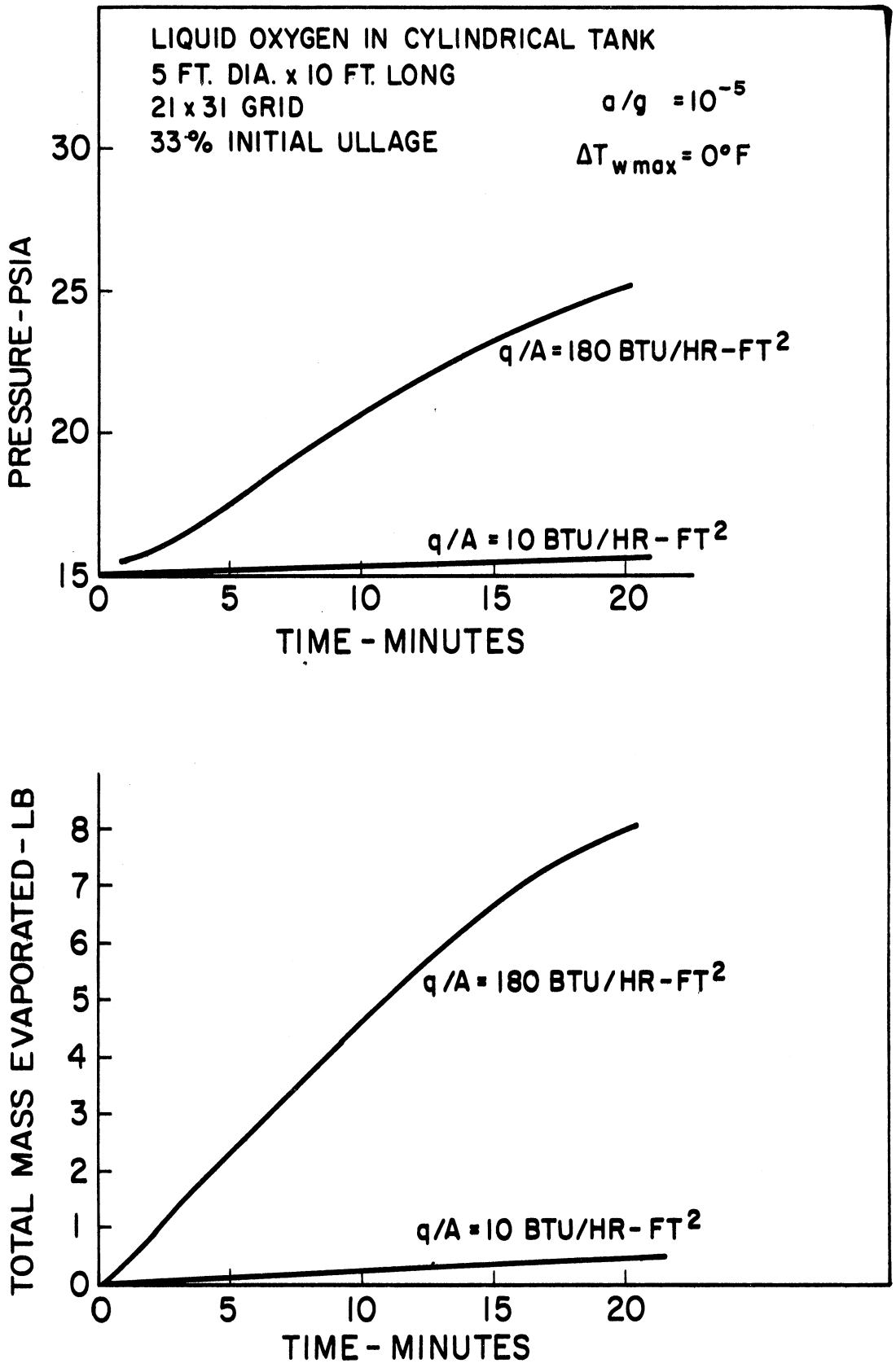

FIGURE 56. EFFECT OF HEAT FLUX ON PRESSURE RISE AND MASS EVAPORATED

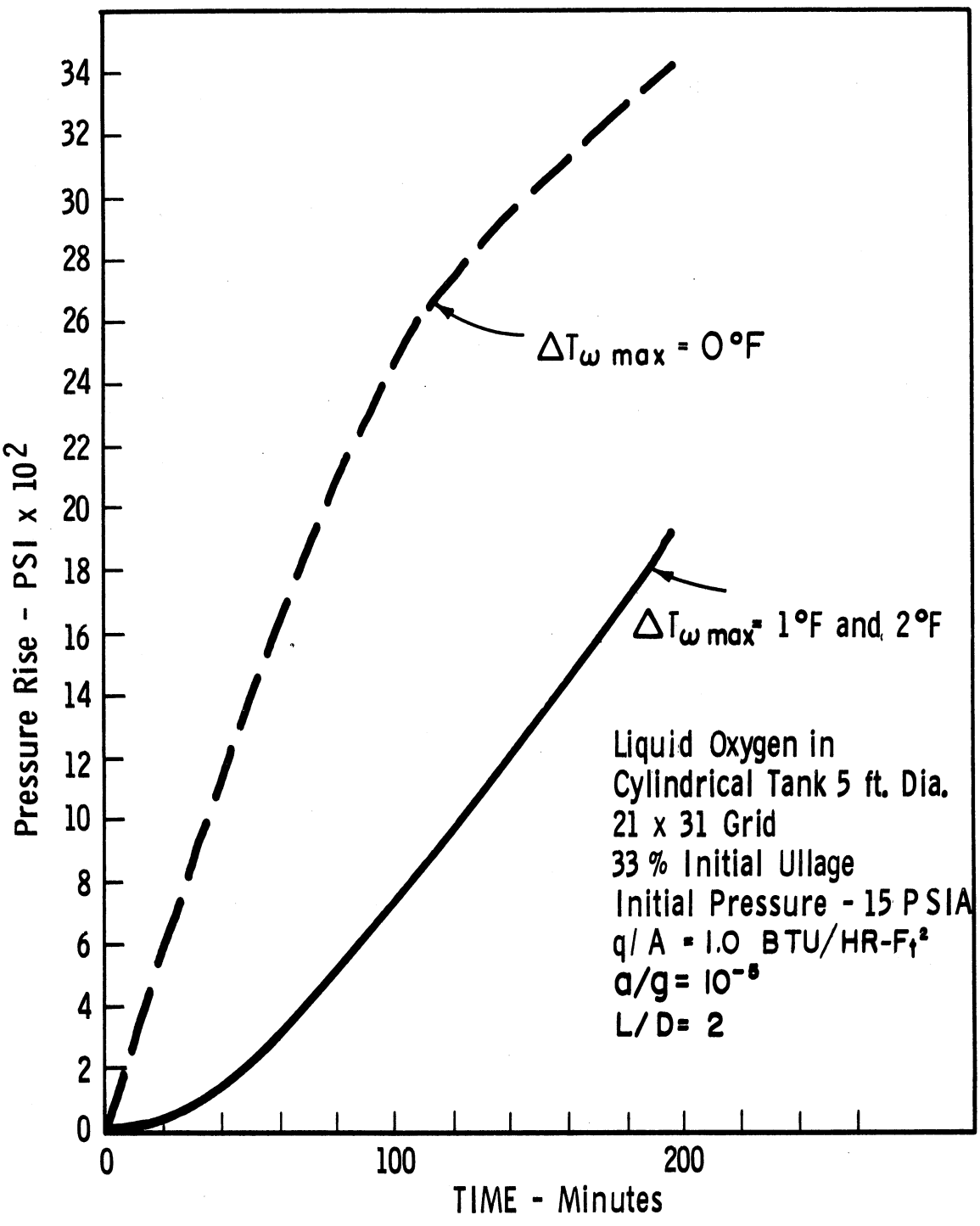

FIGURE 57. PRESSURE RISE IN A CYLINDRICAL LOX CONTAINER FOR AN EXTERNAL HEAT FLUX OF 1.0 BTU/HR-F_t^2

VII. MULTI-PHASE PROCESSES

A. Boiling Heat Transfer

Boiling will exist at a surface when the surface temperature exceeds the saturation or bubble point temperature by a few degrees. This superheat depends upon the type of fluid and surface and the system pressure. It decreases to near zero as the pressure approaches the critical pressure. The word boiling is used to describe the process of vapor bubble generation within a liquid and almost always occurs at a solid surface in heat transfer systems. Two general types of boiling systems exist: pool boiling, a process similar to natural convection, and forced convection boiling. For each of these systems the fluid can be sub-cooled and thus have no net vapor generation or it can be saturated in which case a net vapor generation will occur.

The boiling phenomenon itself is characterized by three regimes, shown in Figure 58, namely, nucleate boiling, transition boiling and film boiling. In addition, two other unique phenomena are observed in boiling heat transfer. These are the conditions of maximum and minimum heat flux, also shown in Figure 58, which separate the transition boiling regime from those of nucleate and film boiling. For systems such as nuclear reactors and electronic equipment in which the heat flux (q/A) is an independent variable the point of maximum heat flux is of utmost importance. Should an attempt be made to increase the power level (and hence q/A) of such systems beyond that of the maximum heat flux corresponding to a given set of circumstances, the surface-fluid saturation temperature difference would increase to that of film boiling at this heat flux. As may be observed from Figure 58 this would result in heat transfer surface temperatures 1000 to 2000F above the fluid saturation temperature. For most fluid-surface combinations this would mean physical

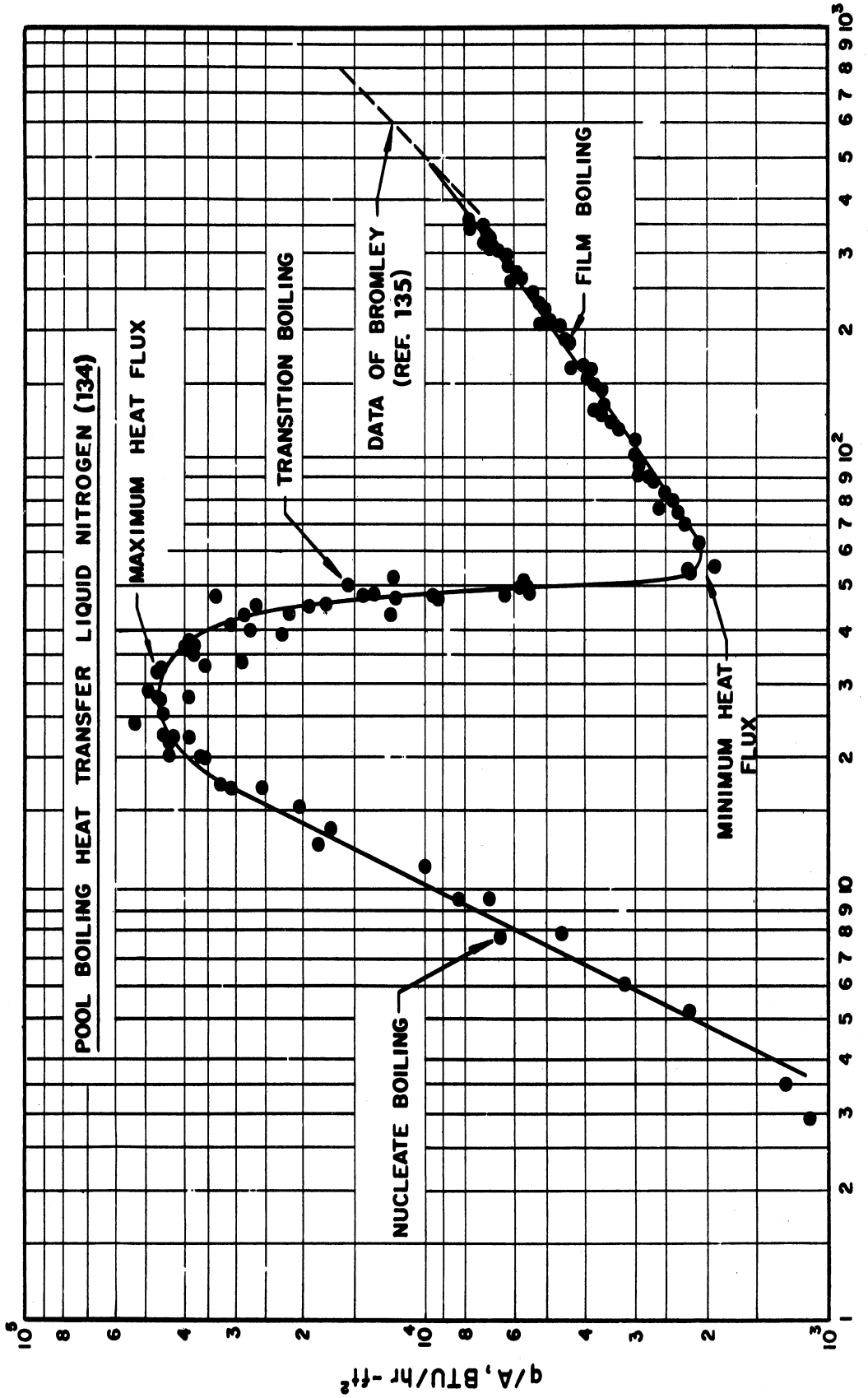

Figure 58. Typical pool boiling characteristic curve.

destruction of the surface. In cryogenic application this consequence is minimized owing to the low saturation temperatures but it still is to be avoided in most instances.

Forced convection boiling has a similar character to that of pool boiling shown in Figure 58, except that non-boiling region is usually more evident in the presentation of the data. Walters (136) has studied the forced convection boiling of liquid hydrogen in a 0.25 inch ID tube and some of his results are given in Figure 59.

The literature of boiling heat transfer is very large. It will be possible in this section to describe only some of the significant results as related to cryogenic heat transfer. Excellent summaries of the subject have been prepared by Westwater (137), Balzhiser, et al. (138), Zuber and Fried (139), Richards, Steward and Jacobs (140), Giarratano and Smith (141, 142), Brentari, et al. (143), Seader, et al. (27), and Tong (144), for both cryogenic and non-cryogenic application. In general, the properties of pool boiling including nucleate, transition and film boiling and the maximum and minimum heat flux can be computed from available correlations and some knowledge of the fluid-surface characteristics. This is less true with forced convection boiling although some progress has been made and will be discussed later. Data on gravic and agravic effects will be given in a separate section.

1. Pool Boiling

a. Nucleate Boiling

Nucleate boiling exists in the $(q/A) - \Delta T$ range from incipient

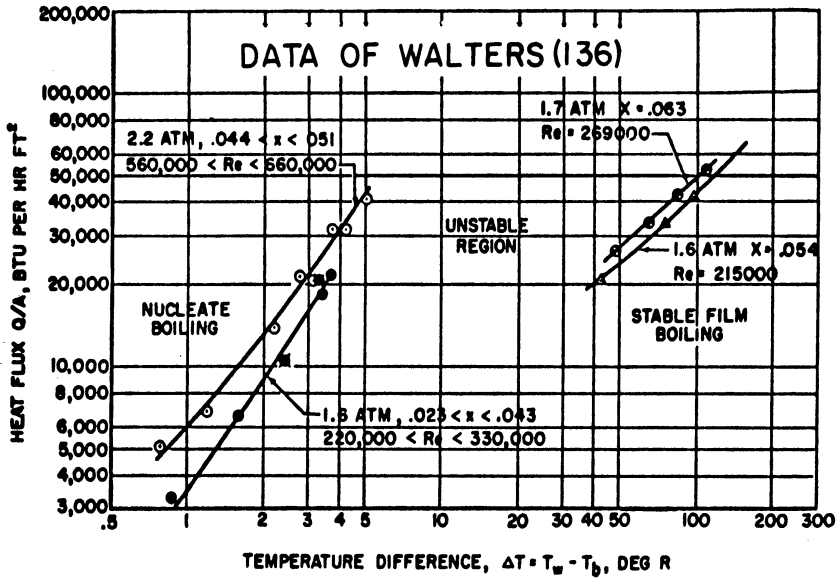

Figure 59. Heat Flux vs. Temperature Difference.

boiling to the point of maximum heat flux. This type of boiling has probably received the greatest attention in terms of the total number of investigations owing to the relative simplicity of conducting measurements. Complete agreement is lacking among the results of the various investigators because of the important influence the kind and nature of the surface has on the process, among other things. This effect has yet to be adequately described. In addition to this variations in system geometry, method of taking data and uncertainities in measurement contribute to the general scatter of data.

This general effect is seen in Figure 60, 61, 62 and 63, taken from Brentari and Smith (142), where the experimental data for nucleate and film boiling for Oxygen, Nitrogen, Hydrogen and Helium are shown. Except for the data of Lyon, et al. (145) the width in the band of the data reflects the spread of each investigator's measurements on a given system. The spread in the data of Lyon, et al. is a result of their study on a range of geometries, orientations and surfaces. For comparision, the correlation for nucleate boiling of Kutateladze (145, Equation 11.21, Equation 88) is included.* The results for the maximum heat flux, the minimum heat flux and film boiling will be discussed later. In general Kutateladze's equation represents the data reasonably well. It should be pointed out that this also will be true of several other correlating equations to be discussed below. Kutateladze's first correlation, originally derived for water and various organic liquids, is

* Kutateladze (145) gives two equations (11.21 and 11.22, p. 129, Reference 145.) His second equation is used by Seader, et al. (27) and Zuber and Fried (139) and given here as Equation (92). Each appears to give approximately the same results, although their $(q/A) - \Delta T$ relationship differ.

$$\frac{h}{k_\ell}\left(\frac{g_o\sigma}{g\rho_\ell}\right)^{1/2} = 3.25(10^{-4})\left(\frac{(q/A)^c p_\ell \rho_\ell}{h_{fg}\zeta_v k_l}\left(\frac{g_c\sigma}{g\rho_\ell}\right)^{1/2}\right)^{0.6}\cdot$$
$$\left(g\left(\frac{\rho_\ell}{\mu_\ell}\right)^2\left(\frac{g_o\sigma}{g\rho_\ell}\right)^{3/2}\right)^{0.125}\cdot\left(\frac{p}{(\sigma g\rho_\ell/g_c)^{1/2}}\right)^{0.7} \quad (88)$$

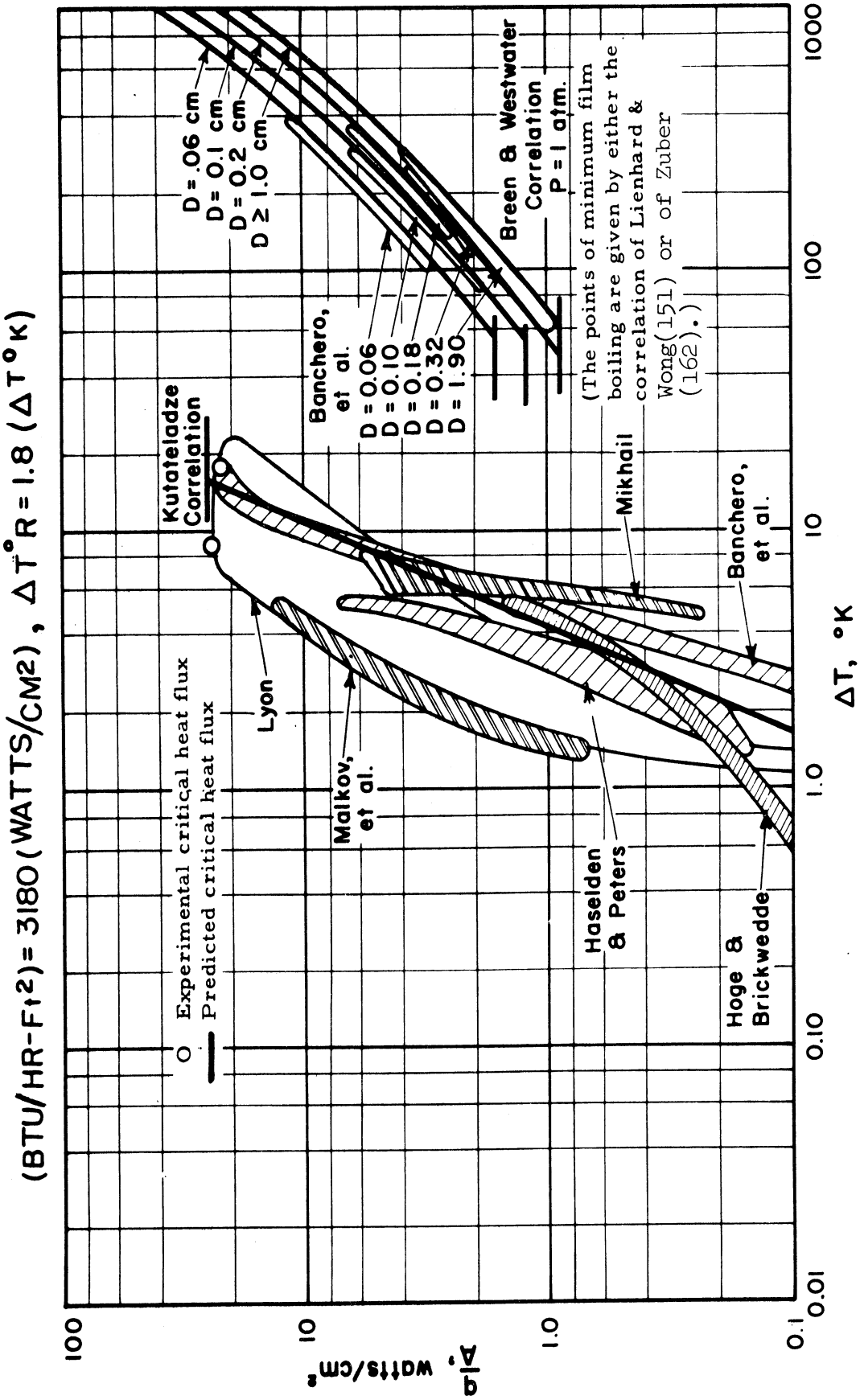

FIGURE 60
Experimental Nucleate and Film Pool Boiling of Oxygen at One Atmosphere Compared with the Predictive Correlations of Kutateladze and Breen and Westwater (142). See Refs. (145-174).

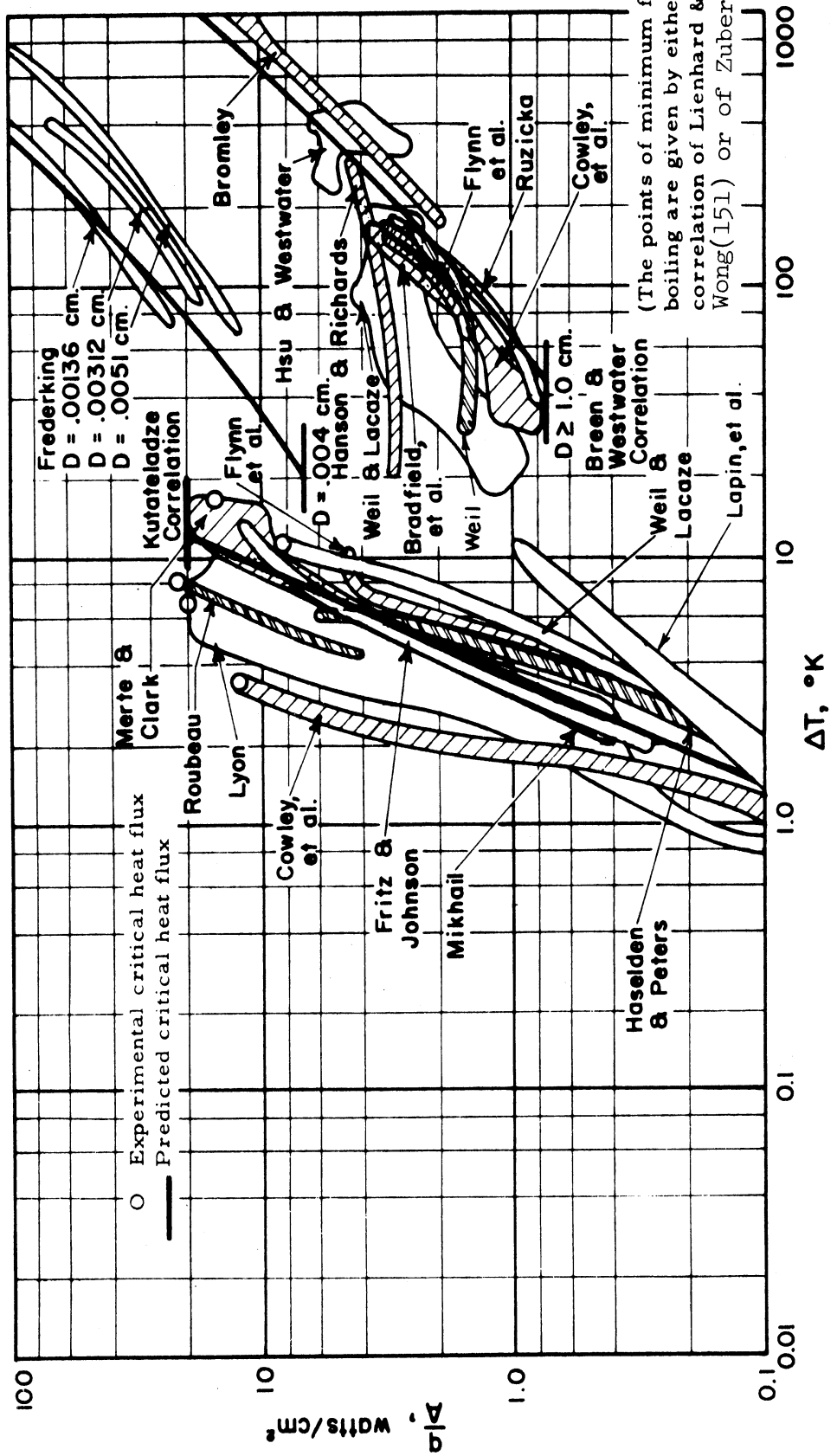

FIGURE 61
Experimental Nucleate and Film Pool Boiling of Nitrogen at One Atmosphere Compared with the Predictive Correlations of Kutateladze and Breen and Westwater (142). See Refs. (145-174).

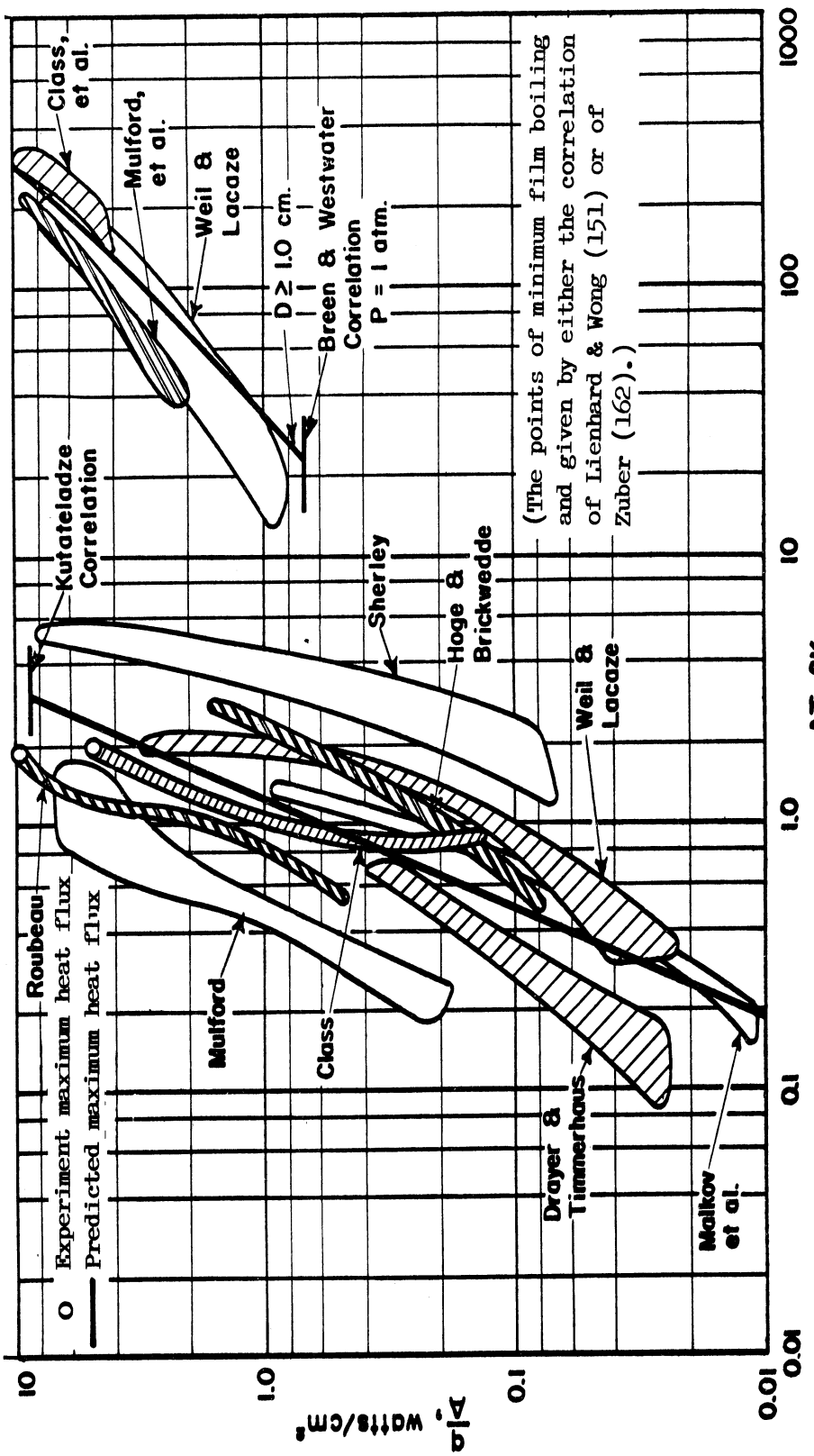

FIGURE 62

Experimental Nucleate and Film Pool Boiling of Hydrogen at One Atmosphere Compared with the Predictive Correlations of Kutateladze and Breen and Westwater (142). See Refs. (145-174).

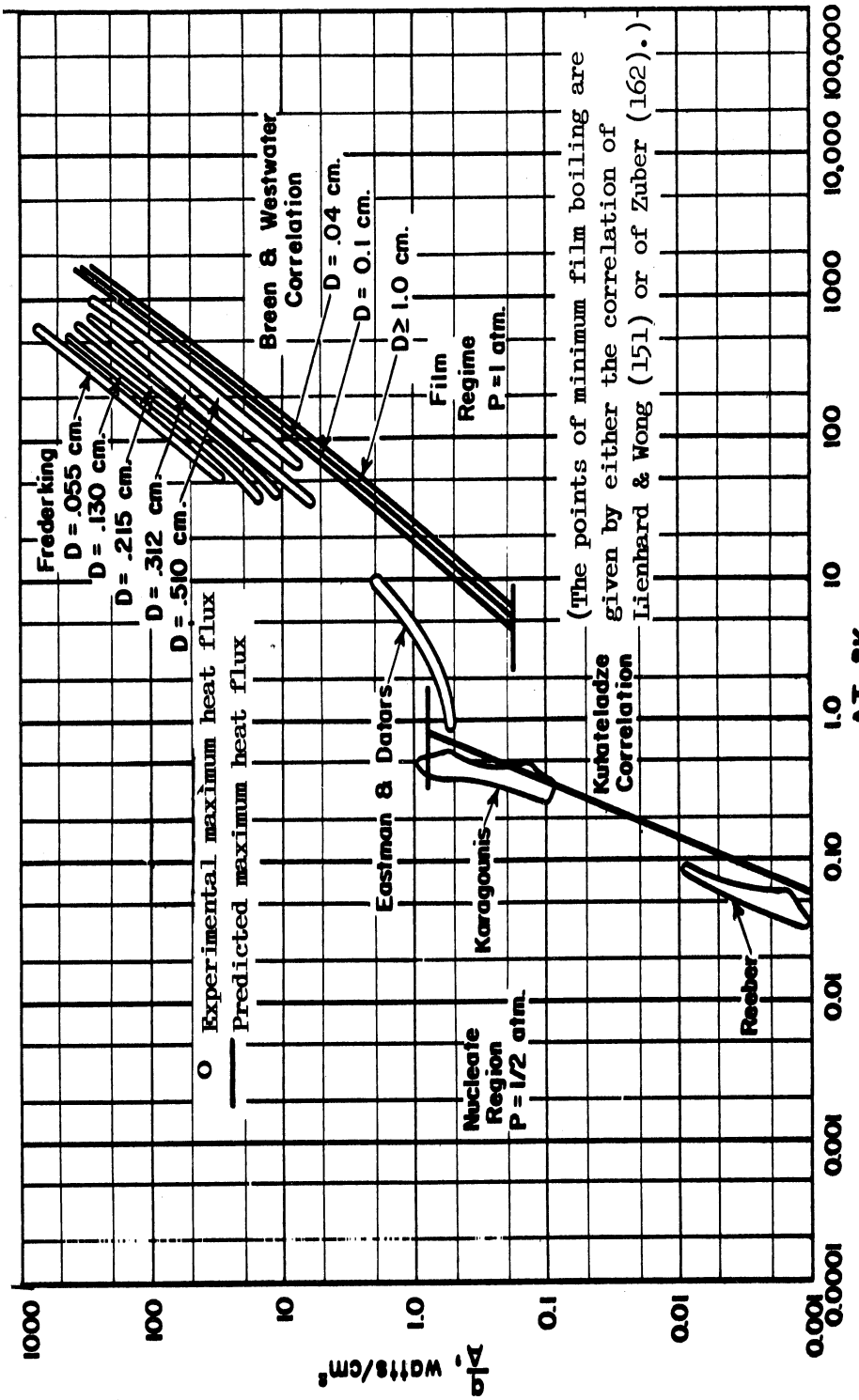

FIGURE 63
Experimental Nucleate and Film Pool Boiling of Helium Compared with the Predictive Correlations of Kutateladze and Breen and Westwater (142). See Refs. (145-174).

From this result the (q/A) - ΔT relationship is,

$$(q/A) = f(p)\ \Delta T^{2.5} \tag{88a}$$

This equation has been computed by Brentari and Smith for a range of pressures as shown in Figures 64, 65, 66 and 67 for O_2, N_2, H_2 and He. Since all data on which equation (88) is based were taken at normal gravity, the influence of g cannot explicitly be found from this result. It is probable the constant $3.25\ (10^{-4})$ is valid only for $g = 32.2\ Ft/SEC^2$. This is also true for the correlations given in Table X. The presence of g in these correlations is primarily for dimensional considerations.

Seader, et al. (27) have arranged several nucleate boiling correlations into the form,

$$\frac{L^* G^*}{\mu_\ell} = \frac{F(p)}{\left(\dfrac{q/A}{\Delta T\ C_{p_\ell}\ G^*}\right)^a Pr^b}\ , \tag{89}$$

which may be written in the form of a Reynolds Number, Stanton Number, Prandtl Number Correlation as

$$Re_B = \frac{F(p)}{St_B^{\,a}\ Pr^b} \tag{90}$$

The characteristic length, L^*, mass velocity, G^*, the property function, $F(p)$, of the exponents a and b are given in Table X. It should be noted that a is the exponent on ΔT in the relation $(q/A) = f(p)\ \Delta T^a$. The value of a depends on the pressure and the nature of the surface.

A comparison of the various correlations in Table X is shown in Figures 69, 70, and 71 for H_2, N_2 and O_2. They all are in fair agreement and generally fall within the range of the experimental data. The correlations of

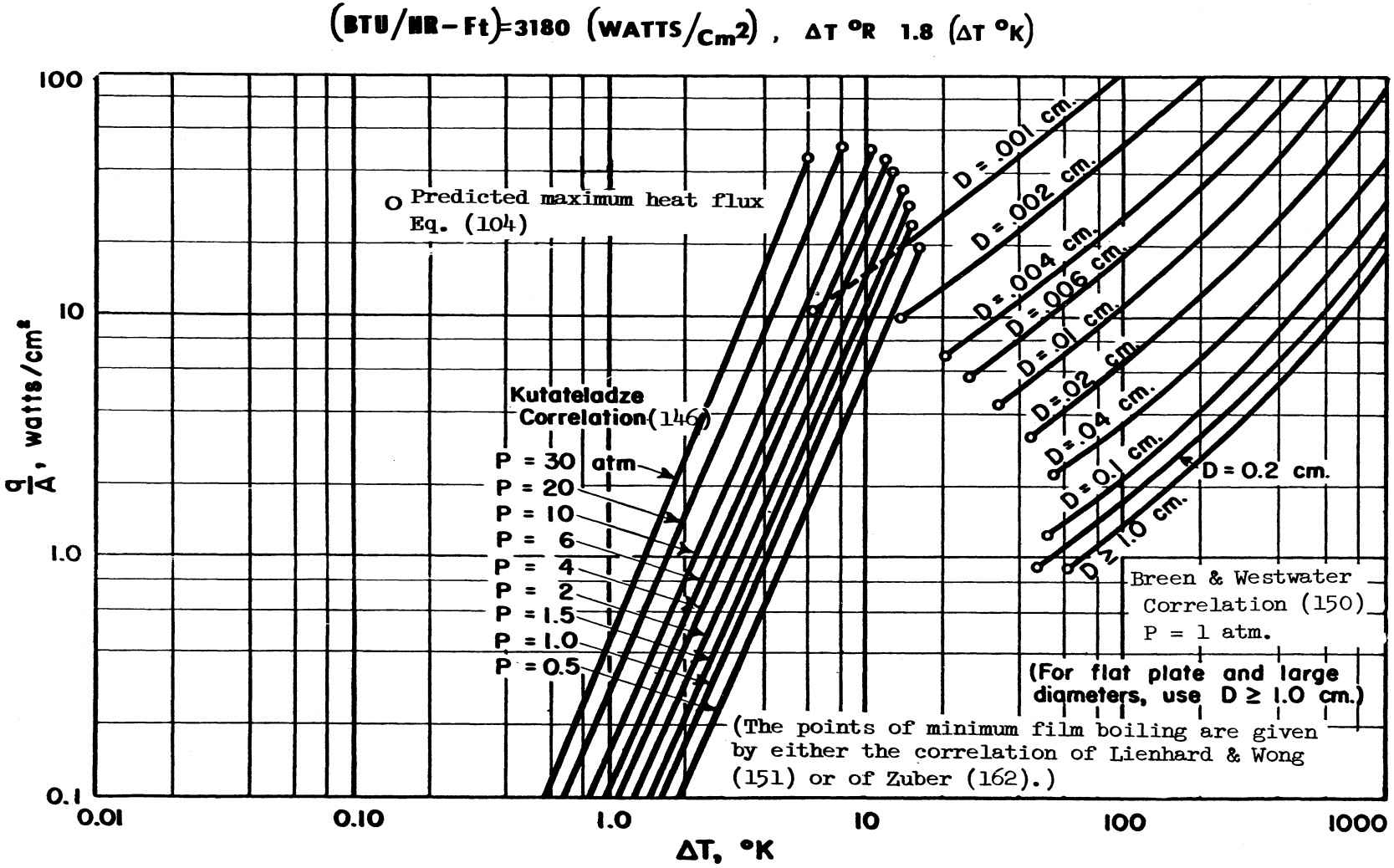

FIGURE 64
Predictive Nucleate and Film Pool Boiling Correlations for Oxygen (142)

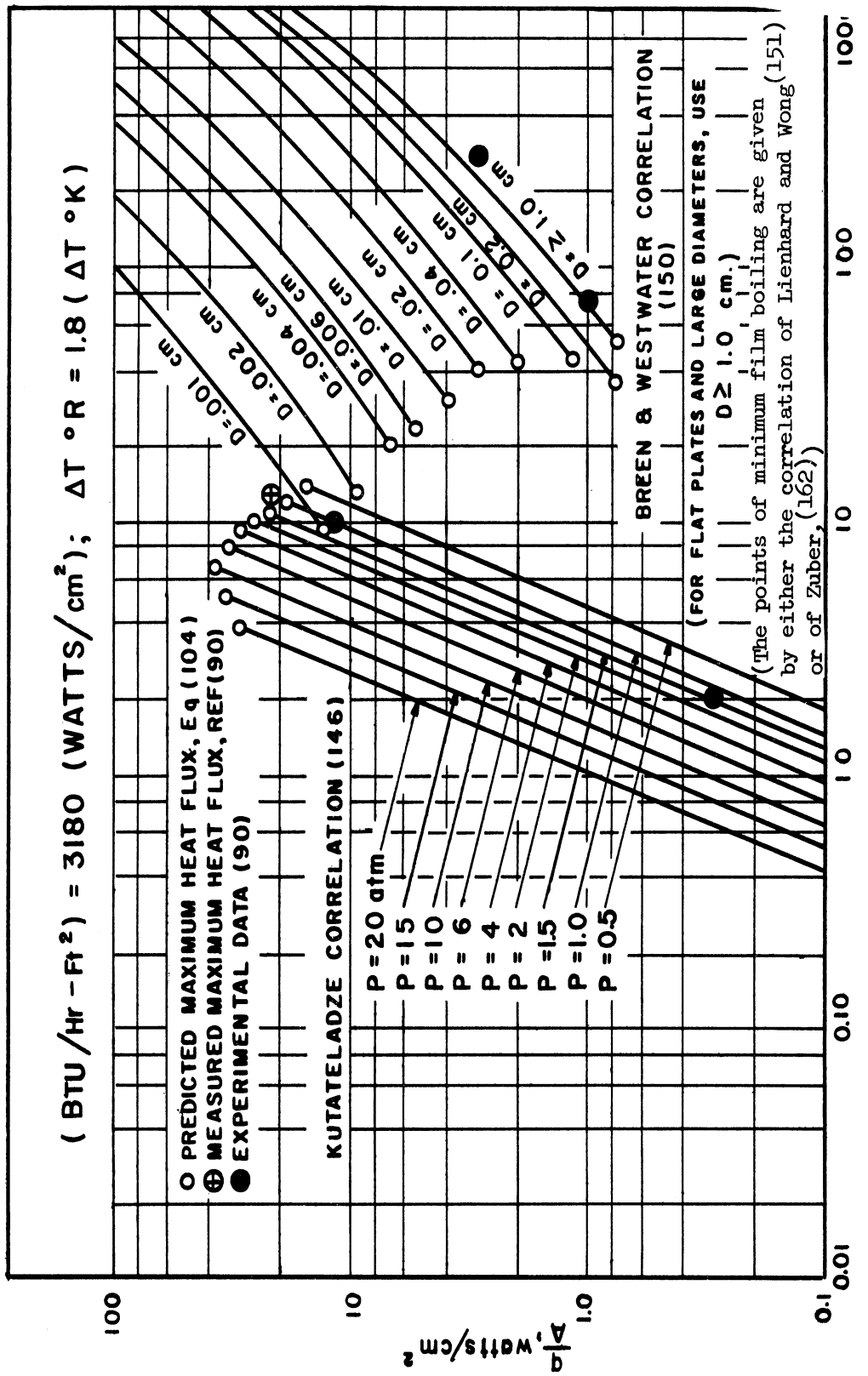

FIGURE 65. PREDICTIVE NUCLEATE AND FILM POOL BOILING CORRELATIONS FOR NITROGEN.(142)

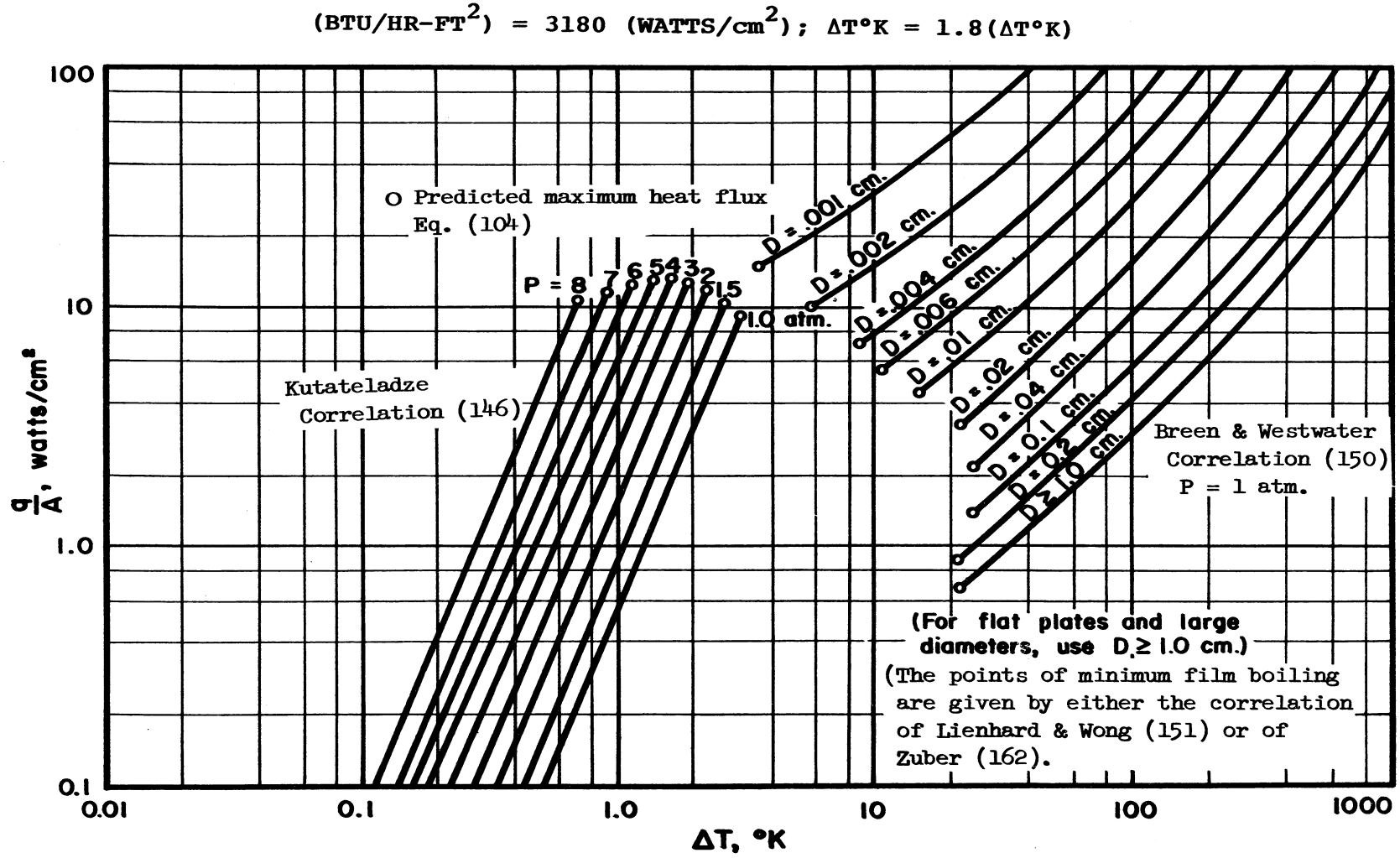

FIGURE 66. PREDICTIVE NUCLEATE AND FILM POOL BOILING CORRELATIONS FOR HYDROGEN.(142)

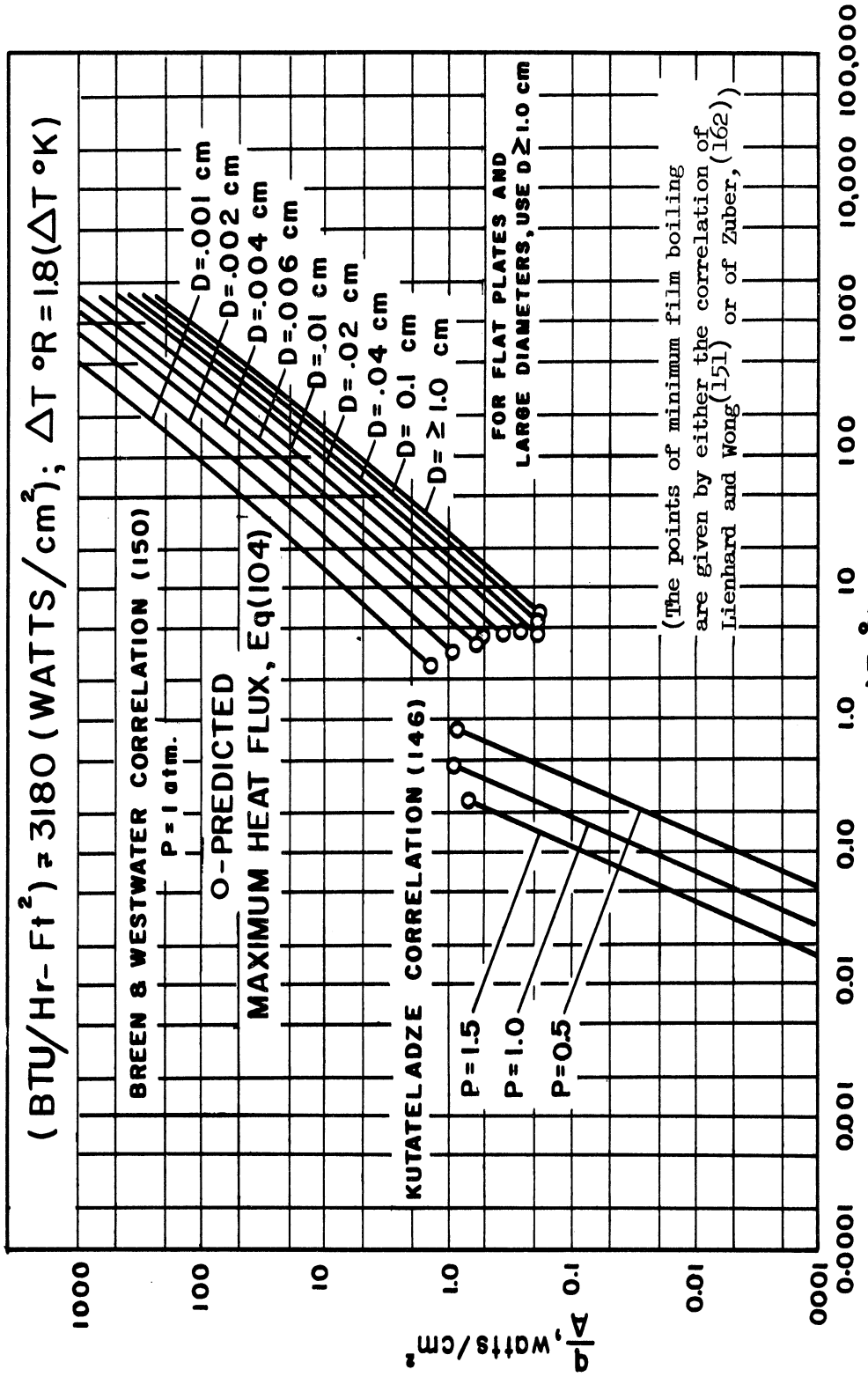

FIGURE 67. PREDICTIVE NUCLEATE AND FILM BOILING CORRELATIONS FOR HELIUM.(142)

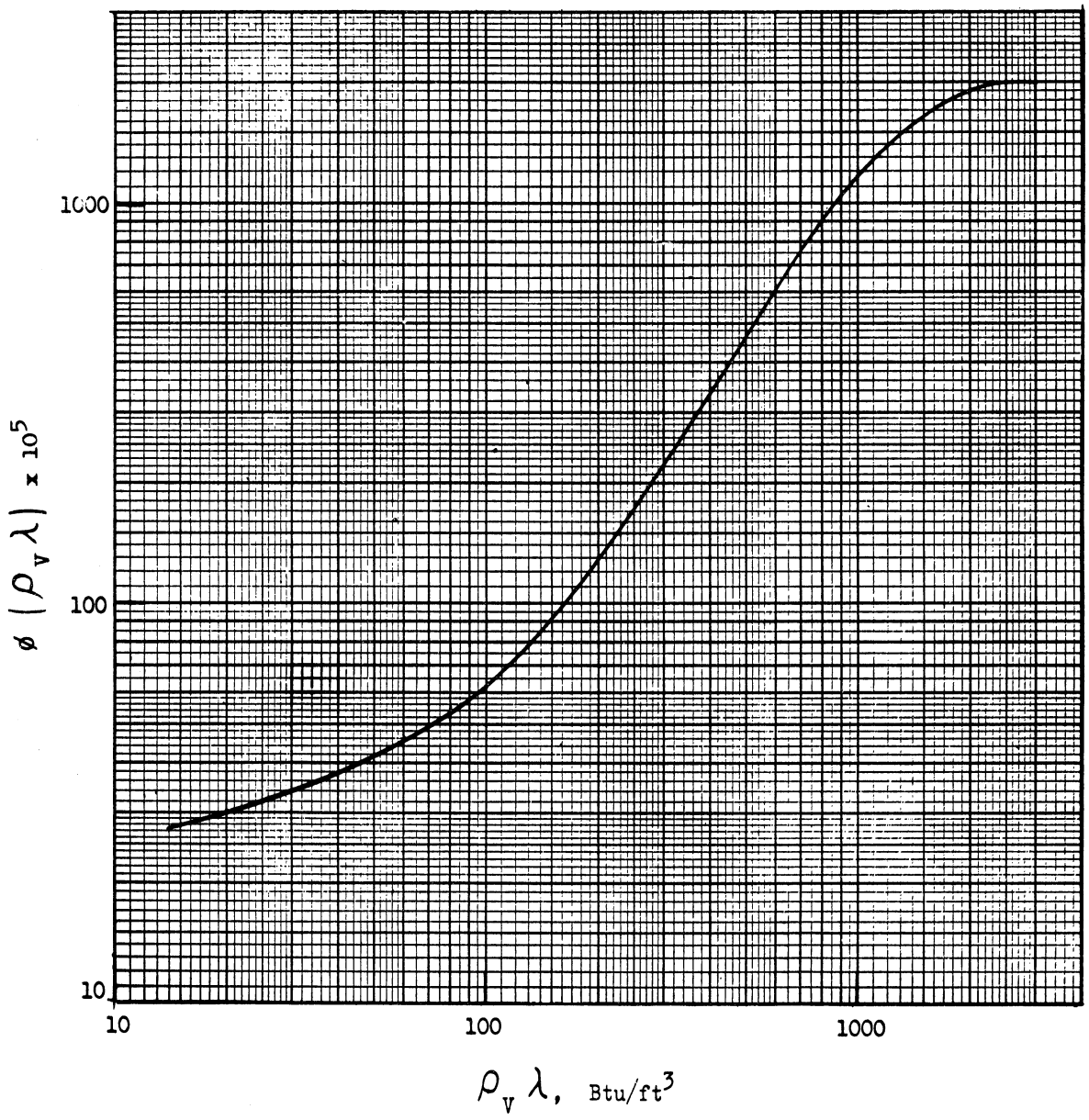

FIG. 68 CORRELATION FACTOR OF LEVY (178)

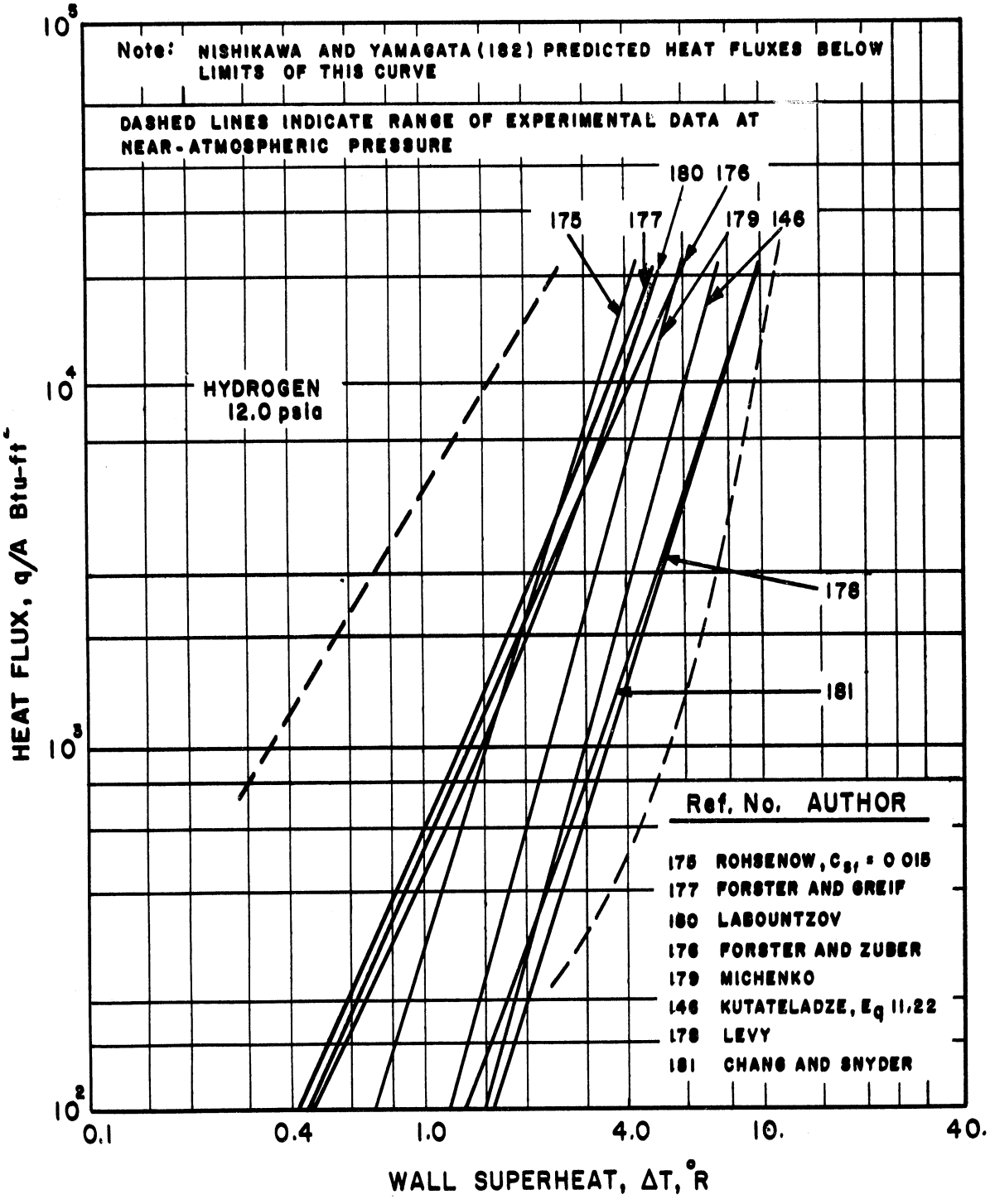

FIGURE 69. POOL NUCLEATE BOILING OF HYDROGEN AT 12.0 PSIA.[27]

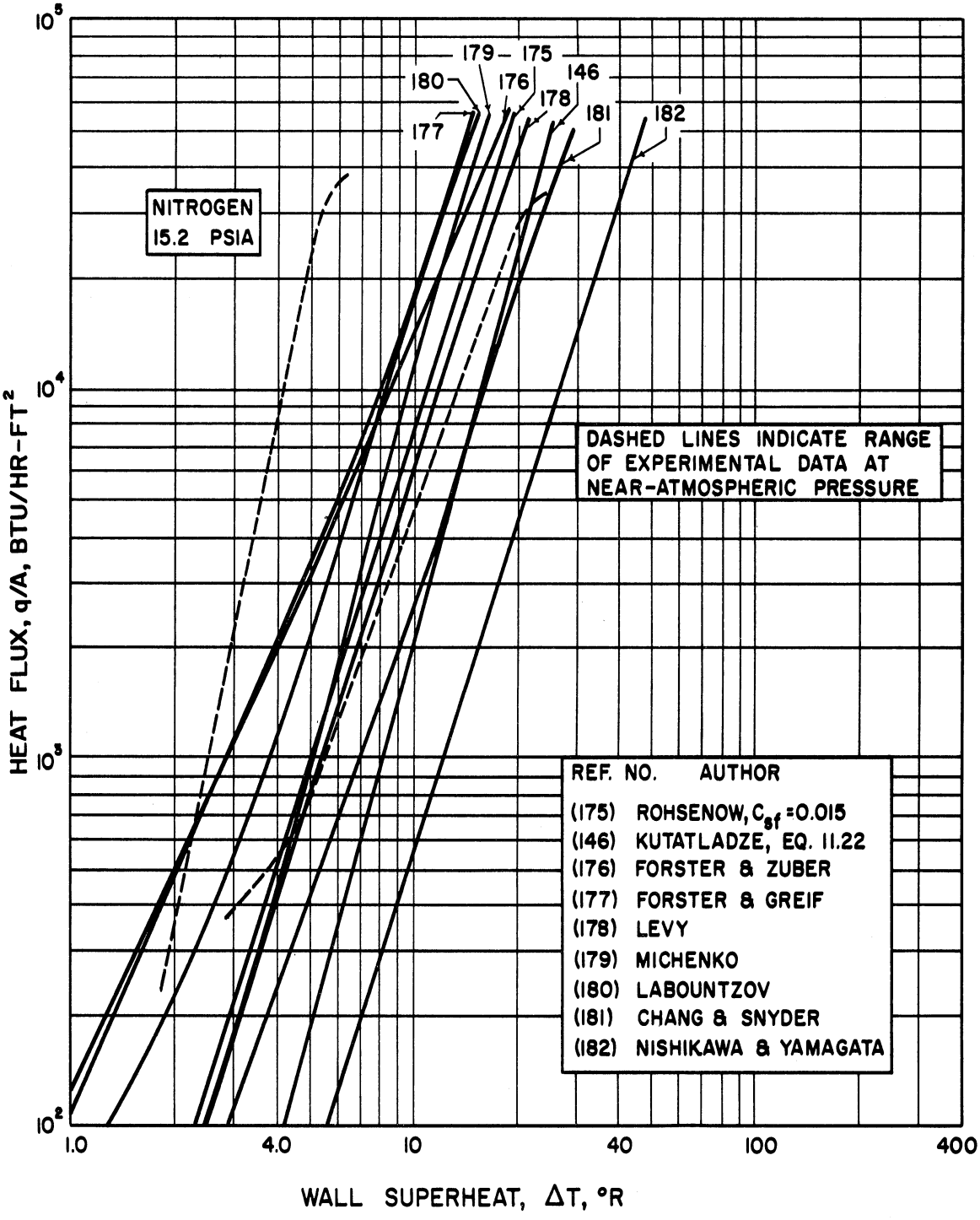

Figure 70. Pool Nucleate Boiling of Nitrogen at 15.2 psia.[27]

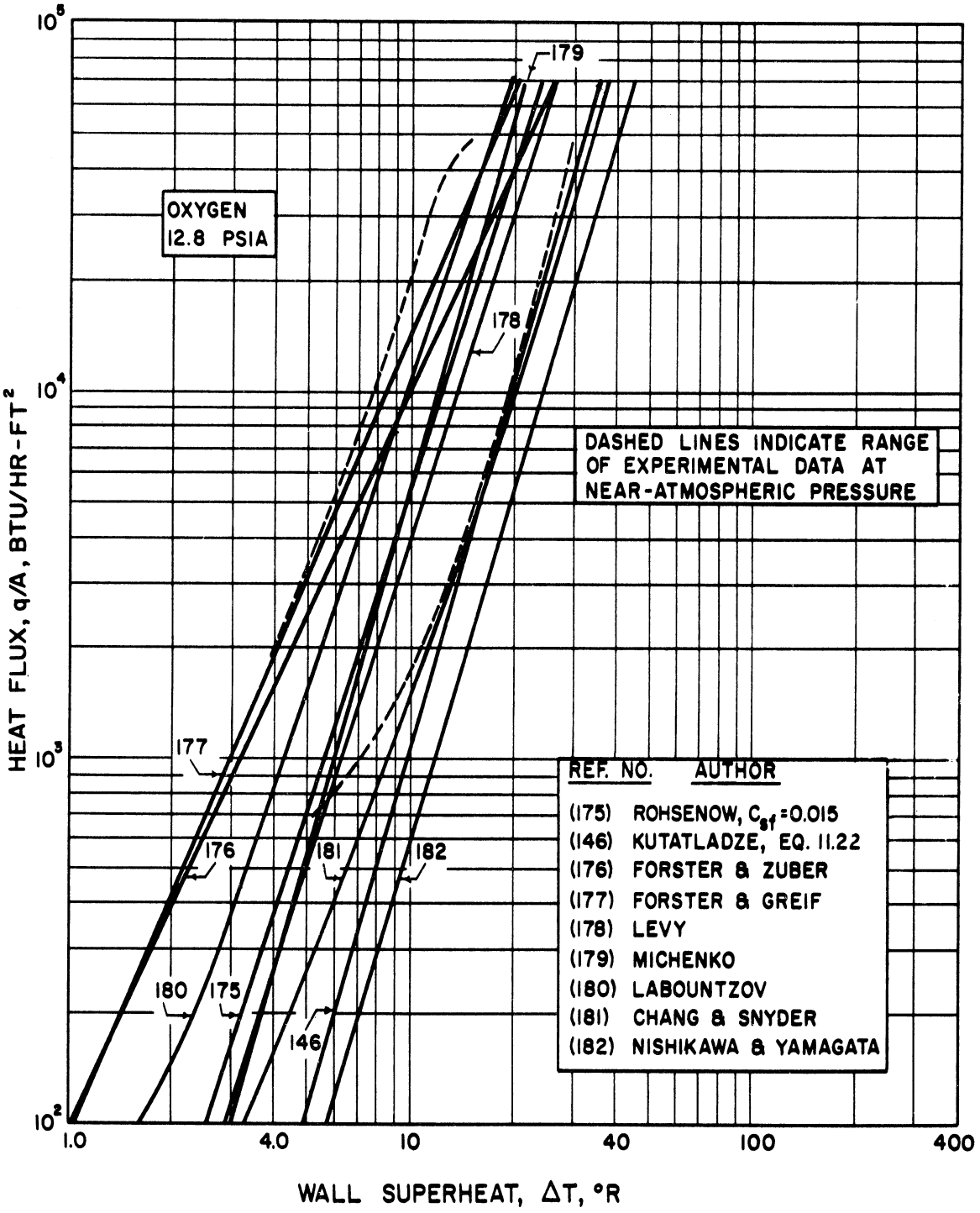

Figure 71. Pool Nucleate Boiling of Oxygen at 12.8 psia.[27]

TABLE X

SUMMARY OF POOL NUCLEATE BOILING EQUATIONS IN GENERALIZED STANTON NUMBER FORM (27)

$$Re_B = \frac{F(p)}{(St)_B^{\,a}\,(Pr)^b} \quad \text{or} \quad \frac{L^*\,G^*}{\mu_L} = \frac{F(p)}{\left[\dfrac{(q/A)}{\Delta T\, C_L\, G^*}\right]^a (Pr)^b}$$

Reference	L^*	G^*	$F(p)$	a	b	Eq. No.
Rohsenow (175)	$\left[\dfrac{g_o\,\sigma}{g\,(\rho_L - \rho_V)}\right]^{1/2}$	$\dfrac{(q/A)}{h_{f_g}}$	2.97×10^5 to 5.08×10^7	3	5.1	91
Kutateladze (146, Eq.11.22)	$\left[\dfrac{g_o\,\sigma}{g\,(\rho_L - \rho_V)}\right]^{1/2}$	$\dfrac{(q/A)\,\rho_L}{h_{f_g}\,\rho_V}$	$3.05 \times 10^{-11} \left\{\dfrac{P}{\sigma \dfrac{g}{g_o}(\rho_L - \rho_V)^{1/2}}\right\}^{7/3}$	$\frac{10}{3}$	$\frac{6.5}{3}$	92
Forster and Zuber (176) and Forster and Greif (177)	$\dfrac{C_{P_L}\,(\rho_L - \rho_V)\,T_s\,\sigma}{(\rho_V\, h_{f_g})^2\, J}$	$\dfrac{(q/A)\,\rho_L}{h_{f_g}\,\rho_V}$	$0.0012 \left[\dfrac{C_L\,\rho_L^{\,2}\,T_s\,\sigma^2\,g_c}{\mu^2\,\rho_V^{\,2}\,h_{f_g}^{\,2}\,J}\right]^{1/4} \left(\dfrac{\rho_L}{\rho_L - \rho_V}\right)$	2	$\frac{19}{24}$	93
Levy (178)	$\dfrac{C_{P_L}\,(\rho_L - \rho_V)\,T_s\,\sigma}{(\rho_V\, h_{f_g})^2\, J}$	$\dfrac{(q/A)\,\rho_L}{h_{f_g}\,\rho_V}$	$\varphi\,(\rho_V\, h_{f_g})$ from graph of Fig. 68	3	1	94

TABLE X

(Continued)

Reference	L*	G*	F(p)	a	b	Eq. No.
Michenko (179)	$\left[\frac{g_o\ \sigma}{g\ (\rho_L - \rho_V)}\right]^{1/2}$	$\frac{(q/A)\ \rho_L}{h_{f_g}\ \rho_V}$	$6.3 \times 10^{-11} \left\{\frac{P}{\left[\sigma \frac{g}{g_o} (\rho_L - \rho_V)\right]^{1/2}}\right\}^{7/3}$	$\frac{10}{3}$	1.0	95
Labountzov (180)	$\frac{C_{P_L} (\rho_L - \rho_V)\ T_s\ \sigma}{(\rho_V\ h_{f_g})^2\ J}$	$\frac{(q/A)\ \rho_L}{h_{f_g}\ \rho_V}$	$\begin{cases} Re_B < 10^{-2}: & 0.00391 \\ Re_B > 10^{-2}: & 0.00260 \end{cases}$	$\begin{matrix} 2 \\ 2.86 \end{matrix}$	$\begin{matrix} 4/3 \\ 1.9 \end{matrix}$	96
Chang and Snyder (181)	$\frac{C_{P_L} (\rho_L - \rho_V)\ T_s\ \sigma}{(\rho_V\ h_{f_g})^2\ J}$	$\frac{(q/A)\ \rho_L}{h_{f_g}\ \rho_V}$	57.2×10^{-4}	2.4	1	97
Nishikawa and Yamagata (182)	$\frac{C_{P_L} (\rho_L - \rho_V)\ T_s\ \sigma}{(\rho_V\ h_{f_g})^2\ J}$	$\frac{(q/A)\ \rho_L}{h_{f_g}\ \rho_V}$	$512 \left[\frac{(\rho_L - \rho_V)\ k_L\ T_s\ g}{M^2\ B\ \rho_V\ h_{f_g}\ J\ g_o}\right] (P/P_{atm})^2\ f_\zeta$ $M = 274.32\ ft^{-1}$ $\quad B = 6.742$ Btu/hr f_ζ is a surface factor (See Ref. 182)	3	1	98

Rohsenow (175), Levy (178) and Michenico (179) were found to fit the nucleate boiling data for liquid nitrogen at one atmosphere from a polished copper sphere 1-inch in diameter (90). These data are shown in Figure 72. This fit was accomplished using a valve of C_{sf} of 0.015 in Rohsenow's original equation. Zuber and Fried (139) report good agreement between the correlations of Rohsenow (175), Michenko (179), Forster and Zuber (176) and Labountzov (180) and experimental data of liquid hydrogen in nucleate boiling from a smooth flat surface, (148) in the pressure range from 0.8 to 5.1 ASM. In this comparison a value of 0.0147 was used for C_{sf} in Rohsenow's correlation, essentially the same as used in Figures 69, 70, 71.

Nucleate boiling heat transfer has been studied for hydrogen, neon, nitrogen and argon by Bewilogua, et al. (183) and for neon by Astruc, et al. (184). Each of these papers reports an hysteresis effect in the transition from natural convection to nucleate boiling, an effect ususally associated with systems in which contamination has been carefully avoided. A different nucleate boiling characteristic was obtained depending on whether the data were taken by increasing or decreasing the heat flux. This is the same effect observed in the pool boiling of water at high pressures reported by Elrod, et al. (185). Experimental data of Astruc, et al. for neon are given in Figure 73, 74, and 75. The data in Figure 73 indicate a very steep nucleate boiling characteristic at low q/A and low pressures, possibly partly a result of the hysteresis effect. A comparison of these results at a pressure of 1 BAR (0.987 ATM.) is made with the measurements of Bewilogua, et al. and Lapin, et al. (186, 187) in Figure 74. Also shown is the nucleate boiling correlation of Kutateladze, Equation (88), indicating a moderate to poor agreement especially at heat flux above 1 watt/cm^2. The hysteresis effect and the difference between the increasing-decreasing heat flux characteristic on nucleate boiling is shown clearly in Figure 75 for a pressure of 4 bars (3.948 ATM.).

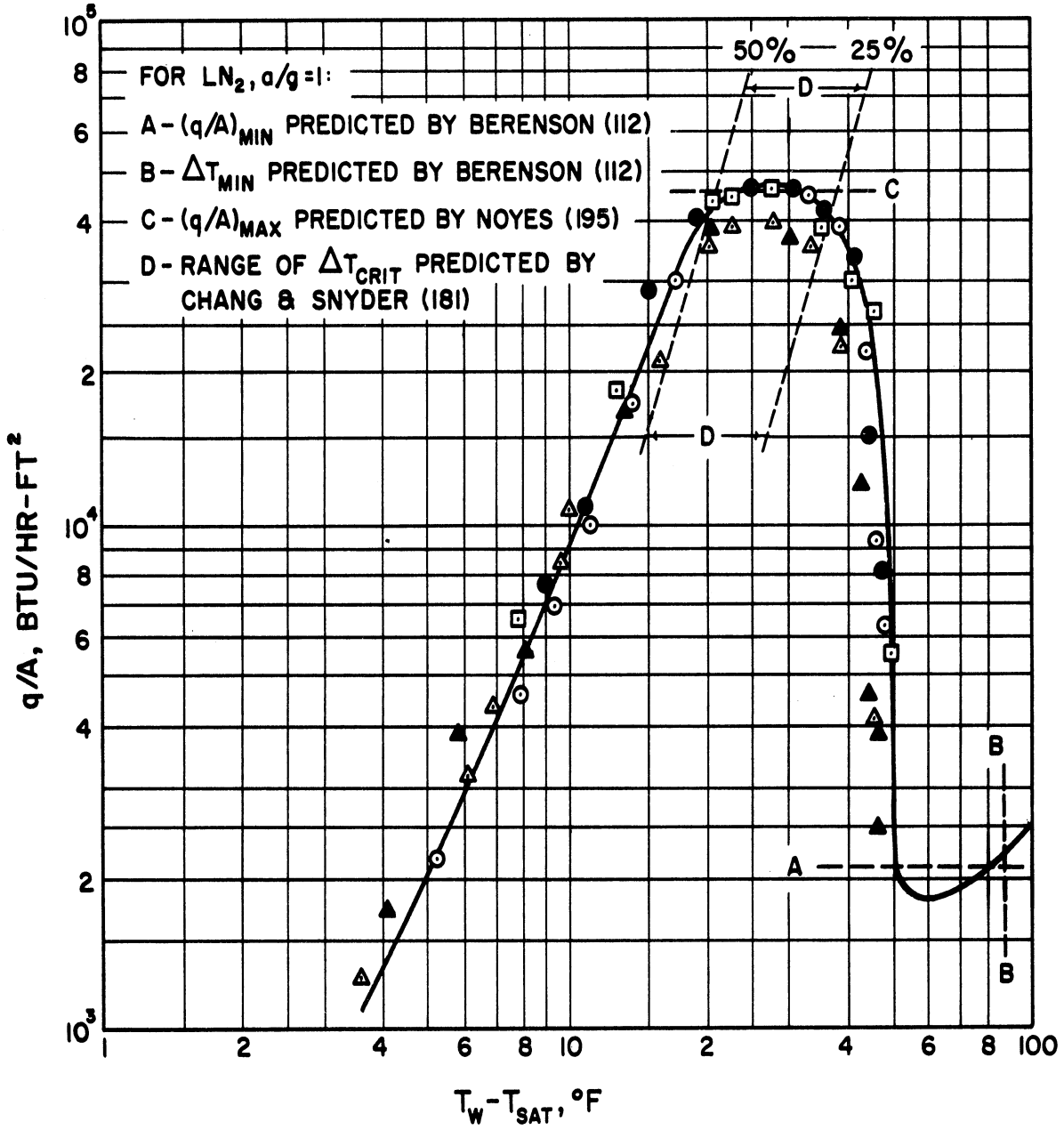

Figure 72. Comparison of Results for Liquid Nitrogen at 1 ATM Reduced Manually and by Digital Computer. a/g = 1, 1-inch Diameter Sphere.(90)

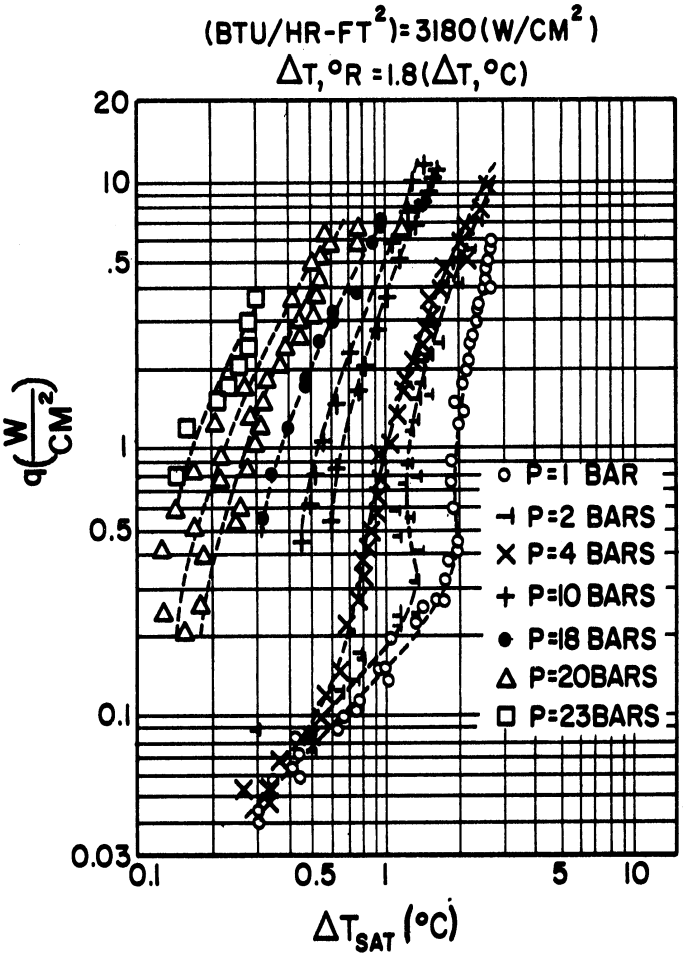

Figure 73. Some Experimental Results on Nucleate Pool Boiling of Neon (Pt Wire, Diam. 0.015 cm).

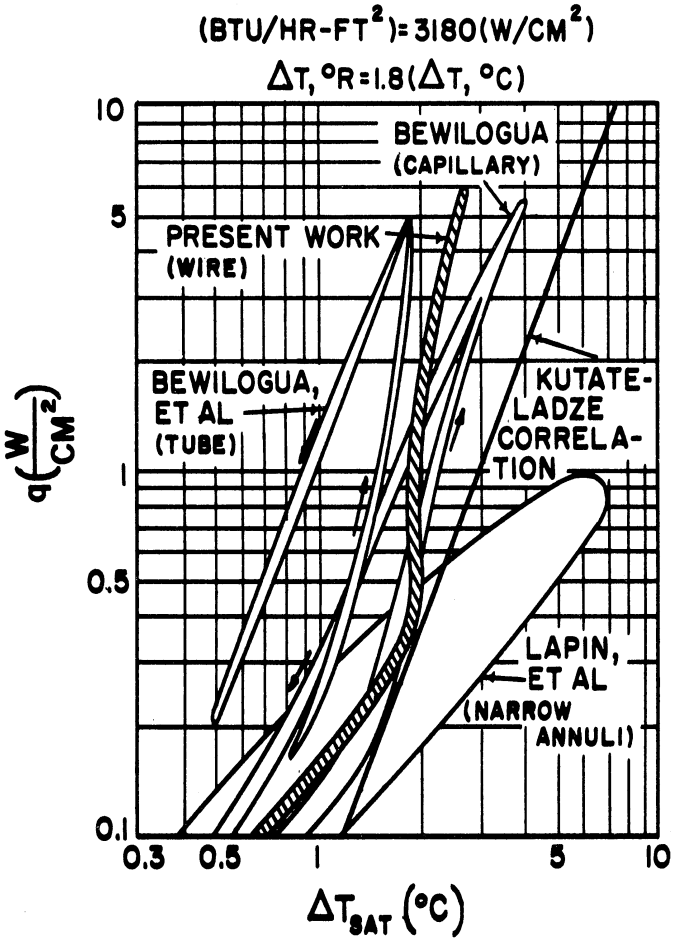

Figure 74. Experimental Nucleate Pool Boiling of Neon at 1 Bar Compared With the Predictive Correlation of Kutateladze.

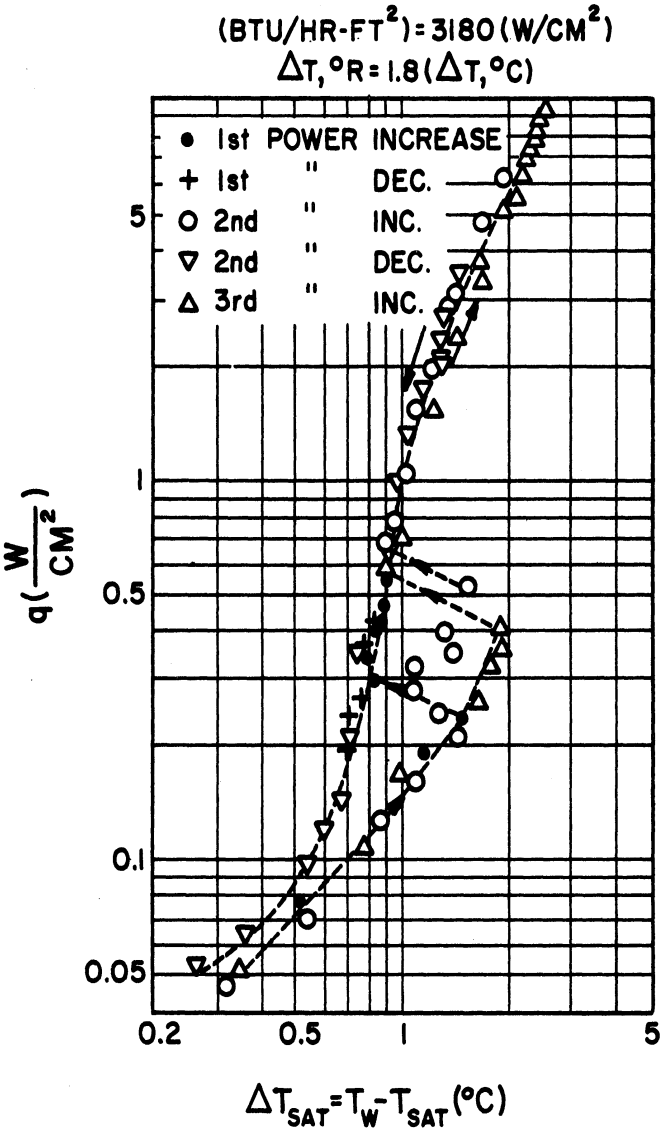

Figure 75. Hysteresis at Very Low Heat Flux in Nucleate Pool Boiling of Liquid Neon. Absolute Pressure Four Bars.

Nucleate boiling data from an 0.811-inch diameter, 4-inch long gold plated cylinder at pressures from 1 ATM to 41.2 ATM (0.9 critical pressure) is reported by Sciance, et al. (188). Their nucleate and film boiling data are given in Figure 76. The correlations of Forster and Grief (177) and Madejski (189) were found unsatisfactory. However, a modified form of Rohsenow's correlation (175) in which pressure dependence was introduced was found to correlate the data for pressures below 0.7 the critical pressure. This equation is

$$\frac{q/A}{h_{fg}\mu_\ell}\left(\frac{g_c\sigma}{g(\rho_L - \rho_V)}\right)^{1/2} = 3.25(10^5)\left(\frac{C_{PL}\Delta T}{h_{fg}}\left(\frac{T/T_c}{P_{r\ell}}\right)^{1.18}\right)^{2.89} . \quad (99)$$

This result is shown in Figure 77 in comparison with the methane data. Equation (99) differs from Rohsenow's correlation by the inclusion of T/T_c and the exponents on the Prandtl number and $c_{p\ell}\Delta T/h_{fg}$.

Lewis, et al. (91) have measured the influence of pressure and sub-cooling on nucleate boiling of N_2 from a 1-inch diameter sphere. Their results for pressures of 1, 3 and 5 ATM and sub-cooling of 16, 22, 25F are shown in Figure 78.

b. Maximum and Minimum Heat Flux

The upper limit of heat flux for nucleate boiling and the lower limit of heat flux for film boiling, Figure 58, are each marked by unique physical states known as the maximum (or, first critical) heat flux and the minimum (or, second critical) heat flux. Each of these states is apparently characterized by a critical stability condition relating to the ability of liquid to maintain contact with the surface. Their physical states have been quite well defined by considerations of the stability of the liquid-vapor interface. In the case

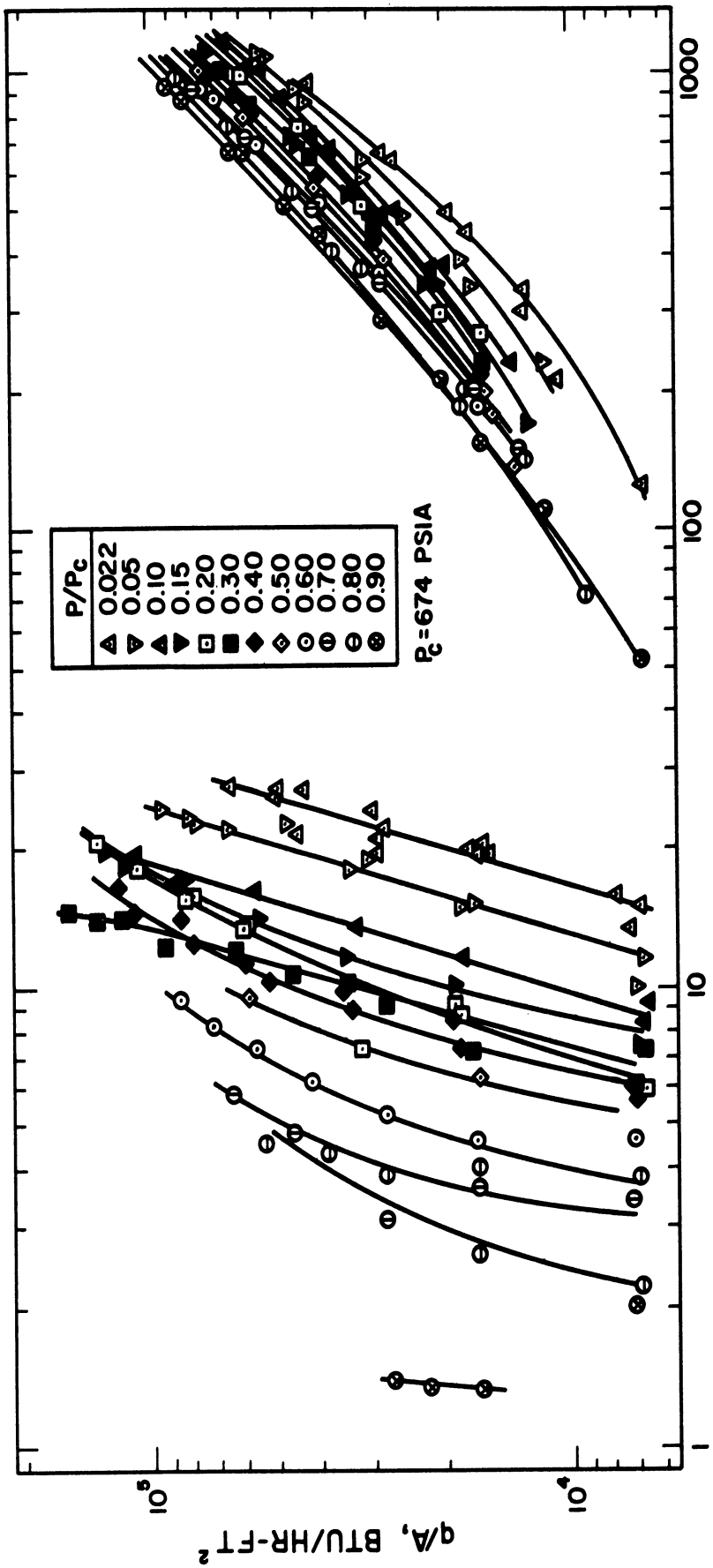

Figure 76. Nucleate and Film Boiling Data for Methane.(188)

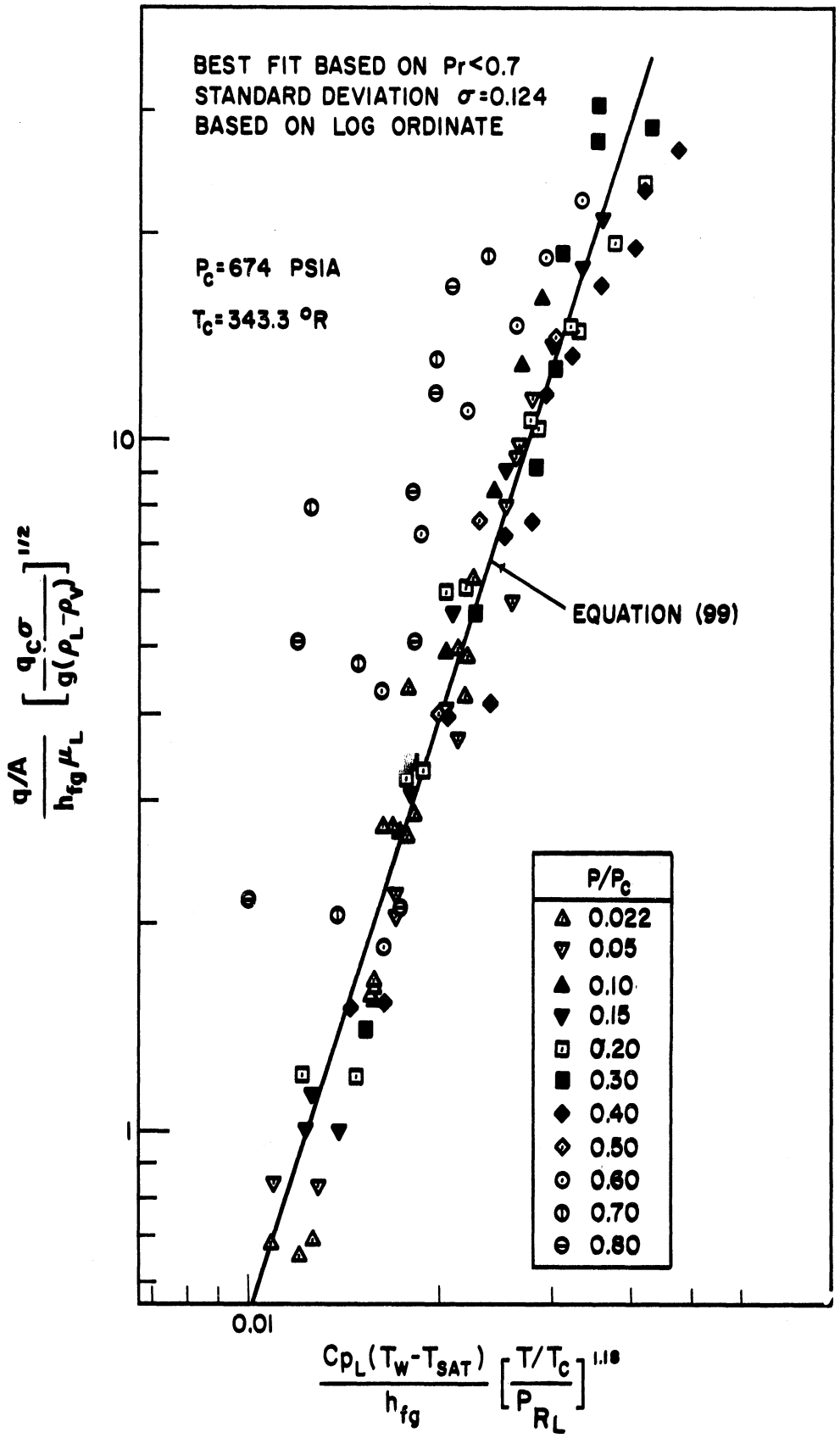

Figure 77. Nucleate Boiling Data for Methane Compared with Proposed Correlation.(188)

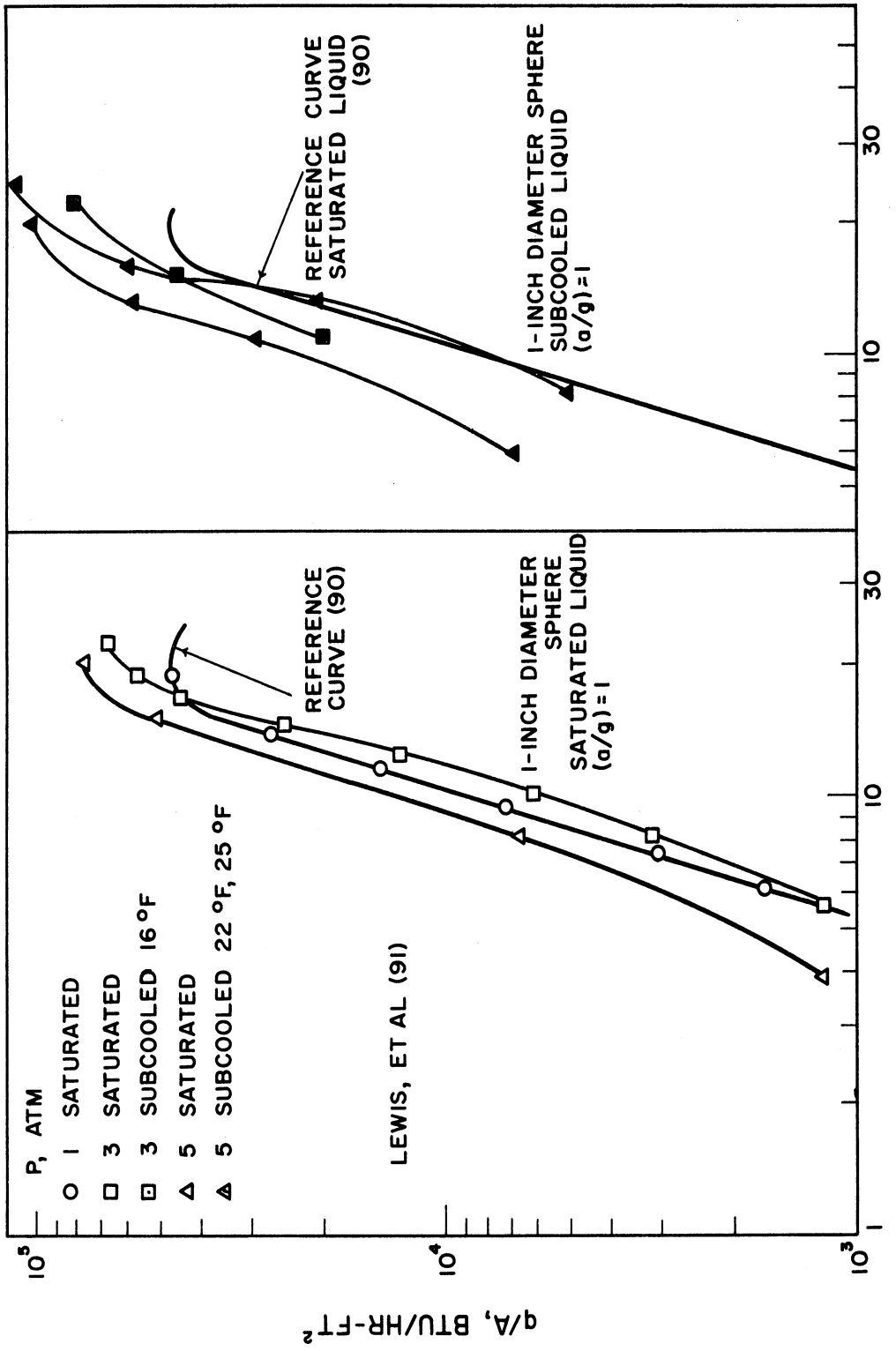

Figure 78. Effects of Pressure and Subcooling on Nucleate Boiling.

of the maximum heat flux the stability theory considers those conditions under which liquid no longer can adequately wet a heated surface. At a certain critical condition of bubble generation, the flow of vapor away from the surface has a destabilizing effect on the flow of liquid to the surface. This has been called the condition of Hemholtz instability. The minimum heat flux, on the other hand, represents a condition where, owing to interfacial stability of an overiding dense phase (for horizontal, upward facing surfaces, at least), the interface is disrupted and vapor alone no longer is in contact with the surface, but liquid comes in contact with it. This condition has been called one of Taylor instability and is described in terms of the critical wave length of an interfacial disturbance. As might be expected the heat flux from a surface behaves in an opposite manner in these liquid-deficient and vapor-deficient states. This effect is clearly evident from Figure 58 and is probably one of the most uniquely distinguishing characteristics of boiling.

Kutateladze (190) was probably the first to point out that the critical heat flux conditions was a matter of hydrodynamic stability. However, Zuber (20), Chang (191) and Berenson (112) first applied the concepts of stability analysis to the process. Borishanskii (192) extended the work of Kutateladze to include the influence of viscosity, which usually is not particularly significant. Other work include that in References (149, 151, 193, 194, 196). A number of correlations for both maximum and minimum heat flux have appeared in the literature. Some of these can be represented by the functions

$$\frac{(q/A)_{max}}{h_{fg}\rho_v} = \Phi_1 \qquad (100)$$

and

$$\frac{(q/A)\ min}{h_{fg}\rho_{v_f}} = \Phi_2 \qquad (101)$$

In most cases the dependence on acceleration is given as $g^{1/4}$. Because of this and the fact that Zuber (20) has shown on the basis of stability analysis that the constant in the correlations is a pure numeric (and not a function of the state of the fluid), each of the equations except that of Rohsenow and Griffith (194) is written with an acceleration dependence of $(a/g)^{1/4}$. This was not in the orginal equations. The value of g is that corresponding to gravitational acceleration on the earth's surface (32.2 ft/sec^2), the condition under which the theories were based and essentially all the measurements were made.

The various functions Φ_1 and Φ_2 are listed in Tables XI and XII, taken from Seader, et al (27). It should be noted that both Φ_1 and Φ_2 have the dimensions of a velocity. Several of the correlations in Table XI are compared with experimental maximum heat flux data for liquid nitrogen (90) in Table XIII. In this comparison the equations of Noyes (195) and Zuber (20) most closely represent the data on liquid nitrogen at 1 atm. The calculation from Noyes' equation is shown as line C in Figure 72. The computed result from the equation of Kutateladze, Equation (104), for $(q/A)_{max}$ is shown in Figures 60, 61, 62 and 63 in comparison with experimental data for O_2, N_2, H_2 and He. The agreement is quite favorable. Since Zuber's and Kutateladze's equations are essentially identical the same agreement could be expected from Zuber's equation. Equation (104) of Kutateladze is also used as the upper limit to his nucleate boiling correlation as shown in Figures 64, 65, 66 and 67 for O_2, N_2, H_2 and He.

TABLE XI

SUMMARY OF POOL NUCLEATE BOILING MAXIMUM HEAT FLUX THEORIES (27)

$$\frac{(q/A)_{max}}{h_{fg}\,\rho_V} = \Phi_1$$

Reference	Φ_1 [Length/Time]	Equation No.
Rohsenow and Griffith (194)	$143\left(\frac{\rho_L - \rho_V}{\rho_V}\right)^{0.6}$, ft/hr	102
Zuber (20)	$\frac{\pi}{24}\left[\frac{\sigma g g_o (\rho_L - \rho_V)}{\rho_V^2}\right]^{1/4}\left(\frac{\rho_L}{\rho_L + \rho_V}\right)^{1/2}\left(\frac{a}{g}\right)^{1/4}$	103*
Kutateladze (190)	$0.16\left[\frac{\sigma g g_o (\rho_L - \rho_V)}{\rho_V^2}\right]^{1/4}\left(\frac{a}{g}\right)^{1/4}$	104
Borishanskii (192)	$\left[\frac{\sigma g g_o (\rho_L - \rho_V)}{\rho_V^2}\right]^{1/4}\left(\frac{a}{g}\right)^{1/4}\left\{0.13 + 4\left[\frac{\mu_L^2 [g(\rho_L - \rho_V)]}{\rho_L (\sigma g_o)^{3/2}}\right]^{1/2}\right\}^{0.4}$	105
Noyes (195)	$0.144\left[\frac{g g_o \sigma}{\rho_L}\right]^{1/4}\left(\frac{\rho_L - \rho_V}{\rho_V}\right)^{1/2}\left(\frac{C_{p_L}\,\mu_L}{k_L}\right)^{-0.245}\left(\frac{a}{g}\right)^{1/4}$	106
Chang and Snyder (181)	$0.145\left[\frac{\sigma g g_o (\rho_L - \rho_V)}{\rho_V^2}\right]^{1/4}\left(\frac{\rho_L + \rho_V}{\rho_L}\right)^{1/2}\left(\frac{a}{g}\right)^{1/4}$	107
Chang (196)	$K\left[\frac{\sigma g g_o (\rho_L - \rho_V)}{\rho_V^2}\right]^{1/4}\left(\frac{a}{g}\right)^{1/4}$ {K = 0.098 vertical; K = 0.13 horizontal}	108
Moissis and Berenson (197)	$0.18\,\frac{\left[\sigma g g_o (\rho_L - \rho_V)\right]^{1/4}\left[\frac{\rho_L + \rho_V}{\rho_L \cdot \rho_V}\right]^{1/2}}{1 + 2(\rho_V/\rho_L)^{1/2} + (\rho_V/\rho_L)}\left(\frac{a}{g}\right)^{1/4}$	109

* In a later discussion of Berenson's paper (112), Zuber gives a range for the constant in Equation (103) to be from 0.120 to 0.157.

TABLE XII

SUMMARY OF POOL FILM BOILING MINIMUM HEAT FLUX THEORIES (27)

$$\frac{(q/A)_{min}}{h_{f_g}(\rho_V)_f} = \Phi_2$$

Reference	Φ_2 [Length/Time]	Equation No.
Zuber and Tribus (193)	$K_1 \left[\frac{\sigma g g_o(\rho_L - \rho_V)}{(\rho_L + \rho_V)^2}\right]^{1/4} \left(\frac{a}{g}\right)^{1/4}$, K_1 = 0.099 to 0.131	110
Zuber and Tribus (193) (alternate approach)	$K_2 \left[\frac{\sigma g g_o}{\rho_L - \rho_V}\right]^{1/4} \left(\frac{a}{g}\right)^{1/4}$ K_2 = 0.109 to 0.144	111
Zuber (20)	$\frac{\pi}{24} \left[\frac{\sigma g g_o(\rho_L - \rho_V)}{(\rho_L + \rho_V)^2}\right]^{1/4} \left(\frac{a}{g}\right)^{1/4}$	112*
Berenson (112)	$0.09 \left[\frac{\sigma g g_o(\rho_L - \rho_V)}{(\rho_L + \rho_V)^2}\right]^{1/4} \left(\frac{a}{g}\right)^{1/4}$	113
Lienhard and Wong (151)	$0.114 \left(\frac{1}{D}\right) \left[\frac{2g(\rho_L - \rho_V)}{(\rho_L + \rho_V)} + \frac{4\sigma g_o}{D^2(\rho_L + \rho_V)}\right]^{1/2} \left[\frac{g(\rho_L - \rho_V)}{g_o \sigma} + \frac{2}{D^2}\right]^{-3/4}$	114

* In a later discussion of Berenson's paper (112), Zuber gives a range for the constant in Equation (112) to be from 0.110 to 0.142.

TABLE XIII

COMPARISON OF $(q/A)_{max}$ CORRELATIONS FOR SATURATED LIQUID NITROGEN (AT ATMOSPHERIC PRESSURE AND a/g = 1) AND EXPERIMENTAL DATA

Investigator	Equation No.	$(q/A)_{max}$, BTU/hr-ft^2
Noyes (195)	(106)	45,000
Chang and Snyder (181)	(107)	56,500
Zuber (20)	(103)	50,100
Kutateladze (190)	(104)	61,000
Borishanskii (192)	(105)	61,000
Chang (196)	(108)	38,500-50,000
Moissis and Berenson (197)	(109)	65,000
Merte and Clark (90)	Experimental	47,000 $\pm$ 1000

Chang and Synder (181) derived an expression for ΔT_{crit} by equating the maximum heat flux, Equation (107) to the product of the ΔT_{crit} and their correlation for h in nucleate boiling, resulting in:

$$\Delta T_{crit} = \begin{Bmatrix} 0.725 \\ 1.450 \end{Bmatrix} \times 10^3 \frac{(h_{fg}\rho_v)^{9/5}\sigma[gg_o\sigma(\rho_\ell-\rho_v)]^{1/4}}{\rho^{1/2}k_\ell[C_pT_s(\rho_\ell-\rho_v)]^{2/5}\Delta P^{7/5}} \left(\frac{a}{g}\right)^{1/4} \qquad (115)$$

The range in the constant arises from the assumption of from 25% to 50% coverage of the heater surface by the bubbles at the maximum heat flux. This range for liquid nitrogen is shown as lines D in Figure 72. The results bracket the experimental value of ΔT_{crit}.

Maximum heat flux data for the cryogenic liquids O_2, N_2, H_2, He and Ne taken by a large number of investigators on plates, cylinders and wires is shown in Figure 79. Comparison is made with Equation (104) but only fair to moderate agreement is found. Astruc, et al (184) found

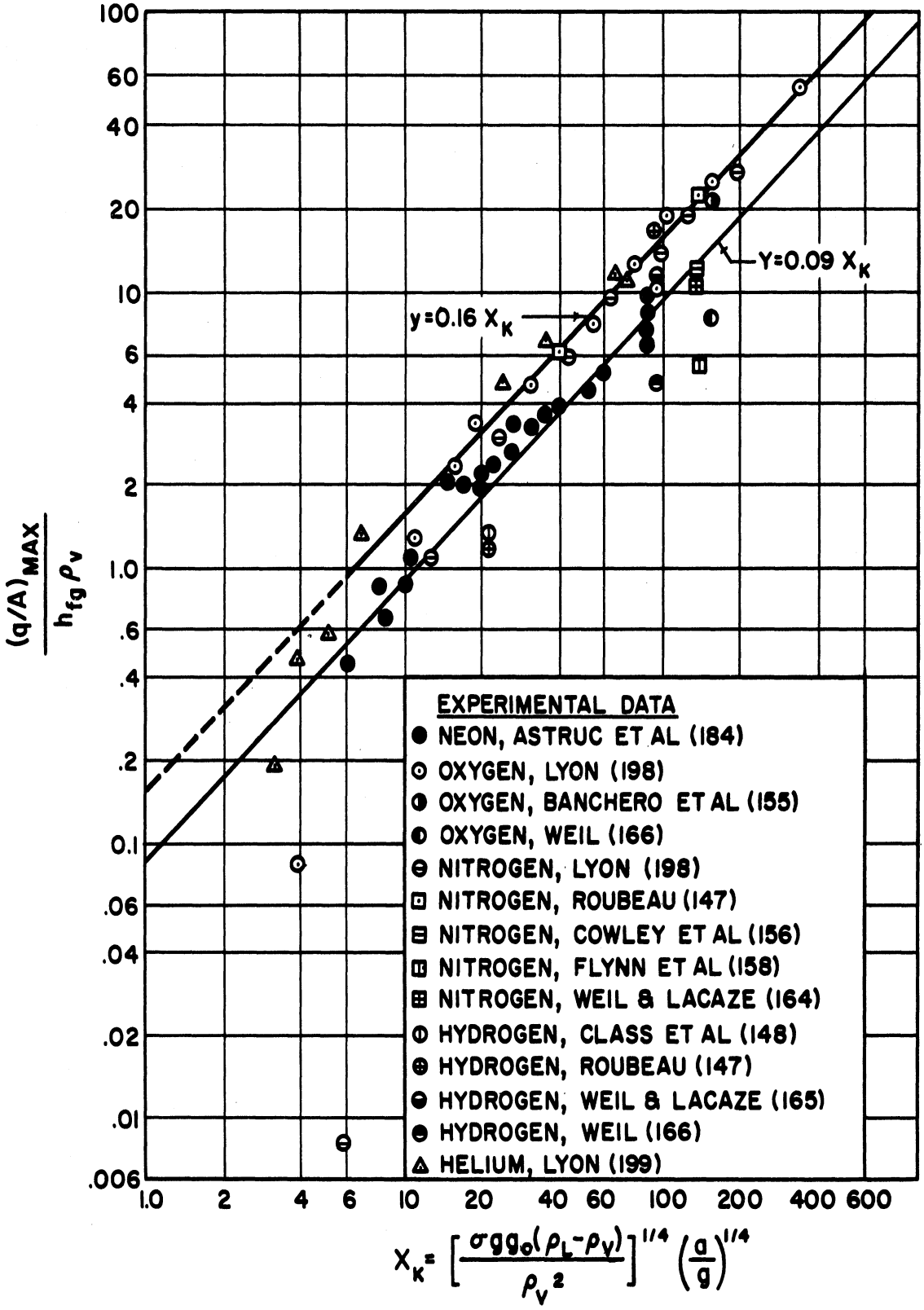

Figure 79. Comparison of the Maximum Nucleate Heat Transfer Fluxes with the Kutateladze Maximum Correlation.

that a best fit with their neon data was with a relation $y = 0.09\chi_k$, whereas the remainder of the data in Figure 49, except for exceptionally low O_2 and N_2 points of Lyon, seemed to correlate best by $y = 0.16\chi_k$, the Kutateladze equation. Interestingly, the approximate mean curve through all the data would be that of Zuber (20), $y = (\pi/24)\chi_k$.

The maximum heat flux data of Science, et al (188) for the boiling of methane outside a 0.811 inch dia. tube over a wide range of pressures is shown in Figure 80 in comparison with Equation (106), the correlation of Noyes (195). An excellent order of agreement is found over the full range of pressures. Noyes' correlation and some cited by McAdams (74) for water and organic liquids are the only equations in which the thermal transport properties of the liquid are considered in the description of the process. The peaking of $(q/A)_{max}$ at P/P_c about 0.30 is typical.

The influence of pressure, subcooling and a/g on the maximum heat flux is shown in Figure 81, from the results of Lewis, et al (91). The effect of both subcooling and pressure is to increase the magnitude of $(q/A)_{max}$. This observed influence of pressure is valid up to about $0.3\ P_{crit.}$, as shown in Figure 90.

A comparison of Berenson's correlation, Equation (113), for the minimum heat flux is shown in Table XIV with experimental liquid nitrogen data at various accelerations (a/g) from 1 to 0.001 (90). The comparison is generally favorable and tends to confirm the $(a/g)^{1/4}$ dependence predicted by the Equations (110 - 113), at least for an (a/g) above approximately 0.10. The calculation from Berenson's Equation is shown as line A in Figure 72.

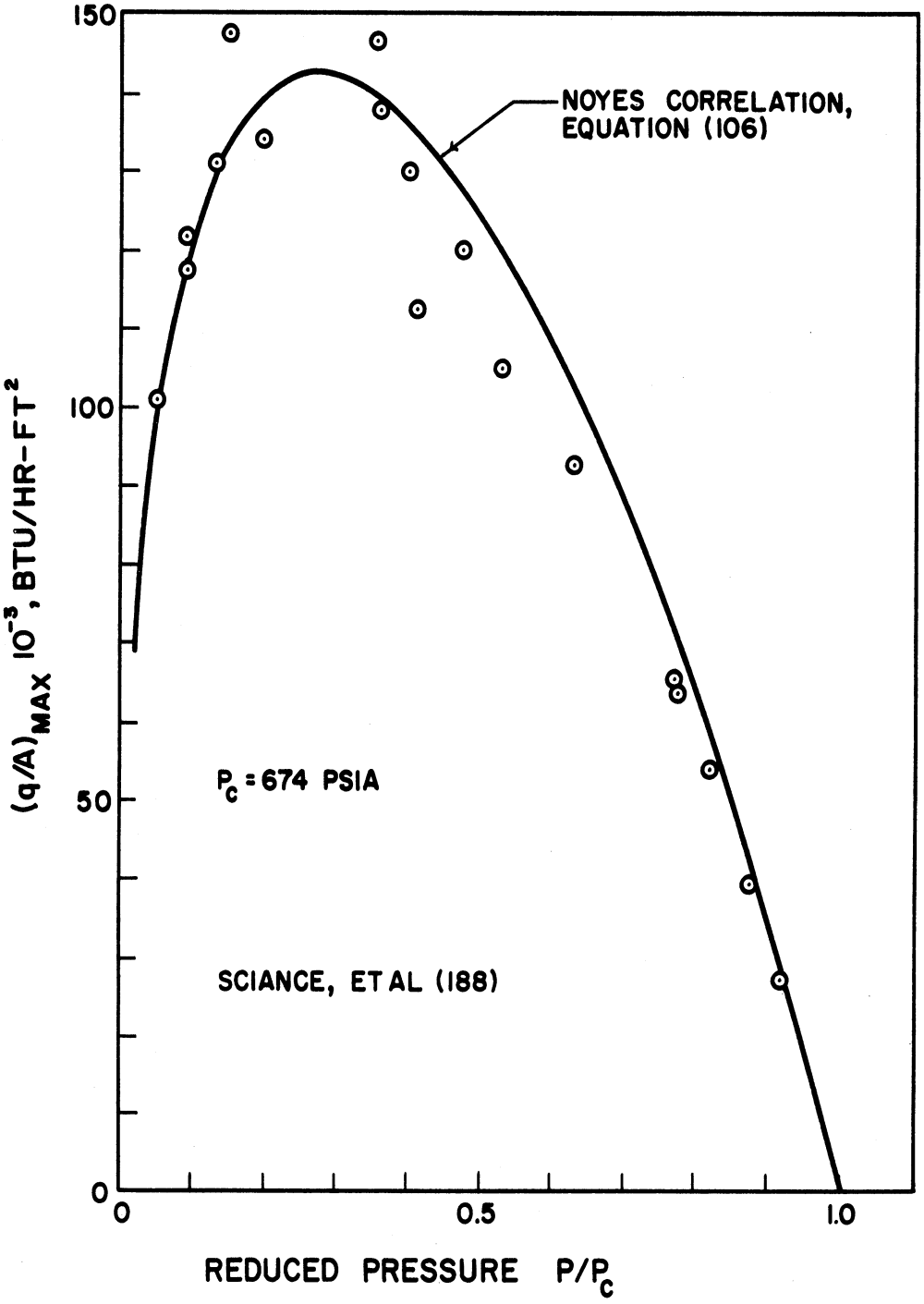

Figure 80. Methane Burnout Heat Flux Compared With the Noyes Correlation,[195] Equation.[106]

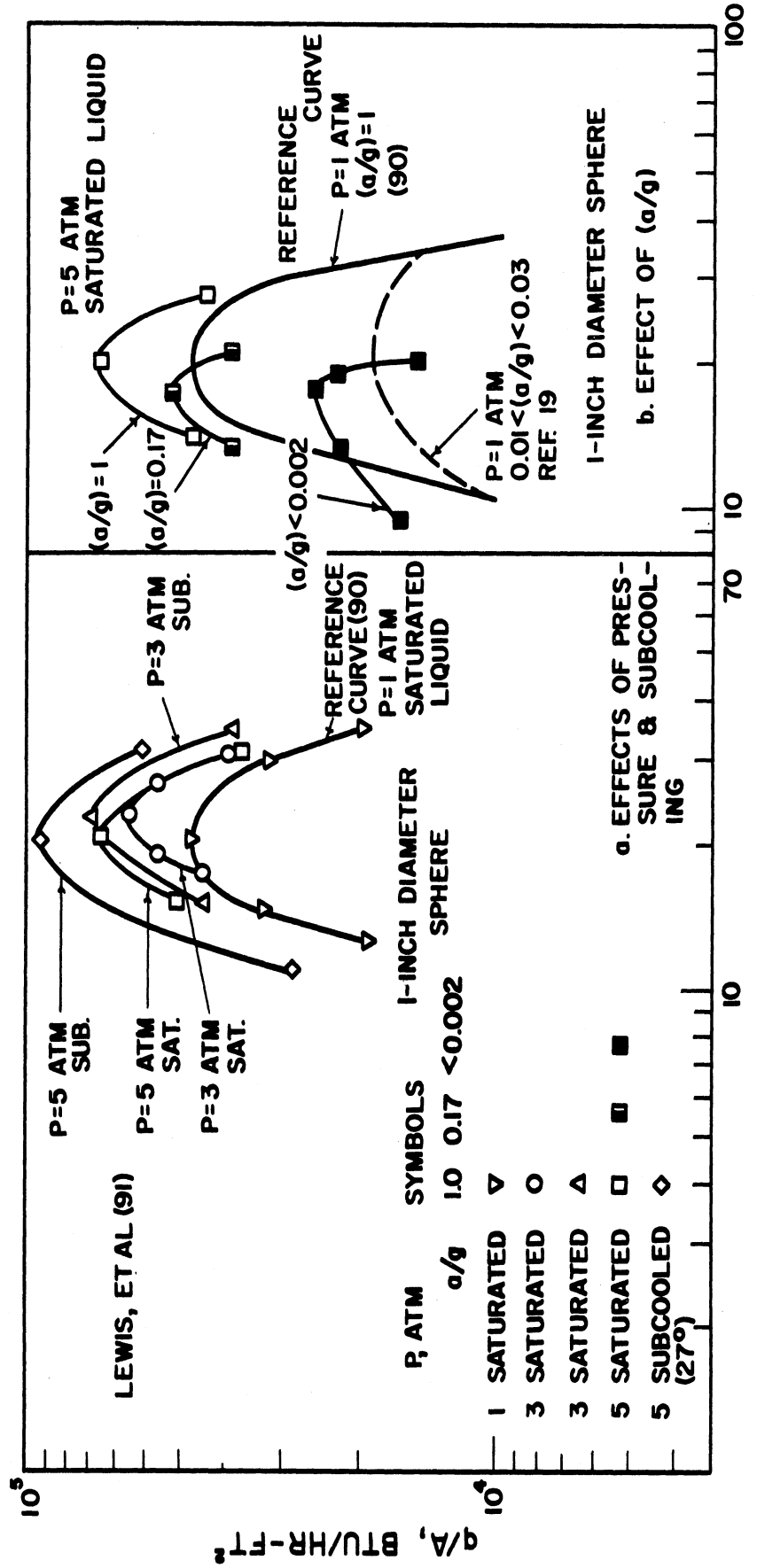

Figure 81. Effects of Pressure, Subcooling, and (a/g) on $(q/A)_{max}$.[91]

TABLE XIV

COMPARISON OF EXPERIMENTAL AND PREDICTED VALUES OF $(q/A)_{min}$, EQUATION (113)

Merte and Clark (90)

a/g	$(q/A)_{min}$-predicted	$(q/A)_{min}$-experimental
1	2100	1700 - 2100
.6	1850	1550
.33	1590	1300 - 1400
.20	1400	1300
.03	875	870 - 1100
.01	666	
.003	491	180 - 530
.001	374	

The correlations of Lienhard and Wong (151) and Zuber (20), Equations (114) and (112), respectively, for the minimum heat flux are given in Figures 60, 61, 62 and 63 for O_2, N_2, H_2 and He in comparison with some experimental data. The comparisons are reasonable. The same correlations are used to establish the lower limit for flim boiling in Figures 64, 65, 66 and 67 for O_2, N_2, H_2 and He. The correlation of Lienhard and Wong is an extension of the concept of Taylor instability introduced by Zuber and takes into account physical systems of small size.

An interesting result is obtained for the ratio $(q/A)_{max}/(q/A)_{min}$ using the correlations of Zuber, Equations (103) and (112). This ratio may be written,

$$\frac{(q/A)_{max}}{(q/A)_{min}} = \left(\frac{\rho_\ell}{\rho_V}\right)^{1/2} \qquad (116)^*$$

Thus, with this simple result the maximum heat flux or the minimum heat flux may be estimated from a measurement of the other. Equation (116) suggests that $(q/A)_{max}$ and $(q/A)_{min}$ approach the same value of high pressures, a reasonable conclusion, confirmed by experience.

An equation for ΔT_{min} was derived by Berenson (112) by equating the minimum heat flux, Equation (113), to $h \cdot \Delta T_{min}$ using his correlation (112) for film boiling, resulting in:

$$\Delta T_{min} = 0.127 \frac{\rho_{vf} h_{fg}}{k_{vf}} \left[\frac{g(\rho_\ell - \rho_v)\mu_f}{(\rho_\ell + \rho_v)^{1/2}}\right]^{1/3} \left[\frac{g_o \sigma}{g(\rho_\ell - \rho_v)}\right]^{1/2} \left(\frac{a}{g}\right)^{-1/6} \qquad (117)$$

This result for liquid nitrogen at $a/g = 1$ is also indicated on Figure 72 as line B. In this case the comparison is only fair.

Lewis, et al (91) studied the influence of pressure and sub-cooling on $(q/A)_{min}$ for liquid nitrogen. Their measurements for pressures of 1, 3 and 5 ATM and an average sub-cooling of 29°F for N_2 boiling on a 1-inch diameter sphere are given in Figure 82. Some data for the transition region are included for completeness. The effect of increase in both pressure and sub-cooling is to increase $(q/A)_{min}$.

---

*Using the range of constants given in the footnotes to Equations (103) and (112), this would be written

$$\frac{(q/A)_{max}}{(q/A)_{min}} = (0.845\text{-}1.436) \left(\frac{\rho_\ell}{\rho_V}\right)^{1/2} \qquad (116a)$$

The results for N_2 in (90) suggest the larger value of the constant best fits the data.

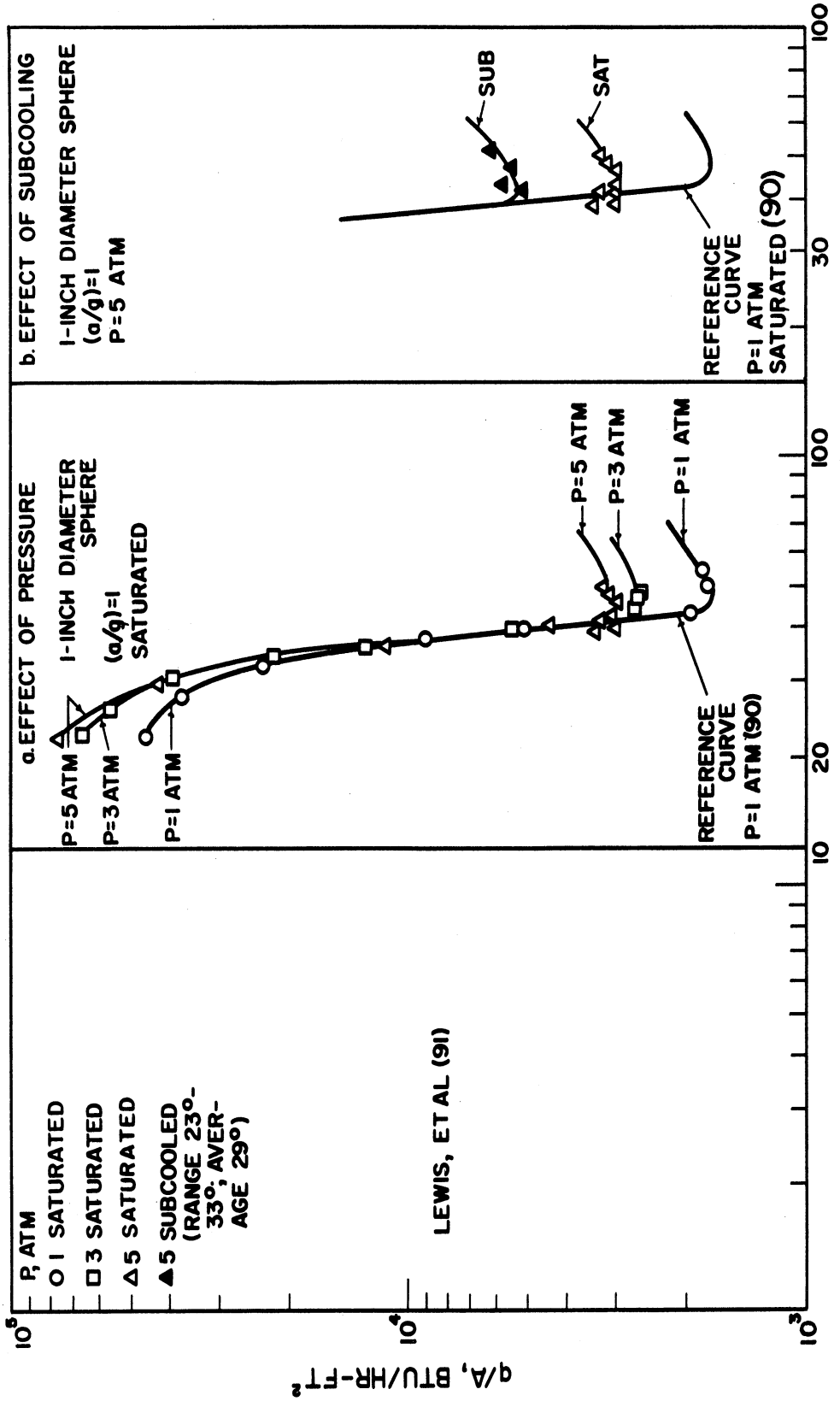

Figure 82. Effects of Pressure and Subcooling on $(q/A)_{min}$ and Transition Boiling.(91)

c. Transition Boiling

The region of transition boiling, Figures 58 and 82 has not been studied very extensively nor is it described by any known correlation equations. It is a region intermediate between the liquid-deficient, maximum heat flux condition and the vapor-deficient, minimum heat flux condition. Because it represents a state transition from basically a liquid-solid , $(q/A)_{max}$, heat transfer process to one in which the heat exchange is between the solid and vapor $(q/A)_{min}$, the heat flux is drastically reduced as the process goes from the maximum to the minimum heat flux condition. Only those physical systems having the surface temperature as the independent variable ever pass through the state of transition boiling. Systems which are controlled by establishing independent levels of (q/A) , such as electrically, chemically or nuclear heated systems, make rapid transition from the points $(q/A)_{max}$ or $(q/A)_{min}$ to either film boiling or nucleate boiling. The data in Figures 28 and 82 were obtained by cooling a copper sphere from a film boiling condition to one of non-boiling. In this way the complete boiling characteristic is obtained.

Presently, the only approach to the treatment of transition boiling is to make recourse to the basic $(q/A) - \Delta T$ data, where they are available. In the absence of data, it is suggested that the points $(q/A)_{max} - \Delta T_{crit}$ and $(q/A)_{min} - \Delta T_{min}$ be established using the correlations of the preceding section. The transition boiling region could then be estimated by fairing-in a suitable curve which would have an appropriate zero-slope at the maximum and minimum points. This will probably not produce data having a high degree of accuracy but could be used for preliminary estimates.

An interesting result in Figure 82 is the relative insensitivity of the transition region to pressure and sub-cooling. More data will be required before conclusions can be made on these effects, however.

d. Film Boiling

Film boiling can exist practically with cryogenic fluids because of their low saturation temperatures. In fact, it is possible to have a heat flux in film boiling greater than that of $(q/A)_{max}$ and still maintain sufficiently low surface temperatures to prevent melting. This may be seen especially for nitrogen in Figure 61 and helium in Figure 63. Because film boiling presents a reasonably well defined physical model (as compared with nucleate boiling) it has been treated analytically. Bromley (135) was one of the first to analyse this process and he modeled his study on the similarity to film condensation. Other such studies include those of Breen and Westwater (150), Frederking and Clark (200) Berenson (112), Chang (191) and Hsu and Westwater (152).

In practical systems the total rate of heat transfer from a surface in film boiling will include an important component of radiation because of the high surface temperatures. This effect is discussed by Brentari, et al (143) who point out that if the surface temperature is below 400 to 425°K (260 to 306°F) the maximum error in neglecting radiation is less than 5% for film boiling of O_2 , N_2, H_2 , and He . The error becomes approximately 50% for a doubling of the surface temperature.

Bromley (135) correlated film boiling to liquid nitrogen on the outside of horizontal cylinder by

$$\frac{hD_o}{k_f} = 0.62 \left(\frac{D_o^3 \rho_f (\rho_\ell - \rho_f) g \, h_{fg}}{k_f \mu_f \Delta T_{sat}} \left(1 + 0.4 \frac{c_{pf} \Delta T_{sat}}{h_{fg}}\right)^2 \right)^{1/4} \qquad (118)$$

For fluids of low latent heat ($c_p\Delta T_{SAT}/h_{fg} \gg 2$) such as helium and hydrogen, Frederking (169) modified this result by the following

$$\frac{hD_o}{k_f} = 0.522\left(\frac{1}{2}\,\frac{\rho_\ell}{\rho_f}\right)^{1/4}\left(\frac{D_o{}^3\rho_f{}^2 g\beta_f\Delta T_{sat.}}{\mu_f^2}\left(\frac{c_p\mu}{k}\right)_f\right)^{1/4} \qquad (119)$$

For circumstances in which $\rho_\ell \approx \rho_f$, i.e., at pressures near the critical pressure, this result is very similar to that for single phase free convection from a horizontal cylinder, Equation (73). Bromley's result assumes the vapor film to be of negligible thickness compared with the cylinder diameter. For small wires this is no longer true. Frederking's results for the film boiling of helium I from small wires and the results of others on the liquids of nitrogen, oxygen and helium for cylinders ranging in diameter from 0.0055 to 8.89 mm are correlated in terms of the Nusselt, Gaashof and Prandtl numbers in Figures 83 and 84. At low values of the Grashof-Prandtl numbers, Figure 83, ($10^{-7} \leq Gr\cdot Pr \leq 10^{-1}$), Frederking's helium data are correlated by

$$\frac{hD_o}{k_f} = 2.5\left(\frac{D_o{}^3\rho_f{}^2\, g\beta_f\Delta T_{sat}}{\mu_f{}^2}\left(\frac{c_p\mu}{k}\right)_f\right)^{0.11} \qquad (120)$$

The constant depends on the type of fluid. It is probably a function of the Prandtl number since the nitrogen data in Figure 83 fall slightly above those of helium for which the constant is equal to 2.5. It is probable the data in Figure 84 also are slightly spread owing a Prandtl number influence. More study is required to clarify this point.

Merte and Clark (134) obtained liquid nitrogen film boiling data from a 1-inch dia sphere using the transient method. These data are given in Figure 58 where they are compared with Bromley's results for a 0.350

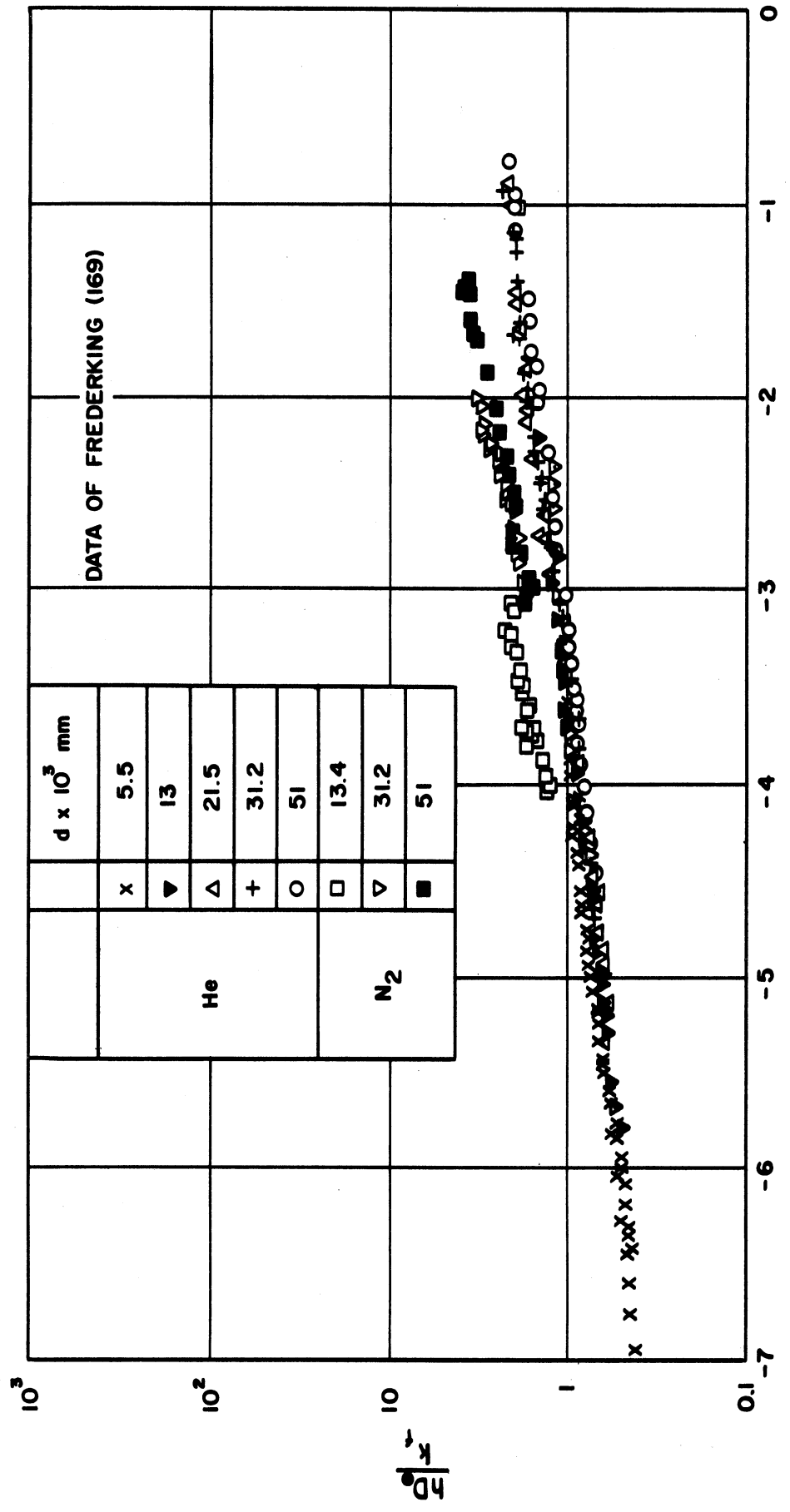

Figure 83. Film Boiling Data for Helium and Nitrogen at Low Grashof-Prandtl Numbers from Cylinders.

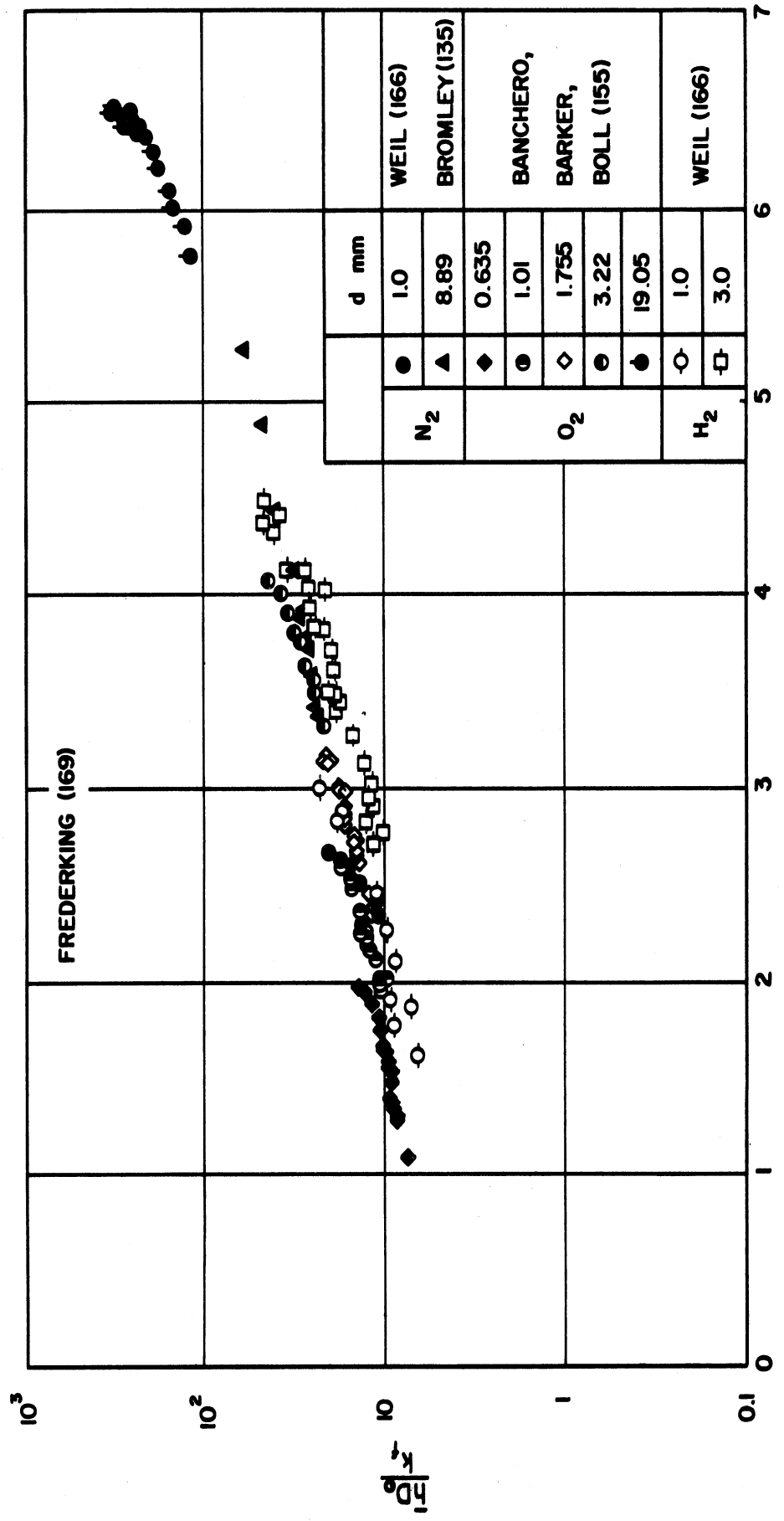

Figure 84. Film Boiling Data for Nitrogen, Oxygen and Hydrogen at High Grashof-Prandtl Numbers From Cylinders.

inch cylinder. The agreement is good. These data have been correlated by Frederking and Clark (200) by

$$\frac{hD_o}{k_f} = 0.14 \left[\frac{D_o^3 \rho_f (\rho_\ell - \rho_f) g}{\mu_f^2} \left(\frac{c_p \mu}{k} \right)_f \frac{h_{fg}}{c_p \Delta T_{sat}} \left(1 + 0.5 \frac{c_p \Delta T_{sat}}{h_{fg}}\right) \right]^{1/3} \tag{121}$$

The results are given in Figure 85 for liquid nitrogen. The similarity of this result with that for turbulent single phase natural convection, Equation (72) or (75) should be noted. Equation (121) has also correlated the film boiling data of Banchero, et al (155).

Lewis, et al (91) studied film boiling with liquid nitrogen from spheres of 1-inch, 1/2-inch and 1/4-inch diameter and from a 3-inch diameter flat disc. They investigated the influence of geometry, orientation and pressure on saturated film boiling and the effect of sub-cooling on film boiling. These data are given in Figures 86, 87, and 88 for pressures of 1, 3 and 5 ATM, average sub-cooling of 26°F and at standard gravity. An effect of size is shown in Figure 86 is consistent with that predicted by Breen and Westwater in Figures 64 to 67. Both increases in pressure and sub-cooling result in increased heat flux in film boiling, as indicated in Figures 87 and 88.

The data in reference (91) as well as that of Merte and Clark (90) are correlated over a range of pressures, sizes and a/g according to the parameters in Equation (121), as shown in Figure 89. The correlation of Frederking and Clark (200) is given for comparison. A reasonably valid correlation is obtained except for the data from the 1/4-inch diameter sphere. Also included are the freon 113 data of Pomerantz (201) taken on a 0.1875-inch dia. cylinder at (a/g) from 1 to 10. These data appear

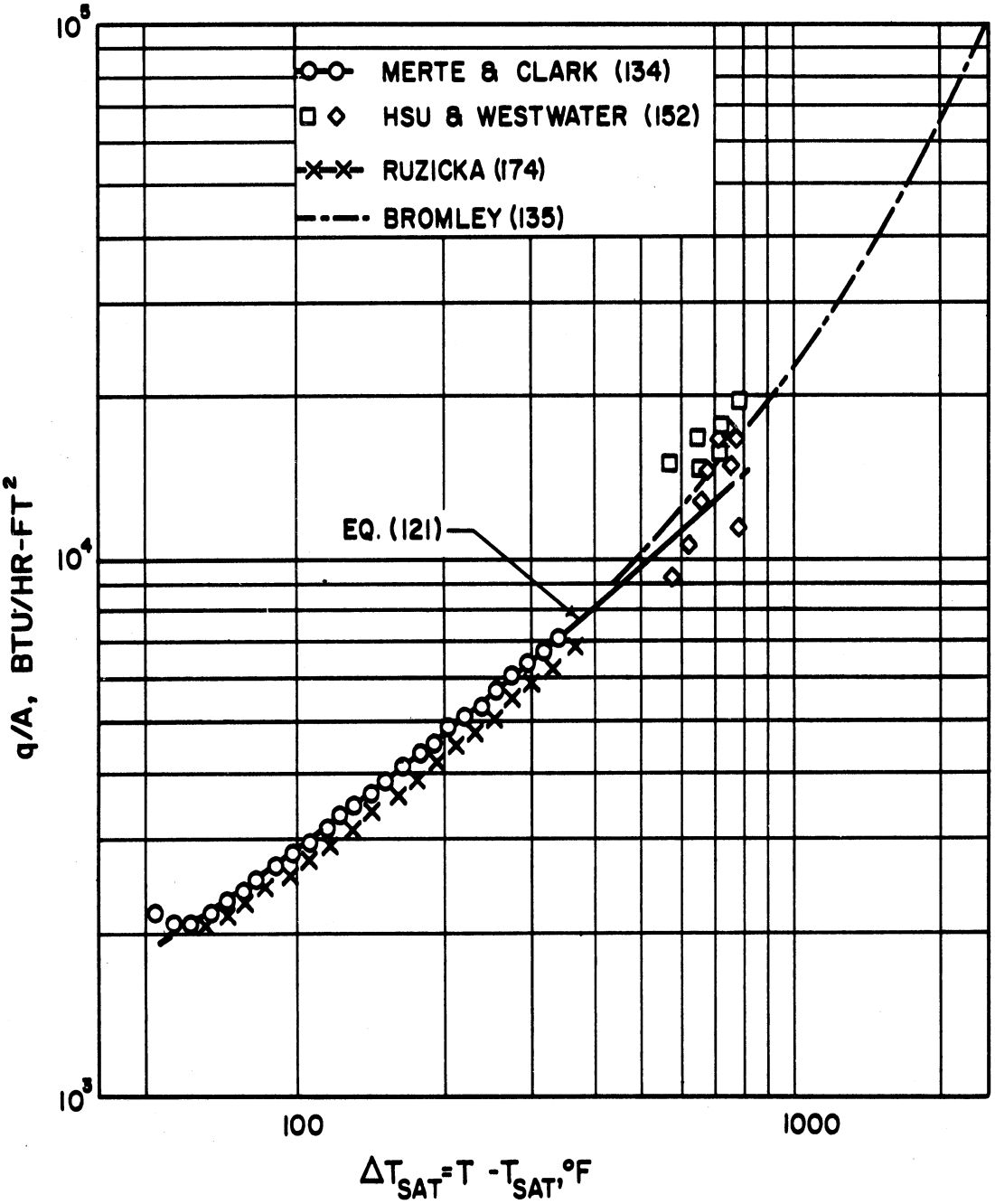

Figure 85. Film Boiling Heat Transfer Data for Nitrogen from a Sphere.(200)

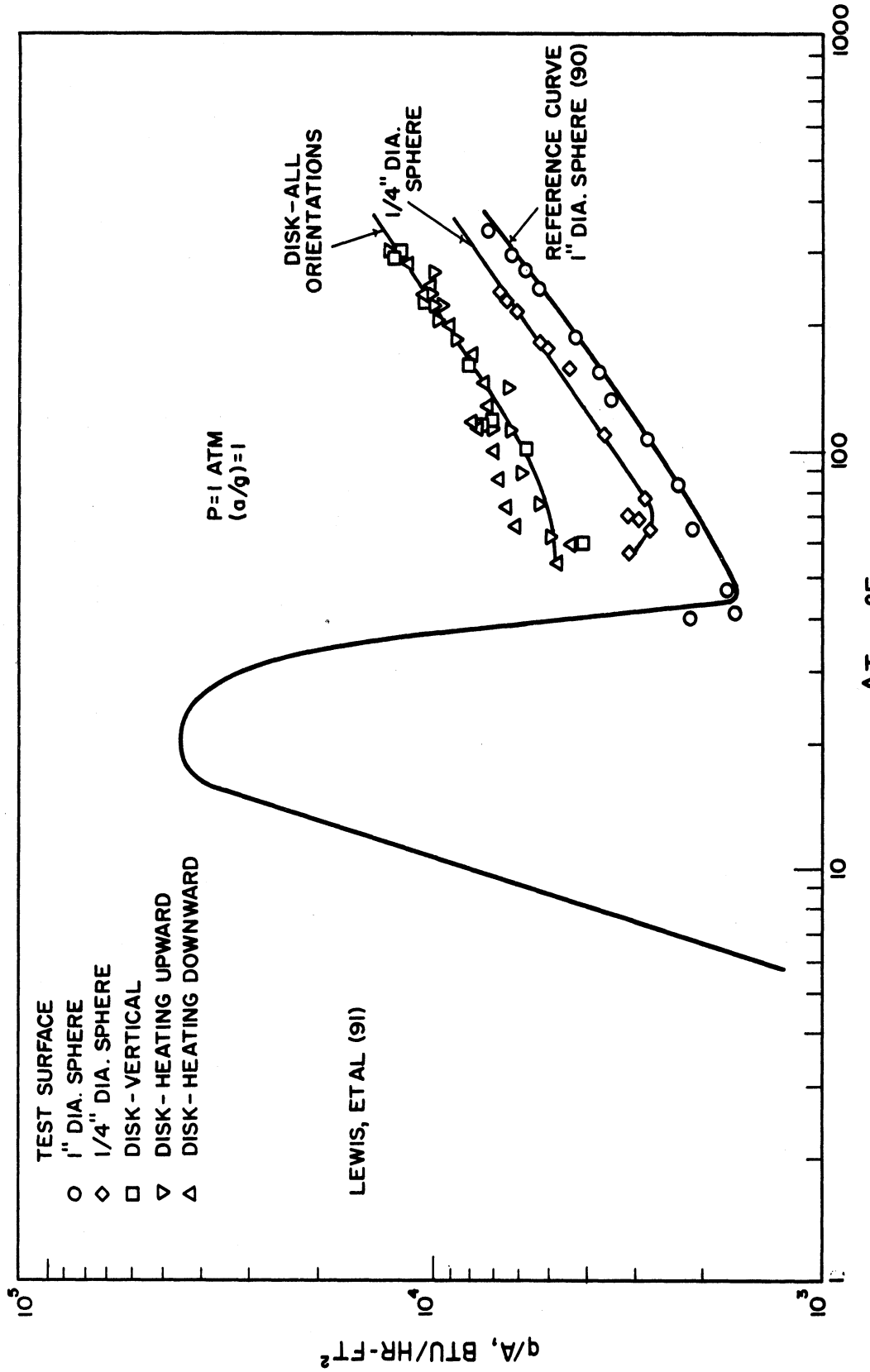

Figure 86. Effects of Geometry and Orientation on Saturated Film Boiling.(91)

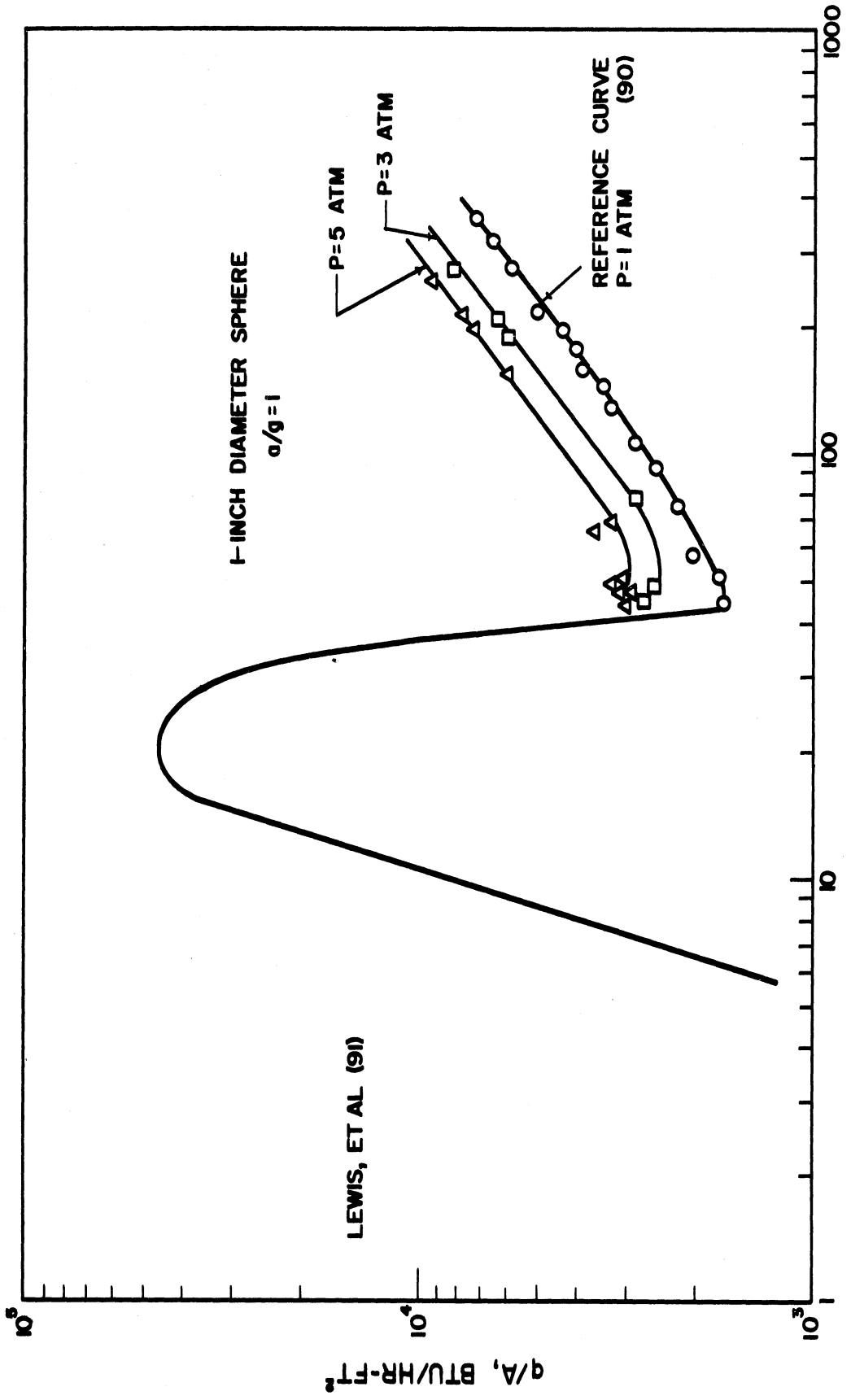

Figure 87. Effect of Pressure on Saturated Film Boiling.(91)

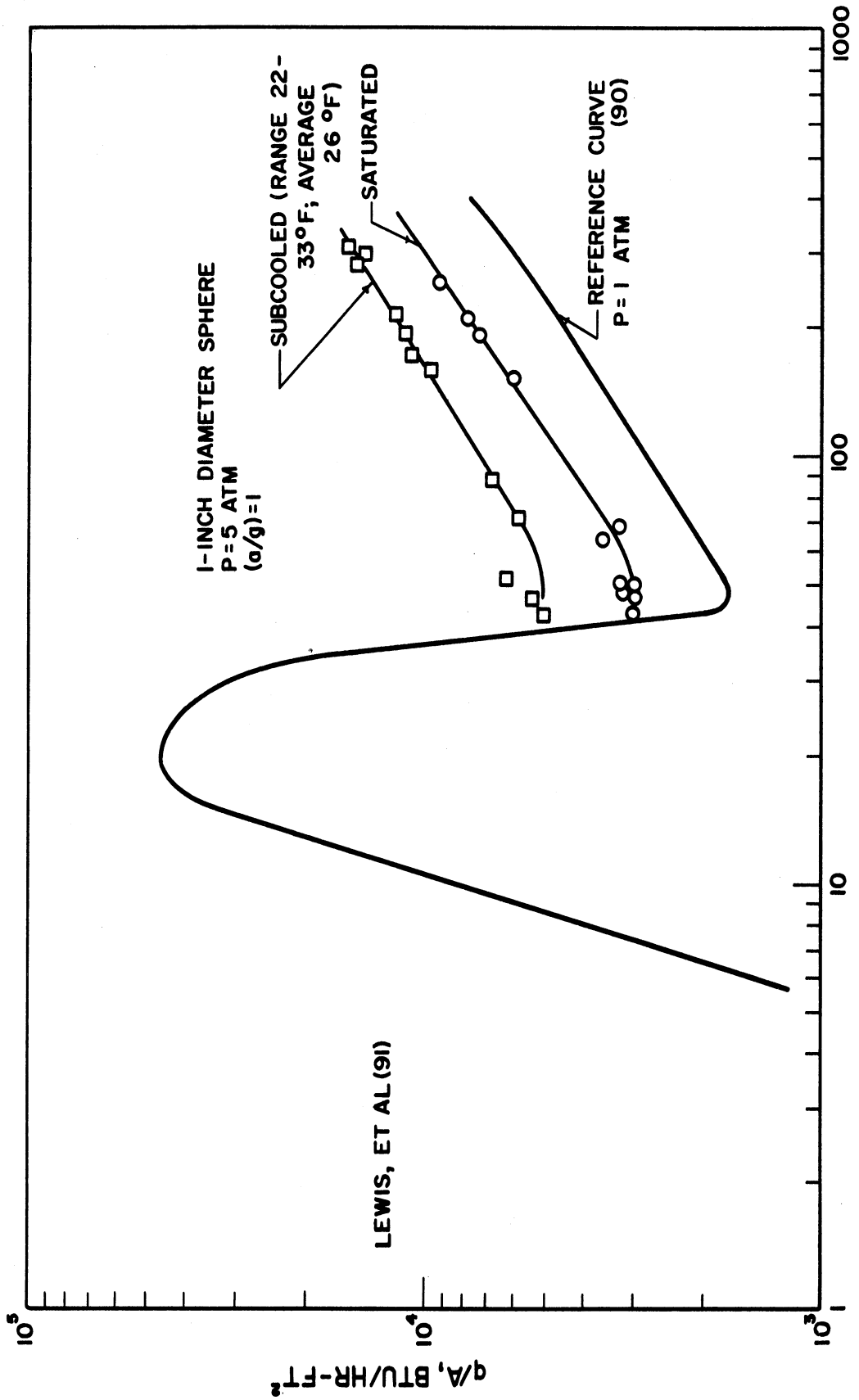

Figure 88. Effect of Subcooling on Film Boiling.(91)

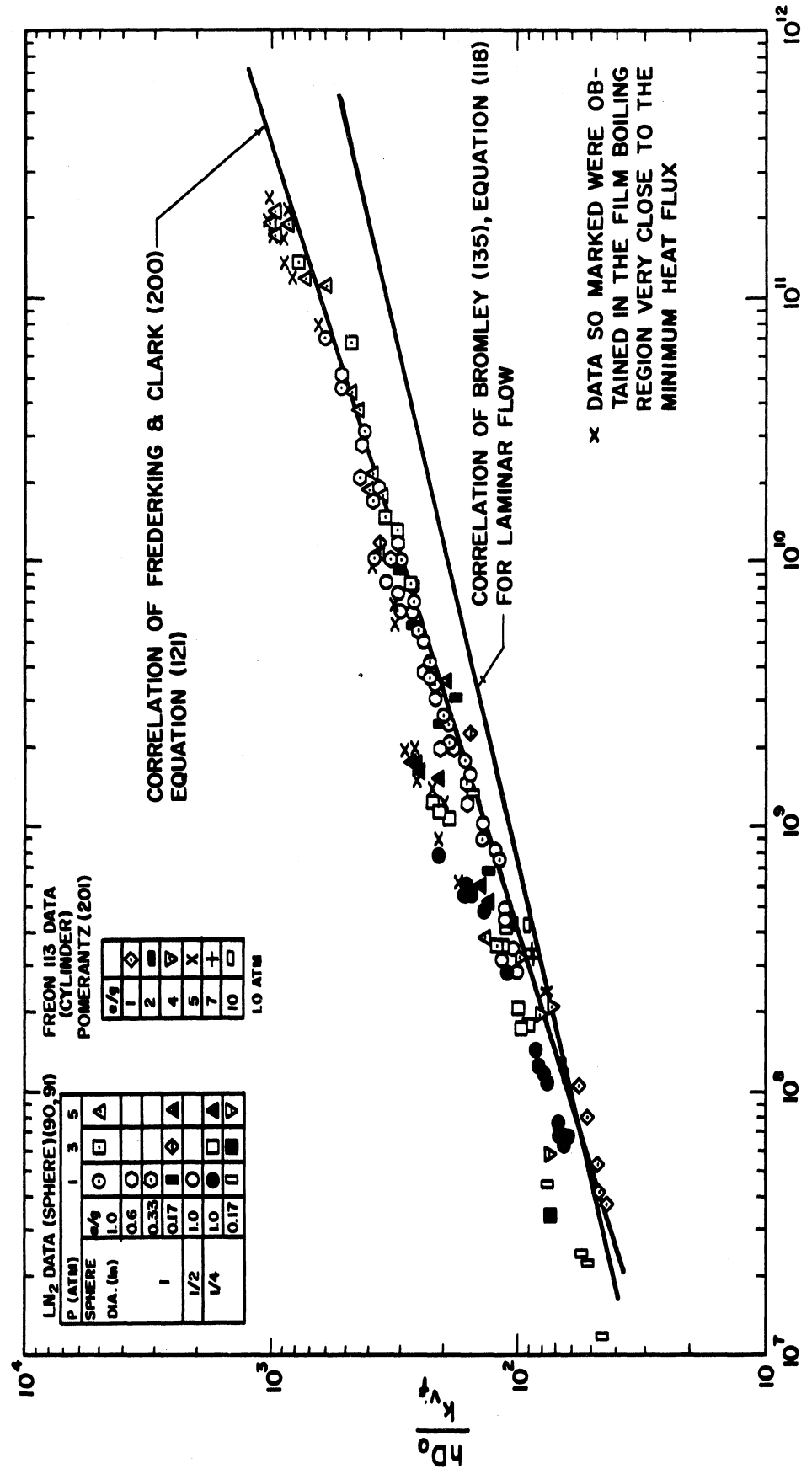

Figure 89. Comparison of Fractional Gravity Film Boiling Data for Liquid Nitrogen and Freon 113.(91)

to correlate well with Equation (121). Manson (202) found that her data for the film boiling in liquid nitrogen from a 3-inch dia. sphere fell about 7% below that predicted by Equation (121). The laminar film boiling correlation of Bromley is shown in Figure 89, indicating that transition to turbulent film boiling at Ra' in the range 10^7-10^8 .

The natural characteristic dimension for film boiling in systems of large physical dimension is probably the "critical" wavelength, λ_d , (112, 203), where

$$\lambda_c = 2\pi \left[\frac{g_o \sigma}{g(\rho_\ell - \rho_v)} \right]^{1/2} \left(\frac{a}{g} \right)^{-1/2} \qquad (122)$$

and

$$\lambda_d = \lambda_c \sqrt{3} \ . \qquad (123)$$

The flat plate data of Lewis, et al (91) for liquid nitrogen was correlated in terms of λ_c as shown in Figure 90. The best fit equation for what is believed to be turbulent film boiling is

$$Nu_\lambda = 0.012 \, Ra'_\lambda{}^{1/2} \ , \qquad (124)$$

where,

$$Nu_\lambda = \frac{h\lambda_c}{k_{vf}}$$

and

$$Ra'_\lambda = \frac{\lambda_c^3 \, \rho_{vf}(\rho_\ell - \rho_{vf}) g}{\mu_{vf}^2} \left(\frac{c_p \mu}{k} \right)_{vf} \left(\frac{h_{fg}}{c_p \Delta T_{sat}} + 0.5 \right) \left(\frac{a}{g} \right)^{2/3} . \qquad (125)$$

Also included in this figure is the laminar film boiling correlation of Berenson (112), which may be written

$$\frac{h\lambda_c}{F_1}^{1/4} = 0.672 \qquad (126)$$

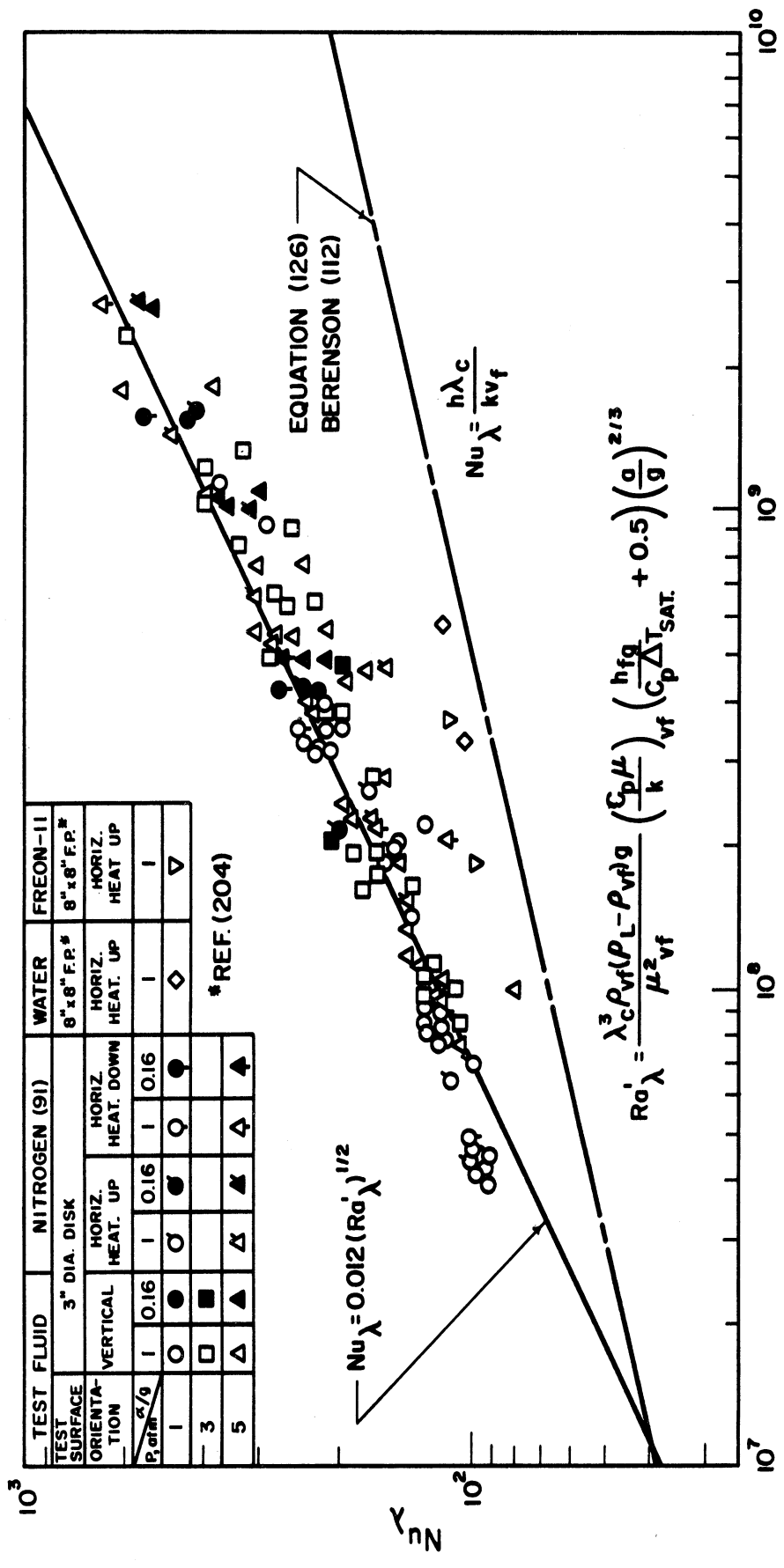

Figure 90. Saturated Film Boiling Correlation for Flat Plates.(91)

where

$$F_1 = \left(\frac{k_v^3 \rho_v (\rho_\ell - \rho_v) g \, h'_{fg}}{\mu_v \Delta T} \left(\frac{a}{g} \right) \right)^{1/4} , \tag{127}$$

and

$$h'_{fg} = h_{fg} \left(1 + 0.5 \frac{c_{pv} \Delta T}{h_{fg}} \right) . \tag{128}$$

The fact that the results fall above Berenson's equation is probably caused by turbulent flow in the vapor film. Although no criterion exists for the transition between laminar and turbulent flow, the results in Figure 90 suggests that is is approximately at Ra'_λ of 10^7. Of some interest in Figure 90 is the relative insensitivity of the data to orientation.

The problem of representing cylindrical systems whose physical dimension is small compared with λ_c was treated by Breen and Westwater (150). Their correlation is

$$\frac{h \, \lambda_c}{F_2}^{1/4} = 0.59 + 0.069 \frac{\lambda_c}{D_o} \tag{129}$$

where,

$$F_2 = \left(\frac{k_v^3 \rho_v (\rho_\ell - \rho_v) g h_{fg2}}{\mu_v \Delta T} \left(\frac{a}{g} \right) \right)^{1/4} \tag{130}$$

and,

$$h'_{fg2} = h_{fg} \left(1 + 0.34 \frac{cp_v \Delta T}{h_{fg}} \right)^2 \tag{132}$$

The functions F_2 and F_1 are virtually identical. Equation (129) was tested on several fluids, including the N_2 data of Bromley (135), that of Banchero, et al (155) for O_2 and the He data of Frederking (169).

The results are shown in Figure 91 and very good agreement is found. For systems in which $\lambda_c/D_o \ll 1$, Equation (129) becomes essentially the same as Berenson's result, Equation (126). Furthermore, under these circumstances h becomes independent of D. Equation (132) also is restricted to laminar flows. By comparing their results with the correlation of Bromley, Eauation (118), Breen and Westwater conclude that Bromley's equation is valid for $0.8 \leq \lambda_c/D_o \leq 8.0$.

The correlation of Breen and Westwater, Equation (129), was used to compute the film boiling curves in Figures 64 to 67. It also is shown in Figure 92 in compraison with the neon film boiling data of Astruc, et al (184) from small diameter wires. The agreement is quite favorable. Minimum heat flux points computed by the equations of Lienhard and Wong (151) and Zuber (162) are also shown.

The film boiling data of Sciance, et al (188) for methane given in Figure 76 is correlated in Figure 93. The correlation of the data from an 0.811-inch dia. cylinder presented by these authors is

$$Nu^* = 0.346 \left[\frac{Ra^* h'_{fg}}{cp_v \Delta T (T/T_c)^2} \right]^{0.276}, \qquad (133)$$

where,

$$Nu^* = \frac{(q/A)}{k_{vf} \Delta T} \left[\frac{g_o \sigma}{g(\rho_\ell - \rho_v)} \right]^{1/2} \left(\frac{a}{g} \right)^{-1/2} \qquad (134)$$

$$Ra^* = \left(\frac{\lambda_c}{2\pi} \right)^3 \frac{g \rho_{vf} (\rho_\ell - \rho_v)}{\mu_{vf}^2} \left(\frac{c_p \mu}{k} \right)_{vf} \left(\frac{a}{g} \right) \qquad (135)$$

Equation (133) is shown in Figure 93 as the solid line.

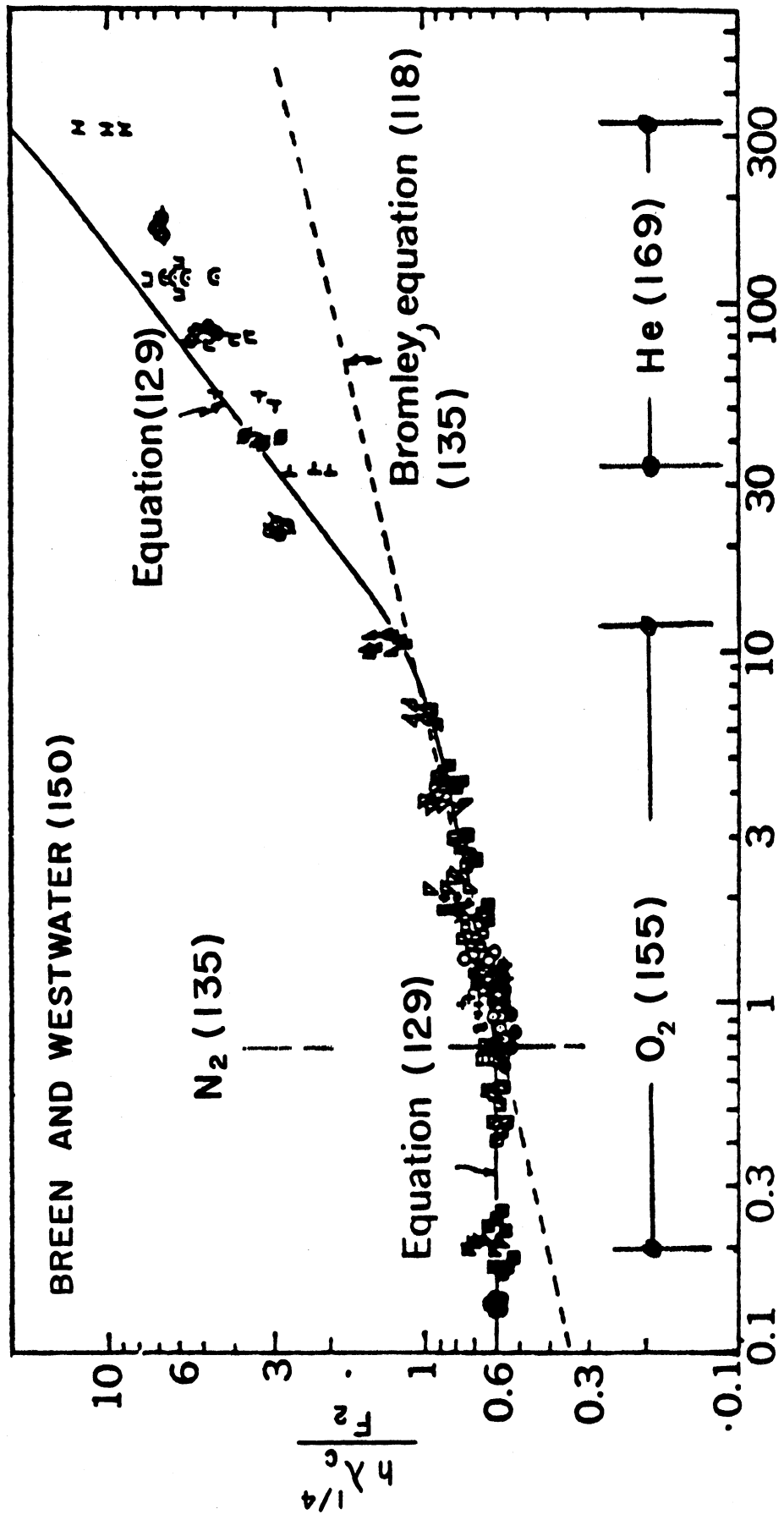

FIGURE 91. GENERAL CORRELATION FOR FILM BOILING ON HORIZONTAL CYLINDERS. THE RANGE OF DIAMETERS IS FROM 0.00022 TO 1.895 IN.

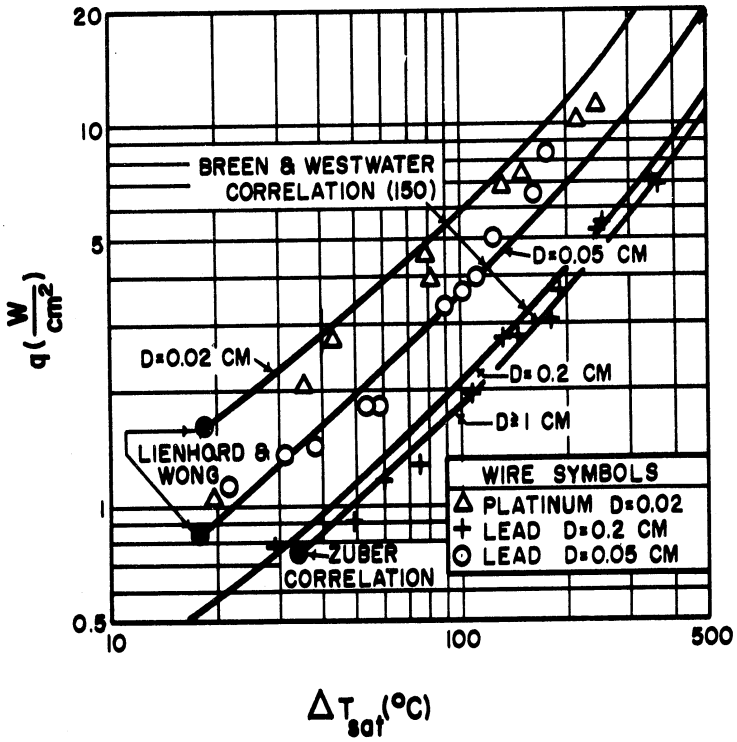

Figure 92. Experimental Film Pool Boiling of Neon at 1 Bar Compared with the Predictive Correlations of Breen and Westwater,[150] Leinhard and Wong,[151] and Zuber.[162]

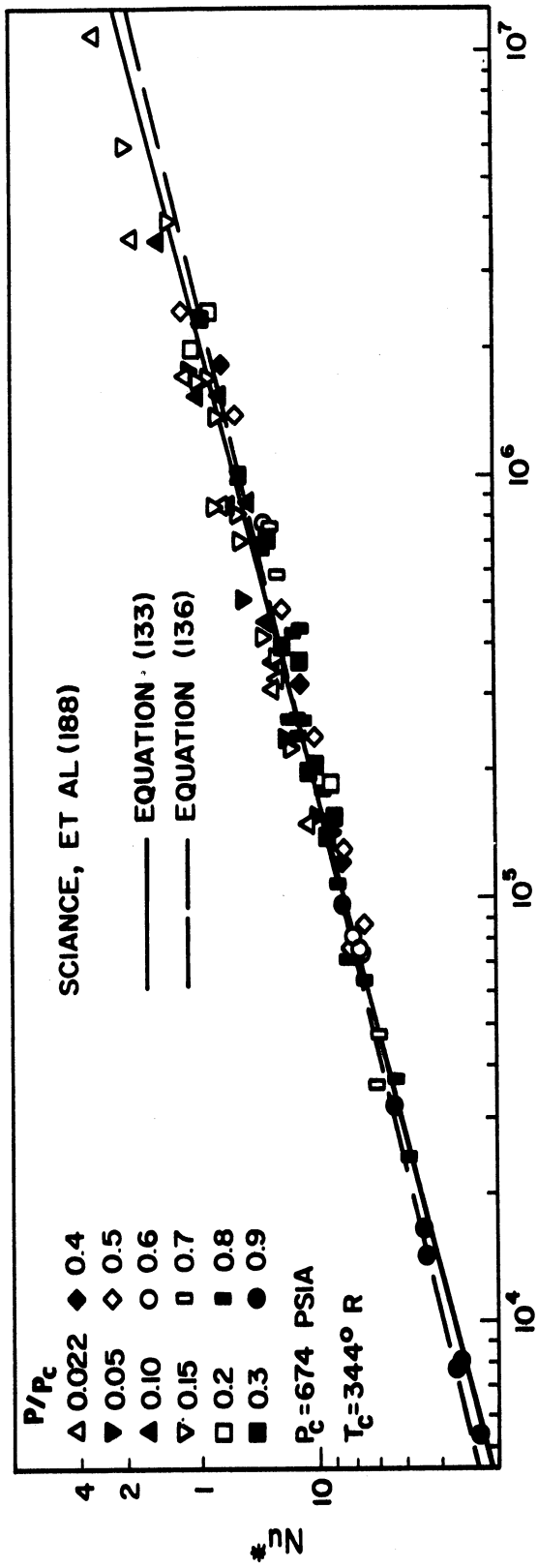

Figure 93. Methane Film Boiling Data Compared with the Proposed Correlation.

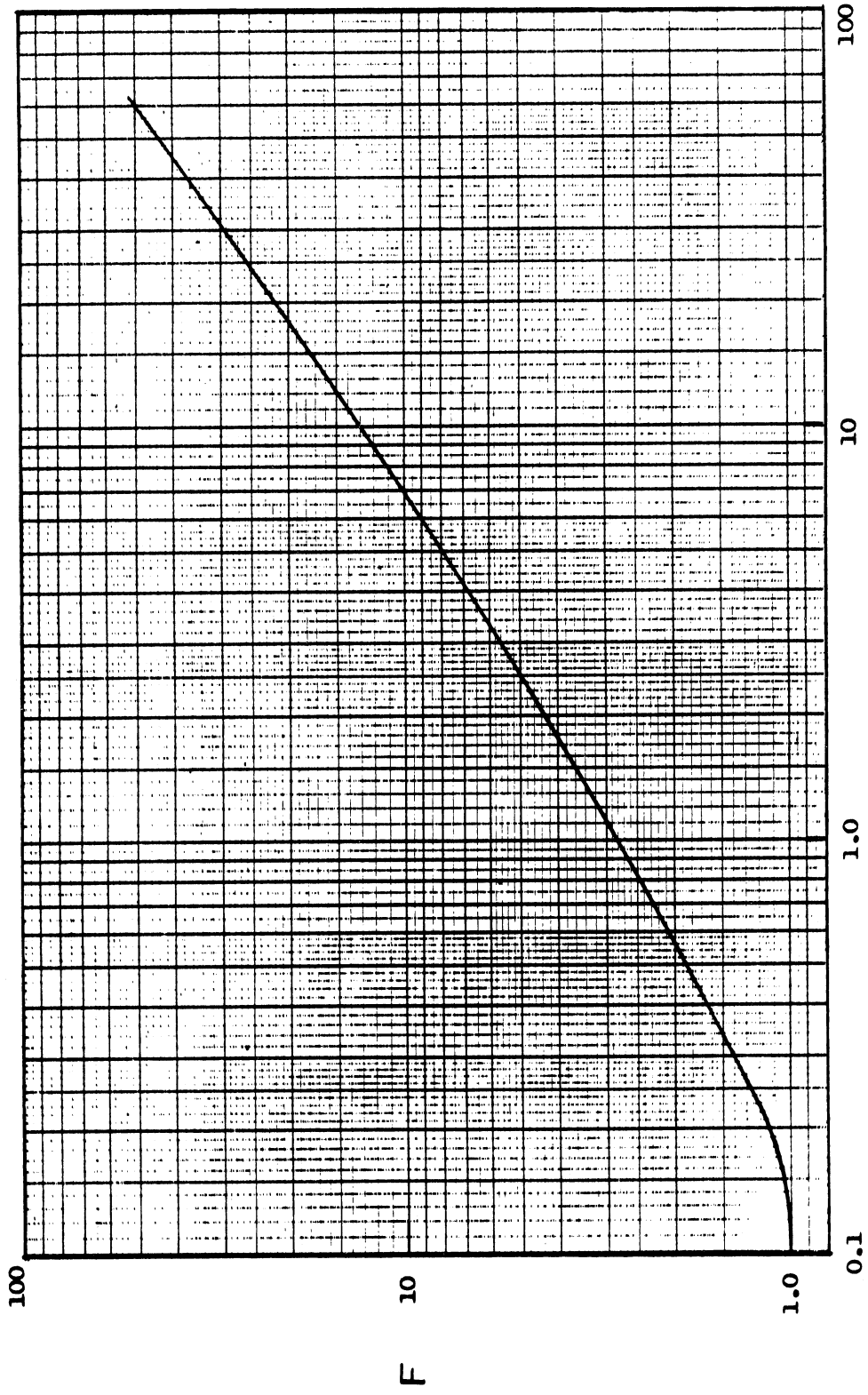

FIGURE 94. REYNOLDS NUMBER FACTOR, F, OF CHEN. (205)

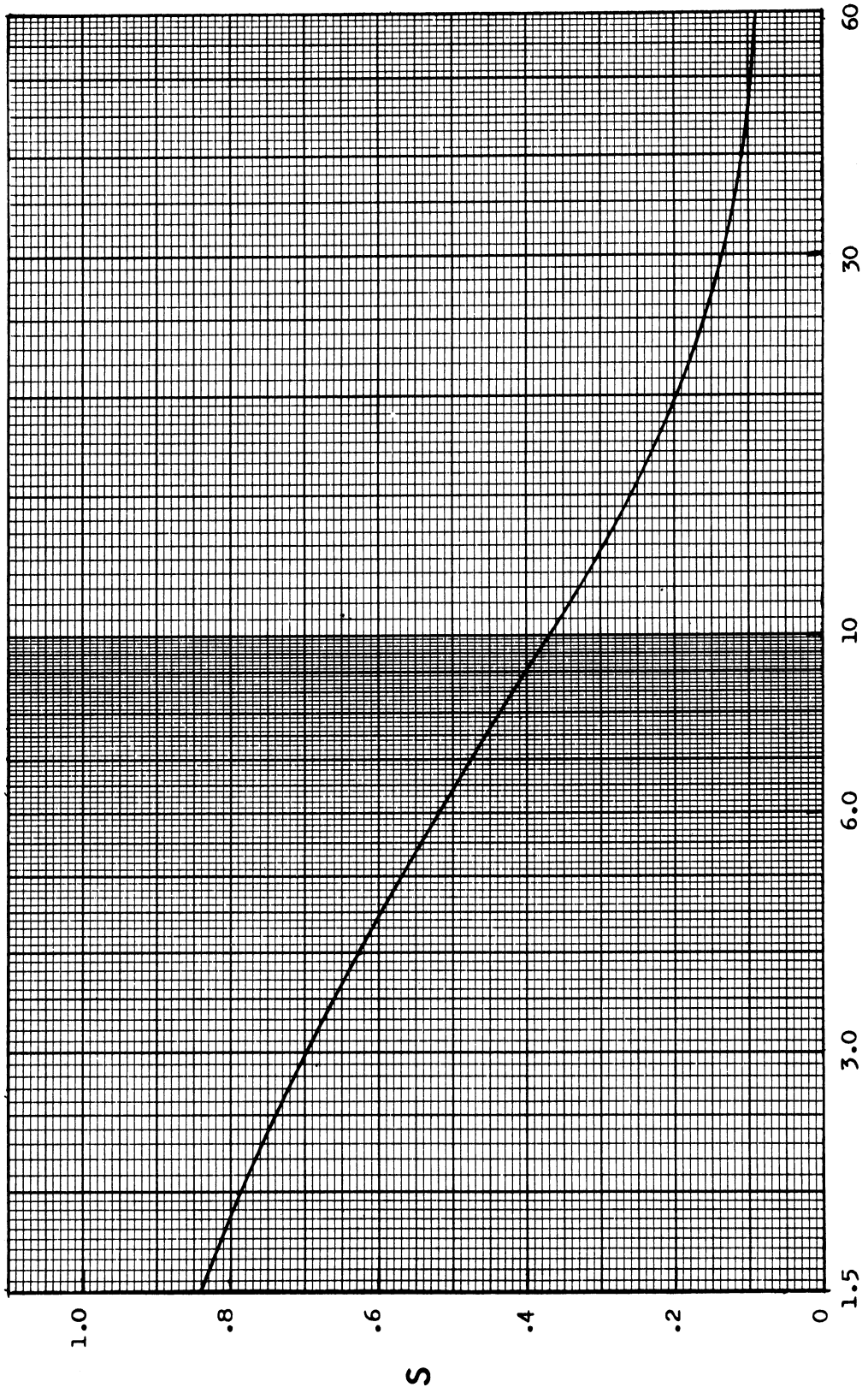

FIG. 95 SUPPRESSION FACTOR, S, OF CHEN (205)

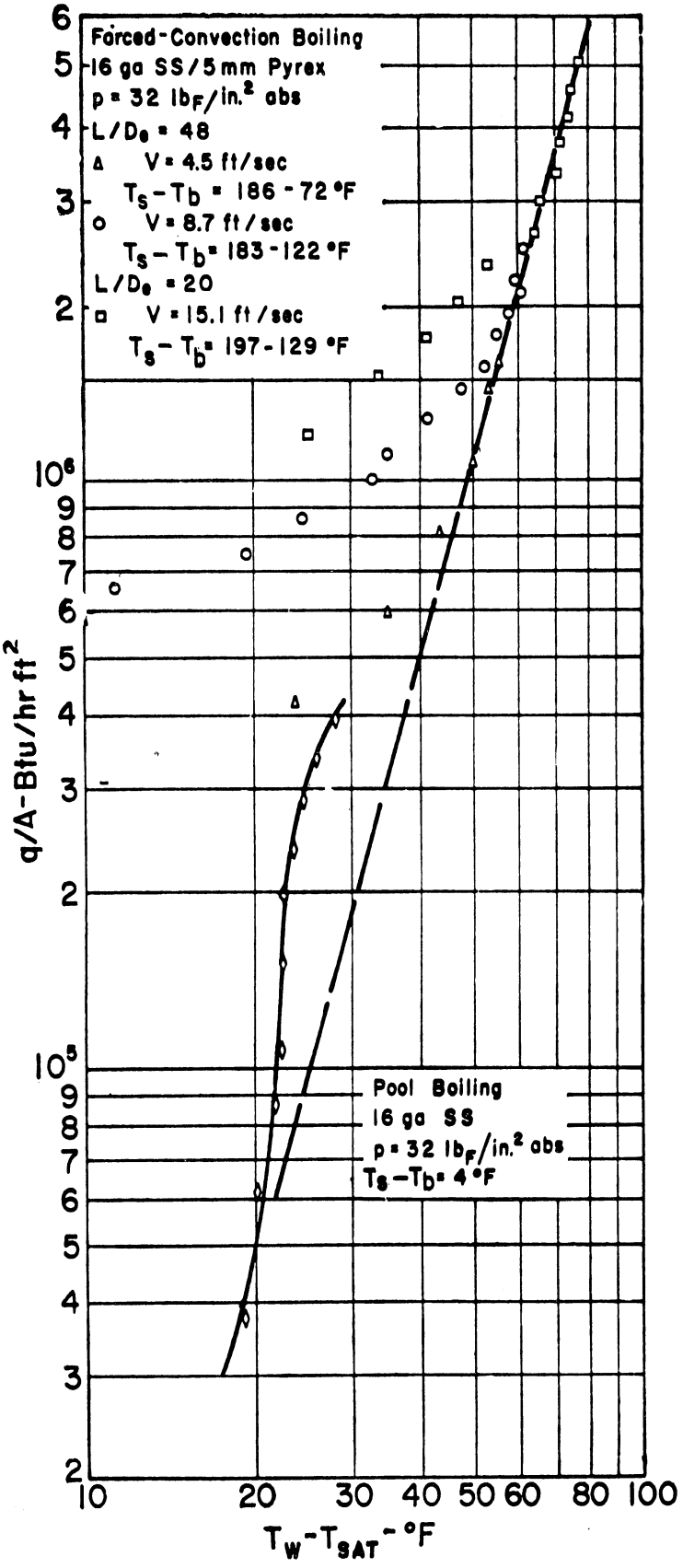

Fig. 96 Forced-convection surface-boiling data and pool-boiling data for stainless-steel tube (38)

These same experimental data can be correlated in the manner of Breen and Westwater (150) by an equation similar to that of Berenson (112) and obtain an equally satisfactorily result. This may be done by fitting the data in Figure 93 by an equation in which the exponent in Equation (133) is changed from 0.276 to 0.250 and determining a new value for the constant. As a result the following equation is obtained

$$\frac{h\,\lambda_c^{1/4}}{F_1} = 0.745\left(\frac{T}{T_c}\right)^{-1/2}. \qquad (136)$$

Equation (136) is shown by the dotted line in Figure 93. This result appears to correlate the data about equally well as Equation (133). Equation (136) has the same asymptotic form as that of Berenson, Equation (126). This is reasonable since the value of λ_c/D_o for the system of Sciance, et al is small and the influence of size (D_o) should not be significant. The range of (T/T_c) for the data in Figure 93 is from 0.75 to 1.0. Thus, Equation (136) could be written,

$$\frac{h\,\lambda_c^{1/4}}{F_1} = C_1(T/T_c)^{-1/2}, \qquad (137)$$

where

$$0.745 \leq C_1(T/T_c)^{-1/2} \leq 0.860.$$

This range of values is slightly higher than that of Berenson but with fair agreement considering the extended conditions and a different geometry of Sciance, et al. Furthermore, Equation (137) is in reasonable correspondence with the asymptotic form of the Breen and Westwater Equation, Figure 91.

2. Forced Convection Boiling

a. Sub-cooled, Nucleate Boiling

Nucleate boiling will occur in forced convection flow when the temperature of a heated surface exceeds the saturation temperature by a few degrees. When the bulk of the fluid is sub-cooled the bubbles which form at the surface condense in the liquid, either while still attached to the surface or after detaching and penetrating the liquid a short distance. The resulting flow phenomena in the region of the surface is enormously complex and not well understood or described at present. Owing to the action of the bubbles themselves the degree of liquid mixing or turbulence is significantly enhanced near the surface. As would be expected the heat transfer rate is significantly increased under these conditions. The process mechanics then appear to be governed by both bubble induced flows and the flow of the bulk liquid as influenced by the presence of the bubbles. Accordingly, most nucleate boiling heat transfer correlations in forced convection boiling attempt to account for these two simultaneous effects.

At present there are very little forced convection, sub-cooled nucleate boiling data available for cryogenic liquids. The liquid hydrogen data of Walters in Figure 59 is one of the few examples. Because of the limited amount of available cryogenic data, essentially all of the correlation methods to be discussed have been developed for non-cryogenic substances. However, it may be expected that they also will apply to cryogenic liquids. Forced convection boiling with cryogenic fluids is reviewed by Seader, et al (27), Giarrantano and Smith (141) and Brentari, et al (143).

The simplest method which has been proposed is to use the pool boiling equations alone for forced convection boiling. Zuber and Fried (139) in a review paper place the work of Kutateladze (146), Michenko (179), Gilmour (278), Labountzov (180) and Forster and Grief (177) in this category. This method, however, seems hazardous in view of the demonstrated variation between some of the forced convection and pool boiling data, especially with regard to the influence of sub-cooling. The data of Bergles and Rohsenow (38) for sub-cooled water, Figure 97, indicates a difference between these two kinds of boiling whereas that of Elrod, et al (185) for saturated boiling in pressurized water shows the data of nucleate pool boiling and forced convection boiling to merge at high heat flux.

Rohsenow (38) and Clark and Rohsenow (63) have suggested that nucleate boiling data be predicted by a superposition of data for non-boiling forced convection and pool boiling. Thus, the heat flux in nucleate boiling, $(q/A)_{NB}$, would be written,

$$(q/A)_{NB} = h(T_w - T_\ell) + (q/A)_{PB}, \qquad (138)$$

where $(q/A)_{PB}$ is the pool boiling heat flux corresponding to $(T_w - T_\ell)$, and h is computed from an appropriate non-boiling correlation, such as

$$\frac{h_x D_e}{r_f} = 0.023\ Re_f^{0.8}\ Pr_f^{0.4} \qquad (52)$$

This method was employed on data for high pressure water at low velocities in tubes (63) where it was observed that at high (fully developed nucleate boiling) heat flux, the flow velocity had no noticeable influence on the process. However, more recent data of Bergles and Rohsenow (277)

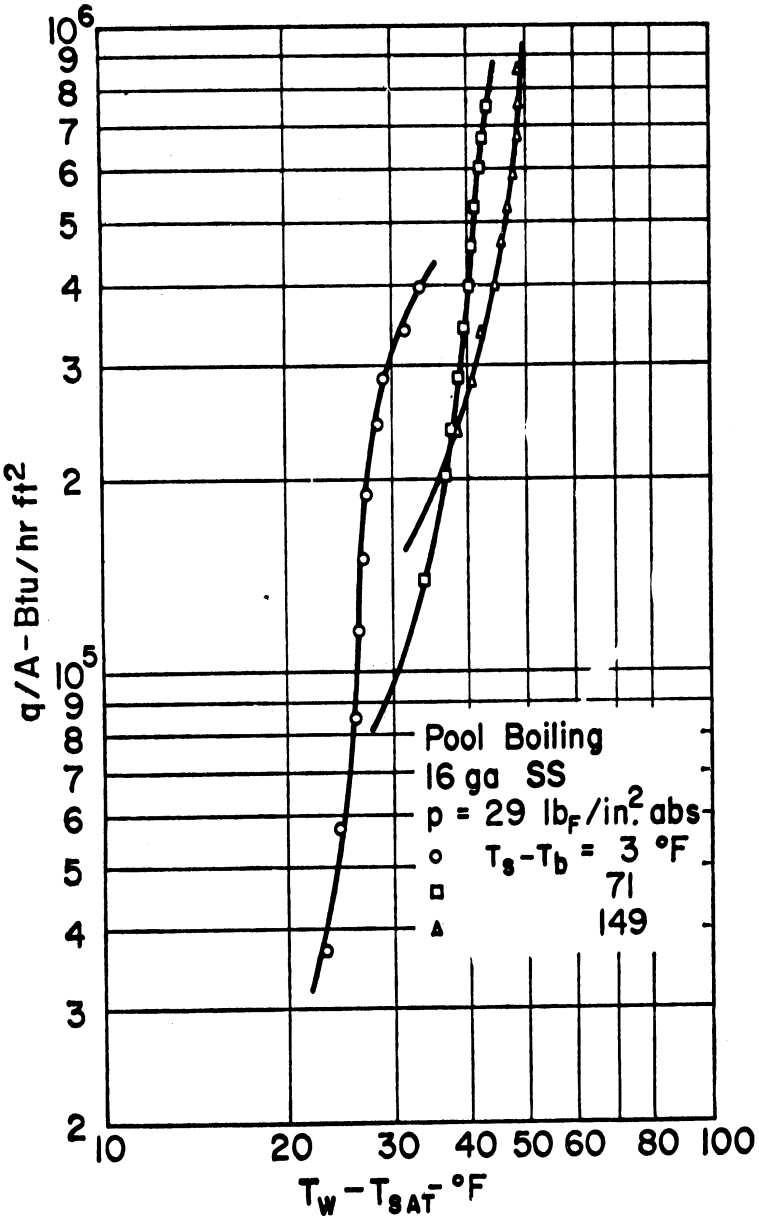

Fig. 97 Influence of subcooling on pool boiling (38)

indicate that nucleate pool boiling and forced convection (fully developed) nucleate boiling are not the same. This suggests that the superposition method of Equation (138) should be used with discretion.

A nucleate boiling correlation designed for saturated liquids has been proposed by Chen (205) and tested against data for water, methanol, cyclohexane, pentane, benzene and heptane. The average deviation of the data from Chen's equation is $\pm$ 11% for a vapor quality range from 1% to 70%. For flow in a vertical tube in the annular or annular-mist flow regime, Chen employed a weighted superposition hypothesis to account for the interaction between the vapor bubbles and the flowing liquid. Thus, the boiling heat flux is written

$$(q/A) = h(T_w - T_{sat})F + (q/A)_{FZ} S, \qquad (139)$$

where h is computed from Equation (52), or equivalent, and $(q/A)_{FZ}$ is the nucleate pool boiling heat flux using the Forster-Zuber correlation, Equation (93). F is a two-phase correction factor given in Figure 94 as a function of the parameter X_{tt}, where

$$X_{tt} = \left(\frac{1-x}{x}\right)^{0.9} \left(\frac{\mu_\ell}{\mu_v}\right)^{0.1} \left(\frac{\rho_v}{\rho_\ell}\right)^{0.5}, \qquad (140)$$

S is a factor which accounts for the influence of the flow in suppressing the growth of the vapor bubbles. This factor is given in Figure 95, as a function of $Re_\ell F^{1.25}$, where

$$Re_\ell = \frac{DG(1-x)}{\mu_\ell}. \qquad (141)$$

Bergles and Rohsenow (277) have studied the relationship between nucleate pool boiling and forced convection nucleate boiling from the same surface to sub-cooled water at low pressures. They conclude

"that the curves for forced convection surface (nucleate) boiling cannot be based on data for saturated pool boiling but must rather be based on actual forced-convection data." This results from the fact that the mechanics of the flow near a heated surface in saturated pool boiling is not similar to that in forced convection boiling, especially where sub-cooling exists, except perhaps at low velocities. Accordingly, the heat transfer rates also will be different. This, of course, complicates the prediction of forced-convection nucleate boiling data as it requires the measurement of these data. The difference between saturated nucleate pool boiling and forced convection nucleate boiling as well as the influence of sub-cooling on nucleate pool boiling are shown in Figures 96 and 97, taken from the paper of Bergles and Rohsenow (277).

A method for the construction of the curve for the intermediate boiling region connecting single phase forced-convection and fully developed forced-convection nucleate boiling is given by Bergles and Rohsenow (277). This procedure, coupled with data for both the single-phase and boiling regions, then permits the construction of the complete (q/A) - Δt heat transfer characteristic curve. Since, the data given in (277) applies specifically to water, this construction method will not be reproduced here.

b. Saturated (Film) Boiling

Heat transfer to a flowing saturated liquid produces bubbles which do not condense but cause a net increase in the vapor fraction of the stream. This is called saturated boiling or, if the vapor fraction is sufficiently large, film boiling, especially if the vapor is concentrated near the surface. One important consequence of this is

the large reduction in stream density which can occur. For flow inside of pipes and tubes the flow then accelerates, causing a momentum pressure-drop which in many instances becomes the predominent component of the total pressure-drop. Under these circumstances, the flow patterns in the stream are also very complex and difficult to define. These conditions contribute to the problem of correlating heat transfer data in this flow regime.

Presently most of the available data is for liquid hydrogren. This includes the work of Hendricks, et al (66), Wright and Walters (78), Walters (136), Chen (205), Graham, et al (206), Chi (207,208) and Core, et al (209). Burke and Rawdon (210) and Laverty and Rohsenow (211) have studied nitrogen in film boiling. A summary of film boiling correlating methods is given in references (27), (141) and (143).

Saturated and film boiling correlations have been formulated in terms of the Martinelli parameters, X_{tt} and the vapor mass fraction (quality) x, where,

$$X_{tt} = \left(\frac{1-x}{x}\right)^{0.9} \left(\frac{\mu_\ell}{\mu_v}\right)^{0.1} \left(\frac{\rho_v}{\rho_\ell}\right)^{0.5} \qquad (140)$$

These correlations are written in terms of the ratio

$$\frac{\text{Nu,exp}}{\text{Nu,calc}} ,$$

where, Nu,exp. is the experimentally determined Nusselt number and Nu,calc. is a Nusselt number computed on the basis of a single phase correlation.

Hendricks, et al (66) proposed that

$$\frac{\text{Nu,exp.}}{\text{Nu,calc,f,t.p.}} = f(\tilde{X}_{tt}) \qquad (142)$$

where,

$$Nu,exp. = \frac{h\ exp.\ D}{k_{f,v}} \tag{143}$$

$$Nu,calc,f,t.p. = 0.023\ Re_{f,m,t.p.}^{0.8}\ Pr_{f,v}^{0.4} \tag{144}$$

$$Re_{f,m,t.p.} = \frac{\rho_{f,m,t.p.}\ V_{avg}\ D}{\mu_{f,v}} \tag{145}$$

$$\rho_{f,m,t.p.} = \frac{1}{(x/\rho_f) + [(1-x)/\rho_\ell]} \tag{146}$$

$$V_{avg} = \frac{w}{\rho_b\ A_c} \tag{147}$$

$$\rho_b = \frac{1}{(x/\rho_v) + [(1-x)/\rho_\ell]} \tag{148}$$

The correlation in the form of Equation (142) is shown in Figure 98 in comparison with experimental data. Although a general agreement is observed, quite a wide scatter exists in the data. Because the experiments were conducted on hydrogen alone, a correlation was sought (141) for the Nusselt number ratio of Equation (142) in terms of the local vapor quality x. The result is shown in Figure 99. There appears to be no significant improvement in the degree of correlation. However, some simplification is introduced since the determination of the ordinate x is easier than X_{tt}.

An improvement in the correlation was obtained by Ellerbrook, et al (212), by recognizing that the data in Figure 98 could be grouped into families of curves identified by constant "Boiling Number", B_o, where,

$$B_o = \frac{(q/A)}{h_{f_g}\ G_{mix}}\ , \tag{149}$$

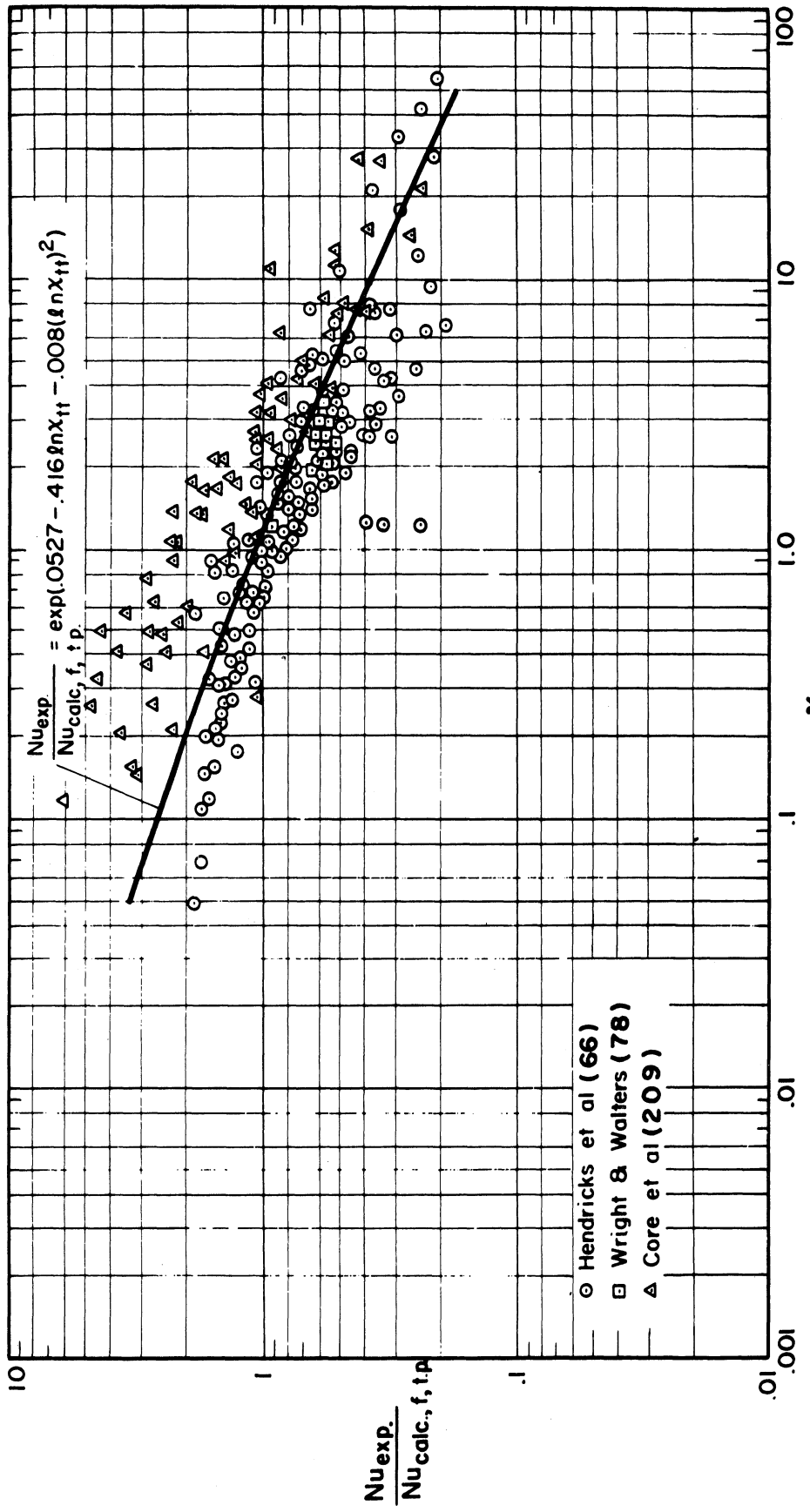

Figure 98 Two-phase Nusselt number ratio vs X_{tt} (141)

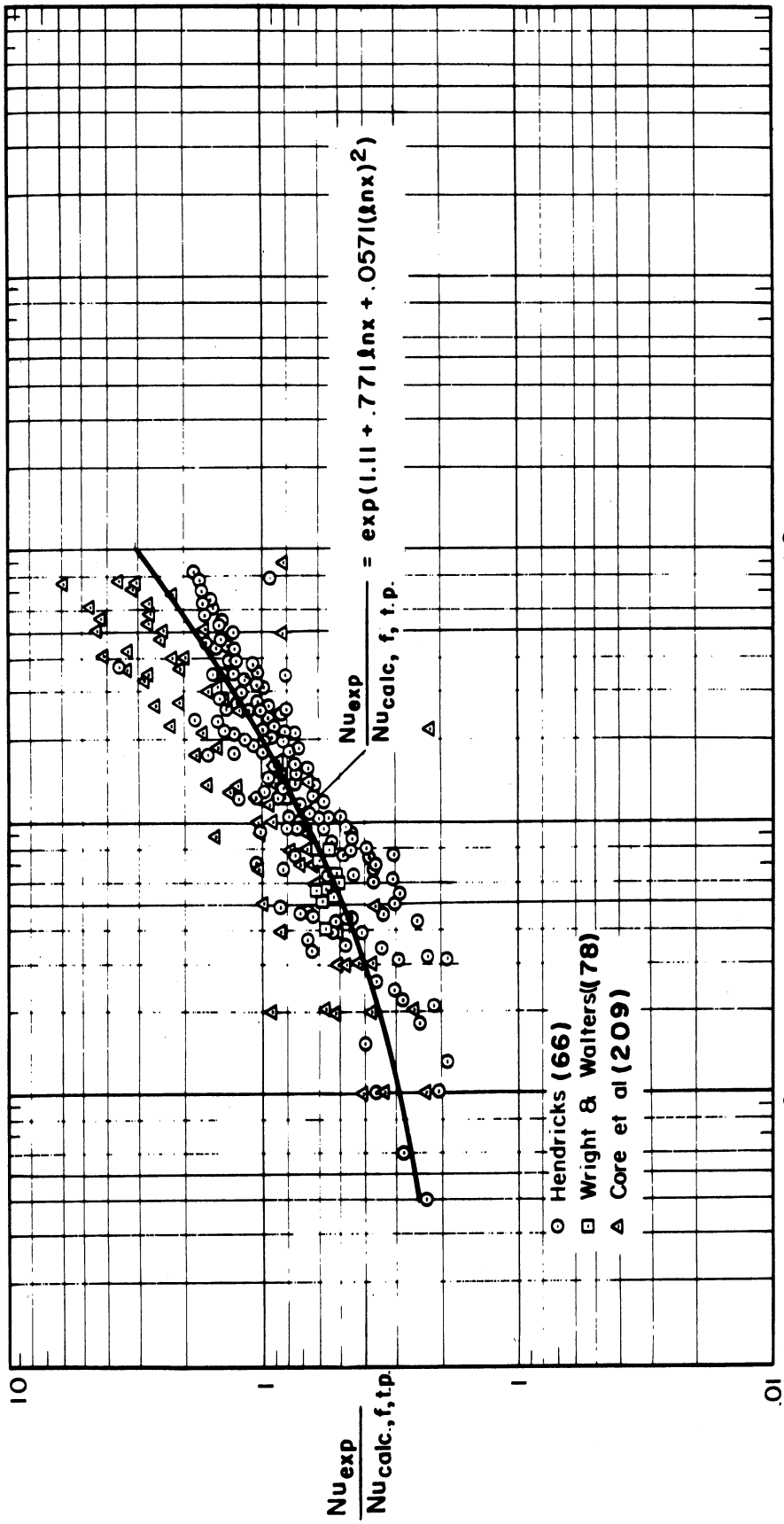

Figure 99 Two-phase Nusselt number ratio vs x(quality) (141)

where,

$$G_{mix} = \frac{w}{A_c} \quad . \tag{150}$$

The separation of the data by boiling number is shown in Figure 100. The boiling number may be interpreted physically as the ratio of the transverse mass velocity of the vapor formed at the wall, $(q/A)/h_{fg}$, to the axial mass velocity of the mixture, G_{mix}.

The boiling number is used to modify Equation (142) to give

$$\frac{Nu, exp.}{Nu, calc, f, t.p.} \; Bo^{-0.4} = f(X_{tt}) \quad . \tag{151}$$

This form of the correlation is shown in Figure 101 where it will be observed that a significant improvement in the correlation has been obtained. The modified Nusselt number ratio is shown in Figure 102 as a function of quality. In this case the degree of correlation also is improved.

c. Maximum Nucleate Boiling Heat Flux (Burnout)

Very little maximum nucleate boiling heat flux data are available for cryogens and no suitably reliable correlations are known to exist at present. The available data are those of Lewis, et al (213) for liquid nitrogen and liquid hydrogen. These data are compared with the following correlations of Lowdermilk, et al (214), originally derived for pressurized water in Figure 103.

$$(q/A)_{max} = \frac{270\, G^{0.85}}{D^{0.2}\,(L/D)^{0.85}} \; ; \quad 1 \leq \frac{G}{(L/D)^2} \leq 150 \tag{152}$$

$$(q/A)_{max} = \frac{1400\, G^{0.5}}{D^{0.2}\,(L/D)^{0.15}} \; ; \quad 150 \leq \frac{G}{(L/D)^2} \leq 10^4 \tag{153}$$

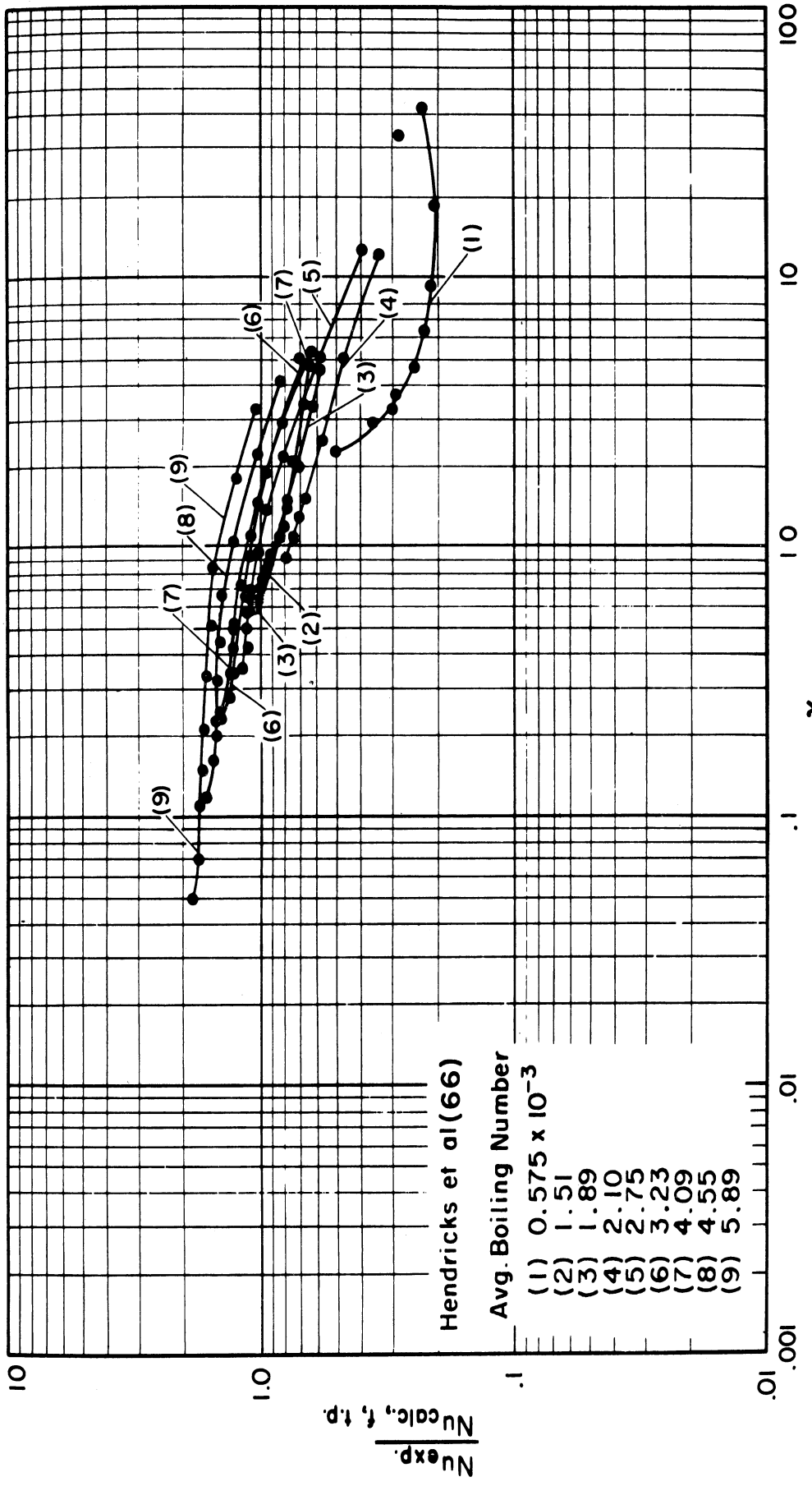

Figure 100 Two-phase Nusselt number ratio vs X_{tt} for only the data of Hendricks, et al (66) illustrating separation of data according to boiling number (141)

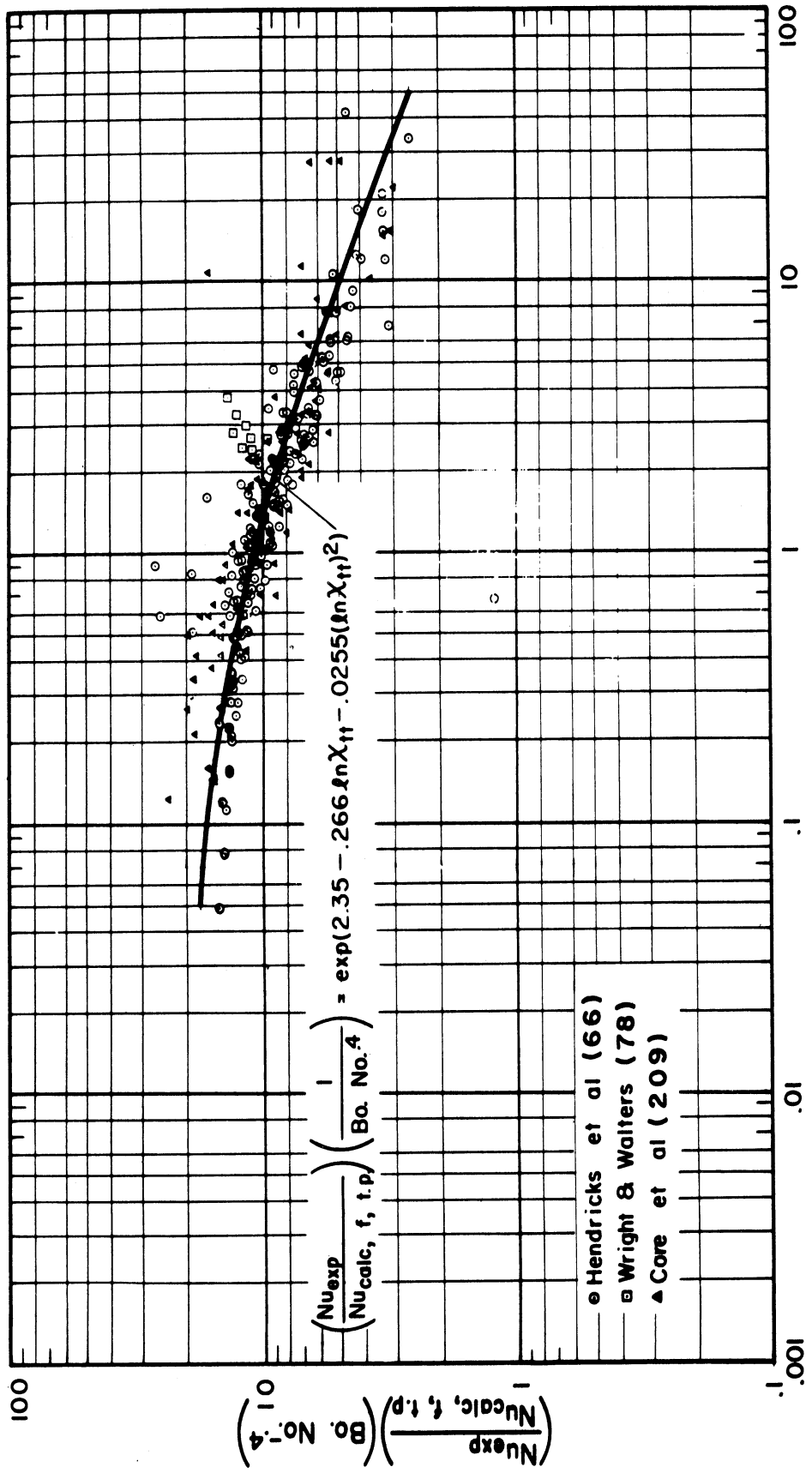

Figure 101 Two-phase Nusselt number ratio times boiling number factor vs X_{tt} (141)

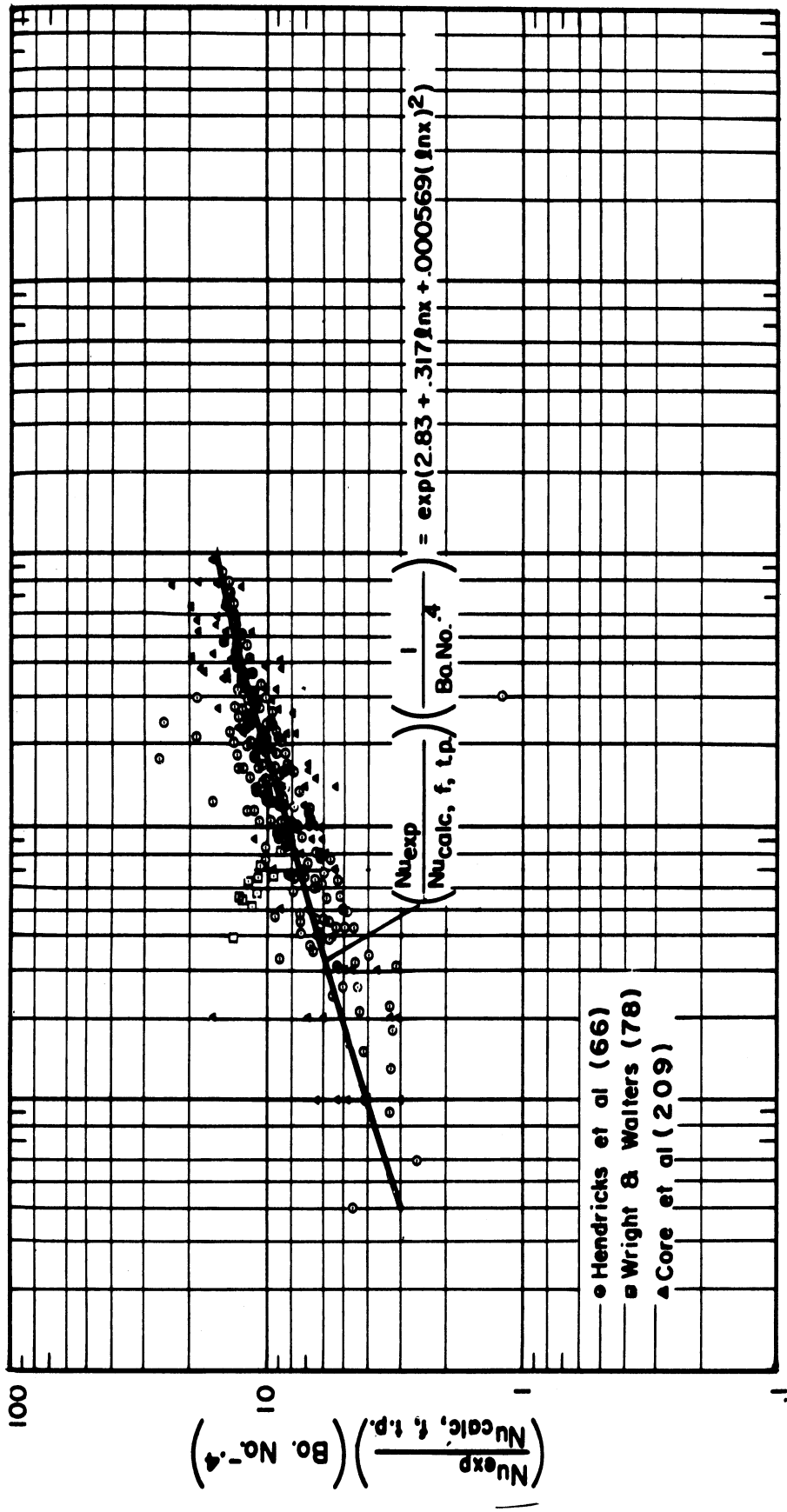

Figure 102 Two-phase Nusselt number ratio times boiling number factor vs x(quality)(141)

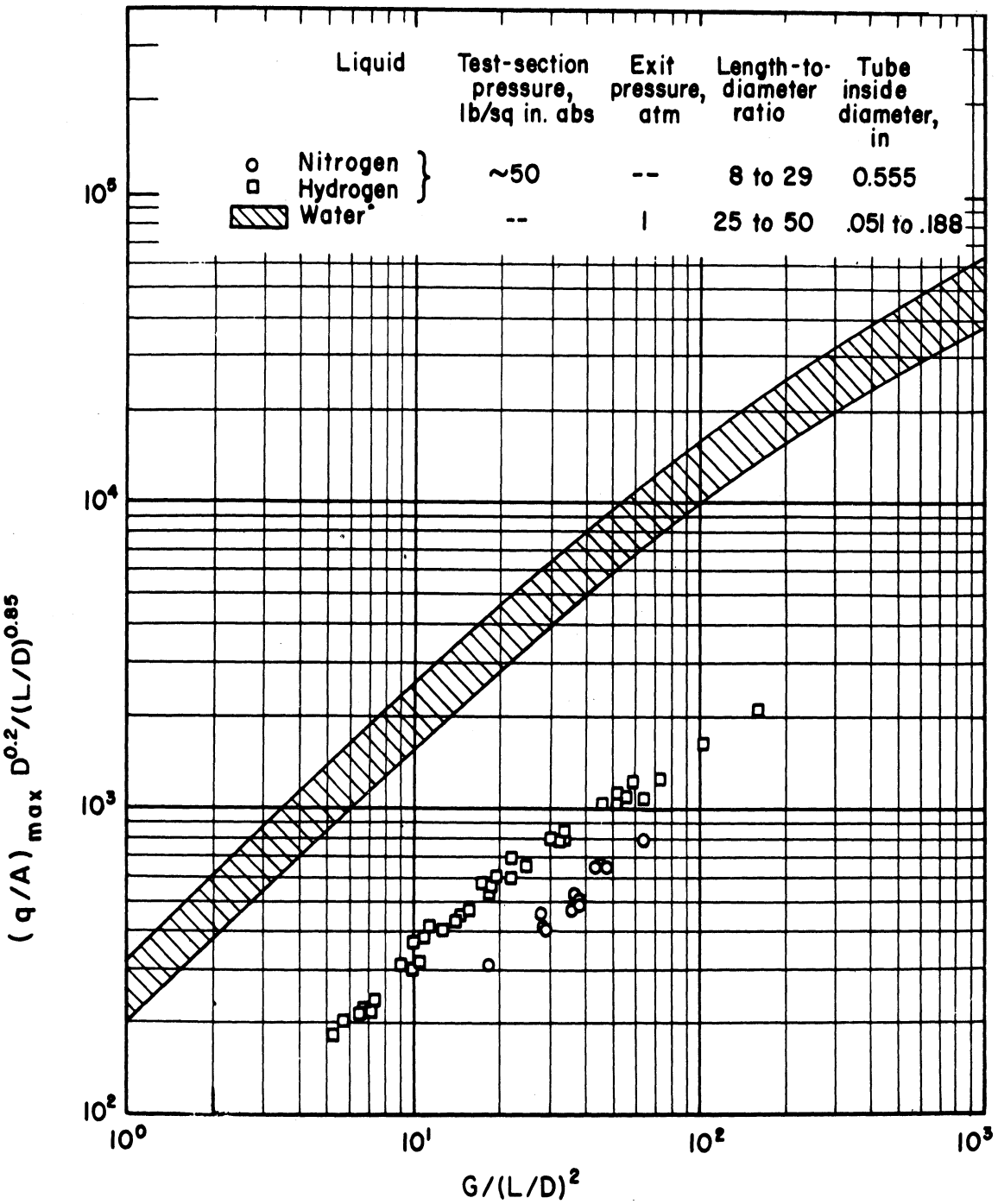

Figure 103 Comparison of maximum critical heat flux for cryogenic liquids with water correlation of Lowdermilk, et al.(214)

As can be seen the correlations agree with the general trend of the data but predict values for $(q/A)_{max}$ which are greater by almost one order of magnitude than those observed for liquid nitrogen and hydrogen. Thus, Equations (152) and (153) should be used with discretion.

d. Pressure Drop in Two-Phase Flow

The total pressure drop in a flowing fluid is caused by the effects of viscous friction, the influence of body forces (such as gravity) and the momentum changes in the flows. For two phase systems subject to heat transfer at the wall, and thus to significant density variations, the latter effect, namely momentum changes, can be the principal factor in the pressure drop. In instances where this is true, the calculation of the pressure drop is greatly simplified providing the mixture densities can be determined. For exit qualities (x_e) above 0.10-0.20, an assumption of a homogenous stream provides a reasonable estimate. An example of this is shown in Figure 104 where the total measured pressure drop across a 0.313-inch I.D. tube, 12-inches long is compared with that computed for simple momentum change. These results are those of Graham, et al (206) for the flow of liquid hydrogen. As can be observed, the two results are essentially identical, especially for the higher exit qualities.

Because of the inherent large temperature difference between a cryogenic fluid and an atmospheric ambient the probability of boiling is great. The design of piping, transfer lines and associated pumping equipment depends on an estimate of two-phase flow phenomena. Two phase pressure drop is classified as adiabatic (without heat transfer) or diabatic (with heat transfer). Two-phase flow and pressure drop have

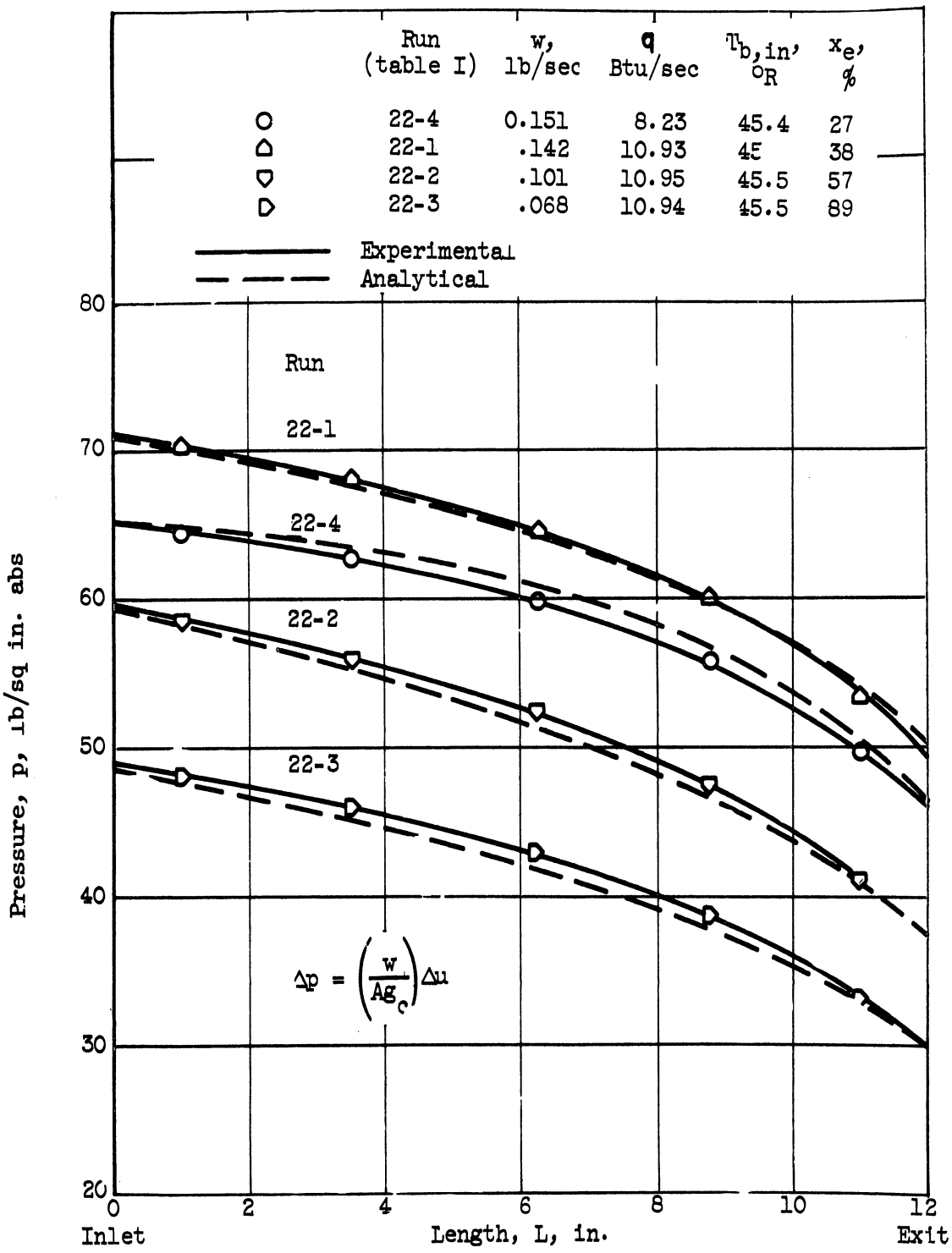

Figure 104. Comparison of experimental and theoretical pressures along length of test section of 0.375-inch-outside-diameter Inconel tube. (206)

been studied by Baker (215), Martinelli and Lockhart (216), Martinelli and Nelson (217), Leonhard and McMordie (218), Hatch and Jacobs (219), Lapin and Baver (220), Chenoweth and Martin (221) and Dukler, et al (222), among others. A simplified calculation method for total pressure drop for low quality flow of saturated freon-11 is given by Sugden, et al (223). Timmerhaus and Sugden (224) give a simplfied method for the calculation of the frictional pressure-drop for freon-11, freon-12 and liquid hydrogen. Their method is similar to that proposed by McAdams, et al (225) and used by Davison, et al (226), who found the two-phase friction factor about 50% greater than smooth tube single phase friction factor.

Baker (215) has described several regimes of adiabatic two-phase flow inside pipes and ducts as, (a) bubble, (b) froth, (c) plug (vapor), (d) stratified (liquid-vapor), (e) wavy, (f) slug (liquid), (g) annular (liquid) and (h) mist (fog or homogeneous). These flow patterns were identified by Baker in terms of certain parameters of the flow as shown in Figure 105. This representation has become known as the "Baker Plot" and has been found to be reasonably valid for pressurized water systems. Lapin and Bauer (220) also have used it to identify the flow regimes for methane. The data points on Figure 105 are those of Leonhard and McMordie (218) for freon-12 and show a reasonable agreement with the flow regime boundaries.

As the "Baker Plot" suggests the flow of two phases is a rather complex phenomenon. Several correlating methods for pressure drop exist in the literature and individual design groups frequently develop limited emperical forms valid for a specific range of application. Often these latter are modifications of existing correlations. In this

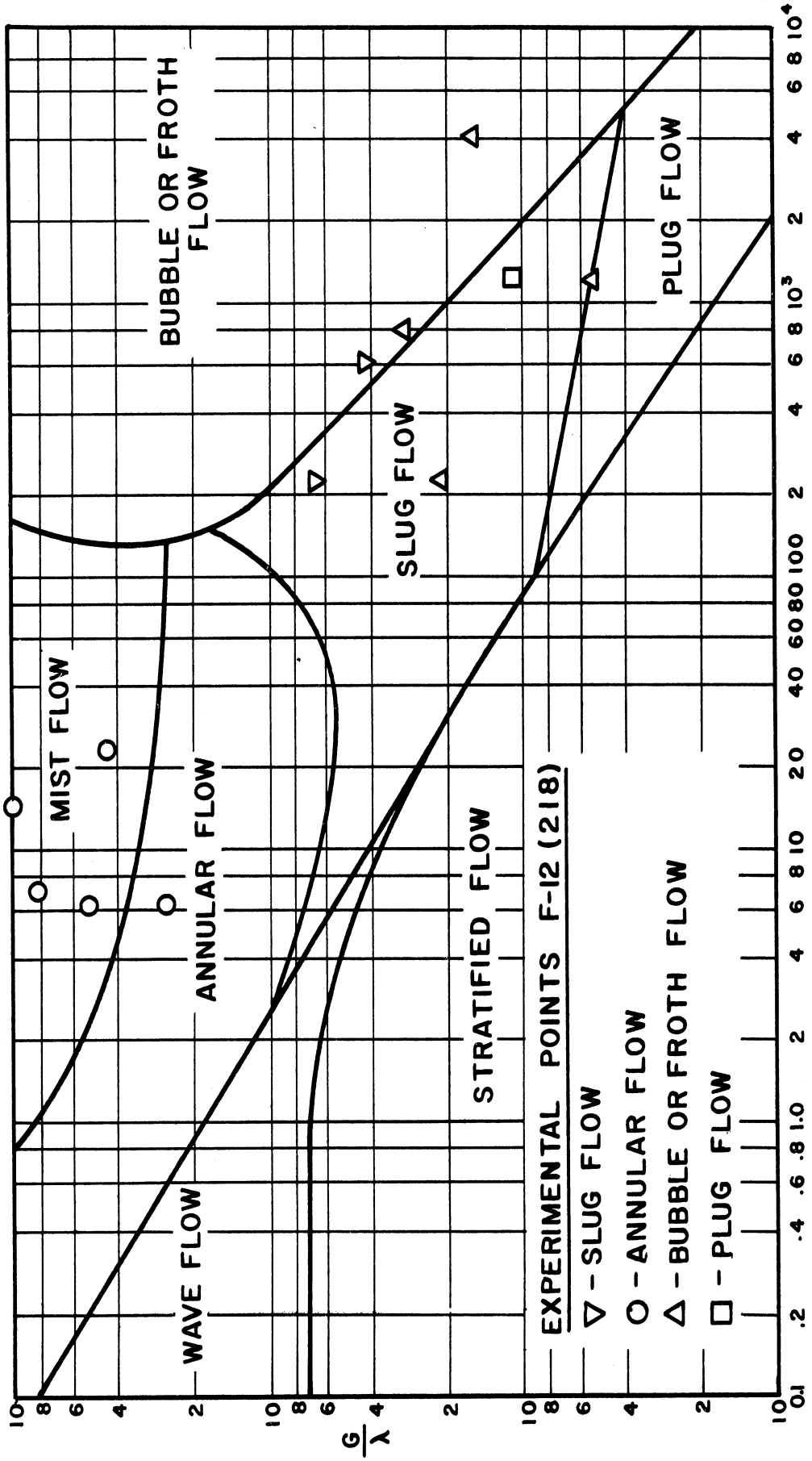

FIGURE 105. BAKER PLOT FOR ADIABATIC TWO-PHASE FLOW.(215)

section it will be necessary to limit the description to but two and these will be those of Martinelli and his co-workers (216,217) for adiabatic and diabatic flow. These Martinelli correlations describe the essential features of the process and introduce the governing parameters. They also recognize a slip-flow between separated phases, something which is necessary for any realistic representation of the process. The Martinelli correlations have enjoyed a remarkable endurance over the years having been used with reasonable success on air-water mixtures at low pressures, on pressurized water systems and for cryogenic fluids. However, it should be mentioned that Lapin and Bauer (220) have found that an extrapulated form of the Chenoweth and Martin (221) correlation was most satisfactory for the calculation of frictional pressure drop for liquid nitrogen and methane.

For the calculation of adiabatic turbulent two phase flow frictional pressure drop, Martinelli and Lockhart (216) present the following equations,

$$\left(\frac{\Delta p}{\Delta L}\right)_{TPF} = \left(\frac{\Delta p}{\Delta L}\right)_{\ell} \phi_{\ell}^{2} \qquad (154)$$

where

$\left(\frac{\Delta p}{\Delta L}\right)_{TPF}$ = frictional pressure drop per unit length in two-phase flow

$\left(\frac{\Delta p}{\Delta L}\right)_{\ell}$ = frictional pressure drop per unit length if liquid only flows in the pipe at rate w_{ℓ}.

The function ϕ_{ℓ} in Equation (154) is given in Figure 106 as a function of X, defined as

$$X^2 = \frac{(\Delta p/\Delta L)_{\ell}}{(\Delta p/\Delta L)_{g}} \qquad (155)$$

where,

$(\frac{\Delta p}{\Delta L})_g$ = frictional pressure drop per unit length if gas only flows in the pipe at rate w_g.

The fractional pipe volume filled by liquid, R_ℓ , and that of the gas, R_g, also is given in Figure 106.

For diabatic flow, the effect of heat transfer is to change the relative vapor-liquid fraction along a pipe. In this case, Martinelli and Nelson (217) found the following equation to describe events at each axial location,

$$\frac{(dp/dL)_{TPF}}{(dp/dL)_o} = (1 - x)^{2-n} \phi_\ell^2(p,x) , \qquad (156)$$

where $(dp/dL)_o$ is the frictional pressure gradient if only liquid were flowing at the total flow rate $w_\ell + w_g$. The constant n is the exponent in the friction factor-Reynolds number relation, $f = C/R_e^n$. For turbulent flow this was taken to be 0.25. The function $\phi_\ell(p,x)$ is found (217) from Figure 106 corresponding to X which may be obtained from the following relation and is equivalent to that given in Equation (155),

$$X = x^{\frac{2-n}{2}} = (\frac{\rho g}{\rho_\ell})^{1/2} (\frac{\mu_\ell}{\mu_g})^{\frac{n}{2}} (\frac{1}{x} - 1)^{\frac{2-n}{2}} \qquad (157)$$

Hence, for a condition in which the pressure level and the axial heat flux distribution (and thus x) is specified, the two-phase frictional pressure drop is computed from,

$$\Delta p_{TPF} = \int_o^L (\frac{dp}{dL})_{TPF} \cdot dL = (\frac{\Delta p}{\Delta L})_o \int_o^L (1-x)^{2-n} \phi_\ell^2(p,x) \cdot dL$$

$$= (\frac{\Delta p}{\Delta L})_o \int_o^{x_e} \frac{(1-x)^{2-n}}{(dx/dL)} \phi_\ell^2 (p,x) \cdot dx \qquad (158)$$

If the axial heat flux is constant, $dx/dL = x_e/L$, and Equation (158) becomes (noting $L = \Delta L$),

$$\left(\frac{\Delta p}{\Delta L}\right)_{TPF} = \left(\frac{\Delta p}{\Delta L}\right)_o \frac{1}{x_e} \int_o^{x_e} (1 - x)^{2-n} \phi_\ell^2 (p,x) \cdot dx \qquad (159)$$

The single-phase pressure drop gradient, $(\Delta p/\Delta L)_o$ is found from,

$$\left(\frac{\Delta p}{\Delta L}\right)_o = 4 \frac{f}{D_e} \frac{\rho_\ell V_o^2}{2g_o} \qquad (160)$$

where,

$$V_o = \frac{w_g + w_\ell}{\rho_\ell A_F} \qquad (161)$$

$$f = \frac{0.046}{Re^{0.25}} \qquad (162)$$

$$Re = \frac{\rho_\ell D_e V_o}{\mu_\ell} \qquad (163)$$

The momentum pressure-drop (217) is computed from,

$$\Delta p_M = \frac{(w_g + w_\ell)^2}{\rho_\ell A_F^2 g_o} \left[\frac{(1 - x_e)^2}{R_{\ell_e}} + \frac{x_e^2}{R_{g_e}} \cdot \frac{\rho_\ell}{\rho_g} - 1 \right], \qquad (164)$$

where R_{ℓ_e} and R_{g_e} correspond to the value of X, Equation (157) evaluated at $x = x_e$. The total pressure drop would then be $\Delta p = \Delta p_{TPF} + \Delta p_M$, the sum of Equations (158) and (164).

This method for estimating two-phase frictional and momentum pressure drop been extensively employed in computing the performance of pressurized water boiling systems. Hatch and Jacobs (219) have used this method to correlate adiabatic and diabatic pressure drop for Freon-11 and hydrogen. Their data are shown in Figure 107, 108 and 109, where the parameter X was evaluated at the mean quality along the

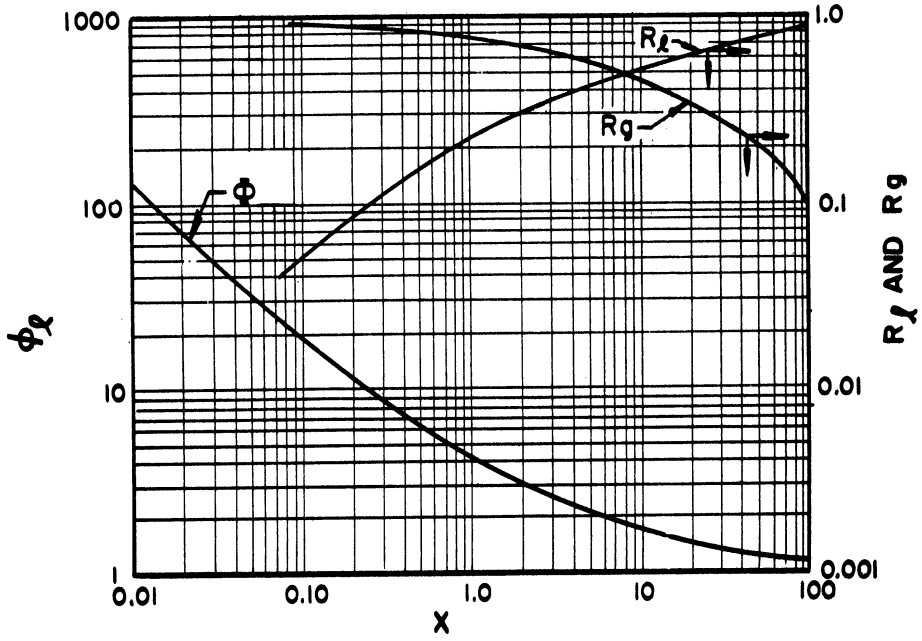

Figure 106. Adiabatic two-phase flow pressure drop function ϕ_ℓ.(216)

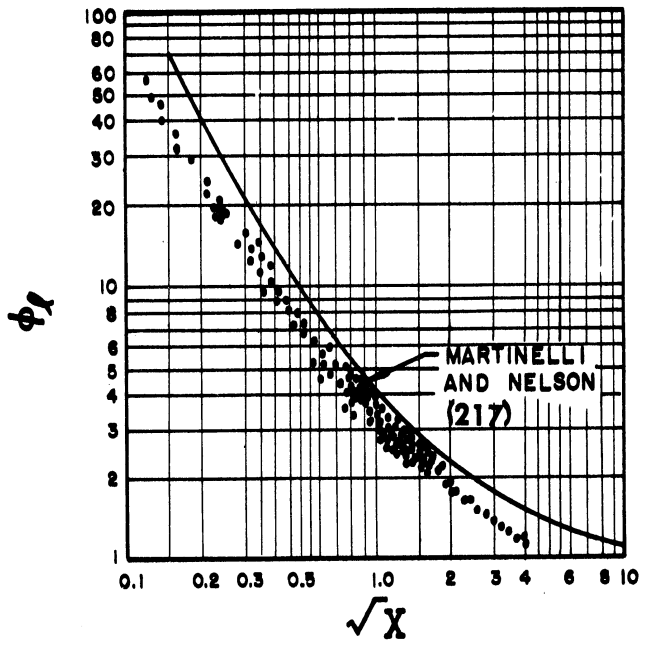

Figure 107. Comparison of two-phase (adiabatic) pressure drop data of Freon-11 with Martinelli-Nelson prediction.(219)

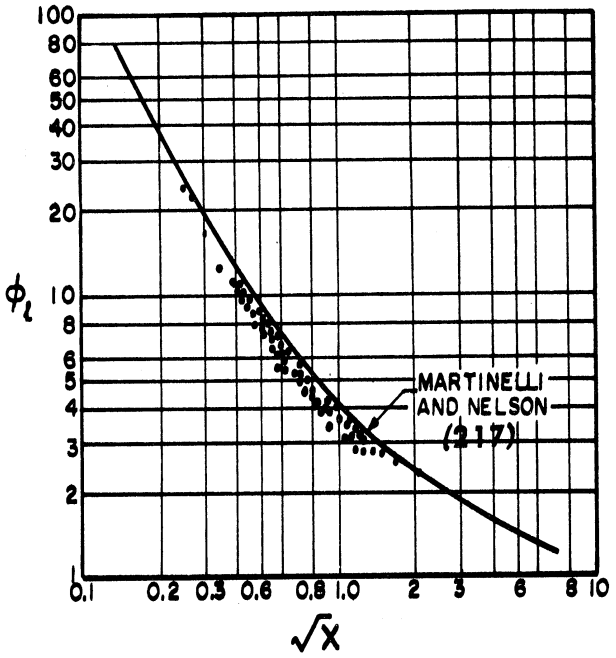

Figure 108. Comparison of two-phase (diabatic) pressure drop data for boiling Freon-11 with Martinelli-Nelson prediction.(217)

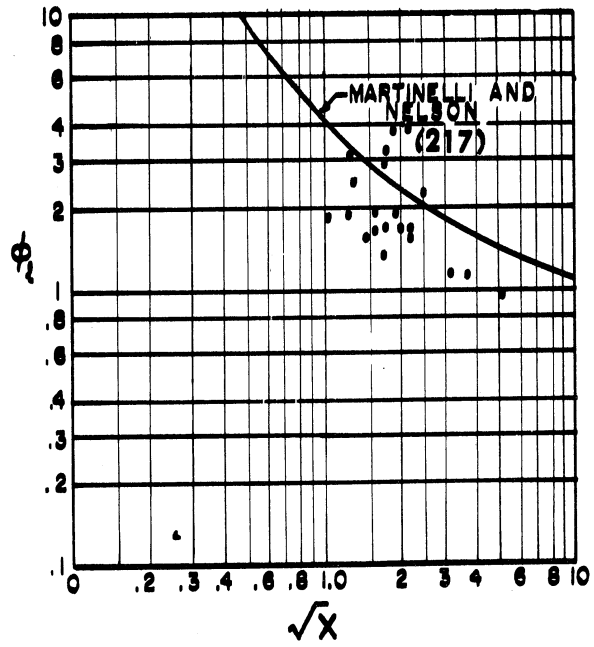

Figure 109. Comparison of two-phase (diabatic) pressure drop data for boiling hydrogen with Martinelli-Nelson prediction.(217)

test section. The Freon-11 data fell below the recommended curve of Martinelli - Nelson by about 20%. The authors attribute this partly to the existence of metastable liquid in the flow. The hydrogen data scatter considerably although the mean correlating line is also below the recommended curve. In both cases the experimental data closely parallel the Martinelli - Nelson correlation. As may be seen from these results two-phase pressure drop can exceed the single-phase pressure drop by several orders of magnitude for the same rates of flow.

3. Gravic and Agravic Effects on Boiling Heat Transfer

In recent years the application of boiling heat transfer data for environments of varying gravity has become of importance. This is a result of the need for information on heat transfer for the design of both high acceleration systems such as booster rockets and re-entry vehicles as well as devices to operate in sub-terrestrial gravity environment as orbiting satellites and deep space probes. Results obtained from these studies will undoubtedly have application in other fields also, as well as providing an improved understanding of the process fundamentals. One important aspect of low-gravity studies to date has been the isolation of gravity or body-force controlled phenomena and an evaluation of their true influence on a process. Also, a low-gravity environment is effective in reducing natural convective motion thus enabling the effects of other forces to be determined.

An approximate listing of the various gravity conditions to be expected for the operations of equipment is shown in Table XV.

Essentially all of the low-gravity heat transfer data have been taken using drop-towers. Some data have been taken with a KC-135

TABLE XV

APPROXIMATE RANGES OF a/g FOR EQUIPMENT OPERATION

Source	Application	Order of Magnitude of a/g
1. Centrifugal	Rotations in Turbines and compressors	10^{5}
2. Vehicle Acceleration	Liftoff and Re-entry of Rockets and Space Vehicles	10
3. Earth Gravity	At Surface of Earth	1
4. Lunar Gravity	At Surface of Moon	10^{-1}
5. Aerodynamic Drag	Drop Tower Experiments	10^{-1} to 10^{-4}
6. Thrust from ullage Control or From Radio-isotope Propulsion*	Typical Thrust: 10 lb_f	10^{-4}
7. Centrifugal (Space Vehicle Rotation)*		
a. To Maintain Vehicle Parallel to Earth Surface	Low Earth Orbit High Earth Orbit	10^{-6} 10^{-8}
b. Limit Cycle to Maintain Vehicle Oriented Towards Sun or Star	Angular Velocity Due to Limit Cycle: 0.05 deg/sec	10^{-8}
8. Aerodynamic Drag*	100 mi Orbit 250 mi Orbit 400 mi Orbit	10^{-6} 10^{-8} 10^{-9}
9. Solar Pressure*	Deep Space Penetration; Low Absorptance Surface	10^{-10}

*Typical Vehicle: 100,000 lb class about 20 ft in diameter (227).

aircraft in a Keplerian trajectory and a few have been taken in a magnetic field using the principle of magnetic levitation. The drop-towers have so far proven to be the most convenient, reliable, accurate and least costly. Their great disadvantage, of course, is the relatively short period of test time permitted (1-4 sec.). Longer duration of test times may be expected when orbital laboratories are put into operation. High gravity heat transfer data have been obtained on centrifuge apparatus. Present capacity enables the attainment of gravity levels up to 1000 times earth gravity in completely instrumented test packages.*

Nucleate and film pool boiling heat transfer data for liquid hydrogen for gravity levels (a/g) from 1 to 7 are reported by Graham, et al (228). Their results are shown in Figure 110. The influence of increased gravity forces is relatively insignificant in nucleate boiling but prominent in film boiling. Clark and Merte (93) and Merte and Clark (92) have studied the effect of gravity fields in the range $1 \leq a/g \leq 21$ on pool nucleate boiling to saturated liquid nitrogen and water at atmospheric pressure. The results of this investigation are given in Figures 111 and 112. As in the case of the data for liquid hydrogen of Graham, et al (228) the influence of increased bouyant forces on nucleate boiling is not significant, at least in the range of bubble dominated boiling. The apparent influence of a/g on the low boiling heat flux in Figures 111 and 112 is attributed to the effect of single phase, natural convection. This is to be expected since single phase natural convection is uniquely related to bouyant forces. Thus, it is apparent that in the region of well-developed boiling it is the dynamic forces associated with the bubbles themselves which govern the process, the

* 10-foot diameter centrifuge installed in the Heat Transfer Laboratory, Department of Mechanical Engineering, The University of Michigan, Ann Arbor, 1963.

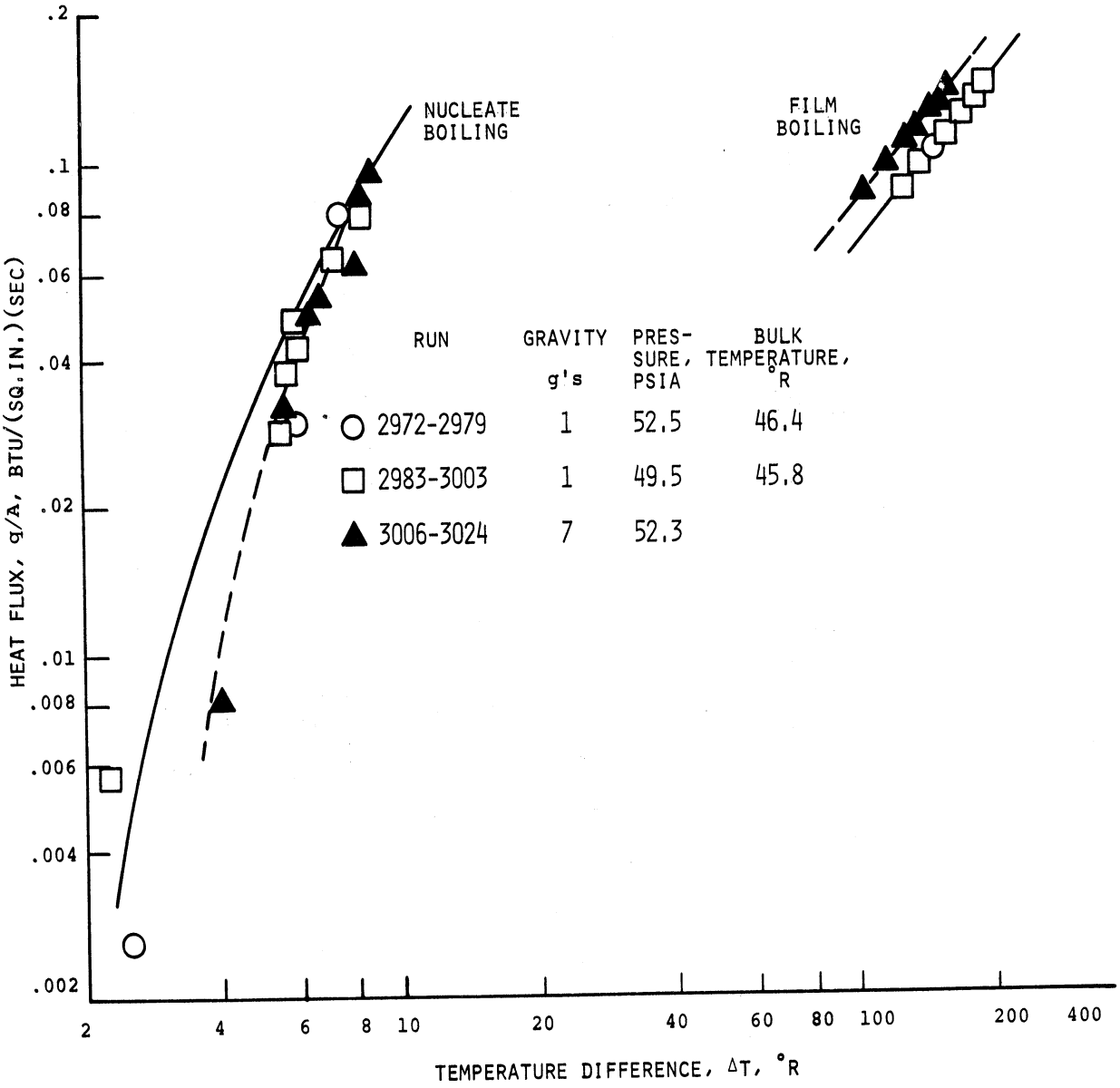

FIGURE 110. COMPARISON OF EFFECTS OF ACCELERATION ON NUCLEATE AND FILM BOILING FOR PARA-HYDROGEN.(228)

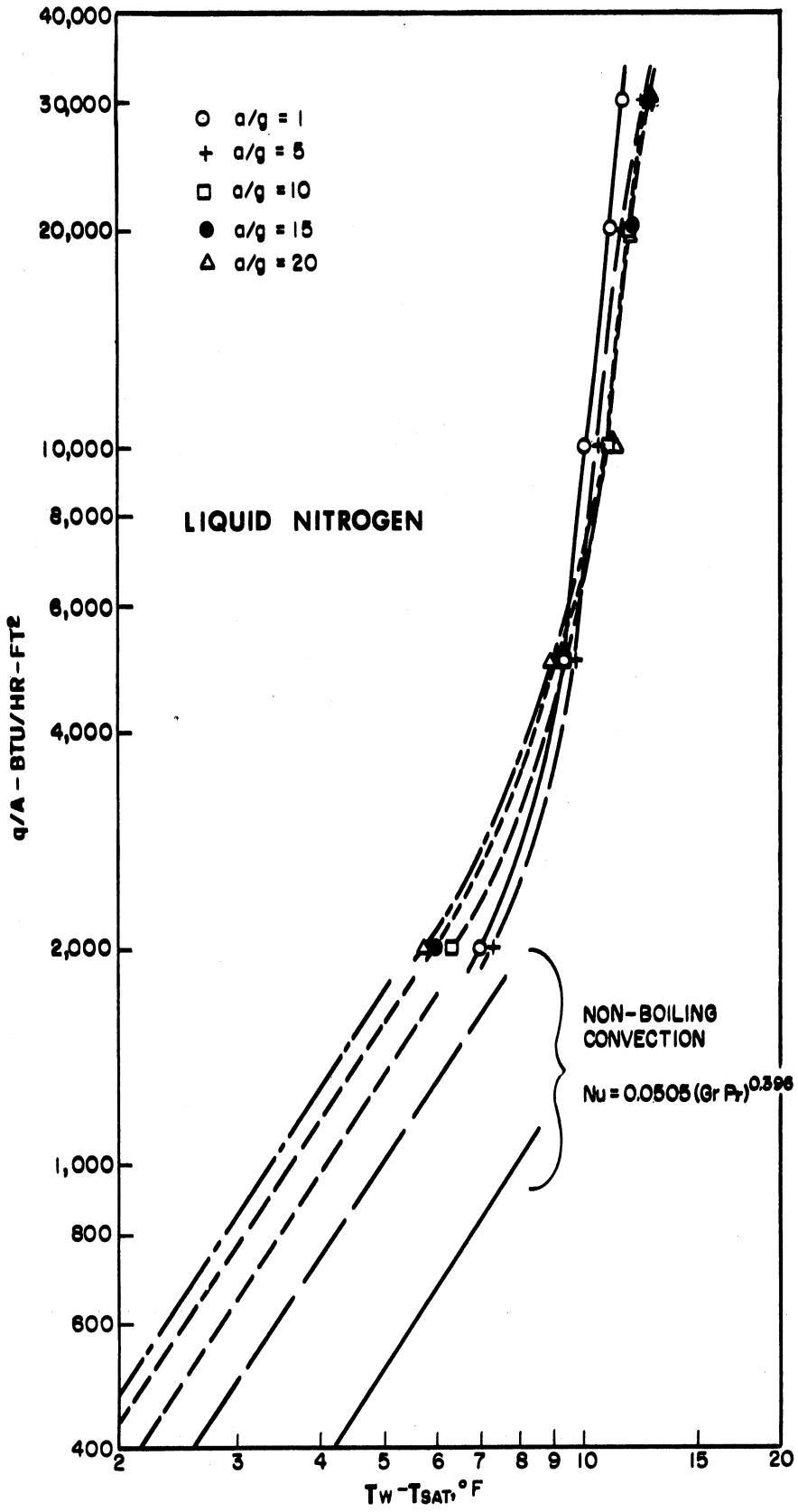

Figure 111. High-Gravity Nucleate Boiling Data for Liquid Nitrogen at Atmospheric Pressure.(193)

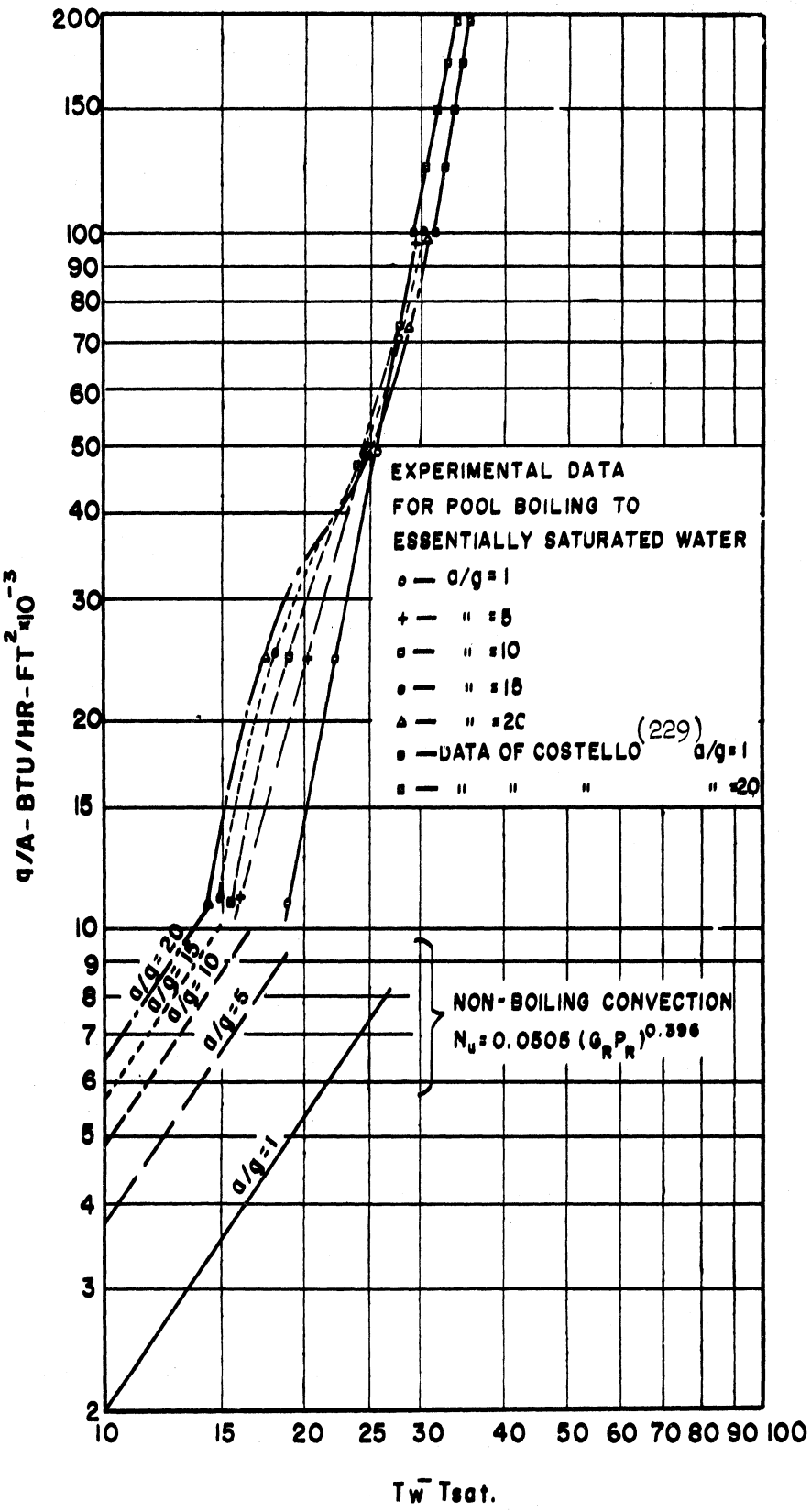

Figure 112. Influence of system acceleration normal to heating surface on convection and pool boiling. (92)

role of bouyant forces not being nearly as significant as previously believed. It is possible, of course, that at very high levels of a/g this condition will no longer prevail. This same effect will be seen in the low-gravity results to be discussed below in which the bouyant (body) forces have been essentially removed.

High gravity data (a/g from 1 to 10) are reported by Pomerantz (201) for Freon-113. His film boiling results were given in Figure 89 and found to correlate reasonably well with Equation 121. Beckman and Merte (230) studied the process of bubble formation and growth photographically in water in the range of gravity (a/g) from 1 to 100. High speed motion pictures of the bubbles taken at 20,000 fps showed some remarkable dynamic effects.

Maximum heat flux data of Ivey (231) for water are shown in Figure 113 for a/g up to 160. The 1/4-power influence of a/g on $(q/A)_{max}$, predicted by Equations 103-109, is seen only to be approximated. Ivey found that an exponent on (a/g) of 0.273 would best fit his data. However, the maximum heat flux data of Merte and Clark(90) for liquid nitrogen at (a/g) ranging from 1.0 to about 0.10 shows a reasonably good agreement with the 1/4-power prediction. These data, taken from drop-tower measurements, are shown in Figure 114. For a/g less than about 0.10 the 1/4-power dependence of a/g seems no longer valid for calculations of the maximum heat flux in pool boiling. This effect is suggested in Figure 114. Lyon, et al (234) have made an extensive study of the influence of a/g on $(q/A)_{max}$ in these very low ranges of acceleration using the unique technique of magnetic levitation. The results of these investigators is shown in Figure 115 for liquid oxygen where comparison is made with measurements of others for water, liquid nitrogen

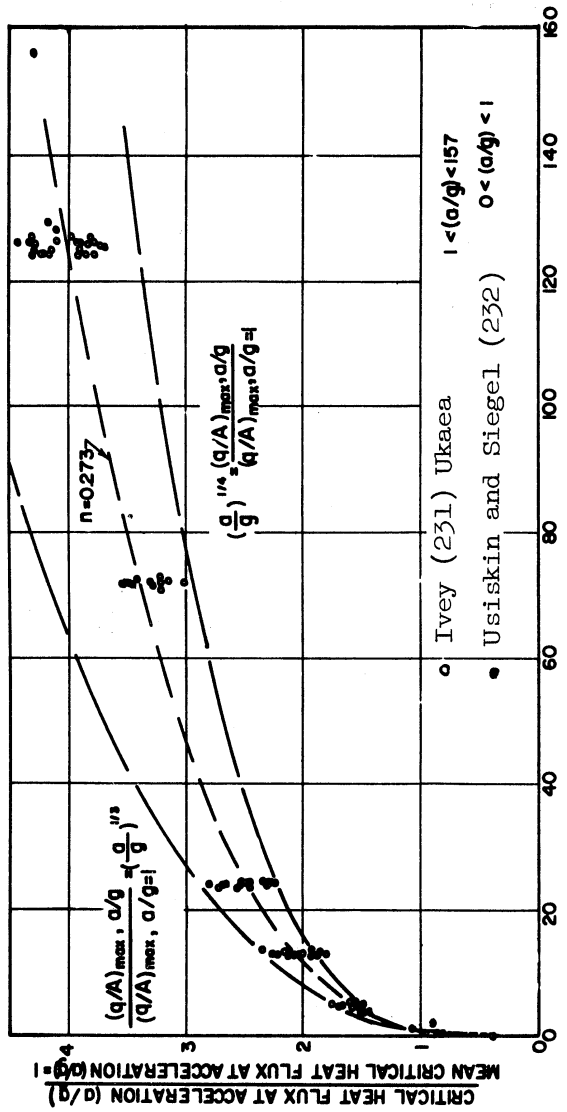

Figure 113. Effect of system acceleration on maximum heat flux in pool boiling.

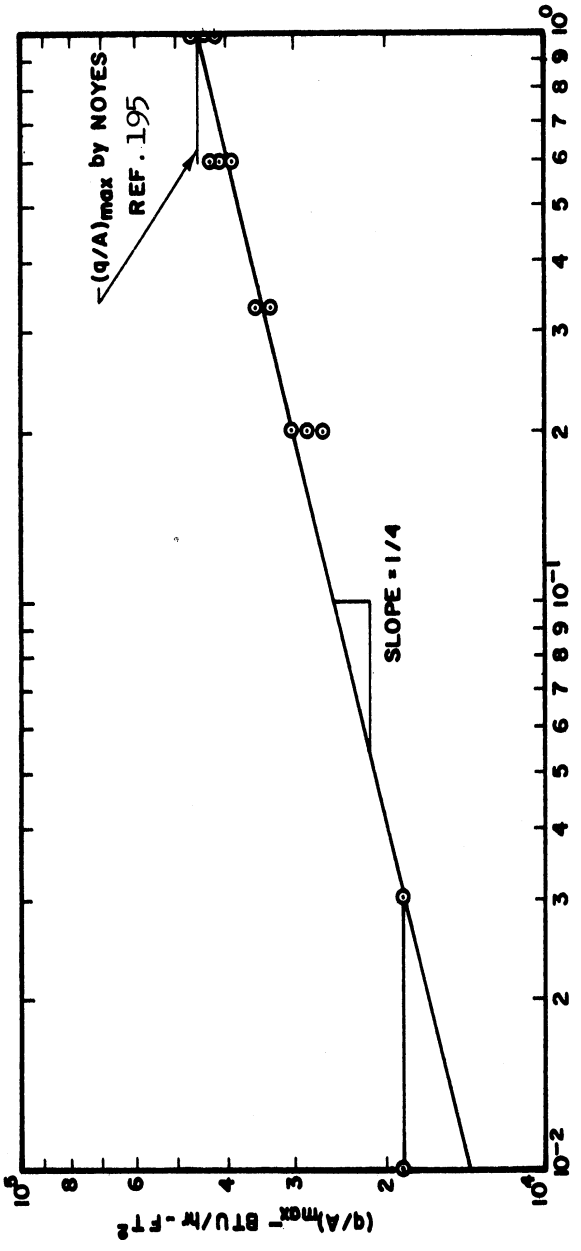

Figure 114. Maximum Heat Flux Data for Liquid Nitrogen from a Sphere During Fractional Gravity. (90)

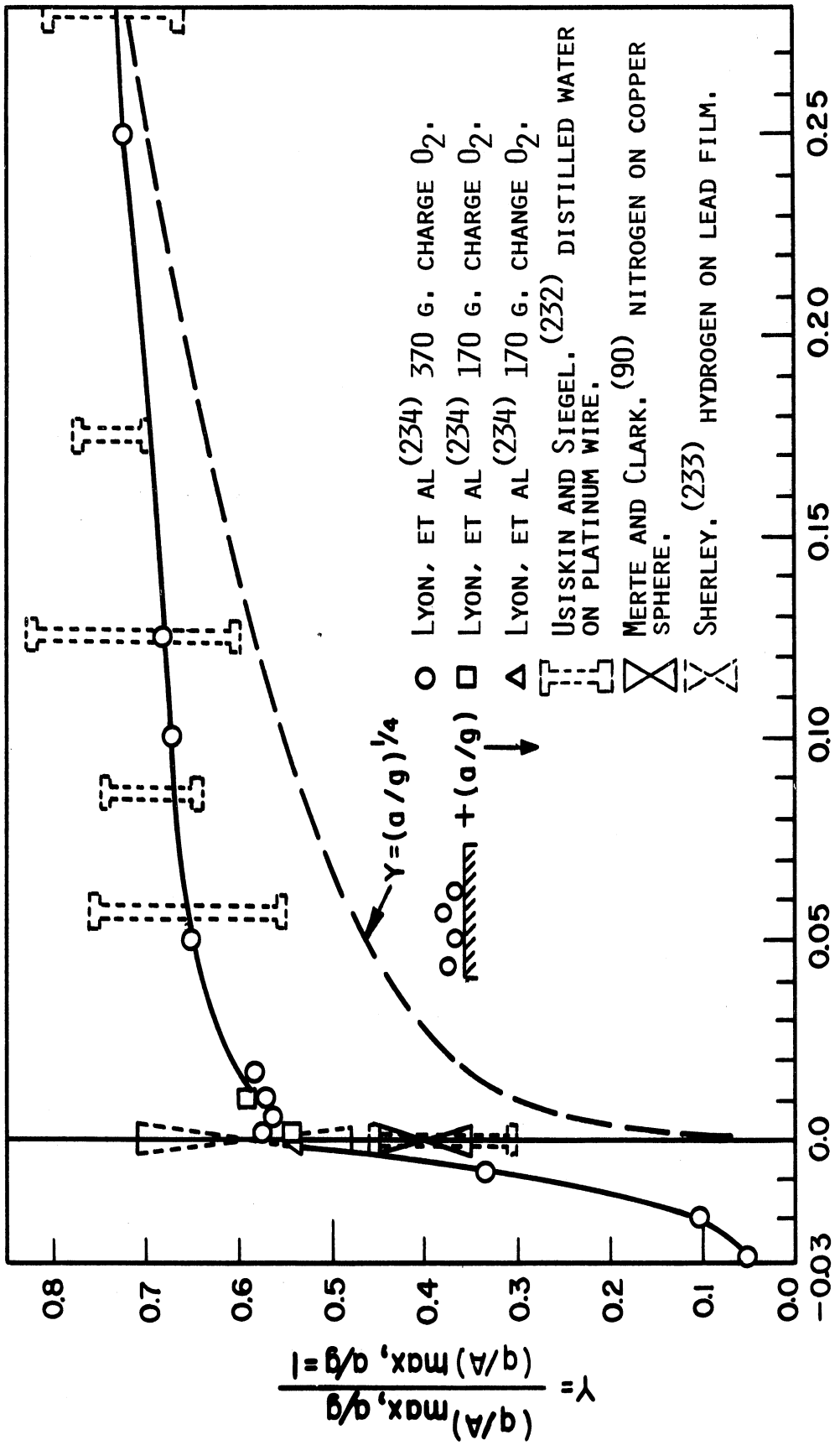

FIGURE 115. NORMALIZED MAX HEAT FLUX AT SMALL RELATIVE VAPOR ACCELERATIONS (CALCULATED FROM BULK LIQUID TEMPERATURES).(234)

and liquid hydrogen. As may be observed, a considerable departure is found from the 1/4-power formula. At very low a/g the actual $(q/A)_{max}$ is significantly greater from that predicted by any of the Equations 103 to 109. At the present, the meaning of this is unclear. It seems probable that owing to the powerful dynamic influence of the bubbles a finite maximum heat flux will exist even at a condition of true zero-g. How the vapor will be removed from the surface under these conditions is unknown and doubtless would present a serious problem for sustained operation at true zero-g. However, at least for a short period following the initiation of zero-g it seems probable that $(q/A)_{max}$ would be finite and a significant fraction of that at normal earth gravity.

An interesting feature of the work of Lyon, et al (234) is the control they could impose over both the magnitude and direction of the acceleration vector (body or bouyant force). Some of their results for a small negative acceleration also are shown in Figure 115. Under these circumstances the maximum heat flux rapidly approaches zero since the forces in the system tend to drive the vapor towards the surface.

Gravity dependence on the minimum heat flux is also predicted in accordance with the 1/4-power relation in Equations 110 to 114, Table XII. A reasonable agreement with experiments using liquid nitrogen in the range a/g from 1.0 to 0.001 is shown in Table XIV.

Low gravity heat transfer data of Merte and Clark (90, 93, 134), for liquid nitrogen in the nucleate and film boiling regions are given in Figure 116. The film boiling data for a/g of 1.0 are in good agreement with the results of others (135, 152, 174) for systems in which the ratio $\lambda c/D$ is small. For the range of a/g from 1.0 to 0.20

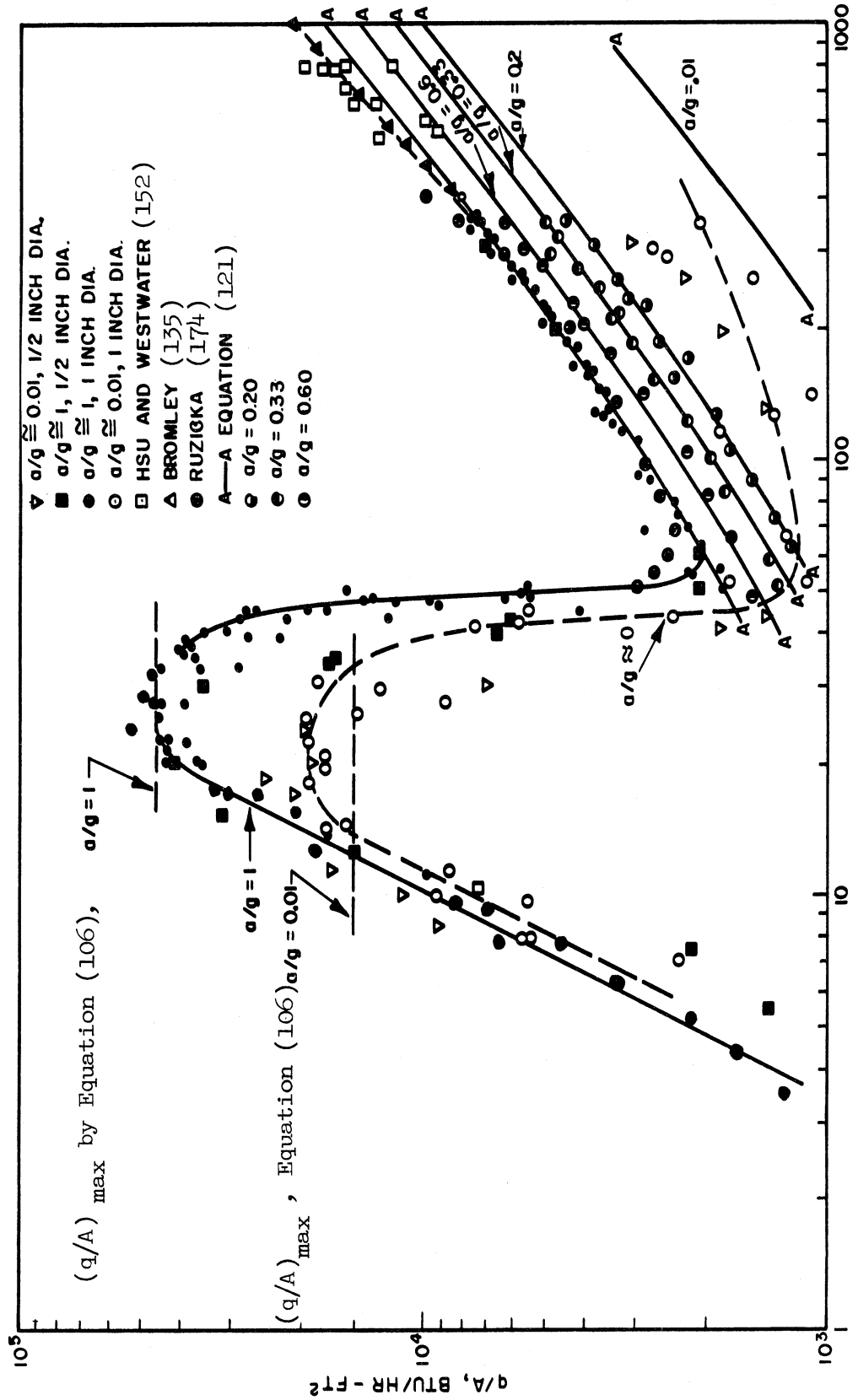

Figure 116. Boiling Heat Transfer to Liquid Nitrogen at Atmospheric Pressure.(90)

these data correlate well with Equation 121 as shown in Figure 89. This indicates that the controlling force in film (pool) boiling is the body force.

The nucleate boiling data in Figure 116 indicates a remarkable lack of sensitivity to the 100-fold reduction in gravity. A similar result is reported for liquid hydrogen by Sherley (233) as shown in Figure 117. Both of these sets of data are consistent with the observations of the influence of high-g on nucleate boiling which was indicated in Figures 110, 111 and 112. These results have led to the aforementioned conclusion that bouyant forces are not of prime significance in the process of nucleate boiling. The role of inertia forces resulting from bubble growth appears to have the principal influence in the process. These observations have suggested the formulation of a Froude number, Fr, criterion to indicate the relative importance of inertia and bouyant forces (235). Adelberg and Forster in a discussion of Reference (232) have formulated the Froude number as

$$Fr = \frac{F_i}{F_b} = \frac{3R^2\dot{R}^2 + R^3\ddot{R}}{R^3(a/g)g} \quad . \tag{165}$$

This result can be evaluated further by introducing the following expression for bubble growth in a superheated liquid derived by Forster and Zuber (176).

$$R\dot{R} = \left[\frac{\Delta T\ c_{p_\ell}\ \rho_\ell}{h_{f_g}\ \rho_v}\ \sqrt{\pi a_\ell}\ \right]^2 \tag{166}*$$

---

*Equation (166) was derived for a uniformly superheated liquid. However, Zuber and Fried (139) report that it has been used as a first approximation to predict bubble growth rates in pool boiling. These authors also employ a factor of 2 on the left side of equation (166) which was not in the original formulation (176). For the present purposes either form would be adequate.

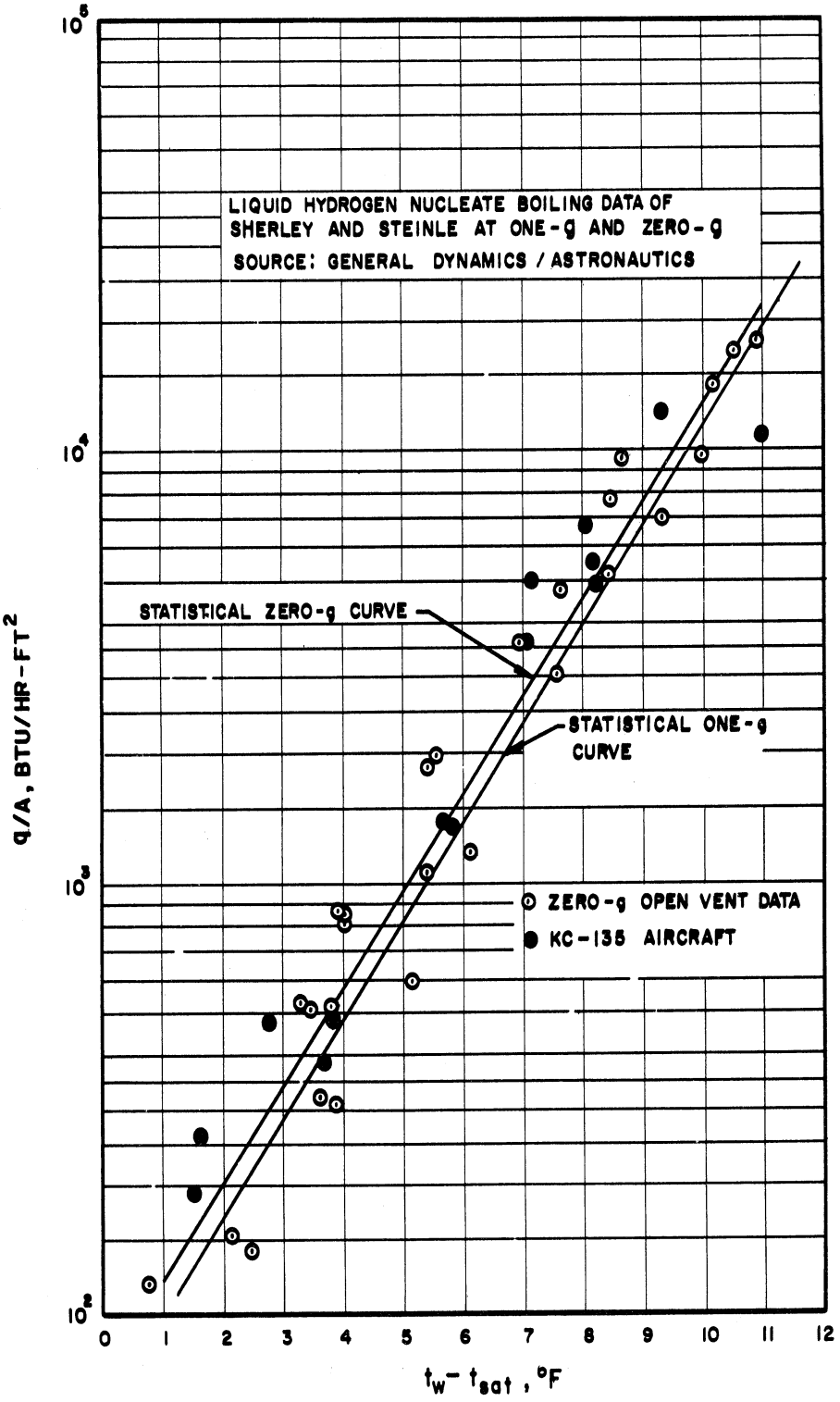

Figure 117. Nucleate boiling data for liquid hydrogen at standard and zero-gravity. (233)

Performing the indicated operations in Equation (165), the bubble Froude number becomes

$$Fr = \frac{2}{R^3(a/g)g}\left[\frac{\Delta T\, c_{p_\ell}\, \rho_\ell}{h_{f_g}\, \rho_v}\sqrt{\pi a_\ell}\right]^4 . \qquad (167)$$

The magnitude of the Froude number in Equation (167) indicates the relative importance of inertia forces and bouyant forces in the growth of a bubble. When the Froude number is of the order of 1 these two forces have approximately equal value. Should this ratio be greater than unity then the inertia forces may be expected to predominate. The opposite will be true for Froude numbers less than unity. Hence, Equation (167) may be employed as a criterion for a satisfactory level of "zero-gravity". As will be noted below, an adequate zero-g condition actually exists when $a/g = 1$ for nucleate boiling of cryogenic liquids and water. Calculations of the Froude number have been made for the liquids of nitrogen, oxygen and hydrogen (93, 235) and are given in Table XVI. Water is included for comparison. The data correspond to those conditions which may be reasonably expected near a heated surface in nucleate boiling where the dynamics of the bubbles have their greatest influence on the heat transfer.

TABLE XVI

FROUDE NUMBER FOR NUCLEATE BOILING (93)

(p=15 psia, a/g=1, ΔT=16°F, R=0.005 inch)

Liquid	Froude Number
N_2	452
O_2	546
H_2	352
H_2O	13,900

As is evident from these calculations the importance of inertia forces far outweigh that of bouyant forces in nucleate boiling. For gravities less than a/g of 1 the effect becomes even more pronounced and it may be expected that at zero-gravity bubble inertia effects are infinitely more significant. Since it is believed that a micro-convection, or stirring effect of the bubbles, is the principal mechanism controlling the heat transfer rate in nucleate boiling it follows that this would be governed by a liquid flow pattern caused by the dynamics of bubble growth. In view of the results in Table XVI the process of nucleate boiling then appears to be gravity-insensitive, except possibly at very high a/g, the important mechanics being the inertial effects of the growing (and collapsing) bubble. In the case of sub-cooled nucleate boiling, inertial effects can be expected to be even greater since the bubble dynamics are more pronounced.

Siegel (236) has presented a comprehensive review of the influence of reduced gravity on heat transfer in the previous volume of Advances in Heat Transfer.

4. Injection Cooling

Another process which has found important application in cryogenic systems is the cooling of a cryogen by the injection of a non-condensible gas of low solubility. One significant application of this has been the injection of gaseous helium into the liquid-oxygen suction lines of large rocket boosters during pre-launch operations. This provides the necessary subcooling by the evaporation of the liquid into the helium bubbles to prevent pump cavitation and engine failure at start-up (237, 238). This process has been analyzed in depth in recent

years. However, in the interest of brevity the available papers on the subject will be cited only.

Larsen, et al (239) analyzed the process of gas injection including the effects of liquid evaporation, gas solubility, gas enthalpy flux, ambient heating and liquid displacement due to the presence of gas bubbles in the system. The analytical model is space-wise lumped and the results compare favorably with measurements on vertical columns of liquid oxygen cooled by the injection of gaseous helium and nitrogen. The production of solid argon by the injection of gaseous helium into liquid argon has been observed in experiments reported by Lytle and Stoner (240). The cooling of liquid hydrogen by helium gas injection has been studied by Schmidt (241). A detailed analytical investigation of the dynamics of single bubbles injected in a liquid is reported by Arpaci, et al (242). Reasonable agreement with the theory was obtained from high speed motion pictures of the dynamics of nitrogen and helium bubbles injected into water.

5. Frost Formation

The problem of frost formation on cooled surfaces is not well defined although it is commonly encountered on cryogenic systems in an atmospheric ambient. Should cryogenic substances be stored in atmospheres other than the terrestrial other kinds of frost can be expected.

The prediction of frost formation in atmospheric air is complicated by several factors. For surface temperatures below the temperature of liquid air the overriding layers of water and carbon dioxide frost have a liquid air substrate. This results in an instability of the growth of the frost causing it to coat a surface in patches. The

shearing action of gravity and aerodynamic drag forces cause a similar destruction of the frost layers. The mechanical structure of frost is largely unknown and its physical properties are not well tabulated. Frost formation from normal ambient air involves a complex process of simultaneous transient heat and mass transfer of at least two or three components (H_2O, CO_2, air) and two or three phases.

A study of frost formation inside of tubes in forced convection is reported by Chen and Rohsenow (244). They attribute the increased heat transfer and pressure drop under conditions of frost to the roughness of the frost surface. Smith, et al (245) analyzed the problem of frost formation on cooled surfaces in forced convection and give results concerning the thermal conductivity of frost. They conclude that the thermal conductivity is a function of the conduction and diffusion paths through the frost.

Barron and Han (243) investigated the formation of frost on vertical flat surfaces in laminar and turbulent natural convection. They observed that a simultaneous mass transfer of water vapor from the moist ambient air to the frost layer increased the rate of heat transfer. This effect was not large, however, being about 5% for a mass fraction of water vapor of 0.10. Their heat transfer data were correlated within $\pm$ 20% by formulations in terms of Nusselt, Grashof, Prandtl and Schmidt numbers and parameters which relate to the effects of mass transfer. On the other hand the predicted mass transfer rates were about 10 times greater than those measured. This was attributed to the interference by frost particles in the boundary-layer to the diffusion of water vapor to the cold surface. The predominant component to the energy transport

was the convective component and the influence of thermal diffusion and diffusion thermo effect was found to be completely negligible. Barron and Han measured the thermal conductivity of the frost and found it to be related to its mean density and mean temperature. Some of their results are given in Figures 118 and 119.

Studies of frost formation also have been reported by Holten (246) Van Gundy and Uglum (247), Arthur D. Little, Inc., (248), The National Bureau of Standards (249) and Loper and Heatherly (250).

Holten (246) investigated the growth of frost on the outside of spherical aluminum containers in a free convection atmospheric ambient and found a definite dependence on the specific humidity. Some of his results are given in Figures 120 to 123. The rate of formation of frost was found to go through a maximum while its surface temperature increased. The fact that the latter did not reach 32°F after long times is attributed to the mechanical failure of the condensate which became excessive after 150 minutes. Thermal conductivity data for the frost is given in Figure 123 as a function of the average temperature. Similar data from reference (248) indicate k-values of frost to range from 0.02 BTU/HR-Ft-F at -275F to 0.035 BTU/HR-Ft-F at -200F, corresponding to frost thicknesses of 0.05 and 0.15 inches, respectively. Reference (248) also reports that only 20-40% of the water vapor that is predicted to diffuse to the cooled surface by mass transfer calculations is retained on the surface as frost, an observation similar to that of Barron and Han (243).

Van Gundy and Uglum (247) conducted experiments on the mechanics of frost on liquid hydrogen cooled surfaces at 20°K for the forced flow of moist air. They report an important influence of the condensation

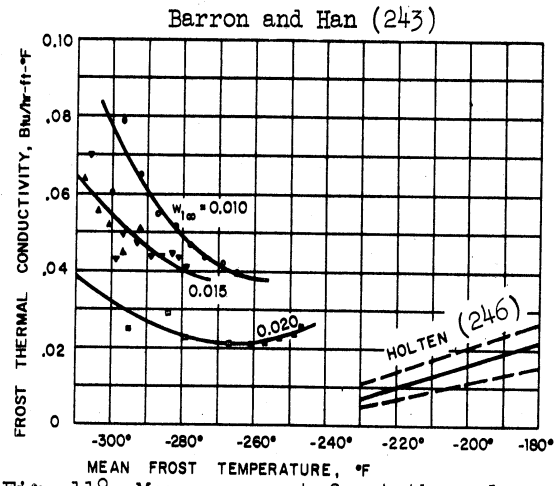

Fig. 118. Mean apparent frost thermal conductivity as a function of the mean frost temperature, $T_f = 0.5(T_w + T_s)$.

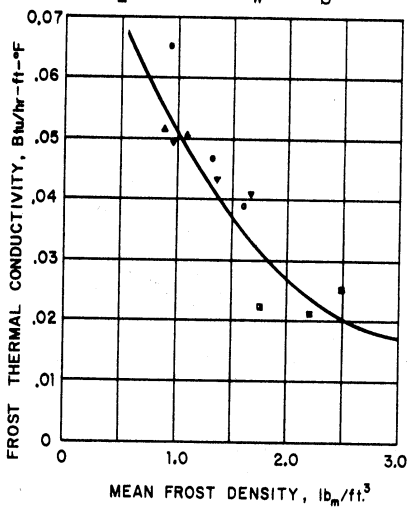

Fig. 119. Mean apparent frost thermal conductivity as a function of mean frost density

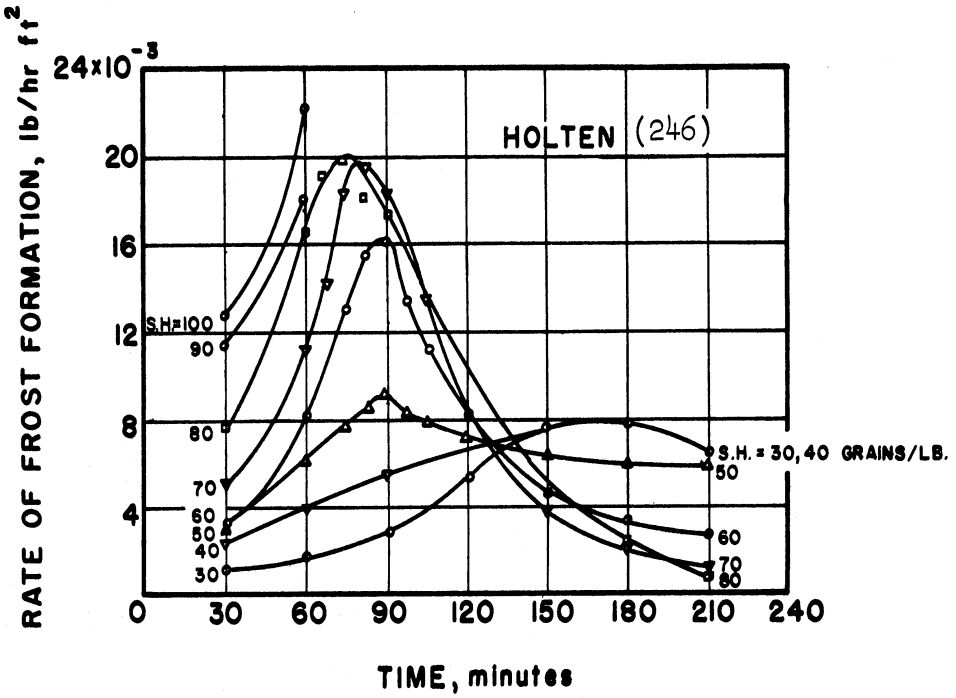

Figure 120. Rate of frost formation as a function of time and specific humidity.

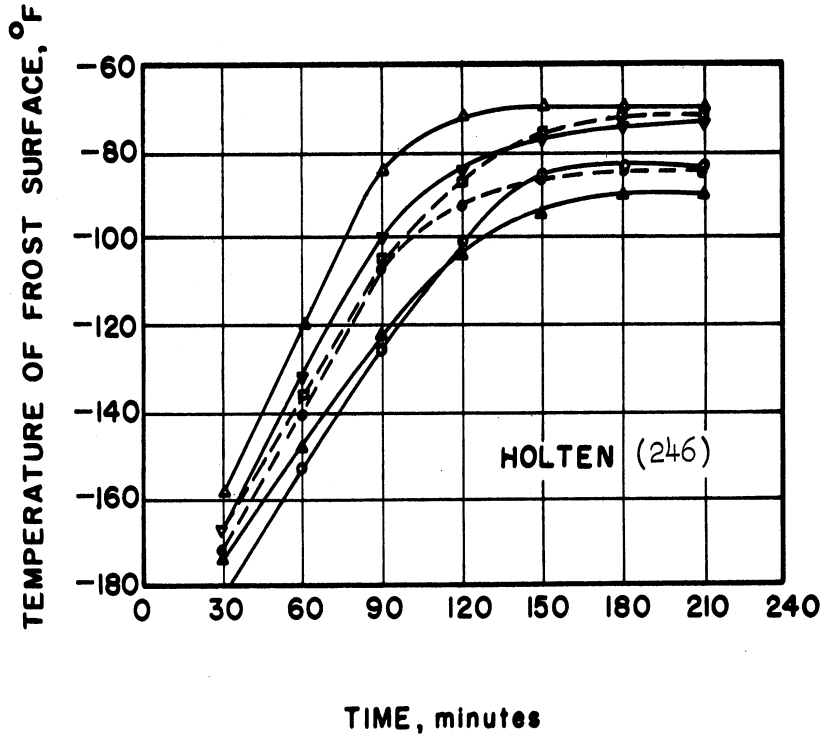

Figure 121. Calculated frost surface temperature as a function of time in natural convection.

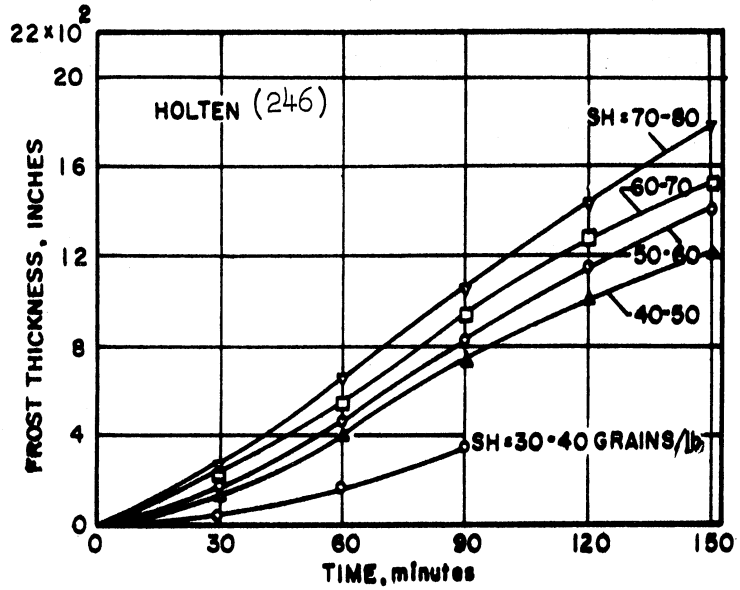

Figure 122. Frost thickness as a function of time and specific humidity.

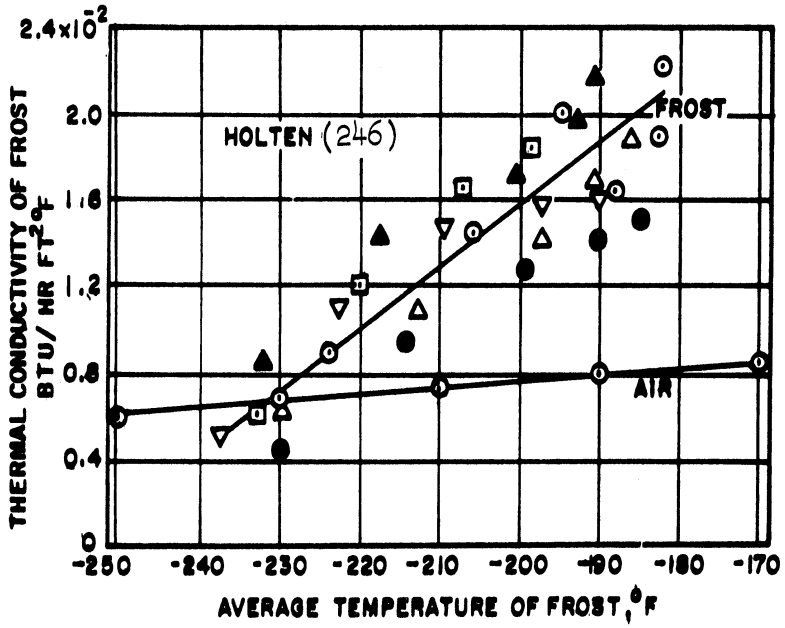

Figure 123. Apparent thermal conductivity of frost as a function of the average frost temperature.

of liquid air. The highest heat flux is obtained when the condensed air can flow off the surface. A low ambient temperature and low humidity was found to inhibit frost formation. Data for the steady frost thickness for this system are given in Figure 124 as a function of the absolute humidity and air velocity.

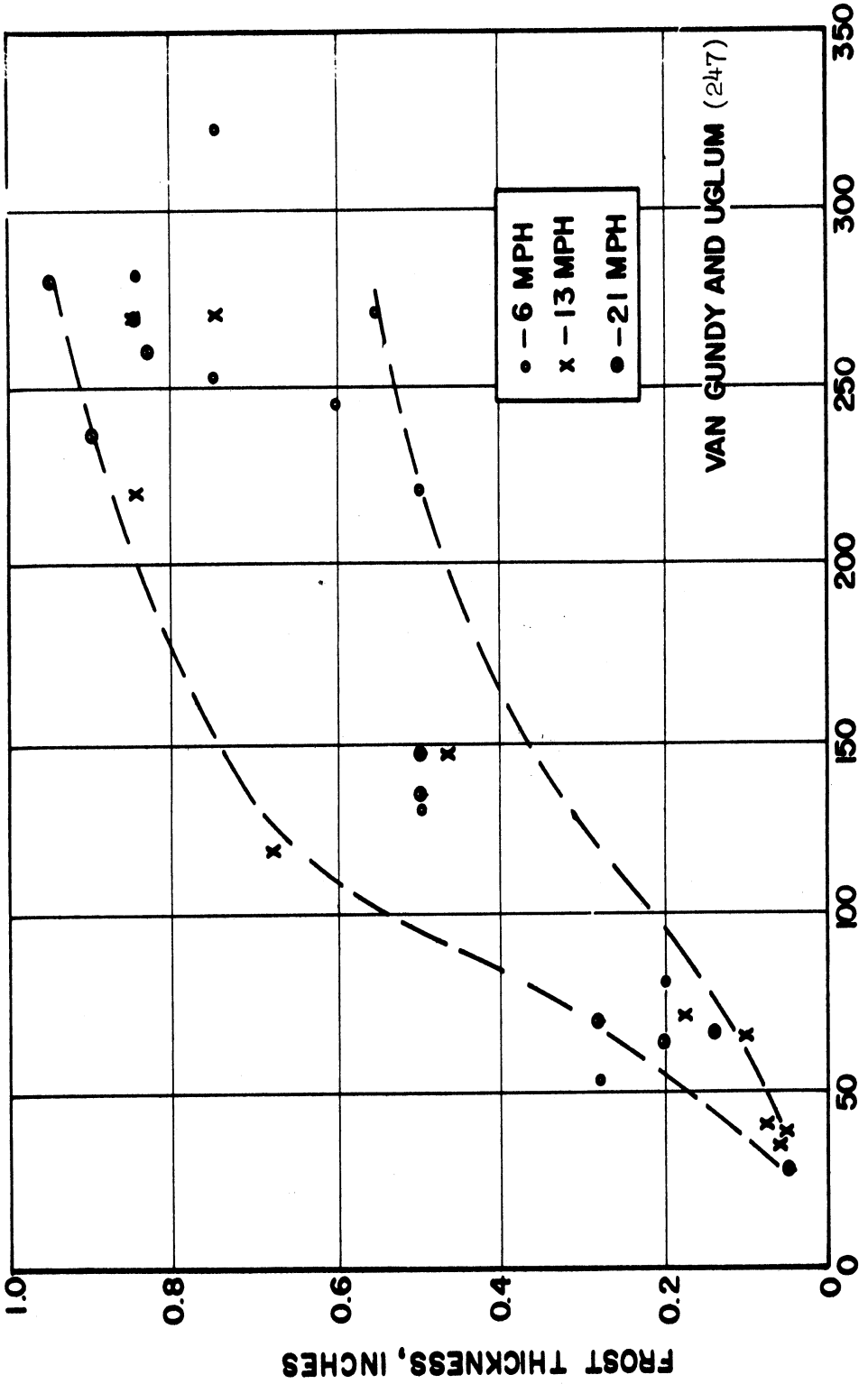

Figure 124. Influence of flow velocity and absolute humidity on frost thickness.

VIII. RADIATION

The principal problems of radiation heat transfer at cryogenic temperatures is the determination of the radiation properties of surfaces. Gaseous radiation is less of a problem since most of the substances which remain as gases at low temperatures are not significant radiators nor absorbers. Radiation enclosure calculation methods such as those of Hottel (74) and Gebhart (252) are valid under these conditions. However, low temperature systems have introduced a new consideration into the treatment of radiation heat transfer. This is the effect of condensed gases on the radiation properties of cold surfaces. Such condensate layers build up complex systems known as cryodeposits on the cold substrate. Much of the work to date has been for systems of H_2O and CO_2, the common cryodeposits from a terrestrial ambient. In general this is an extension of the problem of frost and much yet remains to be learned about these systems. Knowledge of the radiation properties of the cryodeposits is important in connection with studies of cryopumping, simulation of the solar space environment and the storage of cryogenic fluids.

Kropshot (13) gives some values of the total hemispherical emissivities for some common metals at low temperatures. His results are included in Table XVII. Other tabulations of the emissivities of various materials with different surface conditions as a function of temperature include the work of Fulk and Reynolds (253).

The emissive properties of vacuum-deposited metallic coatings on polyester film for low temperature service has been investigated by Ruccia and Hinckley (254). These highly reflective surfaces are

TABLE XVII

SELECTED MINIMUM TOTAL EMISSIVITIES*

Surface	Surface Temp., °K			
	4	20	77	300
Copper	0.0050		0.008	0.018
Gold			0.01	0.02
Silver	0.0044		0.008	0.02
Aluminum	0.011		0.018	0.03
Magnesium				0.07
Chromium			0.08	0.08
Nickel			0.022	0.04
Rhodium			0.078	
Lead	0.012		0.036	0.05
Tin	0.012		0.013	0.05
Zinc			0.026	0.05
Brass	0.018			0.035
Stainless steel, 18-8			0.048	0.08
50 Pb 50 Sn solder			0.032	
Glass, paints, carbon				>0.9
Silver plate on copper		0.013	0.017	
Nickel plate on copper		0.027	0.033	

*These are actually absorptivities for radiation from a source at 300°K. Normal and hemispherical values are included indiscriminately. Data taken from Kropschot (13).

employed in multi-layer, vacuum insulation where, except for aluminum, savings in weight and cost as well as increases in strength are obtained by depositing copper, gold and silver on a polyester substrate. An important factor to be determined is the influence of thickness of the metallic deposit on the radiative properties. Another is the effect of environmental conditions of temperature, humidity and contaminents on the stability and adhesion of the metal film.

The results of Ruccia and Hinckley (254) for the emittance of metallic deposits of aluminum, gold, silver, silicon monoxide protective coating on silver, copper and silicon monoxide protective coating on copper are given in Figure 125. The substrate consisted of 1/4-mil (0,00025 inch) DuPont, type A, polyester film. As the thickness of the deposited metal layer increases the emittance decreases until an asymptote is reached at about 750-1000 Å for silver and aluminum and 1500 Å for gold. The lowest emittance is found for silver with copper, gold and aluminum following next in order of increasing emittance for any thickness. The protective coatings of SiO on silver and copper degrade their emittance by about 40%.

The influence of environment is shown in Table XVIII. The tape test listed consisted of placing a strip of scotch tape over the film to determine the adhesive properties of metallic coating. Except for the 95% relative humidity environment the aluminum coating showed good stability. Gold appears to be less stable in all environments while silver and copper were the least stable, as may be seen in the table.

Cunningham and Young (255) have studied the absorptance of a CO_2 cryodeposit on various substrates at 77°K (139°R). Their measurements

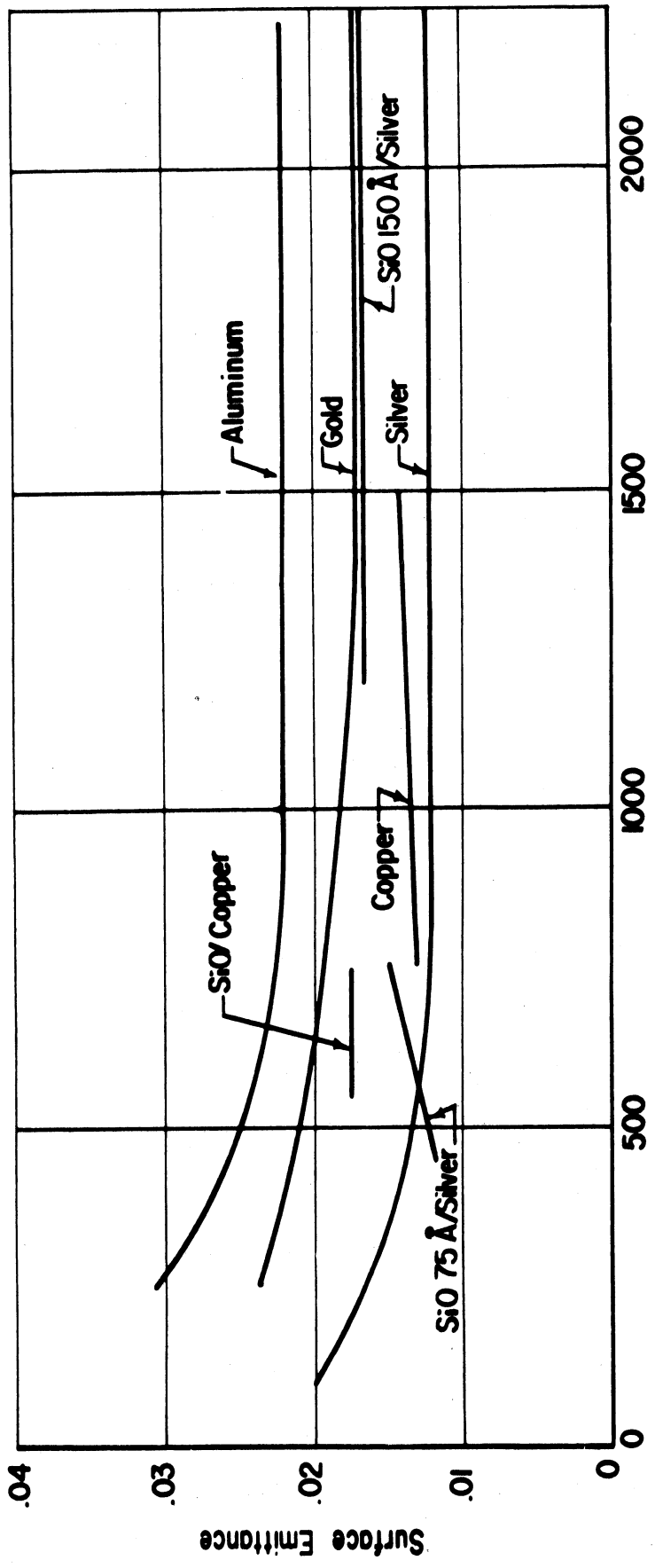

Fig. 125 Emittance of vacuum-metallized polyester film at 553°R for various metal coating materials and thicknesses. (254)

TABLE XVIII

EMITTANCE OF VACUUM-METALLIZED POLYESTER FILM AT 553°R FOR VARIOUS METAL-COATINGS AND MATERIAL THICKNESSES (254)

Environment	Film	Source	Sample No.	Thick-ness, Å	Start	Tape test, %	50 hr	Tape test, %	100 hr	Tape test, %
Air atm., 45% rel. humidity, 95°F	Al	ADL	48	790	0.021	0	0.021	0	0.0195	0
	Au	ADL	35-2	783	0.015	0	0.0159	0	0.0148	0
	Ag	ADL	36	762	0.0133	0	0.0181	10	0.016	10
	SiO/Ag	ADL	42	75/745	0.0160	0	0.0152	1	0.0165	0
	Cu	ADL	58	675	0.013	0	0.0167	0	0.0174	0
	SiO/Cu	ADL	52	75/761	0.0179	0	0.0178	0	0.0173	0
	Al*	NRC	305	376	0.0136[1]	0	0.025	0	0.0291	0
	Au*	Hastings	304-A	1000	0.025	0	0.025	0	0.0234	0
	Au*	Nat.Met.	308	240	0.0214	0	0.0211	0	0.0235	0
Air atm., 95% rel. humidity, 95°F	Al	ADL	49	862	0.0184	0	0.0225	0	0.0206	0
	Au	ADL	35-1	940	0.0140	0	0.0145	0	0.014	0
	Ag	ADL	37	762	0.0111	0	0.0144	20	0.0147	40
	SiO/Ag	ADL	43	75/745	0.0141	0	0.0199	20	0.0175	20
	Cu	ADL	59	675	0.0121	0	0.0437	0	0.0713	0
	SiO/Cu	ADL	53	75/761	0.0174	0	0.0212	10	0.0254	10
	Al	NRC	321	435	0.0225	0	0.0229	0	0.243	0
	Au	Hastings	304B	825	0.021	0	0.023	2	0.0225	30
	Au	Nat.Met.	322	212	0.0211	0	0.027	0	0.0271	0
CO_2 atm., 95°F	Al	ADL	50	862	0.0203	0	0.0192	0	0.0184	0
	Au	ADL	34-1	1020	0.0152	0	0.0148	0	0.0187	0
	SiO/Ag	ADL	44	75/745	0.0150	0	0.0142	0	0.0207	0
	SiO/Cu	ADL	54	75/761	0.0170	0	0.018	0	0.0166	0
	Au	Hastings	333	953	0.0259	0	0.0273	0	0.0299	-
	Au	Hastings	330A	1840	0.0146	0	0.0146	0	0.0153	0
Salt atm., 95°F	Al	ADL	51	862	0.0191	0	0.0187	0	0.0200	0
	Au	ADL	33-2	455	0.0154	0	0.0153	0	0.0152	0
	SiO/Ag	ADL	45	75/745	0.0198	0	0.0179	50	0.0165	100
	SiO/Cu	ADL	55	75/761	0.0228	0	0.0248	0	0.0255	0
	Au	Hastings	336	1050	0.0228	0	0.0225	0	0.0202	40
	Au	Hastings	330B	2072	0.0127	0	0.0160	0	0.0144	0

*Purchased samples are coated on both sides.
[1]Questionable value; previous measurements indicate this value has a range of 0.023 to 0.027.

of the absorptance as a function of deposit thickness is shown in Figure 126. The results for the bare surface (t = 0) agree well with literature values for the black and polished surface and a weighted calculation based on area for the other surfaces. The influence of cryodeposit thickness is to change the absorptance significantly for small thickness but to have essentially no effect for thicknesses greater than about 0.8 mm. For substrates of low absorptivity the effect of the deposit is to increase the absorptivity whereas the opposite effect is observed for high absorptivity substrates. Even for relatively large thickness of CO_2 the absorptivity of the cryodeposit on the various surfaces did not approach a common value. Apparently for a thickness in excess of about 0.8 mm the frost absorbs all radiation in the absorption band thus having no further influence on the radiating characteristics for greater thicknesses.

The absorptance of water vapor and carbon dioxide cryodeposits at 77°K (139°R) for both solar and 290°K (522°R) black body radiation is reported by Caren, et al (256). The substrates consisted of polished aluminum and aluminum coated with a black epoxy paint (cat-a-lac flat black). The absorptance of an H_2O cryodeposit on these substrates is shown in Figure 127 as a function of deposit thickness for black radiation at 522°R. The influence of the H_2O deposit is to increase the absorptance very significantly for the low absorptance substrate. The effect is much less for the painted surface. Agreement with data for H_2O given in Reference 257 is good. The absorptance data for a CO_2 deposit on the same substrates for black radiation at 522°R is given in Figure 128. Agreement with the results of Reference 257 is reasonably good but poor with the data of Cunningham and Young (255).

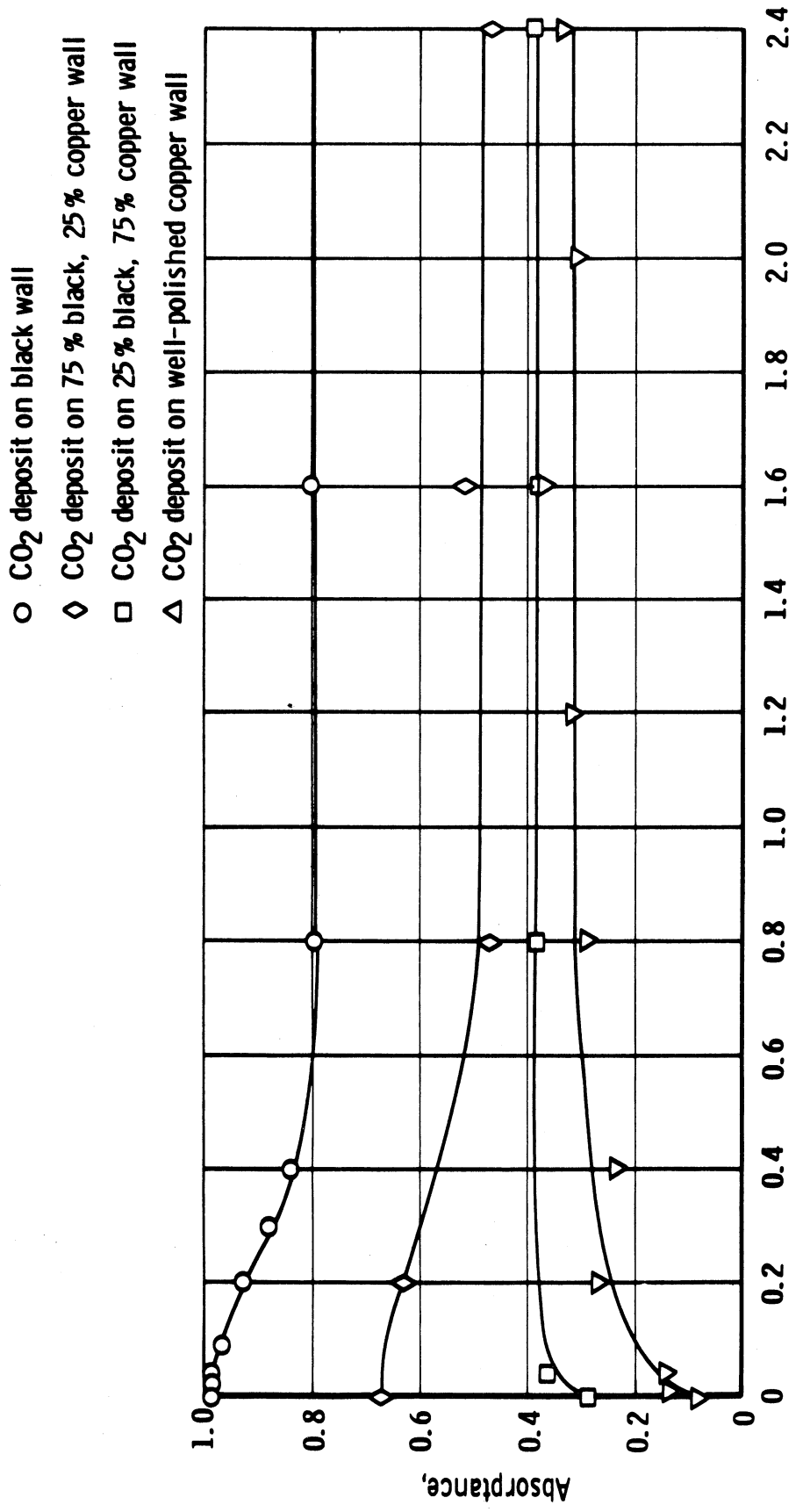

Fig. 126 Effect of Cryodeposit Thickness and Wall Absorptivity on Complex Absorptance (255)

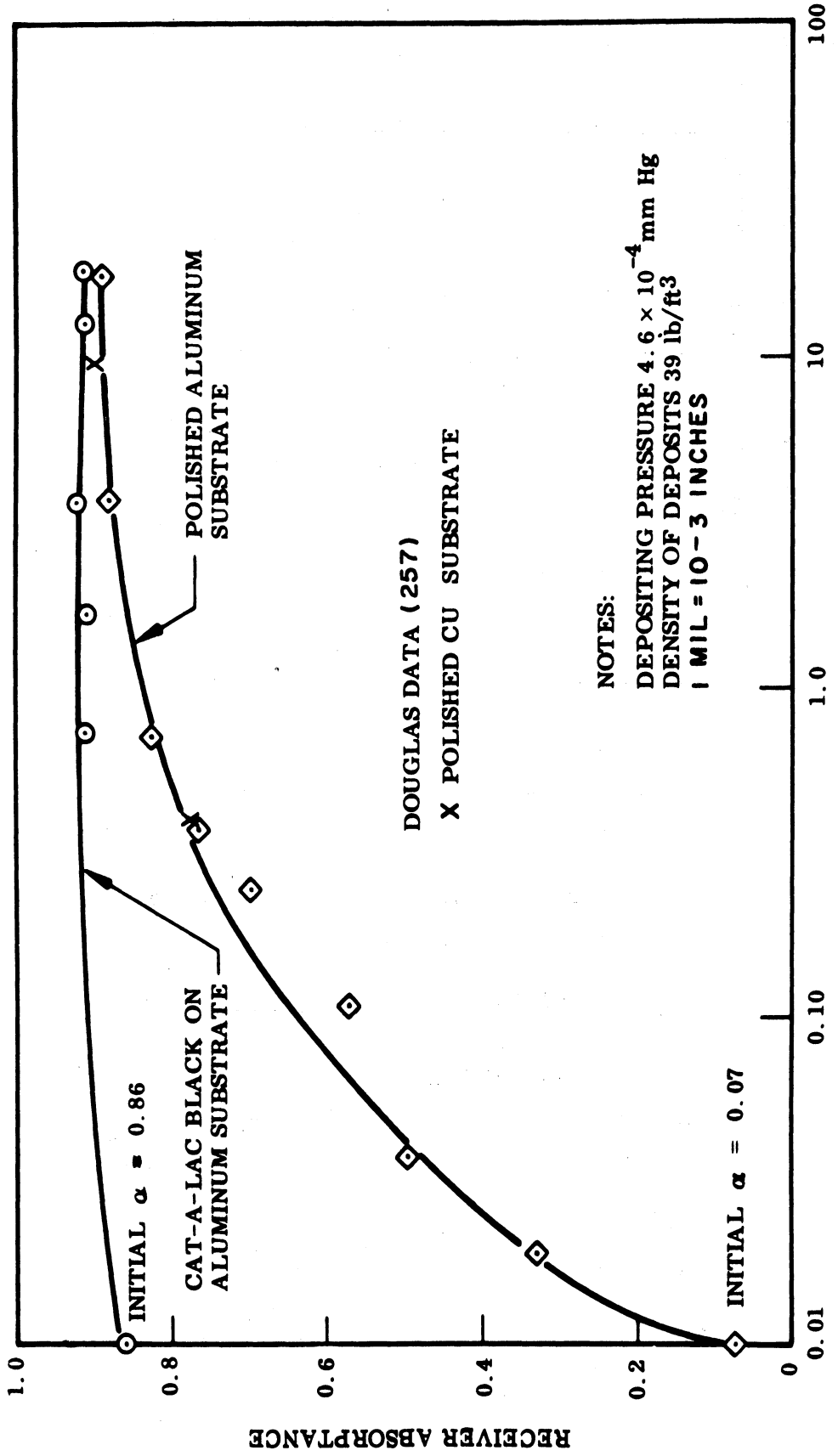

Fig.127 Absorptance of H_2O cryodeposit for room temperature blackbody radiation.(256)

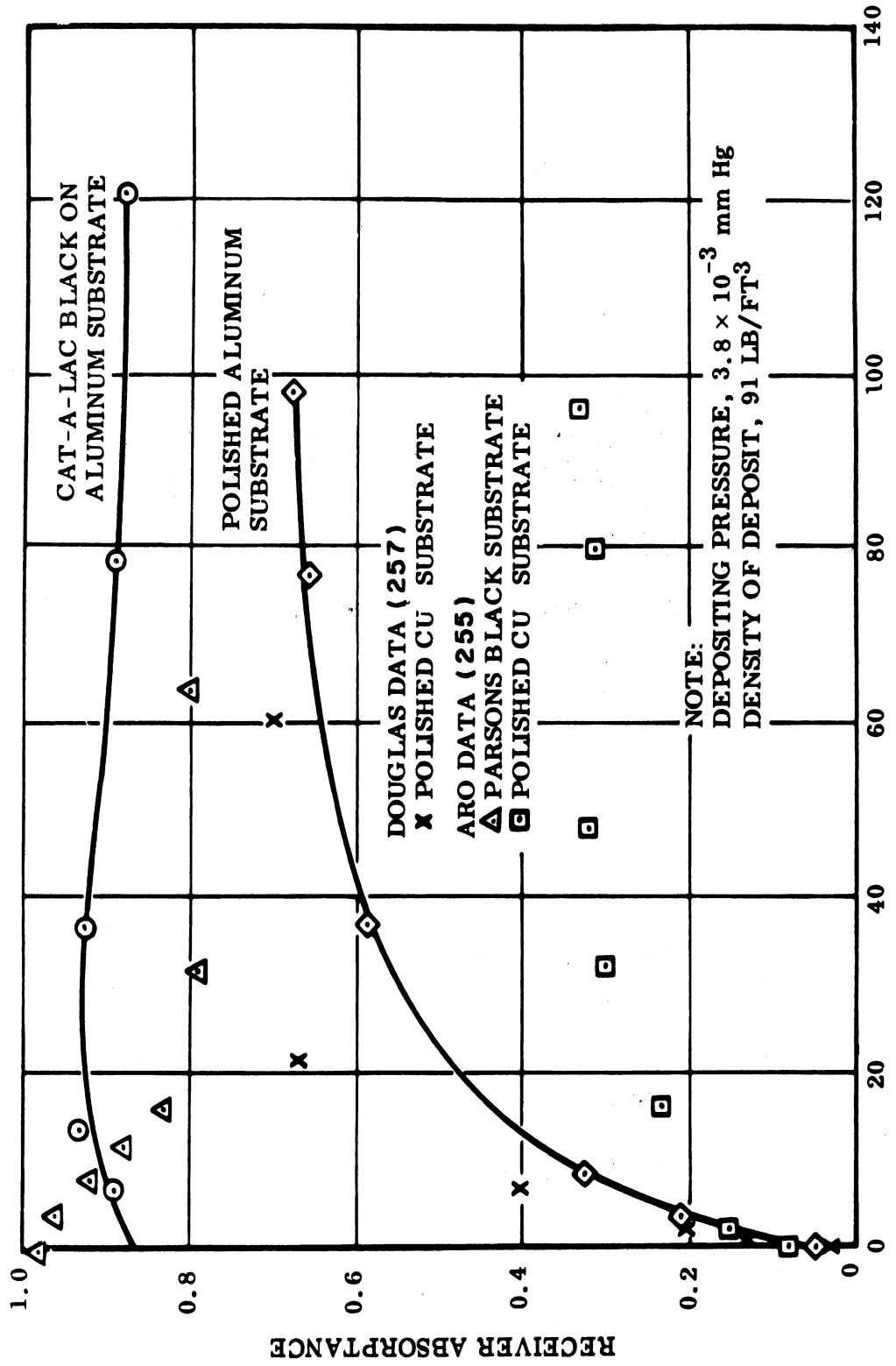

FIGURE 128. ABSORPTANCE OF CO_2 CRYODEPOSIT FOR ROOM TEMPERATURE BLACKBODY RADIATION.(256)

This variation is attributed to differences in the physical nature of the deposits.

A solar source was simulated by using filtered radiation from a Mercury-Xenon lamp. The absorptance of an H_2O cryodeposit under these conditions is shown in Figure 129. In this case the absorptance decreases with deposit thickness for an essentially black substrate.

An analysis of the thermal transport processes in a cryodeposit subject to radiation at the vacuum interface is given by McConnell (258). His results compare favorably with the experimental measurements of Caren, et al (256) for H_2O on a reflecting substrate. Tien and Cravalho (259) survey recent advances in the study of the thermal radiation properties of solids at cryogenic temperatures. For radiative transport between solids they discuss the influence or non-gray surfaces (wave length and temperature dependent properties), non-equilibrium fields and the effect of small surface spacing, a factor of particular significance at cryogenic temperatures. This latter is important because of the concentration of low temperature thermal radiation at long wavelengths. Theoretical studies are needed to provide calculation procedures for the transport of radiation between surfaces whose spacing is of the same order or less than the wavelength at the maximum radiative heat flux.

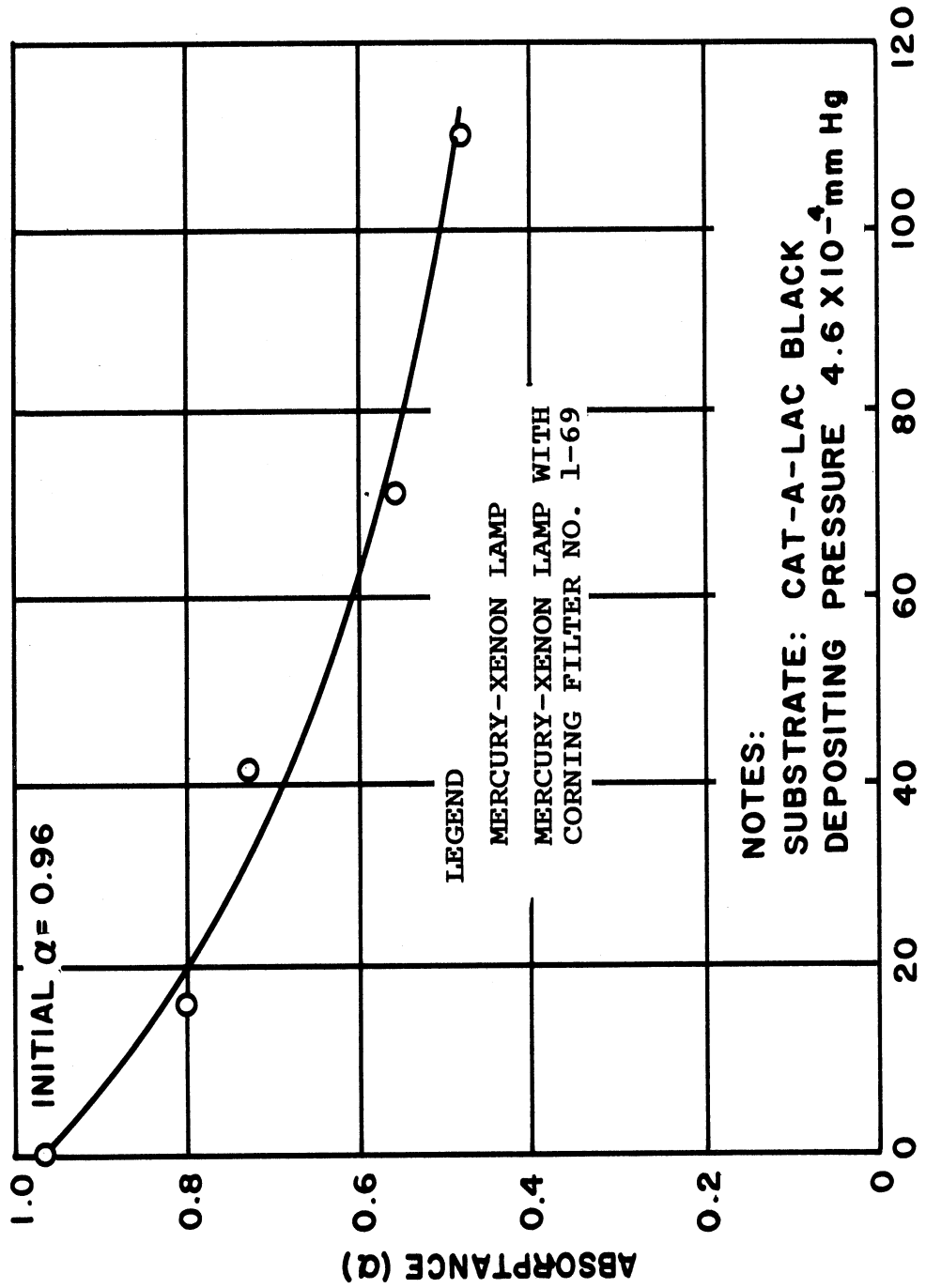

FIGURE 129. ABSORPTANCE OF H_2O CRYODEPOSIT FOR SIMULATED SOLAR ENERGY.(256)

IX. HELIUM II

Helium is unique among the various substances in that it has two known and distinctly different liquid phases. These are indicated in the phase diagram for helium in Figure 130. The liquid phase which exists in the temperature range from about 2.19°K to the critical point at 5.2°K behaves in a classical manner as do ordinary substances and the gaseous phase of helium. However, at temperature below approximately 2.19°K liquid helium undergoes a remarkable transformation. Within a fraction of a degree below 2.19°K the heat conducting ability of the liquid increases in an astonishing manner by a factor of 10^7, as was indicated in Figure 2 and Table II. Also, its heat capacity increases by about a factor of 6 in this temperature region as was shown in Figure 3. Because of these characteristics this phase of the liquid is identified as helium II and sometimes called a "superfluid". The classical liquid phase is known as helium I. An interesting and potentially significant aspect of helium II from a technological view point is the fact that it remains as a liquid down to the lowest attainable temperatures and presumably to the absolute zero as well. This property will enable the fluid to be employed conveniently as a coolant or as a transfer medium for equipment and components designed to operate below 1°K. At the present there are few such applications but they may be expected to increase in the future. Helium II may also be solidified if it is subjected to a sufficiently high pressure. The shape of the heat capacity curve has given the name "Lambda" to the line of transition between helium I and helium II.

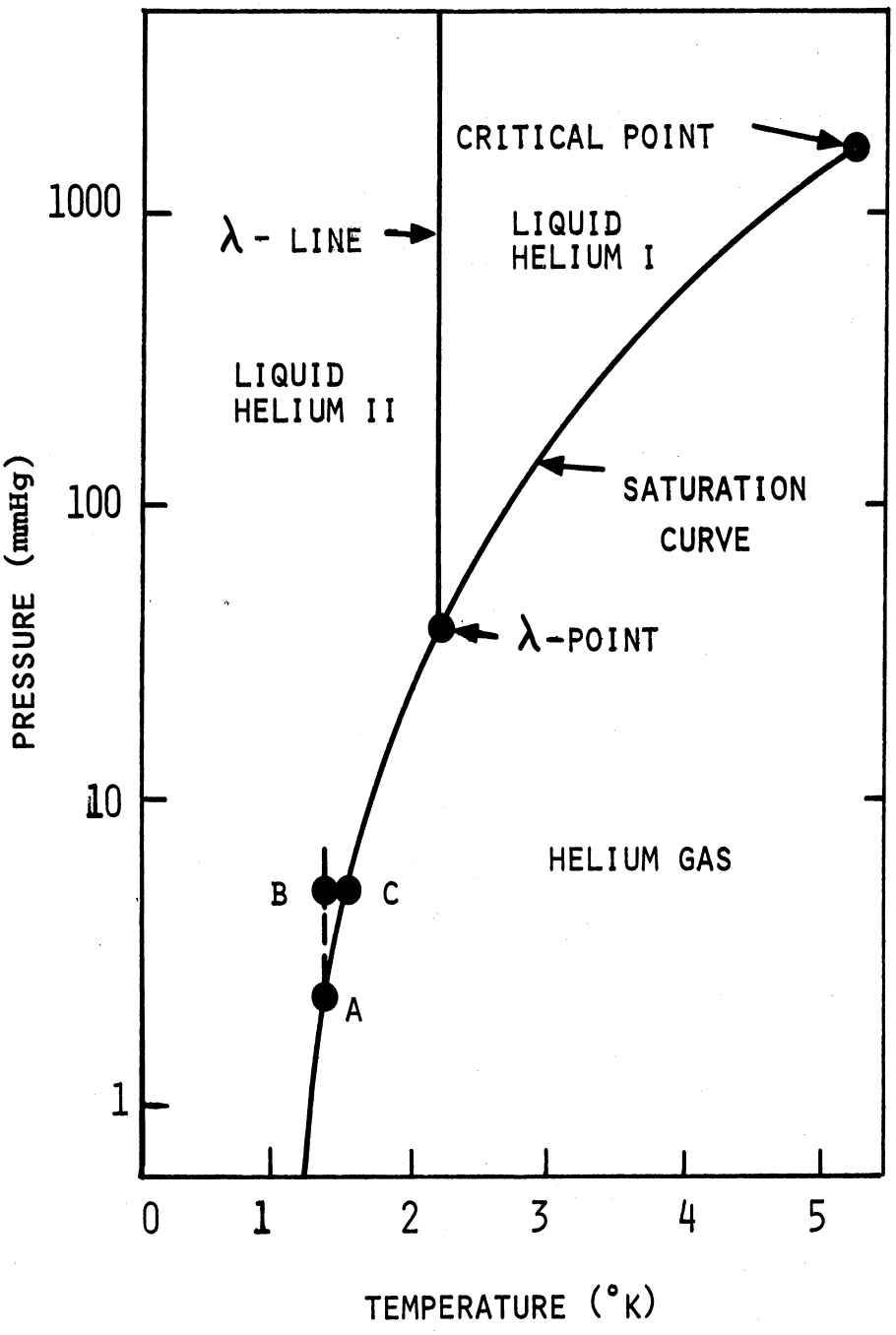

FIGURE 130. PHASE DIAGRAM FOR HELIUM.(261)

The properties of the "superfluid" helium II have long been of great interest to physicists. Much of the known results have been summarized by Lane[22] and Matheson[262] describes a symposium held on this substance consisting of 24 papers treating several aspects of the subject. Some of the extraordinary behavior of helium II, described by Lane, include its superfluidity, the mechano-caloric effect and thermo-mechanical effect, sometimes known also as the fountain effect. In order to explain these observed phenomena, helium II was postulated to be made up of two fluids. One fluid, known as the "superfluid", is without viscosity, entropy or heat capacity while the second fluid has all the properties of a normal substance. It is called the "normal fluid". These two fluids mix in all proportions with helium II consisting of all normal fluid at the λ-point and all superfluid at the absolute zero. These assumptions are largely unproved but they have helped to "explain" certain observed behavior of He II. Obviously, this substance presents a challenge which requires a departure from classical concepts to obtain a quantitative description of its properties.

One of these properties is its extremely great heat conducting ability. The definition of a "thermal conductivity" for He II, as was done in Figure 2, is principally a convenience for comparative purposes as He II does not follow the Fourier concept in the usual sense. If a thermal conductivity is computed for this substance it will be found to be highly temperature sensitive, be a function of the thermodynamic state and be influenced by the geometry and temperature gradient in its system.[263] Another factor in this is the fact that thermal transport ("conduction") in an apparently "stagnant" (zero net mass flow) He II is not a consequence of a strictly diffusive process.

Because of the presence of the superfluid within the mass of He II powerful convective flows are established by the temperature differential. The large apparent thermal conductivity is a result of these internal flows. Nevertheless, there is useful value in formulating the thermal conduction characteristic in terms of an apparent thermal conductivity.

In a presentation of a review of this subject Clement and Frederking[264] give the following expression for the apparent thermal conductivity of He II,

$$k_{App} = C(T)T\,\mu_n^{1/3}\,\rho^{2/3}\,S^{4/3}\left(\frac{\Delta T}{L}\right)^{-2/3}, \qquad (168)$$

where μ_n is the absolute viscosity of the normal fluid, ρ is the total fluid density, S is the liquid entropy per unit mass and $C(T)$ is a function of temperature and shown in Figure 131. The combined property function,

$$k_{App}\left(\frac{\Delta T}{L}\right)^{2/3} = C(T)T\,\mu_n^{1/3}\,\rho^{2/3}\,S^{4/3}, \qquad (169)$$

is shown in Figure 132 and the corresponding values of k_{App} for various values of $(\Delta T/L)$ is given in Figure 133, both taken from Clement and Frederking.[265] The effectiveness of He II as a "conductor" may be seen from Figure 133. The maximum value of k_{App} shown is about 500 watts/cm-°K which may be compared with the thermal conductivity of room temperature copper, Figure 4, which is about 4 watts/cm-°K. For lower values of $(\Delta T/L)$ the k_{App} of He II is even greater. Of particular interest is maximum in the property group $C(T)T\,\mu_n^{1/3}\,\rho^{2/3}\,S^{4/3}$ at approximately 1.9°K as shown in Figure 132 and the rapid reduction in

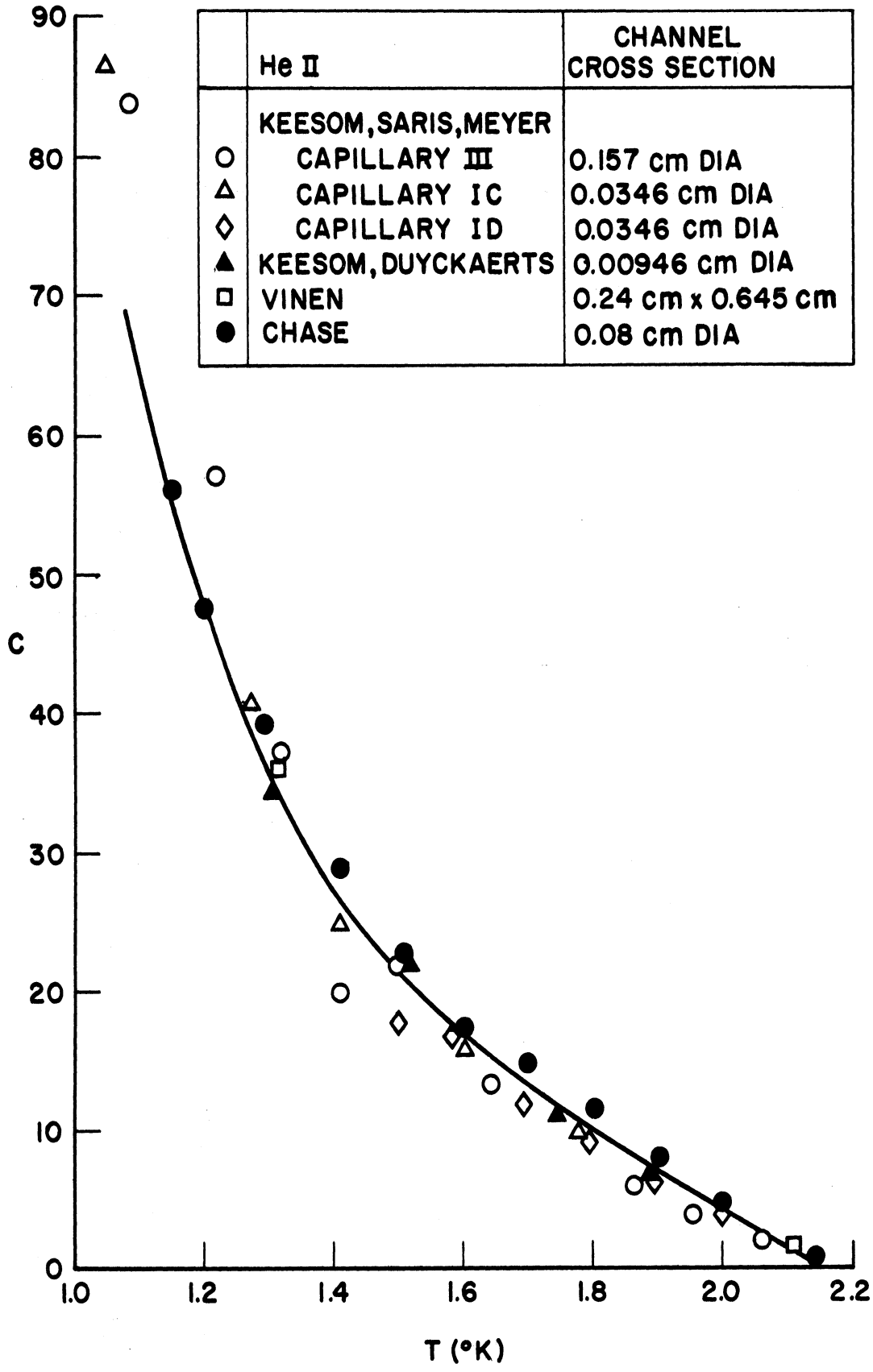

DIMENSIONLESS PARAMETER C(T) FOR SUPERCRITICAL HEAT TRANSPORT IN TUBES AT ZERO MASS FLOW (264)

FIGURE 131

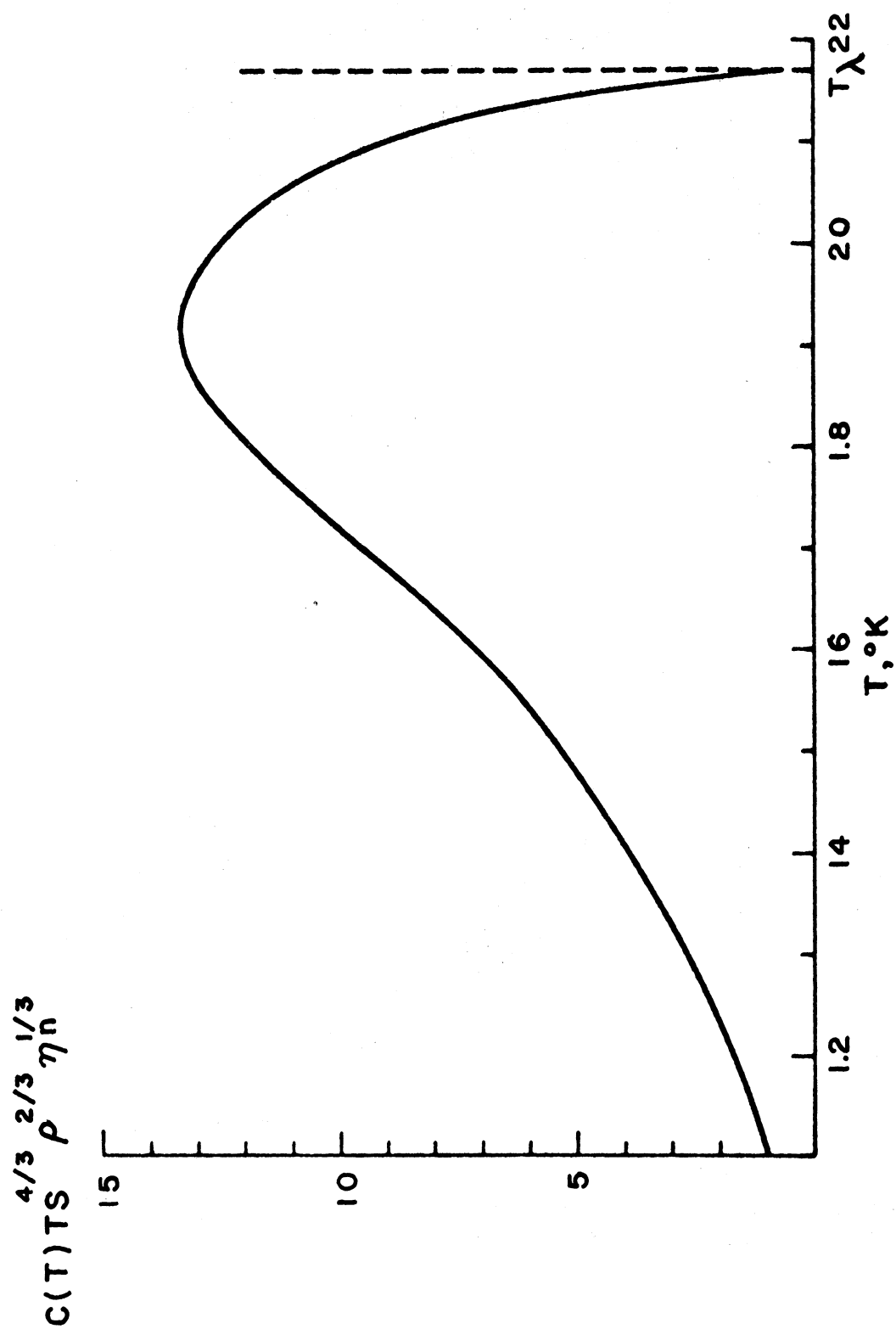

FIGURE 132. PROPERTY FUNCTION $C(T)\ TS^{4/3}\ \rho^{2/3}\ \eta_n^{1/3}$ VS. TEMPERATURE.[265]

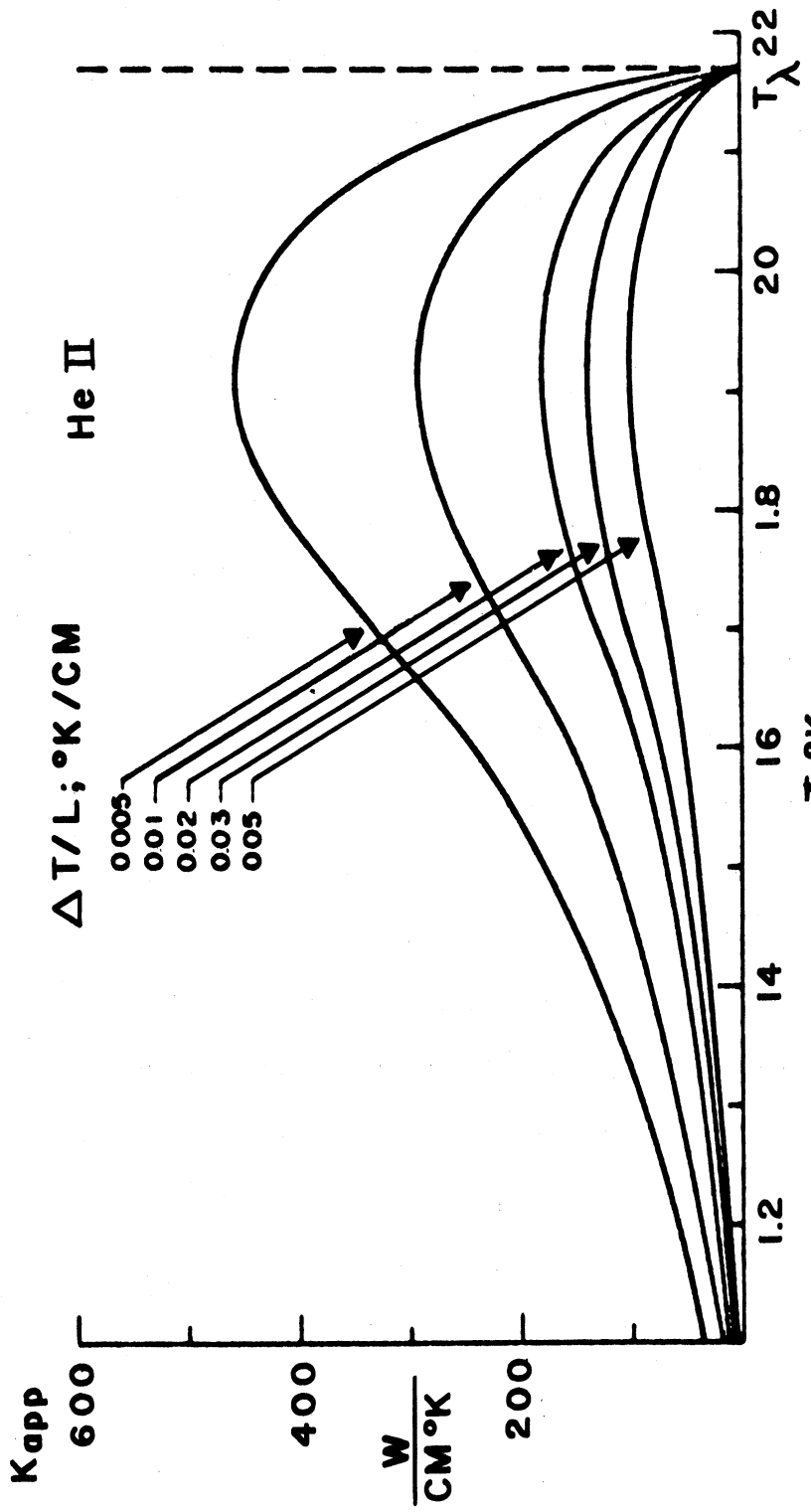

FIGURE 133. APPARENT THERMAL CONDUCTIVITY k_{app} OF He II AS A FUNCTION OF LIQUID TEMPERATURE FOR CONSTANT TEMPERATURE GRADIENTS.(265)

k_{App} as the liquid temperature is either increased to the λ-point or reduced toward the absolute zero. This is a consequence of the liquid becoming completely a normal fluid at the λ-point with the thermal conductivity of liquid He I, and completely a superfluid, but with no heat conducting ability, at 0°K. Because of the large magnitude of k_{App} He II can sustain only very small temperature differentials. Thus, even during large rates of thermal transport the temperature of He II appears uniform.

There is, however, another effect which becomes of importance under these circumstances and has a primary influence on the transport of heat from a solid surface to He II. This is a boundary resistance known as the Kapitza resistance after its discoverer.(266) At low heat flux rates to liquid He II Kapitza observed what appeared to be a temperature discontinuity between the surface and the liquid. It is possible this is an effect to be found with many other fluid-solid systems as well but owing to the large apparent conductivity of He II the temperature discontinuity is more evident in this case. The existence of this phenomenon is supported by theoretical considerations of Khalatnikov(267) who assumed a radiative transport and showed the Kapitza effect to depend on T^3 and the acoustic and elastic properties of both the solid and the liquid. The temperature difference under these circumstances may be expressed in terms of a contact heat transfer coefficient (the reciprocal of a resistance) as

$$h = \frac{(q/A)}{\Delta T} \quad . \tag{170}$$

A limiting value to this coefficient, h_o, corresponding to ΔT equal to zero, may be shown to be written(264)

$$h_o = 4 \sigma_K T^3 , \tag{171}$$

and for larger ΔT but under the restraint that $\Delta T < T$, the coefficient h may be formulated in terms of h_o as[264]

$$\frac{h}{h_o} = f\left(\frac{\Delta T}{T}\right) = 1 + \frac{3}{2}\left(\frac{\Delta T}{T}\right) + \left(\frac{\Delta T}{T}\right)^2 + \frac{1}{4}\left(\frac{\Delta T}{T}\right)^3 . \tag{172}$$

In Equation (171), σ_K is a parameter which depends on the particular properties of the solid and liquid. In most cases it is necessary to determine σ_K empirically as the theory of Khalatnikov, while correctly predicting a solid-fluid property dependence, does not predict its observed magnitude.[268] The temperature dependence is reasonably borne out by experiments with measured exponents ranging between 2.6 and 4.2. Thus, Equation (172) may be written

$$h = 4 \sigma_K T^3 f\left(\frac{\Delta T}{T}\right) , \tag{173}$$

and the corresponding heat flux, $(q/A)_K$, in the range where the Kapitza resistance is controlling becomes

$$(q/A)_K = 4 \sigma_K T^3 \Delta T f\left(\frac{\Delta T}{T}\right) . \tag{174}$$

For a Pt - He II interface Kapitza's data[266] for $\Delta T \ll T$ may be expressed as[264]

$$h_o = 0.065 T^3 , \tag{175}$$*

* The units are watts/cm -°K and T is °K.

and,

$$(q/A)_{K,Pt} = 0.065\ T^3\ \Delta T\ f\left(\frac{\Delta T}{T}\right) . \qquad (176)^*$$

These general types of relationships have been confirmed in several experiments. Clement and Frederking[264] have studied the heat transfer from a silver surface to helium II in a short tube and for conditions of $\Delta T < T$ find that $(q/A)_{K,Ag}$ may be expressed as

$$(q/A)_{K,Ag} = 0.082\ T^3\ \Delta T\ f\left(\frac{\Delta T}{T}\right), \quad \text{watts/cm}^2 \qquad (177)$$

Their data are shown in Figure 134. Agreement between Equation (177) and the data, especially for low values of $\Delta T/T$ is very good. A correlation of the measured (q/A) and that computed by the T^3-relation, Equation (177), is given in Figure 135. The comparison is favorable for low ΔT but a departure is observed at higher ΔT. It seems probable the reason for this is that at higher ΔT the surface temperature exceeds the λ-point temperature and He II no longer is in contact with the solid. This would have the effect of introducing a thin, very low conducting film of helium I between the solid surface and the helium II in the liquid bulk. If this is the case then the measured (q/A) would fall below that predicted by the Kapitza-type theory, which is what is observed. At much larger ΔT a vapor film of He I would be expected to form at the surface. Under these circumstances it is possible that two films, one of He I vapor and the second of He I liquid, could co-exist in a helium II system in film boiling

* The units are watts/cm^2 and both T and ΔT are °K.

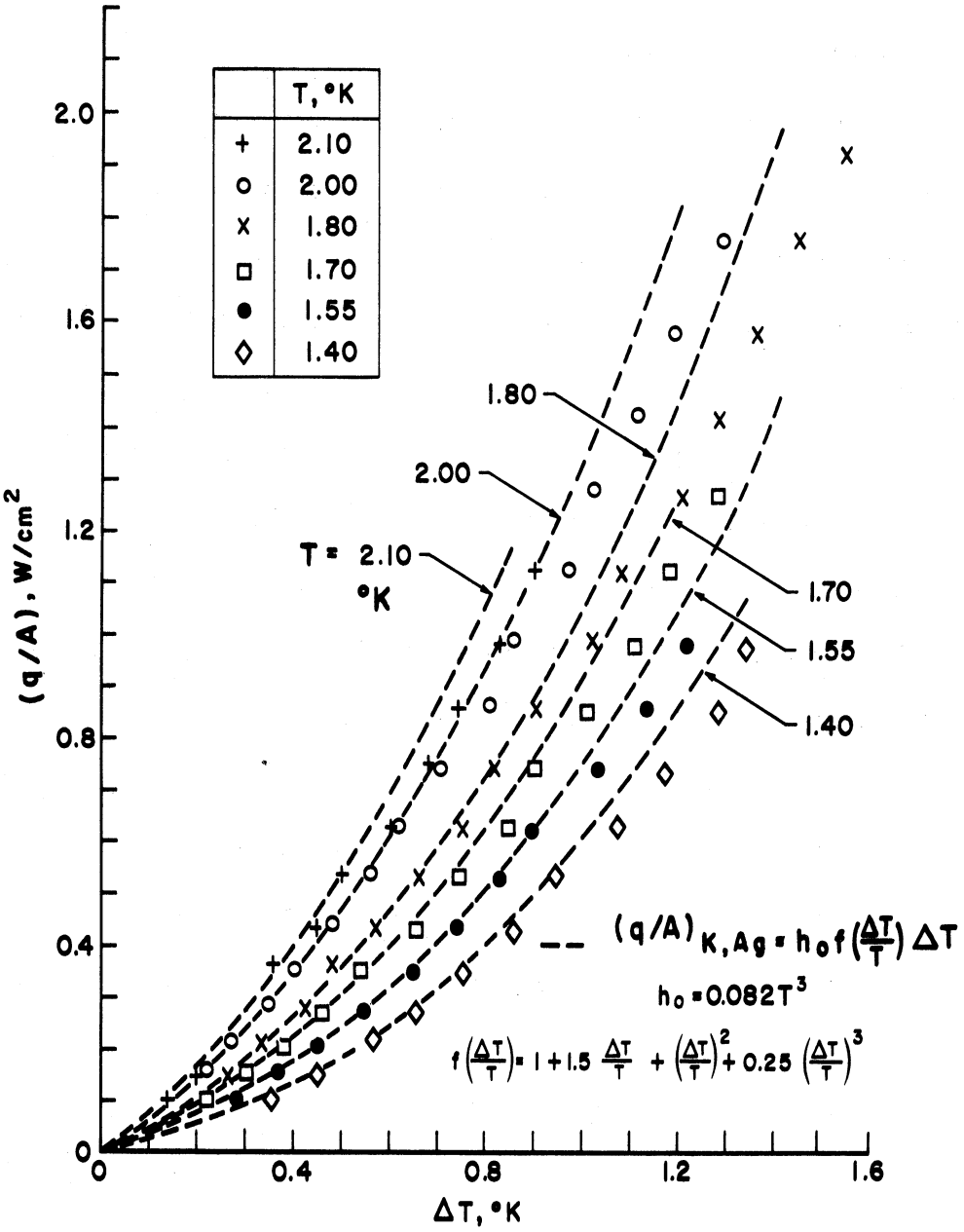

FIGURE 134. COMPARISON OF EXPERIMENTAL HEAT FLOW DENSITY q/A WITH SEMIEMPIRICAL CORRELATION $(q/A)_{K,Ag} = 0.082\ f\Delta T\ T^3$.

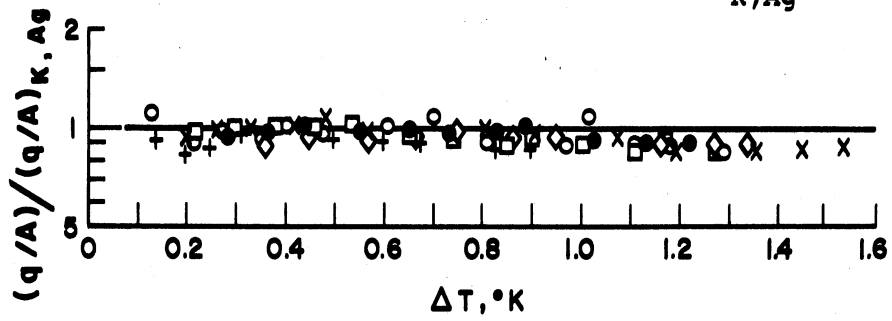

FIGURE 135. RATIO $(q/A)/(q/A)_{K,Ag}$ FOR DATA OF FIGURE 134.

for pressures above that of the λ-point. In this circumstance the temperature discontinuity would probably be shifted to the liquid He I - liquid He II interface.

Thus, for computing heat transfer rates to liquid He II a T^3-relationship of the form of Equation (174) can be employed in which the constant σ_K must be determined for each solid-liquid combination. As a guideline this relationship may be used for ΔT up to the point at which the surface temperature exceeds the λ-point temperature of He II. For conditions of higher surface temperature a He II system goes into other modes of heat transfer. These could involve some vapor formation (boiling) of a He I film or a film boiling condition of He I vapor in contact with a bulk liquid of He II. Because of its large heat transport characteristic bubbles or nucleate boiling have never been observed in helium II. As a guide to engineering calculations in these regions it is probably best to use the available experimental data, most of which is for natural convection processes from small, laboratory type surfaces. Some of these data will be discussed later.

Further evidence of the T^3-relationship for low (q/A) and low ΔT is provided by Irey, et al.[269] and shown here in Figure 136. The test section for these data was a horizontal cylinder of soft-glass, 1.88 mm in diameter and heat transfer was by natural convection from the outside surface of the cylinder to a He II bath.* The data for this combination appear to fit the relationship $h = 0.139\ T^3$ very well. Clement and Frederking[264] have summarized the results of several investigators for heat transfer to liquid helium II from a number of

* In a later paper, Holdredge and McFadden[263] suggest that some of the data of Irey, et al.[269] are probably in error. These are data above the Kapitza range and below a ΔT of about 80°K and thus does not include those in Figure 136.

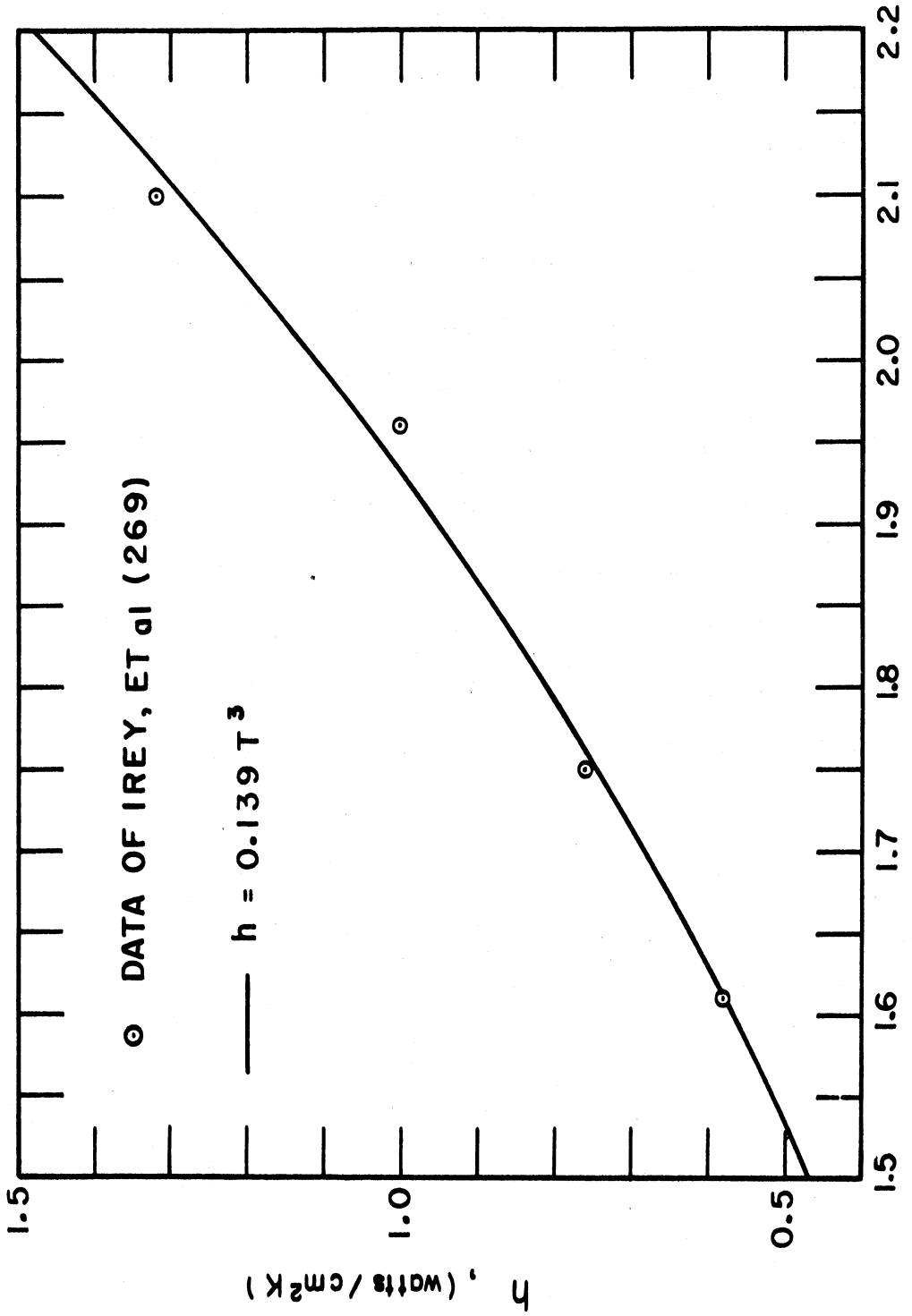

FIGURE 136. VALUES OF h AT SMALL TEMPERATURE DIFFERENCES.(269)

different surfaces for conditions in which the Kapitza effect controls the process. These results are given in Figure 137 where h_o is plotted against T^3. A linear relationship indicates an agreement with Equation (171). As may be seen a reasonable validation of this type of relationship is borne out by most of the data. A low value of h_o will produce the greater boundary ΔT for a given heat flux.

A comparison of natural convection heat transfer data from a 1.79 mm diameter soft-lead glass tube to saturated and unsaturated ("sub-cooled") liquid helium II with the Kapitza resistance theory of Khalatnikov[267] is given by Madsen and McFadden[268] and shown in Figure 138. Good agreement is found for the low ΔT range but as the temperature difference is increased there apparently is an additional thermal resistance being created in the system. Some possibilities as to what this might be were discussed above although the exact nature of this resistance is presently unknown. As may be seen from the data in Figure 138 Khalatnikov's theory is valid to larger ΔT's for a sub-cooled condition than with a saturated liquid. Holdredge and McFadden[263] studied the Kapitza resistance in a saturated He II system with a test section similar to that in Reference 269 in which the influence of depth of immersion was examined. Their results in comparison with the theory of Khalatnikov are given in Figure 139. It is apparent that immersion depth is not an important factor in the Kapitza effect. Since the influence of depth is to establish the pressure level at the test section these results suggest that no vapor phase of helium I exists at the heated surface in these low ΔT regions. An effect of test section size is unobserved as well in this range of ΔT. The

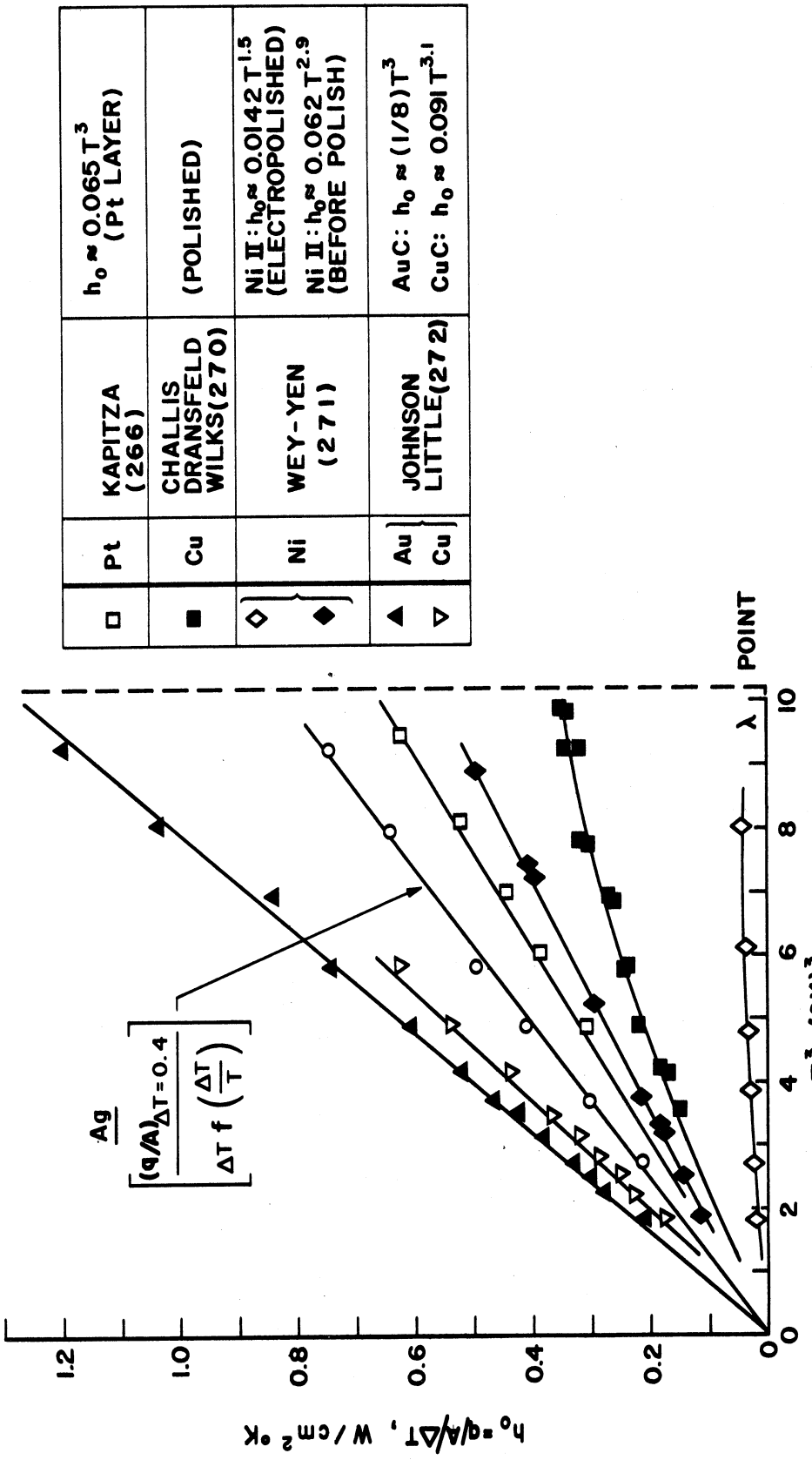

FIGURE 137. COMPARISON OF THE REDUCED HEAT TRANSFER COEFFICIENT WITH THE T^3-RELATIONSHIP FOR FACE-CENTERED CUBIC METALS.

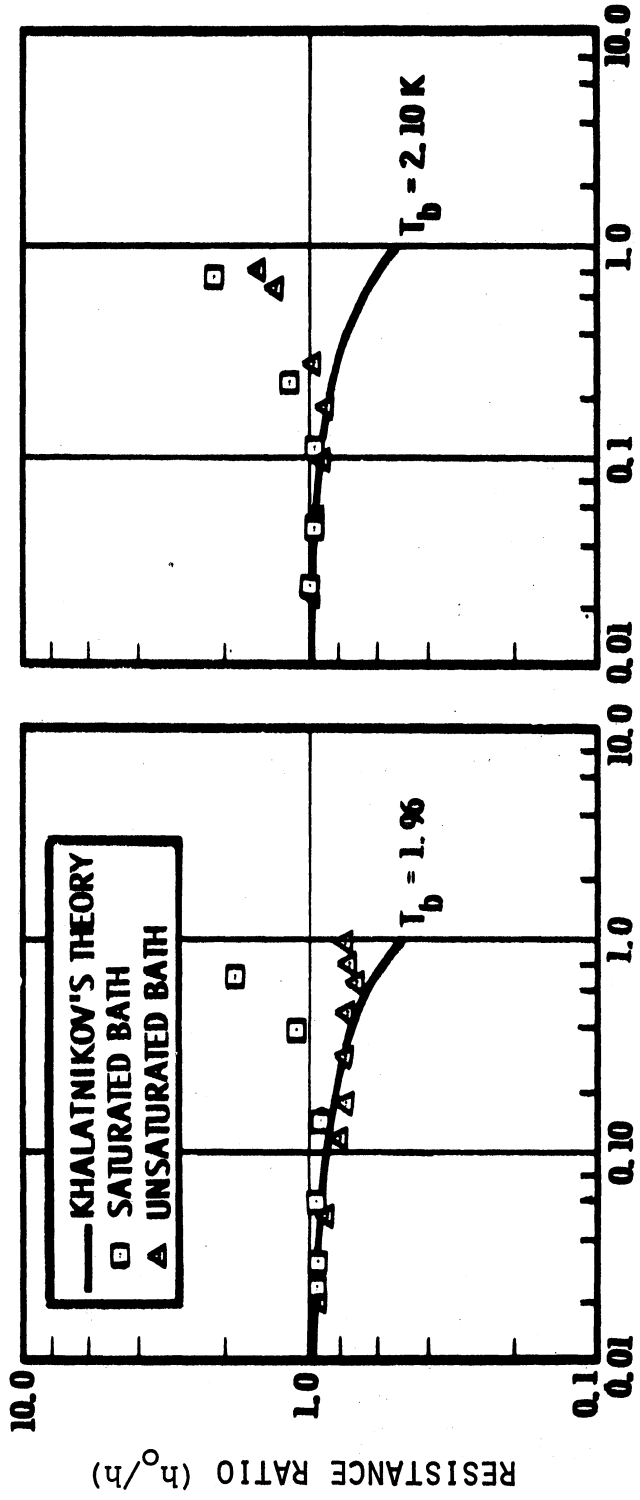

FIGURE 138. VARIATION OF THE KAPITZA RESISTANCE.(268)

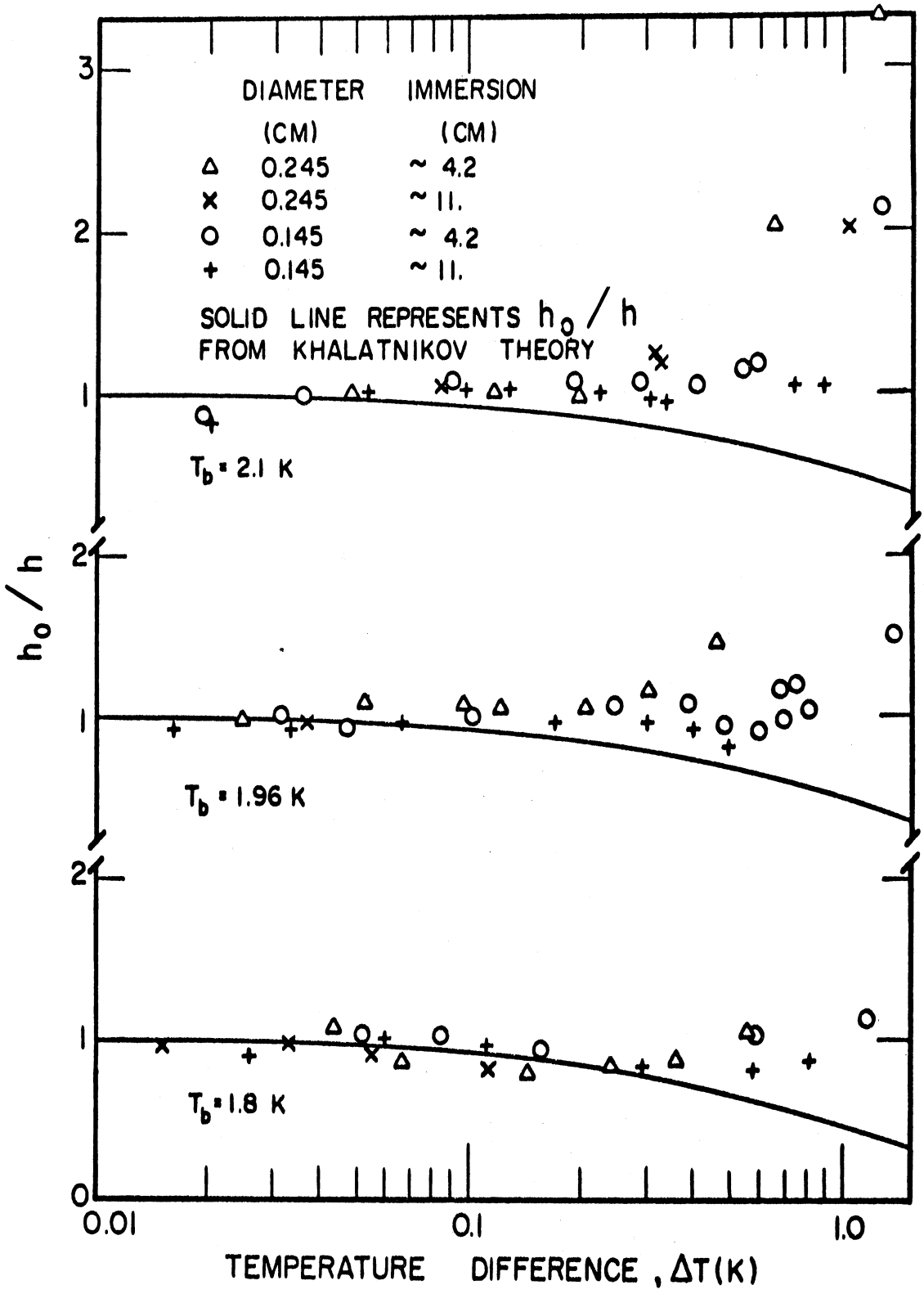

FIG. 139 COMPARISON OF EXPERIMENTAL AND THEORETICAL KAPITZA RESISTANCES (263)

experimental data seem to depart from the Khalatnikov theory at a ΔT of approximately 0.10°K.

Above the ΔT corresponding to the range of the predominance of the Kapitza effect heat is transferred to liquid helium II by a transport mechanism which is largely unknown. It is called non-film boiling but does not appear to be similar to nucleate boiling. Data for this heat transfer process are given in Figures 140 to 143 taken from Holdredge and McFadden[263] and Madsen and McFadden.[268] In each case the test section is a soft-glass cylinder horizontally oriented in a bath of helium II. The data in Figures 140 and 141 are for a saturated liquid with various bulk temperatures, depths and test section size. In these data an influence of size is observed at all bath temperatures suggesting a controlling effect of bouyant forces. Depth, or pressure, does not appear to be significant until fairly large ΔT are obtained. This is thought to be the point for the onset of film boiling and the appearance at the surface of the gaseous phase of helium I. The surface temperature increases with heat flux very significantly at this point and the phenomenon of a maximum heat flux is observed. The effect of "subcooling" on the nonfilm boiling, the maximum heat flux and the transition to film boiling are shown in Figures 142 and 143 for a test section 1.79 mm in diameter.[268] The maximum heat flux is in the range 2 - 4 watts/cm^2 which may be compared to a corresponding value of about 1 watt/cm^2 for helium I as shown in Figure 63 for a pressure of 1/2 atmosphere.

For a heat flux above a certain critical maximum the influence of the superfluid is destroyed, at least locally, in the vicinity of the heated surface. This critical maximum heat flux is similar to the

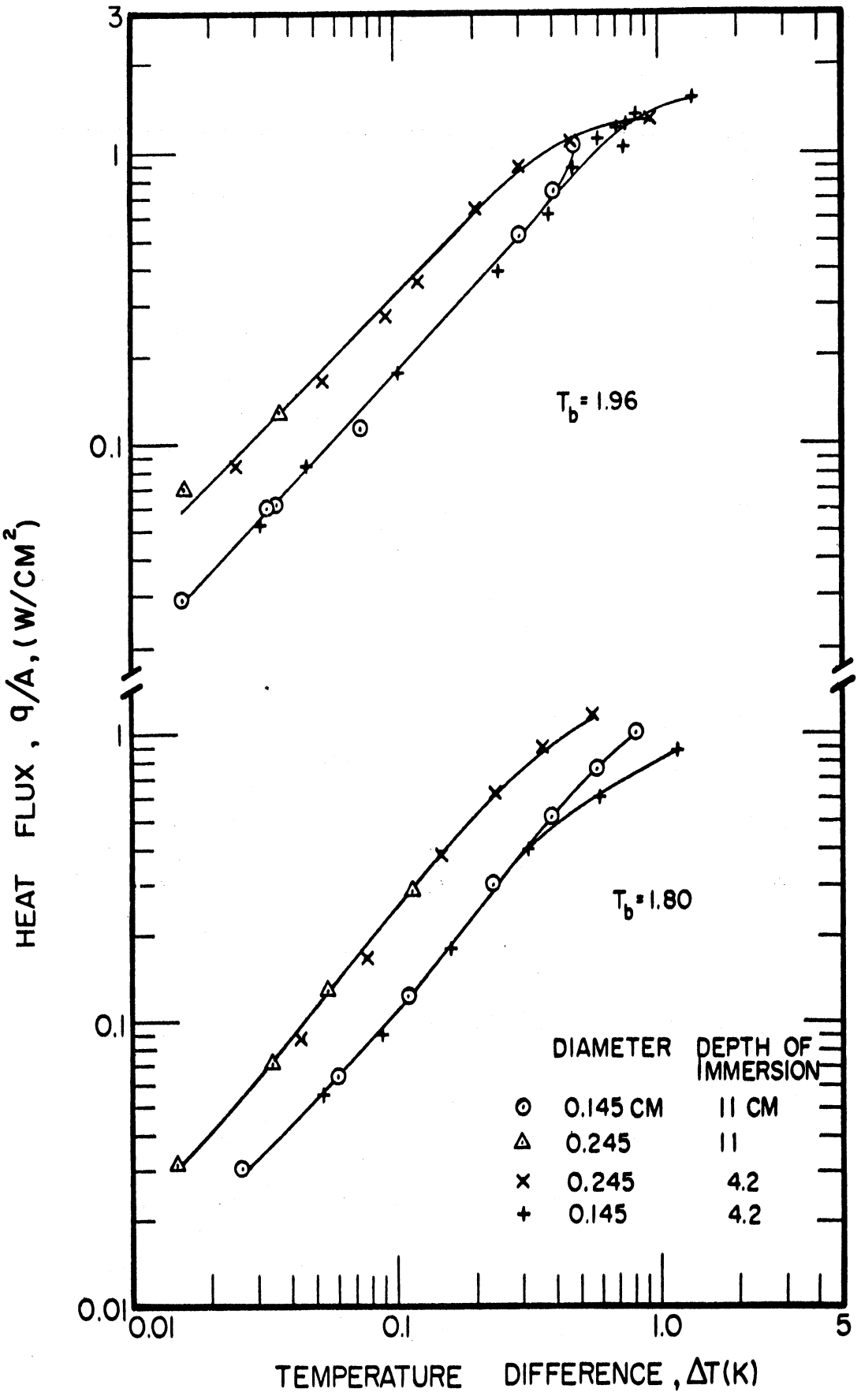

FIG. 140 NON-FILM BOILING HEAT FLUX AS A FUNCTION OF TEMPERATURE DIFFERENCE (263)

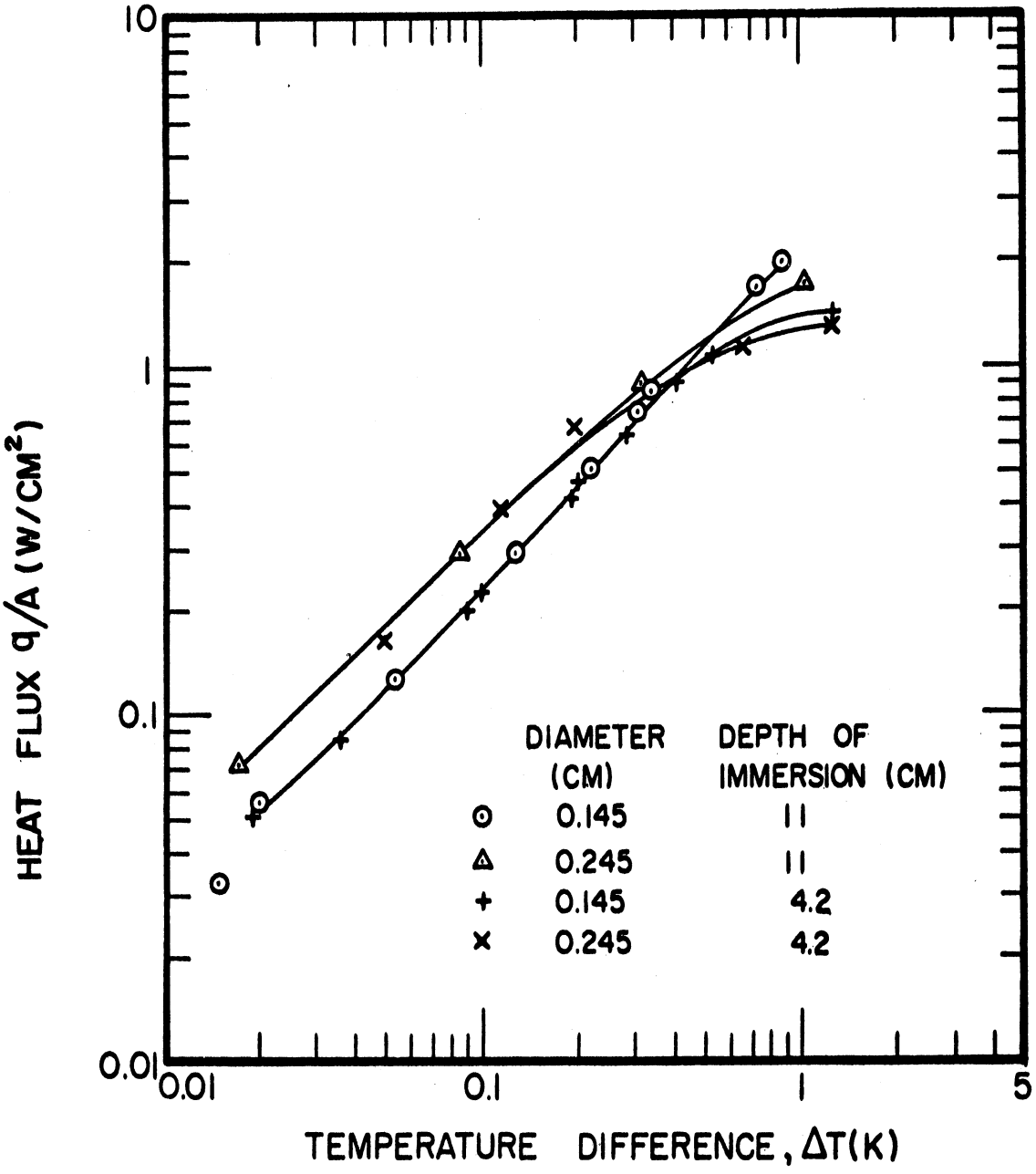

FIG. 141 NON-FILM BOILING HEAT FLUX AS A FUNCTION OF TEMPERATURE DIFFERENCE FOR A 2.1 K BATH (263)

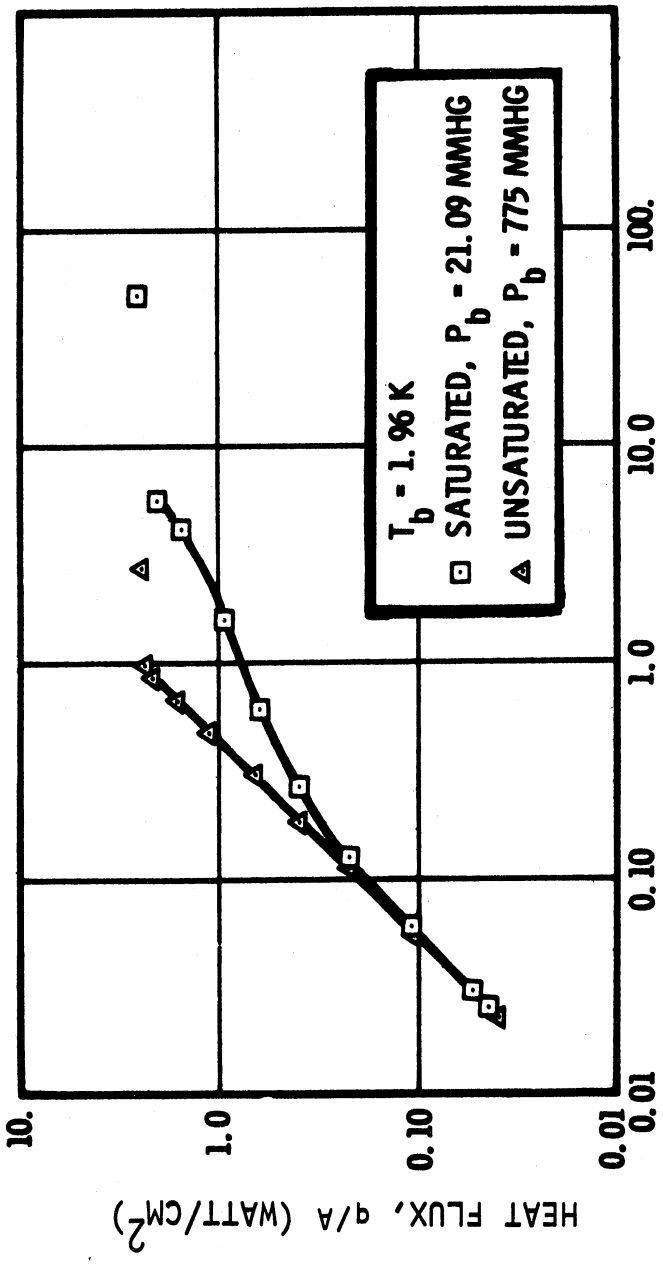

FIGURE 142. BOILING CURVES FOR A BATH TEMPERATURE OF 1.96 K.(268)

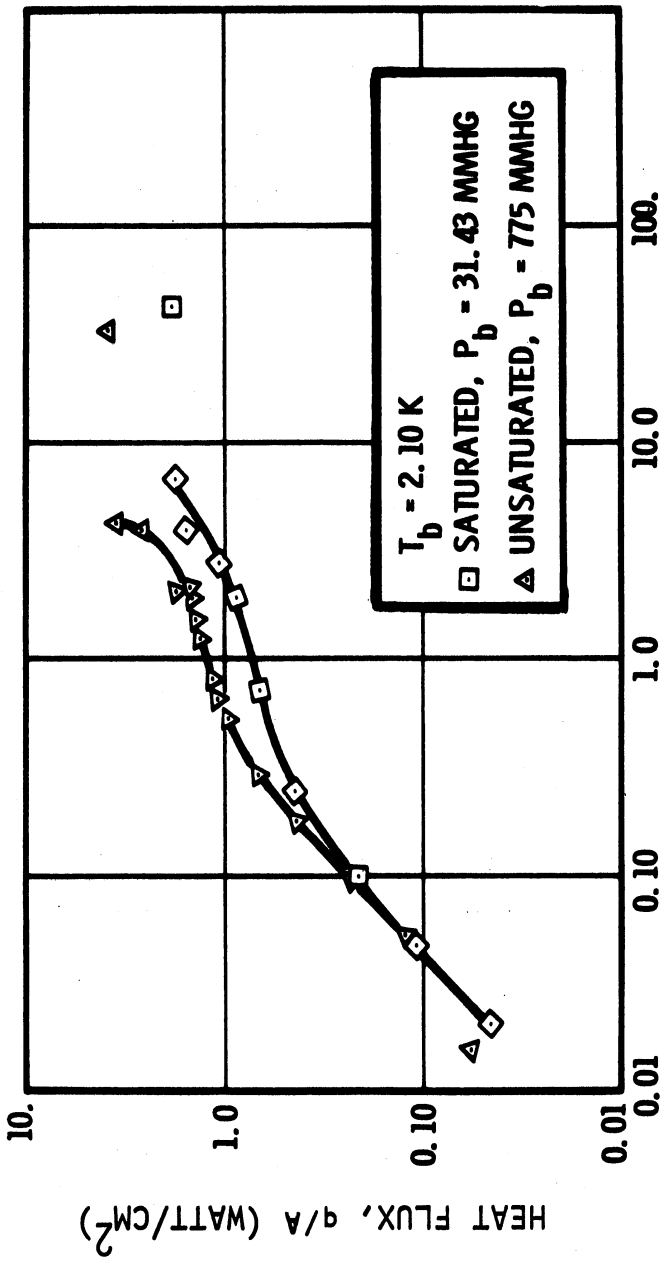

FIGURE 143. BOILING CURVES FOR A BATH TEMPERATURE OF 2.10K. (2b8)

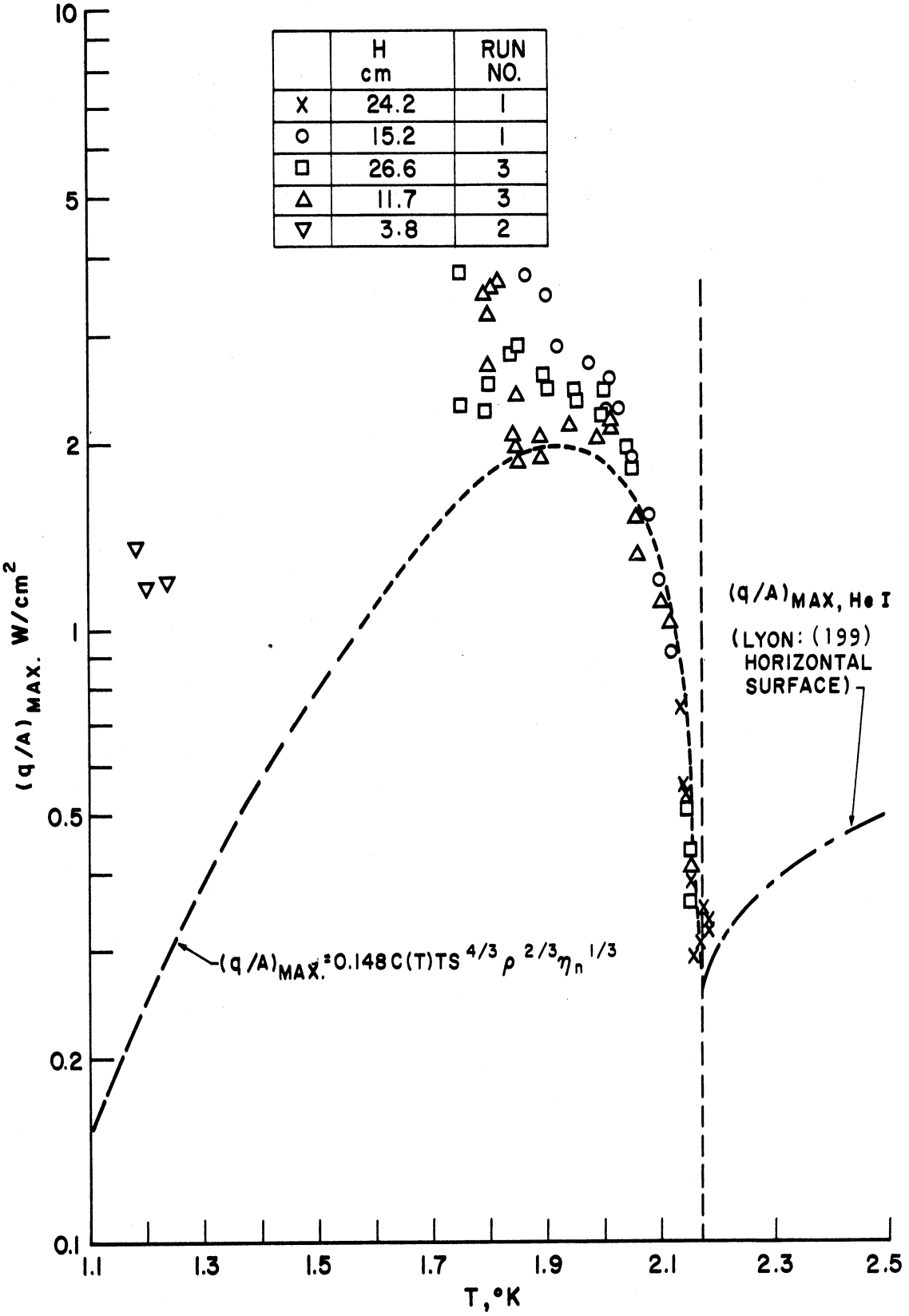

FIGURE 144. MAXIMUM HEAT FLUX AT VARIOUS DEPTHS OF IMMERSION VS. TEMPERATURE.(264)

maximum nucleate boiling heat flux but its mechanism is probably quite different. Clement and Frederking[264] investigated this phenomenon for heat transfer to He II from a horizontal surface through a short tube. In this study the transport processes were of a more bounded type than those cited above in which a test surface was totally surrounded by liquid helium II. The low heat flux-low ΔT data for this bounded system were discussed above and given in Figures 134, 135 and 137. The measured values of $(q/A)_{max}$ are given in Figure 144 for various liquid depths H of the test surface below the He II bath surface. There appears to be very little effect of liquid depth (pressure) on $(q/A)_{max}$. Owing to limitations of pump capacity the pressure was difficult to stabilize at the lower temperatures. In the vicinity of the λ-point, however, the data are very accurate. The magnitudes of $(q/A)_{max}$ are seen to increase from 0.10 watts/cm^2 at the λ-point to approximately 2 - 4 watts/cm^2 at about 1.9°K, the point or maximum apparent thermal conductivity for helium II. The results near the λ-point coincide very well with the low pressure maximum heat flux data of Lyon[199] for helium I. Clement and Frederking have fitted a curve to their data which follows the general characteristic of the heat flux corresponding to the apparent thermal conductivity of helium II. The equation, which fits the data well near the λ-point, is

$$(q/A)_{max} = 0.148\, C(T)T\, \mu_n^{1/3}\, \rho^{2/3}\, S^{4/3} . \qquad (178)$$

The influence of depth of immersion (pressure) on the temperature difference at the maximum heat flux is indicated to be completely

negligible in Figure 145. The temperature difference corresponding to the maximum heat flux is summarized in Figure 146 as a function of bath temperature. The accuracy is limited at the lower temperatures owing to restricted pumping capacities in the experimental apparatus. A lower bound to ΔT_{max} is shown in Figure 146 which is that ΔT from Equation (174), the Kapitza relationship, at which the corresponding heat flux, $(q/A)_K$, is equal to the maximum heat flux, $(q/A)_{max}$, from Equation (178). There is quite a bit of scatter in the data. It should be noted that these ΔT are about the same as those determined for the maximum heat flux in helium I as shown in Figure 63. Clement and Frederking[264] report $(q/A)_{max}$ values for helium II as high as 10 watts/cm^2 but do not give the specific data. Reference is probably made to the small wire data such as that of Frederking.[275]

Maximum heat flux data of the order of 10 watts/cm^2 for a horizontal platinum wire 15 μ diameter is reported by Rinderer and Haenseler[273] for liquid helium II at 1.4°K. The magnitude of $(q/A)_{max}$ was found to depend on liquid height above the test surface.

Lemieux and Leonard[274] investigated the maximum heat flux for a horizontal 76.2 μ diameter 90% platinum - 10% rhodium wire. Depths of immersion below the liquid-vapor interface ranged from 5 to 70 cm. In this way both the pressure at the heated surface and the heat flow path length were varied. A large influence of depth of immersion was found. Figure 147 shows the maximum heat flux data for a depth of 30 cm as a function of liquid bath temperature. Near the λ-point $(q/A)_{max}$ increases very rapidly with bulk temperature reaching a maximum at about 2.0°K. The maximum values are considerably greater

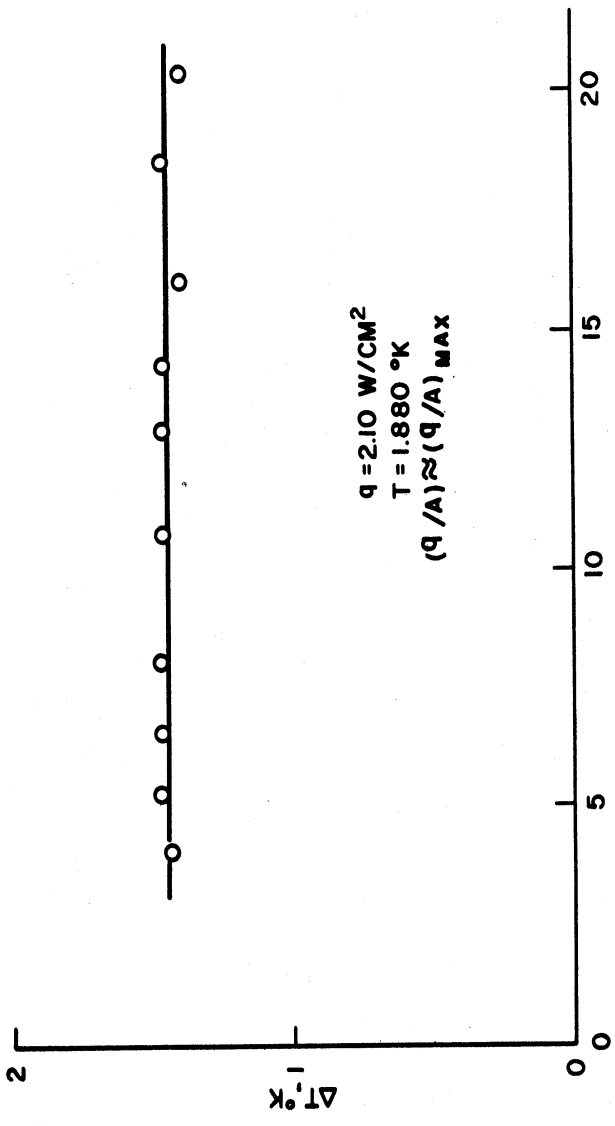

FIGURE 145. SOLID SURFACE EXCESS TEMPERATURE VS DEPTH OF IMMERSION IN THE VICINITY OF THE MAXIMUM HEAT FLUX.(264)

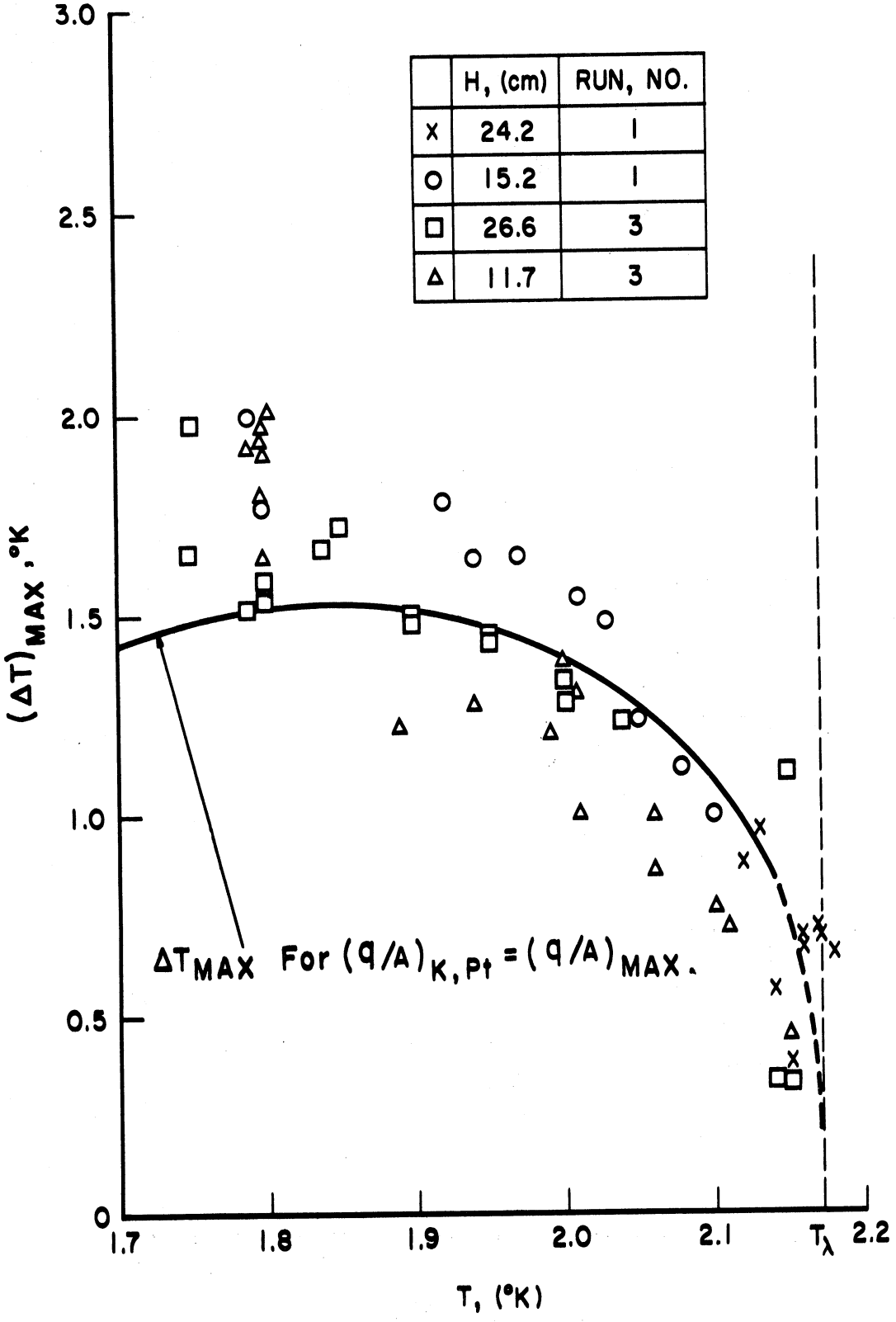

FIGURE 146. TEMPERATURE DIFFERENCES AT THE MAXIMUM HEAT FLUX AS A FUNCTION OF THE BATH TEMPERATURE.(264)

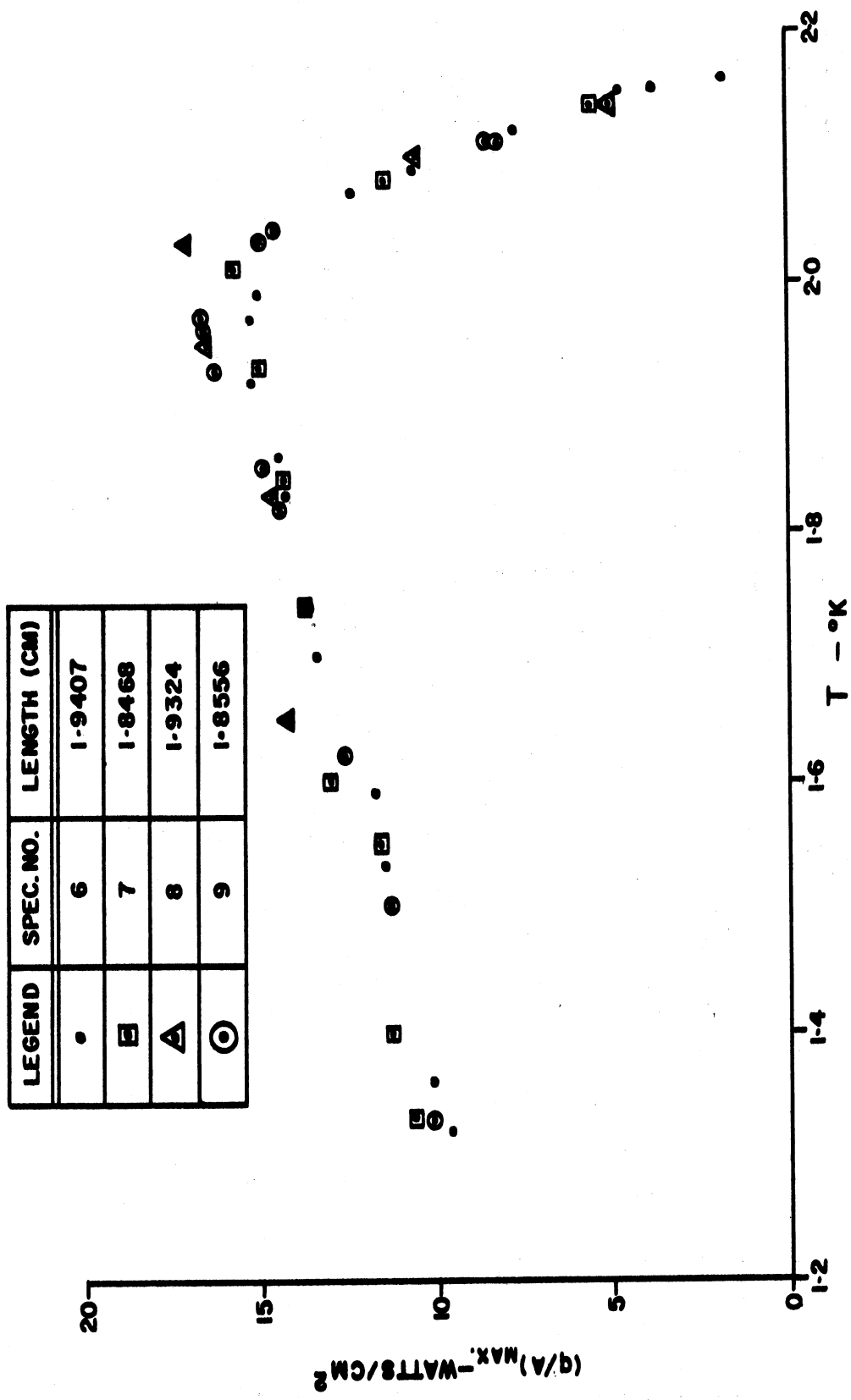

FIG. 147 MAXIMUM HEAT FLUX AS A FUNCTION OF BATH TEMPERATURE AT A DEPTH OF IMMERSION OF 30 CM (274)

for this small diameter wire than for the larger unbounded cylinders [263,268] and the flat (bounded) plate.[264] The smoothed data taken as a function of depth are given in Figure 148. The influence of depth vanishes at the λ-point. A comparison of the data of Lemieux and Leonard with those of others[263,275] as a function of depth is shown in Figure 149 for a bath temperature of 1.96°K. Agreement with the results of Frederking[275] for a 30 μ diameter wire is good. However, for the cylinder (D = 0.245 cm) of Holdredge and McFadden[263] there is no agreement. Apparently, there is a very significant diameter or size influence on $(q/A)_{max}$, perhaps similar to that observed in film boiling for small diameter cylinders by Breen and Westwater.[150]

Lemieux and Leonard[274] report that on reduction of heat flux from a film boiling condition a minimum heat flux is reached, less than $(q/A)_{max}$, at which the system no longer can support the vapor film. For lower heat flux the heat transport reverts to that of the superfluid. Some $(q/A)_{min}$ data are included in Figure 149.

At heat flux rates in excess of $(q/A)_{max}$ a helium II system goes over into film boiling controlled by ordinary fluid and thermal phenomena. Under these conditions the superfluidity effects are destroyed at the heated surface and are replaced with those circumstances which govern the natural convection of a vapor layer in film boiling.[265] The liquid helium II is lifted off the surface but becomes an effective heat sink for the vapor. Since the greater thermal resistance resides in the vapor film the unusually great heat transport ability of the superfluid is no longer effective in promoting heat transfer.

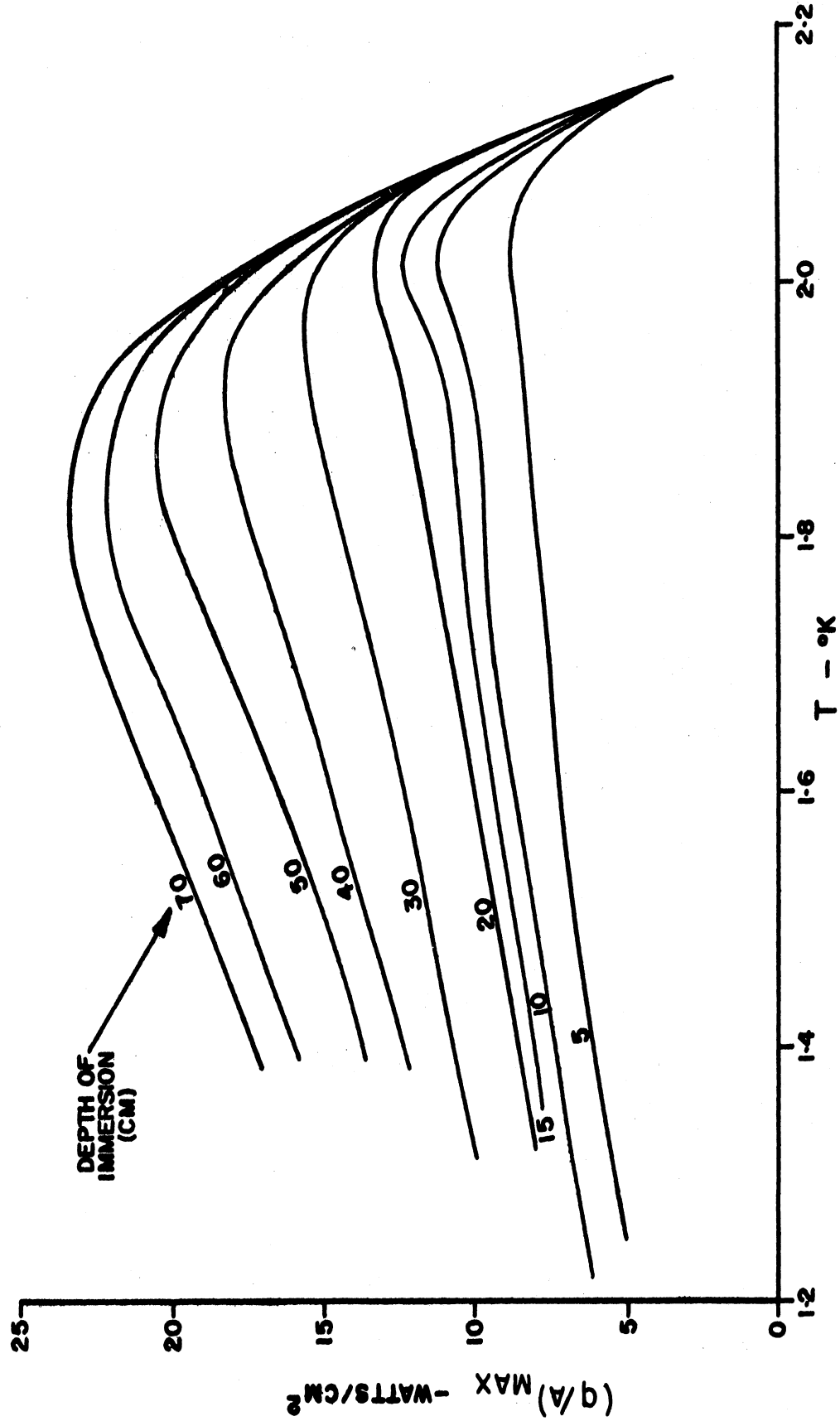

FIG. 148 MAXIMUM HEAT FLUX AS A FUNCTION OF BATH TEMPERATURE & DEPTH OF IMMERSION (274)

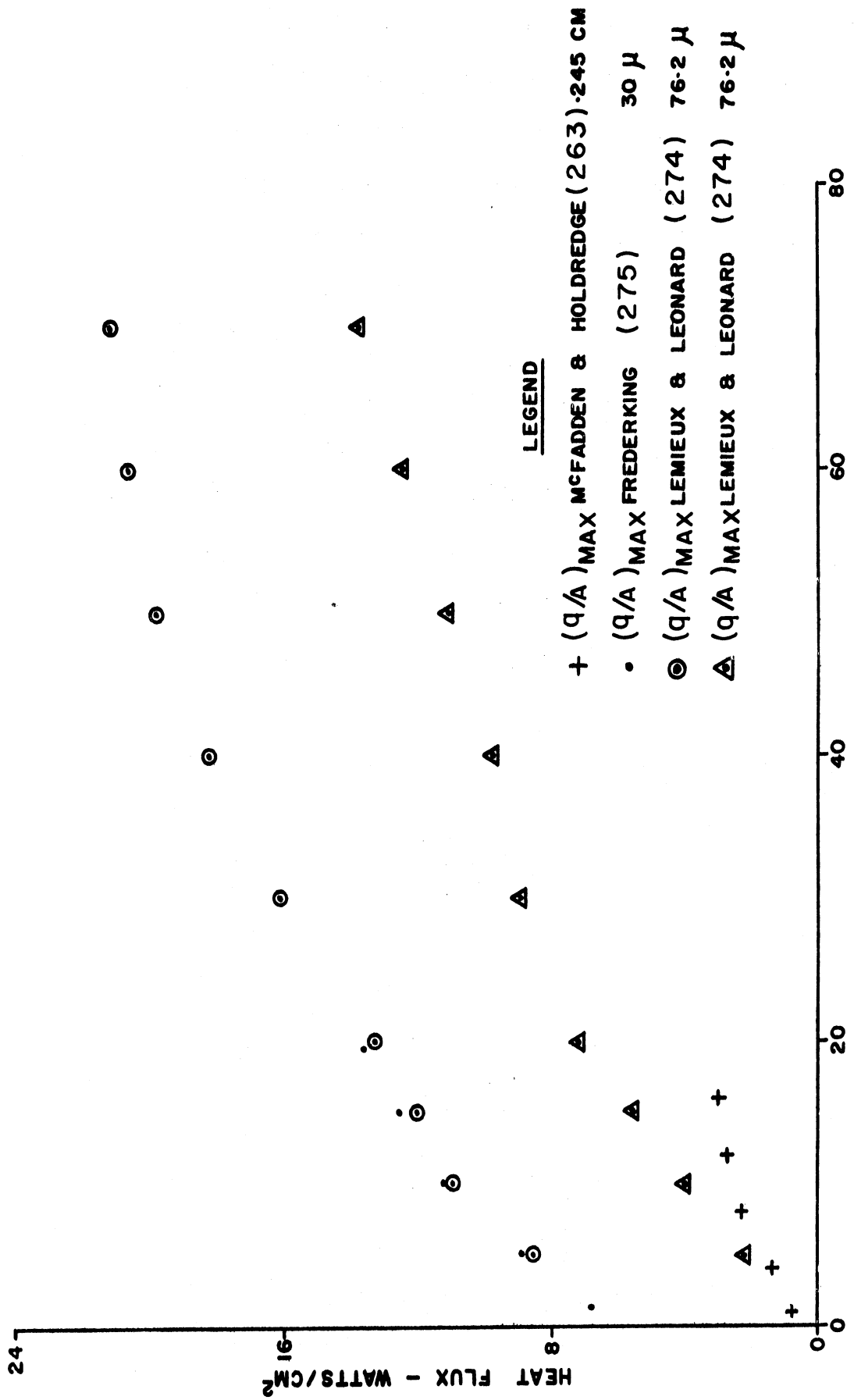

FIG. 149 HEAT FLUX VERSUS DEPTH OF IMMERSION (T = 1·96°K)

Rivers and McFadden[261] have analyzed the transport processes in laminar film boiling in liquid helium II for a flat plate and cylinder. Their results are given for both liquid and vapor films of helium I between the heated surface and the liquid helium II. The process is formulated in terms of the usual transport equations for laminar boundary layer flow but a temperature and velocity discontinuity is introduced at the film-helium II interface. The Nusselt number is determined in terms of the Grashof and Prandtl numbers and two parameters, the "interface enthalpy," H_i and the "interface heat flux," Q_b. The analytical results for the cylinder and flat plate are given in Figures 150 and 151 for films of liquid helium I (Pr = 0.4) and helium gas (Pr = 0.7). The following definitions are used

$$\overline{Nu} = \frac{\bar{h}D}{k_f} \quad , \tag{179}$$

where $D = r$ for a cylinder and L for a plate,

$$Gr = \frac{g\, D^3\, \rho_f\, (\rho_b - \rho_f)}{\mu_f^2} \, , \tag{180}$$

$$H_i = \frac{(\Delta h)_i}{c_{p_f}(\Delta T)_f} \quad , \tag{181}$$

where $(\Delta h)_i$ = enthalpy change at the He II interface, and

$$Q_b = \frac{D(q/A)_b}{k_f(\Delta T)_f} \quad , \tag{182}$$

in which $(q/A)_b$ is an "interface heat flux," a quantity required to compute Q_b but about which little is presently known. From these

results Rivers and McFadden identify three regions. For $Q_b\ Gr^{-1/4} < 0.01$, the heat transfer follows ordinary film boiling characteristics in which the Nusselt number is a function of the Grashof and Prandtl numbers and, of course, H_i. In this region the convective processes dominate. Above $Q_b\ Gr^{-1/4}$ of about 10, the process is described by the asympote $\overline{Nu} = Q_b$. Under these circumstances, the wall heat flux $(q/A)_w$ is identical with that at the interface, $(q/A)_b$. Conductive mechanisms govern the phenomena in this region. For intermediate values of $Q_b\ Gr^{-1/4}$ a transition region exists in which both convection and conduction effects coexist.

Except in the "convection" region, $Q_b\ Gr^{-1/4} < 0.01$, it is necessary to determine $(q/A)_b$ in order to make calculations using the results in Figures 150 and 151. This is the key step in the calculation procedure for the transition region. The "interface heat flux," $(q/A)_b$, is fixed by the state of the liquid helium II and is independent of the processes in the film. Accordingly, it has the role of a "heat sink" and enters the process as a boundary condition. Its magnitude is thought to depend on the bulk temperature of the liquid He II and the interfacial temperature discontinuity. However, its a priori determination has not yet been resolved nor have any quantitative formulations been established for its calculation. Fortunately, in the high ΔT Range where $Q_b\ Gr^{-1/4}$ is less than 0.01, $(q/A)_b$ is much less than $(q/A)_w$, the wall heat flux, and thus it does not influence the process significantly. In this range, however, the classical film boiling correlations are not valid owing principally to the unusual temperature discontinuity and "heat sink," $(q/A)_b$, boundary condition

at the helium II interface. There is presently a need to clarify the role of $(q/A)_b$ and to achieve an explicit expression for its calculation.

Rivers and McFadden[261] report some experimental data of Holdredge for the case of film boiling from a horizontal cylinder in which the liquid helium II is separated from the heated surface by a film of helium I vapor. A comparison of the predicted and measured Nusselt numbers is shown in Figure 152 for primarily a "convective" condition in which $(q/A)_b$ has a subdued role. The comparison is generally favorable for the range of variables considered and the results tend to authenticate the boundary conditions established in the analysis.

A study of isothermal, turbulent flow of liquid helium II at 1.5°K in wide channels (0.003 to 0.015 inch) having an RMS roughness of about 0.0001 inch is reported by Frederking and Schweikle.[276] Their results indicated that under these flow conditions He II behaved similar to ordinary fluids and could be correlated in terms of the usual similarity parameters. Pressure drop data correlated in terms of Reynolds number and friction factor are shown in Figure 153 in comparison with the Blasius formulation for turbulent flow. Although the general nature of the correlation is evident, the magnitude of the friction factor for a given Reynolds number is considerably greater than that predicted by the Blasius expression for smooth surfaces. This increase is significantly greater than would normally be expected for roughend surfaces in the experimental ranges of relative roughness (hydraulic radius/RMS roughness = 30 to 150) and Reynolds number.

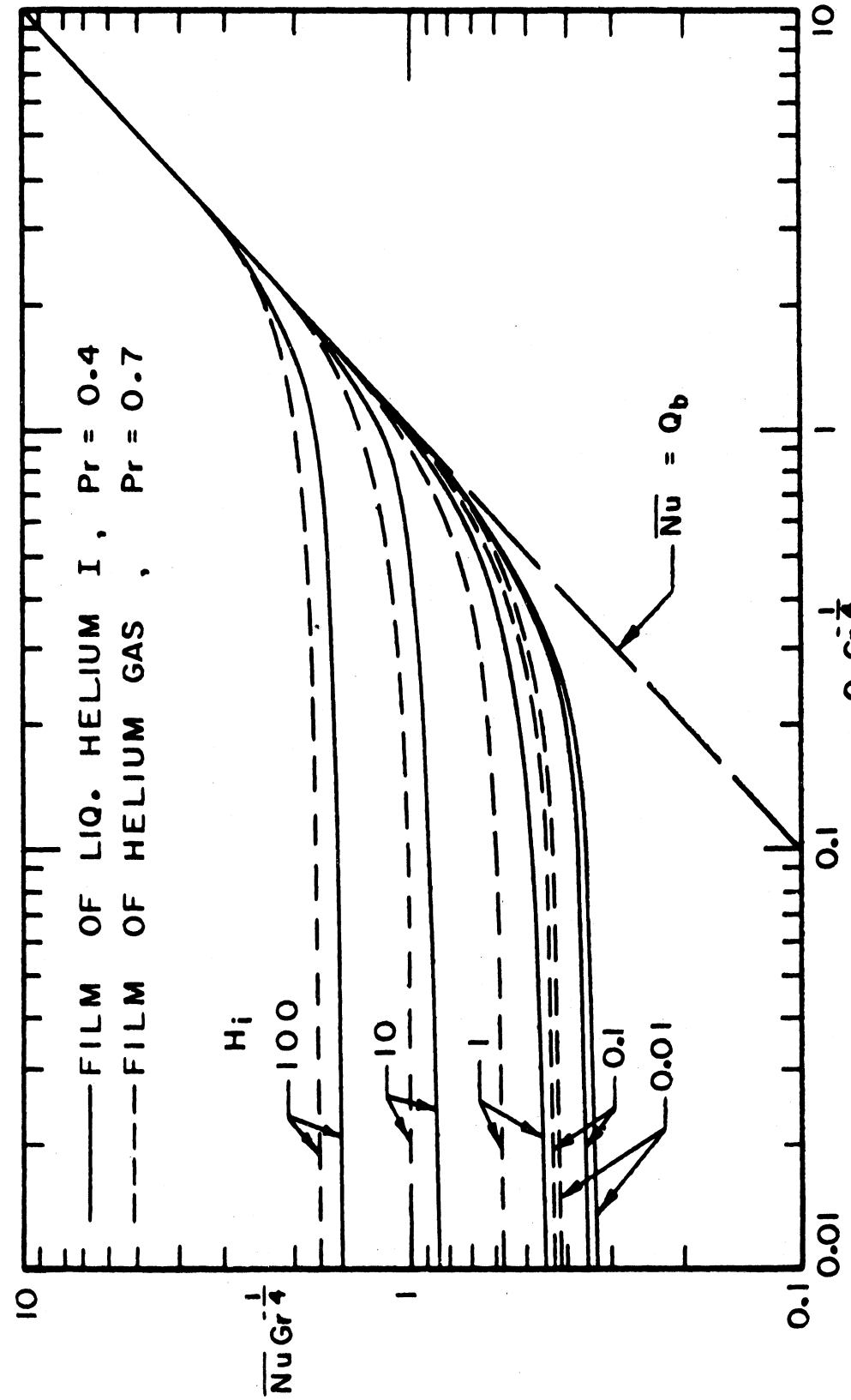

Fig. 150 Calculated results illustrating average heat transfer coefficient ($\overline{Nu} = h_c r/k_f$) for a horizontal circular cylinder (261)

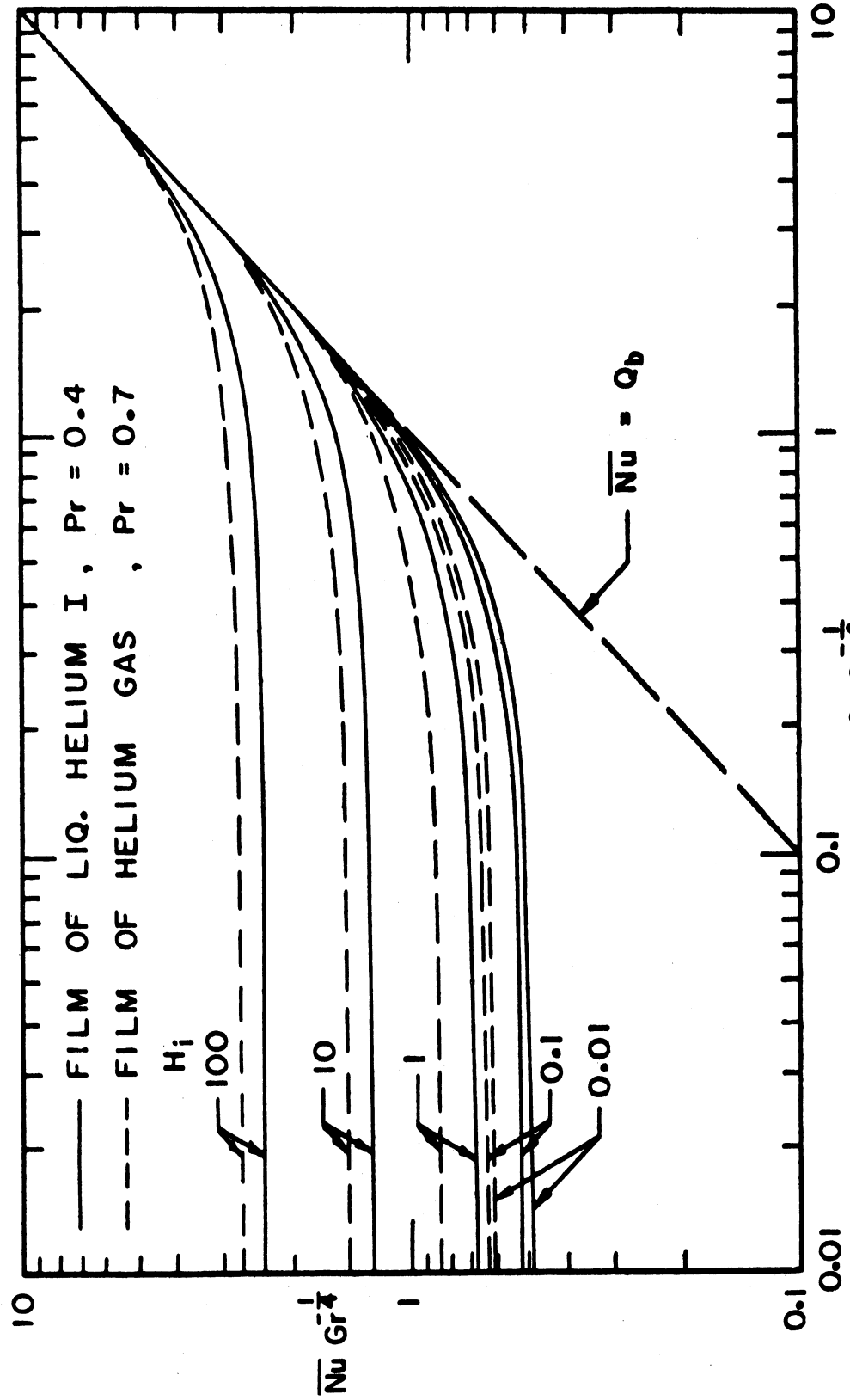

Fig. 151 Calculated results illustrating average heat transfer coefficient ($\overline{Nu} = h_c L/k_f$) for a vertical flat plate (261)

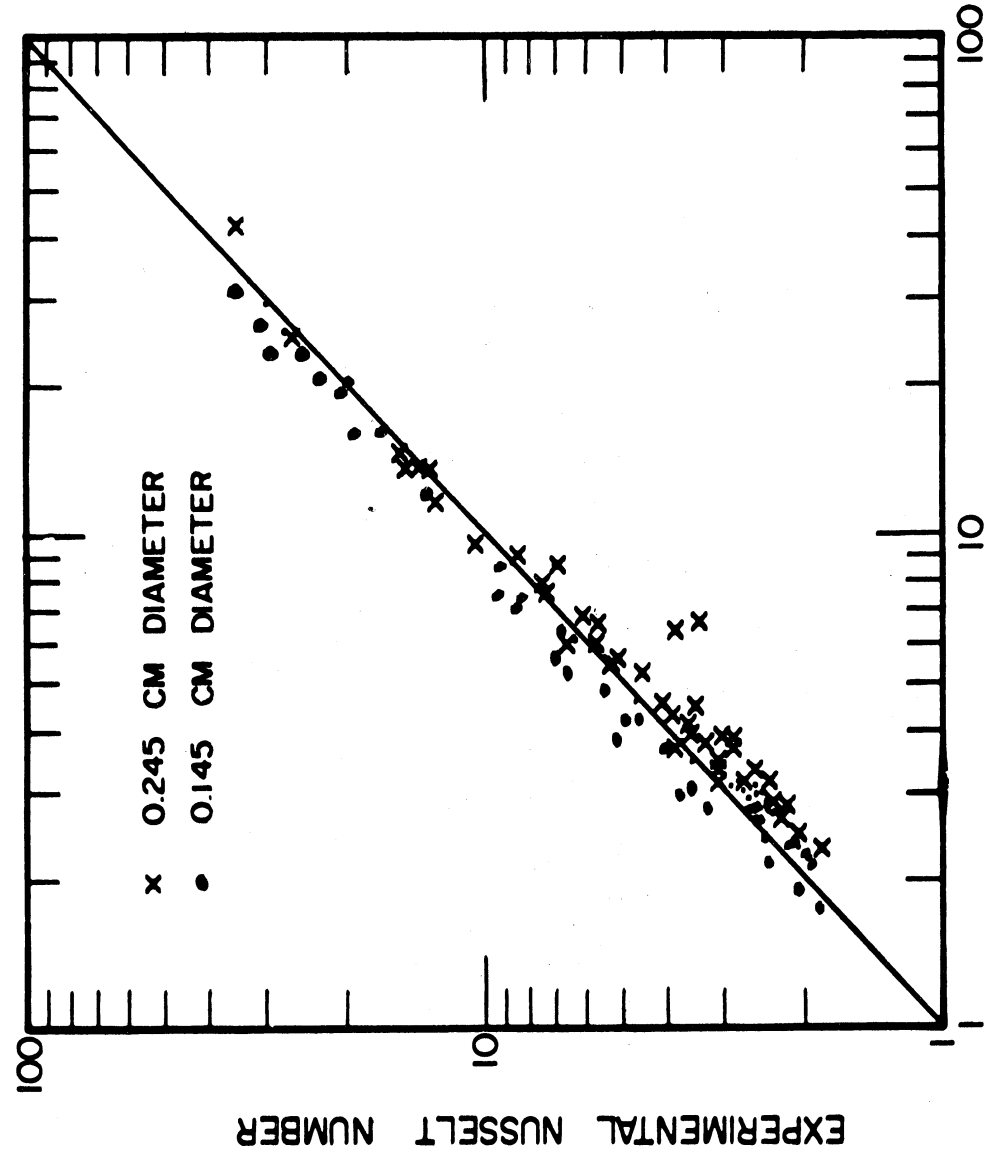

Fig. 152 A comparison of predicted values with experimental values of average Nusselt number for a horizontal circular cylinder (261)

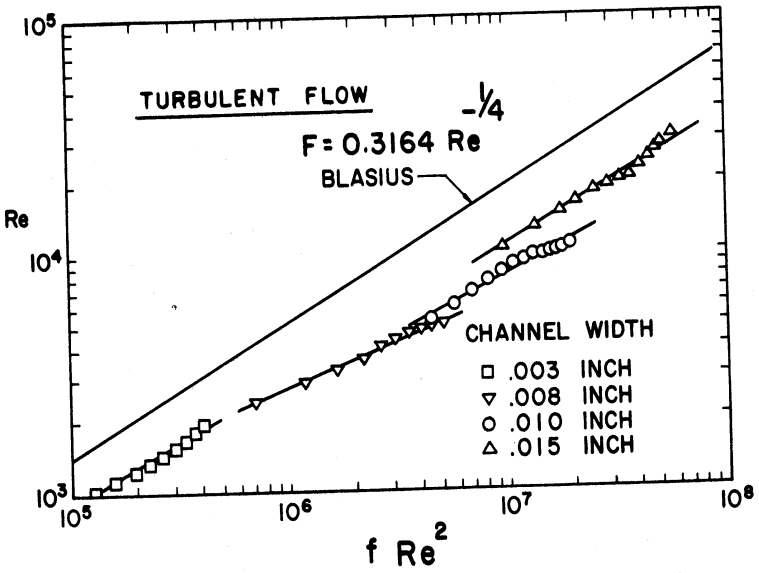

FIGURE 153. DIMENSIONLESS FLOW RATE (REYNOLDS NUMBER) VS DIMENSIONLESS PRESSURE GRADIENT.(273)

The increase in friction factor at Reynolds number as low as 10^3 as a consequence of roughness alone is quite unusual and may be a result of other factors. In Figure 153 the Reynolds number is defined as

$$Re = \frac{\rho V D}{\mu_n} \quad , \tag{183}$$

where ρ is the total liquid density, μ_n the absolute viscosity of the normal fluid and D the hydraulic diameter. The friction factor is defined from

$$\Delta p = f\left(\frac{L}{D}\right) \frac{\rho V^2}{2g_o} \quad . \tag{184}$$

Heat transfer data for zero net mass flow systems also were plotted using similarity parameters but less success was achieved.

ACKNOWLEDGEMENT

The author wishes to express his appreciation to the Industry Program of the College of Engineering, University of Michigan, for providing typing and drafting services on this manuscript and to Mr. Donald L. Danford, Assistant to the Program Director, for his cooperation.

NOMENCLATURE

A	area, ft^2 or cm^2
a	acceleration, ft/sec^2
a,a*	thermal diffusivity, ft^2/hr
$A'(\lambda)$	see Equation (35)
$A''(\lambda)$	see Equation (36)
A_f	flow area, ft^2
B	function for λ_c , see Equation (20)
Bo	boiling number, $(q/A)/h_{fg}\ G_{mix}$
c_p,c_v	heat capacity, BTU/Lb_m-°F, joules/mole-°K
c_o	concentration, Lb_m/ft^3
D',D"	mass diffusivity, ft^2/hr
D_e	equivalent diameter, ft
D_o	outside diameter, ft
E	k(T) integral, see Equation (2), BTU/hr-ft
E_∞	value of E at T_∞ , BTU/hr-ft
E_i	value of E at T_i , BTU/hr-ft
E*	defined by Equation (11)
F	two-phase flow correction factor, see Figure 94
F_1	see Equation (127)
F_2	see Equation (130)
F(p)	see Table X
Fo	Fourier number, $a*t/L^2$
f	friction factor

NOMENCLATURE (CONT'D)

G	for Figure 105 only, vapor mass velocity, w_v/A, $Lb_m/hr\text{-}ft^2$
G	mass velocity, $Lb_m/hr\text{-}ft^2$
G*	see Table X
G_{mix}	see Equation (150)
Gr	Grashof number
g_o	conversion factor, 32.2 $(Lb_m/Lb_f)(ft/sec^2)$
g	gravitional acceleration, ft/sec^2
H	liquid height, ft, Figure 46
H_i	see Equation (181)
h	heat transfer coefficient, $BTU/hr\text{-}ft^2\text{-}°F$, $watts/cm^2\text{-}°K$
h_x	local heat transfer coefficient
h_o	Kapitza effect heat transfer coefficient, Equation (171)
h_g	gas space heat transfer coefficient
h_{fg}	latent heat, BTU/Lb_m
h'_{fg}	see Equation (128)
h_{fg_2}	see Equation (132)
I	see Equation (81)
J	conversion factor 778 $ft\text{-}Lb_f$ = 1 BTU
k	thermal conductivity, $BTU/hr\text{-}ft\text{-}°F$, $watts/cm\text{-}°C$
k',k"	thermal conductivity
k_∞	thermal conductivity at T_∞
k*	see Equation (19)
k_{App}	thermal conductivity of He-II, see Equation (168)

NOMENCLATURE (CONT'D)

L	characteristic length, ft
L*	see Table X
L	for Figure 105 only, liquid mass velocity, w_ℓ/A, $Lb_m/hr\text{-}ft^2$
M_o, M_s	stability modulus, Equations (15, 17)
N_s	biot modulus, Equation (18)
Nu	Nusselt number
p	pressure, psia, mm Hg
p	perimeter, ft
p_c	critical pressure, psia
p''_s	volumetric heat generation, $BTU/hr\text{-}ft^3$
Pr	Prandtl number
q	heat flux, $watts/cm^2$
(q/A)	heat flux, $BTU/hr\text{-}ft^2$
$(q/A)_{max}$	maximum nucleate boiling heat flux
$(q/A)_{min}$	minimum film boiling heat flux
$(q/A)_K$	Kapitza heat flux
Q_b	see Equation (182)
R	residual
R	gas constant, $(Lb_f/Lb_m)(ft/°R)$
Re	Reynolds number
Ra	Rayleigh number, GrPr
R_g	see Figure 106
R_ℓ	see Figure 106

NOMENCLATURE (CONT'D)

St	Stanton number
S	entropy
S	two-phase flow correction factor, Figure 95
T, T', T''	temperature °R, °K
T_m	temperature at maximum value of c_p, °R
T_∞	ambient temperature, °R, °K
T_i	initial temperature, °R
T_s	interfacial temperature, °R
T_{sat}	saturation temperature, °R, °K
ΔT_{sat}	$T_w - T_{sat}$ °R, °K
T_w	wall temperature, °R, °K
T_c	critical temperature °R, °K
t	time, hours, seconds
t^+	universal temperature
u, u', u''	velocity, ft/sec
u^+	universal velocity
v_{fg}	volume for vaporization, ft^3/Lb_m
V	velocity, ft/sec
V_{av}	average velocity
w	mass flow rate, Lb_m/hr
x	coordinate, mass quality
x*	x/L
Δx	grid size
X	interface location

NOMENCLATURE (CONT'D)

y	coordinate
y^*	y/L
z	coordinate
z^*	z/L

Subscripts

b	bulk
f	film
g	gas or vapor
ℓ	liquid
v	vapor
w	wall
∞	ambient

Greek Symbols

α', α''	thermal diffusivity, ft^2/hr
α	absorptance
β	expansion coefficient, $^\circ R^{-1}$
δ_T	see Equation (37)
δ	disturbance parameter
$\Delta(t)$	stratified layer thickness, ft
γ_T	see Equation (38)
ϵ	emittance
η	$z/\Delta(t)$
θ	Debye temperature, $^\circ K$, Figure 5

NOMENCLATURE (CONT'D)

λ_c	critical wave length, ft, cm, Equation (122)
λ_d	most dangerous wave length, ft, cm, Equation (123)
λ	growth rate parameter, Equation (29)
λ	for Figure 105 only $[(\rho_g/0.075)(\rho_\ell/62.3)]^{1/2}$
μ	viscosity, $Lb_m/hr\text{-}ft$
ν	kinematic viscosity, ft^2/hr
ρ	density Lb_m/ft^3, gr/cm^3
σ	surface tension, Lb_f/ft, dynes/cm
σ_T	see Equation (39)
Φ_1	see Equation (100) and Table XI
Φ_2	see Equation (101) and Table XII
ϕ_1	correction factor, Table VI
ϕ_2	correction factor, Equations (62) and (63)
ϕ	correlation factor, see Figure 68
ϕ_ℓ	see Figure 106
ψ	see Equation (82)
ψ	for Figure 105 only, $(73/\sigma)/[(\mu_\ell(62.6)/\rho_\ell)^2]^{1/3}$
X'_{tt}	Martinelli parameter, Equation (68)

REFERENCES

1. D. Alpert, Industrial Research, Vol. 6, No. 6, p. 106, June 1964.

2. K. D. Timmerhaus, R. F. Kamm and J. D. Bays, "Whither Cryogenics", International Advances in Cryogenic Engineering, Vol. 10, p. 1-6, Plenum Press, 1965.

3. F. J. Radd, "Storage Methods for Liquid Methane," 1965 Heat Transfer Conference, Oklahoma State University, Stillwater, Oklahoma.

4. C. E. Schorre, "Liquified Natural-Gas Storage Service," ASME paper 64-WA/PID-10.

5. A. P. Rinfret, "Cryobiology", Advances in Cryogenic Engineering, Vol. 8, 1963, p. 11-16.

6. W. Haumann, "Cryogenic Engineering in Cryobiology", Advances in Cryogenic Engineering, Vol. 8, 1963, pp. 478-83.

7. D. H. Parkinson, "Cryogenic Electronic Developments", International Advances in Cryogenic Engineering, Vol. 10, 1965, pp. 411-18.

8. W. B. Ittner, III, "Cryogenic Electronics", Advances in Cryogenic Engineering, Vol. 8, 1963, pp. 30-36.

9. J. K. Hulm, B. S. Chandrasekhar, H. Riemersma, "High-Field Superconducting magnets", Advances in Cryogenic Engineering, Vol. 8, 1963, pp. 17-29.

10. W. W. Balwanz, "Cryogenic Vacuum Pumping", Advances in Cryogenic Engineering, Vol. 9, 1964, pp. 451-56.

11. E. L. Garloin, "Cryogenic Pumping and Space Simulation", Advances in Cryogenic Engineering, Vol. 8, 1963, pp. 37-45.

12. E. F. Hammel,"Cryo-Engineering in the Nuclear Rocket Program", Advances in Cryogenic Engineering, Vol. 9, 1964, pp. 11-19.

13. R. W. Vance and W. M. Duke, Applied Cryogenic Engineering, John Wiley and Sons, N.Y.C., 1962.

14. R. W. Vance, Cryogenic Technology, John Wiley and Sons, 1964.

15. K. D. Timmerhaus, International Advances in Cryogenic Engineering, Vol. 10, 1965, papers R-1,2,3.

16. R. B. Scott, W. H. Denton and C. M. Nicholls, Technology and Uses of Liquid Hydrogen, Pergamon Press, MacMillan Co., N.Y., 1964.

17. R. S. Hudders, C. J. Dorf and A. H. Holcombe, "Railway Tank Car for Transcontinental Shipment of Liquid Hydrogen", Advances in Cryogenic Engineering, Vol. 8, 1963, pp. 461-66.

18. G. H. Zenner, "Cryogenics and Mechanical Engineering", Mechanical Engineering, Sept. 1961.

19. R. B. Scott, Cryogenic Engineering, D. Van Nostrand Co., 1959.

20. N. Zuber, "On the Stability of Boiling Heat Transfer," Trans. ASME, Vol. 80, No. 3, April 1958, p. 711-20. See also Zuber, N., Discussion of "Film Boiling Heat Transfer From a Horizontal Surface" by P. J. Berenson, J. Heat Transfer, Vol. 83, August 1961, p. 357.

21. "Linde Co. Superinsulation Applied to Space Vehicles," Engineering Development Laboratory, Cryogenic Products Department, Tonawanda, New York.

22. C. T. Lane, Superfluid Physics, McGraw-Hill Book Co., 1962.

23. Behavior of Materials at Cryogenic Temperatures, ASTM publication STP 387, 154 pgs. 1966. ASTM 1916 Race St., Philadelphia, Pa.

24. Symposium on Evaluation of Metallic Materials in Design for low-temperatures, ASTM publication STP 302, 252 pgs., 1962. See Reference (23) for address.

25. Report on Physical Properties of Metals and Alloys From Cryogenic to Elevated Temperatures, ASTM publication DS22 (Formerly STP 296), 210 pgs., 1961, See Reference 23 for address.

26. W. H. Keesom, Helium, Elsevier, Princeton, N. Y., 1942.

27. J. D. Seader, W. S. Miller and L. A. Kalvinskas, "Boiling Heat Transfer for Cryogenics", Final Report, Rocket-dyne Division, North American Aviation, Inc., NASA contract no. NAS 8-5337, George C. Marshall Space Flight Center, Report R-5598, May 11, 1964.

28. J. A. Clark, The Transport of Heat and Mass, in Preparation, John Wiley and Sons, N. Y.

29. V. S. Arpaci, Conduction Heat Transfer, Addison-Wesley, 1966.

30. H. S. Carslaw and J. C. Jaeger, Conduction of Heat in Solids, Second Edition, Oxford Press, 1959.

31. P. J. Schneider, Temperature Response Charts, John Wiley and Sons, 1963.

32. F. Kreith, Principals of Heat Transfer, Second Edition, International Textbook Co.,

33. H. Z. Barakat and J. A. Clark, "On the Solution of the Diffusion Equation by Numerical Methods", Journal of Heat Transfer, November 1966, p. 421.

34. Kropschot, R. H., Chap. 6, "Low Temperature Insulation" Applied Cryogenic Engineering, R. W. Vance and W. M. Duke. Editors, John Wiley and Sons, New York, 1962.

35. Kropschot, R. H., Chap. e, "Insulation Principles", Cryogenic Technology, R. M. Vance, Editor, John Wiley and Sons, 1963.

36. Cline, D. and R. H. Kropschot, "The Thermal Properties of Powder Insulators in the Temperature Range 300°-4°K", Report R-240, Cryogenic Engineering Laboratory, NBS, Boulder, Colorado.

37. Advances in Cryogenic Engineering, K. D. Timmerhaus, Editor, Plenum Press, New York, Vol. 1-14, 1954-1963.

38. W. M. Rohsenow, "Heat Transfer with Evaporation," Heat Transfer, University of Michigan Press, 1953.

39. P. M. Riede and D. I-J. Wang, "Characteristics and Applications of Some Super Insulations", Advances in Cryogenic Engineering, Plenum Press, Vol. 5, p. 204, 1960.

40. J. A. Paivanas, O. P. Roberts and D. I-J. Wang, "Multishielding - An Advanced Super Insulation Technique," Advances in Cryogenic Engineering, Plenum Press, Vol. 10, p. 197, 1965.

41. R. H. Kropschot and R. W. Burgess, "Perlite for Cryogenic Insulation", Advances in Cryogenic Engineering, Plenum Press, Vol. 8, p. 425, 1963.

42. J. F. Jaskins and J. Hertz, "Thermal Conductivity of Plastic Foams From - 423 to 75°F", Advances in Cryogenic Engineering, Plenum Press, Vol. 7, p. 353, 1962.

43. R. N. Miller, C. D. Bailey, R. T. Beall and S. M. Freeman, "Foams and Plastic Films for Insulation Systems", Advances in Cryogenic Engineering, Plenum Press, Vol. 8, p. 417, 1963.

44. J. A. Clark, "A Review of Pressurization, Stratification and Interfacial Phenomena", International Advances in Cryogenic Engineering, Plenum Press, Vol. 10, p. 260, 1965.

45. R. W. Schrage, Interphase Mass Transfer, Columbia University Press, 1953.

46. G. Balekijan and D. L. Katz, "Heat Transfer From Super-Heated Vapors to a Horizontal Tube," AIChE Journal, Vol. 4, No. 1, March 1959, p. 43.

47. M. Saad and D. A. Oliver, "Linearlized Time Dependent Free Surface Flow in Rectangular and Cylindrical Tanks," Proceedings, 1964 Heat Transfer and Fluid Mechanics Institute, Stanford University Press, 1964.

48. H. M. Satterlee and W. C. Reynolds, "The Dynamics of the Free Liquid Surface in Cylindrical Containers Under Strong Capillary and Weak Gravity Conditions, "Technical Report No. LG-2, Department of Mechanical Engineering, Stanford University, Stanford, California, May 1, 1964.

49. E. L. Knuth, "Nonstationary Phase-Changes Involving a Condensed Phase and a Saturated Vapor," The Physics of Fluids, Vol. 2, No. 1, Jan-Feb. 1959, p. 84.

50. J. A. Clark, "Transient Condensation of Insulating Substrates for Cryogenic Application," Advances in Cryogenic Engineering, Vol. 7, 1962, p. 360.

51. W. J. Yang, "Phase Change of one Component Systems in a Container," AIChE Preprint No. 48, Sixth National Heat Transfer Conference, Boston, Mass., August 11 to 14, 1963.

52. W. J. Yang and J. A. Clark, "On the Application of the Source Theory to the Solution of Problems Involving Phase Change. Part I - Growth and Collapse of Bubbles," Journal of Heat Transfer, Transactions ASME, May 1964.

53. P. D. Thomas and F. H. Morse, "Analytic Solution for the Phase Change in a Suddenly Pressurized Liquid-Vapor System," Advances in Cryogenic Engineering, Vol. 8, 1963, p. 550.

54. E. L. Knuth, "Evaporations and Condensations in One-Component Systems," Journal, American Rocket Society, September 1962, p. 1424.

55. W. J. Yang and J. A. Clark, "On the Application of the Source Theory to the Solution of Problems Involving Phase Change; Part 2, Transient Heat and Mass Transfer in a Multi-Component Liquid-Vapor System," Journal of Heat Transfer, Vol. 86, August 1964, p. 443-49.

56. W. J. Yang, P. S. Larsen and J. A. Clark, "Interfacial Heat and Mass Transfer in a Suddenly Pressurized, Binary Liquid-Vapor System," Journal of Engineering for Industry, (ASME), Vol. 87, No. 4 November 1965, p. 413-19.

57. J. A. Clark, H. Merte, Jr. and H. Z. Barakat, "Finite-difference Solution of Stratification and Pressure Rise in Containers", Proceedings, Semi-International Symposium, Japanese Society of Mechanical Engineers, Tokyo, Japan, 1967.

58. D. H. Liebenberg and F. J. Edeskuty, "Pressurization Analysis of a Large Scale Liquid Hydrogen Dewar," International Advances in Cryogenic Engineering, Plenum Press, Vol. 10, p. 284, 1965.

59. B. Baily and J. R. Churgay, "Pressurant Gas Behavior in Pressurized Discharge Apparatus", Memo to J. A. Clark, Heat Transfer Laboratory, Department of Mechanical Engineering, University of Michigan, August 1, 1962.

60. M. E. Nein and J. F. Thompson, "Experimental and Analytical Studies of Pressurization Systems for Cryogenic Propellants," Propulsion Division, NASA, Marshall Space Flight Center, Huntsville, Alabama, July 1964.

61. D. F. Gluck and J. F. Kline, "Gas Requirements in Pressurized Transfer of Liquid Hydrogen," Advances In Cryogenic Engineering, Vol. 7, 1962, p. 219.

62. W. Olsen, NASA Lewis Research Center, Cleveland, Ohio, Personal Communication to J. A. Clark, June 19, 1964.

63. J. A. Clark and W. M. Rohsenow, "Local Boiling Heat Transfer to Water at Low Reynolds Numbers and High Pressures," Transactions ASME, May 1954, pp. 553-63.

64. H. L. Hess and H. R. Kunz, "A Study of Forced Convection Heat Transfer to Supercritical Hydrogen", Journal of Heat Transfer, February 1965, p. 41-49.

65. E. J. Szetela, "Heat Transfer to Hydrogen Including the Effects of Varying Fluid Properties", Journal, American Rocket Society, August 1962, p. 1289-93.

66. R. C. Hendricks, R. W. Graham, Y. Y. Hsu and A. A. Medeiros, "Correlation of Hydrogen Heat Transfer in Boiling and Supercritical Pressure States", Journal, American Rocket Society, February 1962, p. 244-53.

67. R. H. Richards, W. G. Steward and R. B. Jacobs,"A Survey of the Literature on Heat Transfer From Solid Surfaces to Cryogenic Fluids," NBS TN 122, Boulder Laboratories, October 1961.

68. C. C. Wright, "Design, Construction and Testing of A Helium-to-Hydrogen Heat Exchanger", Advances in Cryogenic Engineering, Vol. 5, Plenum Press, 1960, p. 244-54.

69. W. H. Kahl, Linde Co., Tonawanda, N.Y., Personal Communication to J. A. Clark.

70. W. M. Kays and A. L. London, Compact Heat Exchangers, McGraw-Hill Book Co., 1964.

71. D. H. Pope, W. R. Killian and R. J. Corbett, "Single-Phase Flow Tests with Liquid Hydrogen", Advances in Cryogenic Engineering, Vol. 5, Plenum Press, 1960, p. 441-50.

72. J. R. Bartlit and K. D. Williamson, Jr., "Further Experimental Study of H_2O-LH_2 Heat Exchangers", Advances in Cryogenic Engineering, Vol. 5, 1966, p. 561-68.

73. J. H. Hargis and H. A. Stokes, "Thermal Design of Cryogenic Heat Exchangers for Space Vehicle Pressurization Systems", Proceeding, Conference on Propellant Tank Pressurization and Stratification, Vol. I, Gedrge C. Marsall Space Flight Center, NASA, Huntsville, Ala., January 20, 21, 1965.

74. W. H. McAdams, Heat Transmission, 2nd Edition, McGraw-Hill Book Co., 1954.

75. W. R. Thompson and E. L. Geery, "Heat Transfer to Cryogenic Hydrogen at Supercritical Pressure," Advances in Cryogenic Engineering, Vol. 7, Plenum Press, 1963, p. 391-401.

76. J. R. McCarthy and H. Wolf, "Forced Convection Heat Transfer to Gaseous Hydrogen at High Heat Flux and High Pressure in a Smooth, Round Electrically Heated Tube", Journal, American Rocket Society, Vol. 30, April, 1960, p. 423.

77. H. Wolf and J. R. McCarthy, "Heat Transfer to Hydrogen and Helium with Wall to Fluid Temperature Ratios to 11.09", Abstract 100, AIChE Annual Meeting, Washington, D. C., Dec. 4-7, 1960.

78. C. C. Wright and H. H. Walters, "Single Tube Heat Transfer Tests to Gaseous and Liquid Hydrogen", WADC Tech. Report 59-423, August 1959.

79. M. F. Taylor and T. A. Kirchgessner, "Measurements of Heat Transfer and Friction Coefficients for Helium Flowing in a Tube at Surface Temperatures up to 5900°R, NASA TN D-133, October, 1959.

80. R. B. Fleming, "The Effect of Flow Distribution in Parallel Channels of Counterflow Heat Exchangers," Advances in Cryogenic Engineering, Vol. 12, Plenum Press, 1967, p. 352-362.

81. P. G. Kroeger, "Plated-Tube Heat Exchanger: Analytical Investigation of a New Concept", Advances in Cryogenic Engineering, Vol. 12, Plenum Press, 1967, p. 340-351.

82. P. G. Kroeger, "Performance Deterioration in High Effectiveness Heat Exchangers Due to Axial Heat Conduction Effects", Advances in Cryogenic Engineering, Vol. 12, Plenum Press, 1967, p. 363-372.

83. W. A. Benser and R. W. Graham, "Hydrogen Convective Cooling of Rocket Nozzles," ASME Paper no. 62-AV-22.

84. H. H. Koln, "A Closed-Loop Cooling System For Superconducting Bubble Chamber Magnets" Proceedings, International Symposium on Magnet Technology, Stanford Linear Accelerator Center, Stanford, California, 1965, p. 611-612.

85. H. H. Koln, M. J. Leopold and R. D. Hay, "Heat Transfer by the Circulation of Supercritical Helium", Advances in Cryogenic Engineering, Vol. 11, Plenum Press, 1966, p. 530-535.

86. J. G. Knudsen and D. L. Katz, Fluid Dynamic and Heat Transfer, McGraw-Hill, 1959.

87. L. G. Desmond and E. W. Sams, NACA, Research Memorandum, ESO H23, November 1950.

88. D. A. Wiederecht and G. Sonnemann, "Investigation of the Non-Isothermal Friction in the Turbulent Flow of Liquids", ASME Paper 60-WA-82, 1960.

89. S. K. Fenster, G. J. VanWylen and J. A. Clark, "Transient Phenomena Associated with the Pressurization of Liquid Nitrogen Boiling at Constant Heat Flux", Advances in Cryogenic Engineering, Vol. 5, Plenum Press, 1960, p. 226.

90. H. Merte and J. A. Clark, "Boiling Heat Transfer with Cryogenic Fluids at Standard, Fractional and Near Zero Gravity", Journal of Heat Transfer, Vol. 86, August 1964, p. 351-60.

91. H. Merte and E. W. Lewis, "Boiling of Liquid Nitrogen in Reduced Gravity Fields with Subcooling", Heat Transfer Laboratory, Department of Mechanical Engineering, University of Michigan, Ann Arbor, 1967.

92. H. Merte and J. A. Clark, "Pool Boiling in an Acceleration System", Journal of Heat Transfer, August 1961.

93. J. A. Clark and H. Merte, "Boiling Heat Transfer to a Cryogenic Fluid in Both Low and High Gravity Fields", Proceedings (Commission V), International Congress of Refrigeration, Munich, Germany, August 1963.

94. Evaluation of AS-203 Low Gravity Orbital Experiment", Technical Report HSM-R421-67, Contract NAS 8-4016, Schedule II, Fluid Mechanics and Thermodynamics Research Section, Space Division, Chrysler Corporation, Huntsville, Alabama, January 13, 1967.

95. F. E. Swalley, W. D. Ward and L. E. Toole, "Low Gravity Fluid Behavior and Heat Transfer Results From the S-IVB-203 Flight", Proceedings, Conference on Long-term Cryo-propellant Storage in Space", George C. Marshall Space Flight Center, NASA, Huntsville, Ala., October, 12-13, 1966.

96. Platt, G. K., M. E. Nein, J. L. Vaniman and C. C. Wood, "Feed System Problems Associated with Cryogenic Propellant Engines," Paper 687A, SAE-ASNE, National Aeronautical Meeting and Production Engineering Forum, April 1963.

97. Arpaci, V. S., J. A. Clark and W. O. Winer, "Dynamic Response of Fluid and Wall Temperatures During the Pressurized-Discharge of a Liquid from a Container," Advances in Cryogenic Engineering, Vol. 6, 1961, p. 310.

98. Arpaci, V. S. and J. A. Clark, "Dynamic Response of Fluid and Wall Temperatures During Pressurized-Discharge for Simultaneous, Time-Dependent Inlet Gas Temperature, Ambient Temperature, and/or Ambient Heat Flux," Advances in Cryogenic Engineering, Vol. 7, 1962, p. 419.

99. Clark, J. A., G. J. Van Wylen and S. K. Fenster, "Transient Phenomena Associated with the Pressurized-Discharge of a Cryogenic Liquid from a Closed Vessel," Advances in Cryogenic Engineering, Vol. 5, 1960, p. 467.

100. Arpaci, V. S., persoaal communication to J. A. Clark, October 1963. See also, J. A. Clark, et al., "Pressurization of Oxygen Container," Progress Report No. 6, ORA Project 04268, University of Michigan, October 1963.

101. Epstein, M., H. K. Georgius and R. E. Anderson, "A Generalized Propellant Tank Pressurization Analysis," International Advances in Cryogenic Engineering, Vol. 10, 1965, p. 290.

102. Roudebush, W. H., "An Analysis of the Problem of Tank Pressurization During Outflow," NASA TN, Lewis Research Center, Cleveland, Ohio, 1964.

103. Burke, J. C., W. R. Byrnes, A. H. Post and F. E. Ruccia, "Pressurized Cooldown of Cryogenic Transfer Lines," Proceedings of the 1958 Cryogenic Engineering Conference, 1959.

104. Moore, R. W., A. A. Fowle, B. M. Bailey, F. E. Ruccia and R. C. Reid, "Gas Pressurized Transfer of Liquid Hydrogen," Advances in Cryogenic Engineering, Vol. 5, 1960, p. 450.

105. Bowersock, D. C., Jr., and R. C. Reid, "An Analytical Method for Estimating Gas Requirements in the Pressurization and Transfer of Cryogenic Fluids," Advances in Cryogenic Engineering, Vol. 6, 1961, p. 261.

106. Bowersock, D. C., Jr., R. Gardner and R. C. Reid, "Pressurized Transfer of Cryogenic Fluids," Proceedings of the 1958 Crylgenic Engineering Conference, 1959.

107. Humphrey, J. C., "Pressurized Transfer of Cryogenic Fluids from Tanks in Liquid Nitrogen Baths," Advances in Cryogenic Engineering, Vol. 6, 1961, p. 281.

108. Coxe, E. F. and J. W. Tatom, "Analysis of the Pressurizing Gas Requirements for an Evaporated Propellant Pressurization System," Advances in Cryogenic Engineering, Vol. 7, 1962, p. 234.

109. Canty, J. M., "Pressure Pheonomena in Transferring Saturated Cryogenic Fluids," Advances in Cryogenic Engineering, Vol. 6, 1961, p. 272.

110. Momenthy, A. M., "Propellant Tank Pressurization System Analysis," Advances in Cryogenic Engineering, Vol. 9. 1964, p. 273.

111. G. J. VanWylen, S. K. Fenster, H. Merte, Jr. and W. A. Warren, "Pressurized Discharge of Liquid Nitrogen from an Uninsulated Tank," Proceedings of the 1958 Cryogenic Engineering Conference, 1959.

112. P. J. Berenson, "Film Boiling Heat Transfer from a Horizontal Surface," Journal of Heat Transfer, Vol. 83, No. 3, August 1964, p. 351-59.

113. P. M. Ordin, S. Weiss and H. Christenson, "Pressure-Temperature Histories of Liquid Hydrogen under Pressurization and Venting Conditions," Advances in Cryogenic Engineering, Vol. 5, 1960, p. 481.

114. M. E. Nein and R. R. Head, "Experiences with Pressurized-Discharge of Liquid Oxygen from Large Flight Vehicle Propellant Tanks," Advances in Cryogenic Engineering, Vol. 7, 1962, p. 244.

115. J. F. Thompson, "Modification of Rocketdyne Tank Pressurization Computer Program," PTF-64-83, NASA-MSFC, Memorandium R-P and VE-PTF-64-M-83, 1964.

116. L. E. Scott, R. F. Robbins, D. B. Mann and B. W. Birmingham, "Temperature Stratification in a Nonventing Helium Dewar," Journal of Research, NBS, Vol. 64C, No. 1, 1960, p. 19.

117. B. H. Anderson, and M. J. Kolar, "Experimental Investigation of the Behavior of a Confined Fluid Subjected to Nonuniform Source and Wall Heating," NASA TN D-2079, November 1963.

118. R. G. Schwind, and G. C. Vliet, "Observation and Interpretations of Natural Convection and Stratification in Vessels," Proceeding, 1964 Heat Transfer and Fluid Mechanics Institute, Stanford University Press, 1964.

119. D. O. Barnett, T. W. Winstead and L. S. McReynolds, "An Investigation of LH_2 Stratification in a Large Cylindrical Tank or Saturn Configuration," International Advances in Cryogenic Engineering, Vol. 10, 1965, p. 314.

120. E. Y. Harper, J. H. Chin, S. E. Hurd, A. M. Levy and H. M. Satterlee, "Analytical and Experimental Study of Liquid Orientation and Stratification in Standard and Reduced Gravity Fields", Preliminary Report, Lockheed Missiles and Space Co., June 1964, Contract NAS 8-11525, Marshall Space Flight Center.

121. D. M. Tellup and E. Y. Harper, A.I.A.A. Journal, No. 8, 1954, August, 1963.

122. G. C. Vliet, J. J. Brogan, T. S. Sheppard, F. H. Morie and F. L. Hines, "Stratified Layer Flow Model - A Numerical Approach to Temperature Stratification in Liquids Contained in Heated Vessels," A.I.A.A. Preprint No. 64-37, January, 1964.

123. J. M. Ruder, "Stratification in a Pressurized Container with Sidewall Heating," A.I.A.A. Journal, Vol. 2, No. 1, January 1964, p. 135.

124. E. Y. Harper, S. E. Hurd and J. O. Donaldson, "A Study of Liquid Stratification in a Cylindrical Container," Lockheed Missiles and Space Co., Report 803973, March 1964.

125. J. W., Tatom, W. H. Brown, L. H. Knight and E. F. Coxe, "Analysis of Thermal Stratification of Liquid Hydrogen in Rocket Propellant Tanks," Advances in Cryogenic Engineering, Vol. 9, 1964, p. 265.

126. J. H. Robbins, and A. C. Rogers, "An Analysis on Predicting Thermal Stratification in Liquid Hydrogen," Manuscript submitted to A.I.A.A., April 1964, Advance copy sent to author.

127. T. E. Bailey, and R. F. Fearn, "Analytical and Experimental Determination of Liquid Hydrogen Temperature Stratification," Advances in Cryogenic Engineering, Vol. 9, 1964, p. 254.

128. T. E. Bailey, R. VandeKoppel, G. Skartvedt and T. Jefferson, "Cryogenic Propellant Stratification Analysis and Test Data Correlation," A.I.A.A. Journal, Vol. 1, No. 7, July 1963, p. 1657.

129. T. E. Bailey, and others, "Analytical and Experimental Determination of Liquid Hydrogen Temperature Stratification," Final Report, Contract NAS 8-5046, Martin Company, Denver, Colorado, April 1963, Contractor to Marshall Space Flight Center.

130. H. Z. Barakat and J. A. Clark, "Analytical and Experimental Study of the Transient Laminar Natural Convection Flow in Partially Filled Liquid Containers", Proceedings Vol. II, Third International Heat Transfer Conference, Chicago Ill., August 1966.

131. H. Z. Barakat, "Transient Laminar Free-Convection Heat and Mass Transfer in Two-Dimensional Closed Containers Containing Distributed Heat Source", ASME paper 65-WA/HT-28, 1965.

132. C. S. Suh, personal communication to J. A. Clark, August 1967.

133. S. C. Huntley, "Temperature-Pressure-Time Relations in a Closed Cryogenic Container", Advances in Cryogenic Engineering, Vol. 3, 1960, p. 342.

134. H. Merte and J. A. Clark, "Boiling Heat Transfer Data for Liquid Nitrogen and Standard and Near-Zero Gravity", Advances in Cryogenic Engineering, Vol. 7, 1962.

135. L. A. Bromley, "Heat Transfer in Stable Film Boiling", Chemical Engineering Program, Vol. 46, 1950, p. 221-7.

136. H. H. Walters, "Single Tube Heat Transfer Tests with Liquid Hydrogen", Advances in Cryogenic Engineering, Vol. 6, 1961, p. 509.

137. J. W. Westwater, "Boiling of Liquids", Advances in Chemical Engineering, Academic Press, 1956, p. 1-76.

138. R. E. Balzhiser, et a.. "Literature Survey on Liquid Metal Boiling" Final Report - Phase I, ASD Technical Report 61-594, December 1961.

139. N. Zuber and E. Fried, "Two Phase Flow and Boiling Heat Transfer to Cryogenic Liquids", American Rocket Society, Propellants, Combustion and Liquid Rockets Conference, April 1961.

140. R. J. Richards, W. G. Steward, and R. B. Jacobs, "A Survey of the Literature on Heat Transfer from Solid Surfaces to Cryogenic Fluids", NBS TN 122, Boulder Laboratories, October 1961.

141. P. J. Giarratano and R. V. Smith, "Comparative Study of Forced Convection Boiling Heat Transfer Correlations for Cryogenic Fluids", Advances in Cryogenic Engineering, Vol. 11, 1966, p. 492.

142. E. G. Brentari and R. V. Smith, "Nucleate and Film Pool Boiling Design Correlations for O_2, N_2, H_2 and He", International Advances in Cryogenic Engineering, Plenum Press, 1965

143. E. G. Brentari, P. J. Giarratano and R. V. Smith, "Boiling Heat Transfer for Ocygen, Nitrogen, Hydrogen and Helium", NBS Tech. Note No. 317, Boulder, Colorado, 1965.

144. L. S. Tong, Boiling Heat Transfer and Two-Phase Flow, John Wiley and Sons, 1965.

145. D. N. Lyon, P. G. Kosky and B. N. Harnon, "Nucleate Boiling Heat Transfer Coefficients and Peak Nucleate Boiling Fluxes for Pure Liquid N_2 and O_2 on Horizontal Platinum Surfaces from Below 0.5 ATM to the Critical Pressure", Advances in Cryogenic Engineering, Vol. 9, 1964, p. 77-87.

146. S. S. Kutateladze, Heat Transfer in Condensation and Boiling, Translation Series AEC-tr-3770, issued August 1959.

147. P. Roubeau, "Echanges thermiques dans l'azote et l'hydrogene bouillant sous pression," Prog. Refr. Sci. Tech. Vol 1, 49-53 (1960).

148. C. R. Class, J. R. DeHaan, M. Piccone, and R. B. Cost, "Boiling Heat Transfer to Liquid Hydrogen from Flat Surfaces", Adv. Cryo. Engr. Vol 5, 254-261 (1960).

149. N. Zuber, M. Tribus, and J. W. Westwater, "The hydrodynamic crisis in pool boiling of saturated and subcooled liquids," Proc. 2nd Int. Conf. Heat Trans., Boulder Colo., 230-236 (1961). Also, "Hydrodynamic aspects of boiling heat transfer," AECU-4439 (1959).

150. B. P. Breen, and J. W. Westwater, "Effect of diameter of horizontal tubes on film boiling heat transfer," Chem. Engr. Prog. Vol. 58, No. 7, 67-72 (1962).

151. J. H. Lienhard, and P. T. Y. Wong, "The dominant unstable wavelength and minimum heat flux during film boiling on a horizontal cylinder," Journal of Heat Transfer, Vol. 86, May 1964, p. 220-27.

152. Y. Y. Hsu, and J. W. Westwater, "Film boiling from vertical tubes," A. I. Ch. E. J. Vol. 4, No. 1, 58-62 (1958). Also, approximate theory for film boiling on vertical surfaces, CEP Symposium Series 56, No. 30 15-24 (1960).

153. J. E. Sherley, "Nucleate boiling heat-transfer data for liquid hydrogen at standard and zero gravity," Adv. Cryo. Engr. Vol. 8, 495-500 (1963)

154. N. R. Mikhail, "Studies in Heat Transfer to Boiling Liquids at Low Temperatures, Ph. D. Diss., Dept of Chem. Engr. (Imp. Coll. of Sci. and Tech., London, 1952).

155. J. T. Banchero, G. E. Barker, and R. H. Boll, "Heat Transfer characteristics of boiling oxygen, fluorine, and hydrazine," Proj. M834, Engr. Res. Inst., U of Mich. (1951).

156. C. W. Cowley, W. J. Timson, and J. A. Sawdye, "A method for improving heat transfer to a boiling fluid," Ind. Engr. Chem. Proc. Design Devel, Vol. 1, No. 2, 81-84 (1962).

157. D. E. Drayer, and K. D. Timmerhaus, "An experimental investigation of the individual boiling and condensing heat transfer coefficients for hydrogen," Adv. Cryo. Engr. Vol. 7, 401-412 (1962).

158. T. M. Flynn, J. W. Draper, J. H. Roos, "The nucleate and film boiling curve of liquid nitrogen at one atmosphere," Adv. Cryo. Engr. Vol. 7, 539-545 (1962).

159. G. G. Haselden, and J. I. Peters, "Heat transfer to boiling liquid oxygen and liquid nitrogen," Trans. Inst. Chem. Engr. Vol. 27, 201-208 (1949).

160. H. J. Hoge, and F. G. Brickweede, "Rate of heat transfer from a horizontal heated copper tube in boiling liquid hydrogen or oxygen," A-366 (1942). (See Reference 142).

161. A. Karagounis, "Heat transfer coefficient for liquid helium," Int. Inst. Refrig., Comm. 1 and 2, Louvain, Belgium, 195-199, (1966).

162. N. Zuber, "On the Stability of Boiling Heat Transfer," Trans. ASME, Vol. 80, No. 3, April 1958, p. 711-721.

163. M. D. Reeber, "Heat transfer to boiling helium," J. Ap. Phys., Vol. 34, No. 3, 481-483 (1963).

164. L. Weil, and A. Lacaze, "Coefficients d'echange thermiqud dans l'azote bouillant," Acad. des Sci. Tome 230 No. 1, 186-188 (1950).

165. L. Weil, and A Lacaze, "Exchanges de chaleir dans l'hydrogene bouillant sans pression atmospherique," J. Phys. Rad. Vol. 12, 890 (1951).

166. L. Weil, "Heat transfer coefficients of boiling liquified gases," Proc. 8th Intern. Congr. Refrig., London (1951).

167. W. S. Bradfield, R. O. Barkdoll, and J. T. Byrne, Convair Sci. Res. Lab., Res. Note 37, NP-10317 (1960).

168. P. C. Eastman, and W. R. Dators, "Film boiling in liquid helium," Cryogenics, 40-41 (March 1963).

169. T. H. K. Ferderking, "Film boiling of helium I and other liquified gases on single wires," A.I.Ch.E.J. Vol. 5, No. 3, 403-406 (1959).

170. J. J. Fritz, and H. L. Johnson, "Design and operating of Liquid nitrogen-cooled solenois magents", Rev. Sci. Instr. Vol. 21, No. 5, 416-420 (1950).

171. W. B. Hanson, and R. J. Richards, National Bureau of Standards, Boulder, Colorado (unpublished 1956).

172. M. P. Malkov, A. G. Zeldovitch, A. B. Fradkov, and I. B. Danilov, "Industrial separation of deuterium by low-temperature distillation," Proc. 2nd U. N. Intern. Conf. on Peaceful Uses of Atomic Energy, Vol. 4, 491-498 (1958).

173. R. N. Mulford, and J. P. Nigon, Heat exchange between a copper surface and liquid hydrogen and nitorgen, LA-1416, Los Alamos Sci. Lab. (1952).

174. J. Ruzicka, "Heat transfer to boiling nitrogen," Bull. Inst. Intern. Froid, Annexe 1958-1, 323-329 (1958).

175. W. M. Rohsenow, "A Method of Correlating Heat-transfer Data for Surface Boiling of Liquids", Trans. ASME, Vol. 74, 1952, p. 969-75.

176. H. K. Forster and N. Zuber, "Bubble Dynamics and Boiling Heat Transfer", A.I.Ch.E. Journal, Vol. 1, 1955, p. 532-35.

177. H. K. Forster and R. Greif, "Heat Transfer to a Boiling Liquid-mechanism and Correlations", Journal of Heat Transfer, Vol. 81, 1959, p. 43-53.

178. S. Levy, "Generalized Correlation of Boiling Heat Transfer," Journal of Heat Transfer, Vol. 81, 1959, p. 37-42.

179. N. Michenko, "On the Problem of Heat Transfer in Nucleate Boiling," Teploenergetika, Vol. 7, No. 6, 1960, p. 17-21.

180. D. A. Labountzov, "Generalized Correlation for Nucleate Boiling", Teploenergetika, Vol. 7, No. 5, 1960, p. 76-80.

181. Y. P. Chang and N. W. Snyder, "Heat Transfer in Saturated Boiling", ASME-A.I.Ch.E. Heat Transfer Conference, Storrs, Conn., Chem. Eng. Symposium Series, Vol. 56, No. 30, 1960, p. 25-38.

182. K. Nishikawa and K. Yamagata, "On the Correlation of Nucleate Boiling Heat Transfer", Int. Journal of Heat Transfer, Vol. 1, 1960, p. 219-35.

183. L. Bewilogua, R. Knoner and G. Wolf, "Heat Transfer in Boiling Hydrogen, Neon, Nitrogen and Argon," Cryogenics, Vol. 6, No. 1, February 1966, p. 36-40.

184. J. M. Astruc, P. Perroud, A. Lacaze and L. Weil, "Pool Boiling Heat Transfer in Liquid Neon", Advances in Cryogenic Engineering, Vol. 12, Plenum Press, 1967, p. 387-395.

185. W. C. Elrod, J. A. Clark, E. R. Lady and H. Merte, "Boiling Heat Transfer Data at Low Heat Flux," Journal of Heat Transfer, Vol. 89, August 1967.

186. A. Lapin, L. A. Wenzel and H. C. Totten, "Study of Nitrogen and Neon Pool Building on a Short Vertical Pipe", AIChe Journal, Vol. 11, No. 2, 1965, p. 197-201.

187. A Lapin, L. A. Wenzel and H. C. Totten, "Heat Transfer Characteristics of Boiling Nitrogen and Neon in Narrow Annuli", AIChE Journal, Vol. 11, No. 3, 1965, p. 503-8.

188. C. T. Sciance, C. P. Colver and C. M. Sliepcevich, "Pool Boiling of Methane Between Atmospheric Pressure and the Critical Pressure", Advances in Cryogenic Engineering, Vol. 12, 1967, p. 395-409.

189. J. Madejski, "Theory of Nucleate Pool Boiling", Int. Journal of Heat and Mass Transfer, Vol. 8, No. 1, January 1965, p. 155.

190. S. S. Kutateladze, "A Hydrodynamic Theory of Changes in the Boiling Preoces Under Free Convection Conditions", Izv. Akad. Nauk, USSR, OTD. Teck. Navk, No. 4, 1951, p. 529.

191. Y. P. Chang, "Wave Theory of Heat Transfer in Film Boiling", Journal of Heat Transfer, Vol. 81, No. 1, February 1959, p. 1-12.

192. V. M. Borishanskii, "An equation Generalizing Experimental Data on the Cessation of Bubble Boiling in a Large Volume of Liquid", Zhurn. Tek . Fiz., Vol. 26, 1956, p. 452; Translated in Soviet Physics-Technical Physics, Vol. 1, American Institute of Physics, N. Y., p. 438.

193. N. Zuber and M. Tribus, "Further Remarks on the Stability of Boiling", UCLA Report 58-5, January 1958.

194. W. M. Rohsenow and P. Griffith, "Correlation of Maximum Heat Flux Data for Boiling of Saturated Liquids," Chem. Eng. Progress Symposium, Series 18, Vol. 52, 1956, p. 47-49.

195. R. C. Noyes, "An experimental Study of Sodium Pool Boiling Heat Transfer," Journal of Heat Transfer, Vol. 85, No. 2, May 1963, p. 125-32; See Also discussion by J. A. Clark, p. 129.

196. Y. P. Chang, "Some Possible Critical Conditions in Nucleate Boiling", Journal of Heat Transfer, Vol. 85, No. 2, May 1963, p. 89-100.

197. R. Moissis and P. J. Berenson, "On the Hydrodynamic Transition in Nucleate Boiling", Journal of Heat Transfer, Vol. 85, No. 3, August 1963, p. 221-9.

198. D. N. Lyon, "Peak Nucleate Boiling Fluxes and Nucleate Boiling Heat Transfer Coefficients for Liquid N_2 , Liquid O_2 and Their Mixtures in Pool Boiling at Atmospheric Pressure", Int. Journal of Heat and Mass Transfer, Vol. 7, No. 10, Oct. 1964, p. 1097.

199. D. N. Lyon, "Boiling Heat Transfer and Peak Nucleate Boiling Fluxes in Saturated Liquid Helium Between the λ-point and Critical Temperatures", Int. Advances in Cryogenic Engineering, Vol. 10, 1965, p. 371-80.

200. T.H.K. Frederking and J. A. Clark, "Natural Convection Film Boiling on a Sphere," Advances in Cryogenic Engineering, Vol. 8, Plenum Press, 1963, p. 501-506.

201. M. L. Pomerantz, "Film Boiling on a Horizontal Tube in Increased Gravity Fields", Journal of Heat Transfer, Vol. 86, No. 2, May 1964, p. 213-220.

202. L. Manson, "Cooldown of Shrouded Spherical Vessels in Liquid Nitrogen", Advances in Cryogenic Engineering, Vol. 12, 1967, p. 373-381.

203. R. Bellman and R. H. Pennington," Effects of Surface Tension and Viscosity on Taylor Instability", Quarterly of Applied Mathematics, Vol. 12, 1954, p. 151.

204. E. K. Hosler and J. W. Westwater, "Film Boiling on a Horizontal Plate", ARS Journal, Vol. 32, 1962, p. 553-58.

205. J. C. Chen, "A Correlation for Boiling Heat Transfer to Saturated Fluids in Convective Flow", ASME Paper No. 63-HT-34, ASME-AIChE Heat Transfer Conference, Boston, Mass., August 1963.

206. R. W. Graham, R. C. Hendricks, Y. Y. Hsu and R. Friedman, "Experimental Heat Transfer and Pressure Drop of Film Boiling Liquid Hydrogen Flowing Through a Heated Tube," Advances in Cryogenic Engineering, Vol. 6, 1961, p. 517-24. See also NASA TN D-765, May 1961, by the same title and written by the same authors.

207. J. W. H. Chi, "Cooldown Temperatures and Cooldown Time During Mist Flow," Advances in Cryogenic Engineering, Vol. 10, 1965, p. 330-40.

208. J. W. H. Chi, "Slug Flow and Film Boiling of Hydrogen," ASME Paper 65 WA/HT-32, 1965.

209. T. C. Core, J. F. Harkee, B. Misra and K. Sato, "Heat Transfer Studies," WADD-60-239, 1959.

210. J. C. Burke and A. H. Rawdon, "An Experimental Study of Heat Transfer to Two-Phase Film-Boiling Nitrogen," ASME Paper 65-HT-37, 1965.

211. W. F. Laverty and W. M. Rohsenow, "Film Boiling of Saturated Nitrogen Flowing in a Vertical Tube," ASME Paper 65 WA/HT-26, 1965.

212. H. H. Ellerbrook, J. N. B. Livingood and D. M. Straight, "Fluid Flow and Heat Transfer Problems in Nuclear Rockets," NASA SP-20, Dec. 1962.

213. J. P. Lewis, J. H. Goodykoontz and J. F. Kline, "Boiling Heat Transfer to Liquid Hydrogen and Nitrogen in Forced Flow," NASA TN D-1314, 1962.

214. W. H. Lowdermilk, C. D. Lanzo and B. L. Siegel, "Investigation of Boiling Burnout and Flow Stability for Water Flowing in Tubes," NACA TN 4382, Sept. 1958.

215. O. Baker, "Simultaneous Flow of Oil and Gas," Oil and Gas Journal, Vol. 53, No. 12, July 1954, p. 185-95.

216. R. C. Martinelli and R. W. Lockhart," Proposed Correlation of Data for Isothermal Two-Phase, Two-Component Flow in Pipes," Chem. Eng. Progress, Vol. 45, No. 1, Jan. 1949, p. 39.

217. R. C. Martinelli and D. B. Nelson," Prediction of Pressure-Drop During Forced Circulation Boiling of Water," Trans. ASME, Vol. 70, 1948.

218. K. E. Leonhard and R. K. McMordie, "The Non-Adiabatic Flow of Evaporating Cryogenic Fluid Through a Horizontal Tube," Advances in Cryogenic Engineering, Vol. 6, 1961, p. 481.

219. M. R. Hatch and R. B. Jacobs, "Prediction of Pressure Drop in Two Phase Single Component Flow," AIChE Journal, Vol. 8, No. 1, 1962, p. 18.

220. A. Lapin and E. Baver, "Pressure Drop of Two-Phase Single Component Isothermal Upward Flow of Nitrogen and Methane at High Pressures," Advances in Cryogenic Engineering, Vol. 12, 1967, p. 409-19.

221. J. M. Chenoweth and M. W. Martin, "A Pressure Drop Correlation for Turbulent Two Phase Flow of Gas-Liquid Mixtures in Horizontal Pipes," Petro. Refiner, Vol. 34, No. 10, 1955, p. 151.

222. A. E. Dukler, Moye Wicks III and R. G. Cleveland, "Frictional Pressure Drop in Two-Phase Flow: A. A Comparison of Existing Correlations for Pressure Loss and Holdup," AIChE Journal, Vol. 10, 1964, p. 38-43.

223. R. P. Sugden, K. D. Timmeriaos and D. K. Edmonds, "A Pressure-Drop Study of Freon-11, Near Saturation," Advances in Cryogenic Engineering, Vol. 12, 1967, p. 420-26.

224. K. D. Timmeriaos and R. P. Sugden, "Pressure Drop Considerations in the Transfer of Fluids," Advances in Cryogenic Engineering, Vol. 10, 1965, p. 367-74.

225. W. H. McAdams, W. K. Woods and L. C. Heroman, Jr., "Vaporization Inside Horizontal Tubes: II. Benzene-Oil Mixtures," Trans. ASME, Vol. 64, 1942, p. 193-200.

226. W. F. Davison, P. H. Haldie, C. G. R. Humpherys, A. H. Markson, A. R. Mumforo and T. Ravese, "Studies of Heat Transmission Through Boiler Tubing at Pressures From 500 to 3300 Pounds," Trans. ASME, Vol. 65, 1943, 553-91.

227. J. C. Elizalde, "Orbital Tests to Investigate Thermal Behavior of Cryogens Under Weightlessness," Proceedings, Conference on Propellant Tank Pressurization and Stratification, Vol. II, p. 245, NASA, Huntsville, Ala., Jan. 20, 21, 1965.

228. R. W. Graham, R. C. Hendricks and R. C. Ehlers, "Analytical and Experimental Study of Pool Heating of Liquid Hydrogen Over a Range of Accelerations," NASA TN D-1883, Feb. 1965. See also Inter. Advances in Cryogenic Engineering, Vol. 10, Plenum Press, 1965, p. 342-353.

229. C. P Costello and W. E. Tothill, "Effects of Acceleration on Nucleate Boiling," Chemical Engineering Progress Symposium Series, Vol. 57, No. 32, 1961, p. 189.

230. W. A. Beckman and H. Merte, Jr., "A Photographic Study of Boiling in an Accelerating System," Journal of Heat Transfer, Vol. 87, No. 3, Aug. 1965, p. 374-80.

231. H. J. Ivey, "Preliminary Results on the Effects of Accelleration on the Critical Heat Flux in Pool Boiling," Reactor Development Division Report AEEW-R99, AEE, Dorchester, Dorset, England, Sept. 1961.

232. C. M. Usiskin and R. Siegel, "An Experimental Study of Boiling in Reduced and Zero-Gravity Fields," Journal of Heat Transfer, Vol. 83, No. 3, Aug. 1961.

233. J. E. Sherley, "Nucleate Boiling Heat Transfer Data for Liquid Hydrogen at Standard and Zero Gravity," Advances in Cryogenic Engineering, Vol. 8, Plenum Press, 1963, p. 495.

234. D. N. Lyon, M. C. Jones, G. L. Ritter, C. Chiladakis and P. G. Kosky, "Peak Nucleate Boiling Fluxes for Liquid Oxygen on a Flat Horizontal Platinum Surface at Bouyancies Corresponding to Accelerations Between Zero and 1 g_E," AIChE Journal, Vol. 11, No. 5, 1965, p. 773-80.

235. J. A. Clark and H. Merte, "Nucleate, Transition and Film Boiling Heat Transfer at Zero Gravity," Physical and Biological Phenomena in a Weightless State, Vol. 14, Advances in the Astronautical Sciences, Edited by E. T. Benedikt and R. W. Halliburton, Western Periodicals Co., North Hollywood, California, 1963, p. 177-195.

236. R. Siegler, "Effects of Reduced Gravity on Heat Transfer, "Advances in Heat Transfer, Vol. IV, Edited by T. F. Irvine and J. P. Hartnett, Academic Press, 1967.

237. W. O. Randolph and J. L. Vaniman, "Subcooling of Cryogenic Liquids by Injection of Non-Condensible Gas," Geo. C. Marshall Space Flight Center, MTP-S and M -P-61-19, Oct. 17, 1961.

238. "Cryogenic Subcooling by Helium Injection," Geo. C. Marshall Space Flight Center, Memo M-S+M-PE No. 327, Oct. 24, 1961.

239. P. S. Larsen, J. A. Clark, W. O. Randolph and J. L. Vaniman, "Cooling of Cryogenic Liquids by Gas Injection," Advances in Cryogenic Engineering, Vol. 8, 1963, Plenum Press, p. 507-20.

240. F. W. Lytle and J. T. Stoner, "Cryogenic Cooling by Noncondensible Gas Injection," Science, Vol. 148, No. 3678, June 25, 1965, p. 1721-23.

241. A. F. Schmidt, "Experimental Investigation of Liquid Hydrogen Cooled by Helium Gas Injection," Advances in Cryogenic Engineering, Vol. 8, 1963, Plenum Press, p. 521.

242. V. S. Arpaci, J. A. Clark and P. S. Larsen, "The Dynamics of Gas-Vapor Bubbles in Binary Systems," Proceeding of the Royal Society, A, Volume 283, 1965, p. 50-63.

243. R. F. Barron and L. S. Han, "Heat and Mass Transfer to a Cryosurface in Free Convection," Journal of Heat Transfer, Vol. 87, No. 4, 1965, p. 499-506.

244. M. M. Chen and W. M. Rohsenow, "Heat, Mass and Momentum Transfer Inside Frosted Tubes - Experiment and Theory," Journal of Heat Transfer, Vol. 86, No. 3, August 1964, p. 334-41.

245. R. V. Smith, D. K. Edwards, E. G. F. Brentau and R. J. Richards, "Analysis of Frost Phenomena on a Cryosurface," Advances in Cryogenic Engineering, Vol. 9, 1964, p. 88-98.

246. D. C. Holten, "A Study of Heat and Mass Transfer to Uninsulated Liquid Oxygen Containers," Advances in Cryogenic Engineering, Vol. 6, 1961, p. 499.

247. D. A. Van Gundy and J. R. Uglum, "Heat Transfer to an Un-insulated Surface at 20°K", Advances in Cryogenic Engineering, Vol. 7, K. D. Timmerhaus, Editor, 1962.

248. "Atmospheric Heat Transfer to Vertical Tanks Filled with Liquid Oxygne," Special Report No. 50, to AFBMD, WDSOT, Arthur D. Little, Inc., Nov. 1, 1958.

249. NBS, Cryogenic Engineering Laboratory, "Summary Report of Work Done on Liquid Oxygen" ABMA Project Order 1657-00-60, NBS Project 81411.

250. J. L. Loper, and E. R. Heatherly, "Vapor Losses in Cylindrical Containers of Aluminum and Fiberglas Laminate Filled with Liquid Nitrogen and Exposed to Climatic Heating," Tech. Note No. G-002, August 4, 1955, Structures and Mechanics Laboratory, ABMA, Huntsville, Ala.

251. J. C. Aydelott, "Normal Gravity Self-Pressurization of 9-Inch (23 cm) Diameter Spherical Liquid Hydrogen Tankage," NASA TN D-4171, October 1967.

252. B. Gebhardt, Heat Transfer, McGraw-Hill Book Co., 1961, p. 117.

253. M. M. Fulk and M. M. Reynolds in American Institute of Physics Handbook, Edited by D. E. Gray, McGraw-Hill Book Co., 1957.

254. F. E. Ruccia and R. B. Hinckley, "The Surface Emittance of Vacuum-Metallized Polyester Film," Advances in Cryogenic Engineering, Vol. 12, Plenum Press, 1967, p. 300-308.

255. T. M. Cunningham and R. L. Young, "The Radiative Properties of Cryodeposits," Advances in Cryogenic Engineering, Vo. 8, Plenum Press, 1963, p. 85-93.

256. R. p. Caken, A. S. Gilcrest and C. A. Zierman, "Thermal Absorptances of Cryodeposits for Solar and 290°K Blackbody Sources," Advances in Cryogenic Engineering, Vol, 9, Plenum Press, 1964, p. 457-63.

257. B. C. Moore, "Effect of Gas Condensate on Cryopumps," American Vacuum Society, Los Angeles, California, 1962.

258. D. G. McConnell, "Absorptance of Thermal Radiation by Cryodeposit Layers," Advances in Cryogenic Engineering, Vol. 11, Plenum Press, 1966, p. 328-38.

259. C. L. Tien and E. G. Cravalho, "Thermal Radiation of Solids at Cryogenic Temperatures," Paper No. 306 AIChE Symposium, "Advances in Cryogenic Heat Transfer," 1967 AIChE National Meeting, Nov. 30, 1967 New York City.

260. J. A. Clark, et al., Progress Report No. 25, ORA Project 07461, NASA, University of Michigan, August 1967.

261. W. J. Rivers and P. W. McFadden, "Film Free Convection in Helium II," Journal of Heat Transfer, Vol. 88, No. 4, Nov. 1966, p. 343-51.

262. C. C. Matheson, "Symposium on Superfluid Helium," Cryogenics, February 1966, p. 1-10.

263. R. M. Holdredge and P. W. McFadden, "Boiling Heat Transfer from Cylinders in a Saturated Liquid Helium II Bath," Advances in Cryogenic Engineering, Vol. 11, 1966, p. 507-16.

264. B. W. Clement and T. H. K. Frederking, "Thermal Boundary Resistance and Related Peak Flux During Supercritical Heat Transport from a Horizontal Surface Through a Short Tube to a Saturated Bath of Liquid Helium II," Proceedings, International Institute of Refrigeration, Commission I, June 16-18, 1966, Boulder, Colo.

265. B. W. Clement and T. H. K. Frederking, "Destruction of Superfluidity caused by Heat Transport from a Hott Wall Through a Wide Tube to a Bath of Liquid Helium II," Proceedings, 3rd International Heat Transfer Conference, Vol. I., August 1966, Chicago, p. 299-305.

266. P. L. Kapitza, "The Study of Heat Transfer in Helium II," Journal of Physics (USSR, Vol. 4, 1941, p. 181.

267. I. M. Khalatnikov, "Heat Exchange Between a Solid Body and Helium II," Journal of Experimental and Theoretical Physics, (USSR), Vol. 22, 1952, p. 687.

268. R. A. Madsen and P. W. McFadden, "Heat Transfer to an Unsaturated Bath of Liquid Helium II," Advances in Cryogenic Engineering, Vol. 13, 1968.

269. R. K. Irey, P. W. McFadden and R. A. Madsen, "Heat Transfer to a Saturated Bath of Liquid Helium II", International Advances in Cryogenic Engineering, Vol. 10, 1965, p. 361-71.

270. L. J. Challis, K. Dransfeld and J. Wilks, "Heat Transfer Between Solids and Liquid Helium II," Proceedings of the Royal Society, A, Vol. 260, 1961, p. 31-46.

271. Wen-Yen Kuang, "An Investigation of the Temperature Discontinuity at the Boundary Between a Solid and Superfluid Helium," Soviet Physics, (JETP), Vol. 15, 1962, p. 365.

272. R. C. Johnson and W. A. Little, "Experiments on the Kapitza Resistance," Physical Review, Vol. 130, 1963, p. 596.

273. L. Rinderer and F. Haenseler, "Heat Transfer in Superfluid Helium," Helv. Phy. Acta., Vol. 32, 1959, p. 322

274. G. P. Lemieux and A. C. Leonard, "Maximum and Minimum Heat Flux in He II for a 76.2μ Diameter Horizontal Wire at Depths of Immersion Up to 70 cm," Advances in Cryogenic Engineering, Vol. 13, 1968.

275. T. H. K.Frederking, "Waermeuebergang bei der Verdampfung der verfluessigten Gase Helium und Stickstoff," Forschung, Vol. 27, 1961, p. 17-62.

276. T. H. K. Frederking and J. D. Schweikle, "Thermohydrodynamic Flow Similarity of He II in Wide Channels at Supercritical Velocities," Low Temperature Physics-LT9 (Part A), Plenum Press, 1965.

277. A. E. Bergles and W. M. Rohsenow, "The Determination of Forced-Convection Surface Boiling Heat Transfer", Journal of Heat Transfer, Vol. 86, Aug. 1964, p. 365-72.

278. C. H. Gilmour, "Nucleate Boiling - A Correlation", Chem. Eng. Prog., Vol. 54, No. 10, 1958, p. 77-79.